UNIVERSITY OF CALIFORNIA

Los Angeles

Understanding Mechanisms of Motility in *Trypanosoma brucei*

A dissertation submitted in partial satisfaction of the requirements for the degree Doctor of Philosophy in Microbiology, Immunology and Molecular Genetics

By

HoangKim Tran Nguyen

2014

© Copyright by

HoangKim Tran Nguyen

2014

ABSTRACT OF THE DISSERTATION

Understanding Mechanisms of Motility in *Trypanosoma brucei*

by

HoangKim Tran Nguyen

Doctor of Philosophy in Microbiology, Immunology and Molecular Genetics

University of California, Los Angeles 2014

Professor Kent L. Hill, Chair

Trypanosoma brucei are protozoan parasites that present a tremendous medical and economic burden on poverty-stricken areas of sub-Saharan Africa. These pathogens are estimated to affect nearly 60 million people and are considered one the world's most neglected diseases. A key aspect for parasite pathogenicity and transmission is the mechanism of motility. Recent advances have revealed that in addition to the ability to swim in incredibly viscous environments, *T. brucei* parasites are capable of forming multicellular communities upon surface exposure. Although this behavior is ubiquitous in microbiology, this is the first described pathogenic protozoa capable of coordinating motility for polarized movement as a multicellular group. Through both forward and reverse genetic screens, this study outlines efforts to define

signaling pathways and genes required for this surface-induced behavior. In particular, cAMP has been implicated in this process and a biased screen was performed to identify cAMP effectors that are required for social motility.

At individual level, motility in *T. brucei* is achieved by a single flagellum that is attached along the length of the cell body. The *T. brucei* flagellum has a canonical 9 + 2 axoneme structure that is highly conserved in organisms with motile flagella. A previous phylogenetic study identified 50 genes as the Core components of Motile Flagella (CMF). This dissertation expanded the original study and compared 115 diverse eukaryotic genomes. CMF22 was identified as a broadly conserved gene that was present in almost all organisms with motile flagella but not in organisms that lack flagella or have immotile flagella. Biochemical fractionation, localization by epitope tagging and RNAi knockdown was used to characterize CMF22. These experiments have demonstrated that CMF22 is an axonemal protein required for propulsive motility. High-resolution cryo-electron tomography of CMF22 knockdown mutants revealed the requirement of CMF22 for assembly of the proximal lobe of the nexin-dynein regulatory complex (N-DRC). Finally, mutagenesis experiments of the putative IQ motif and AAA domain of CMF22 have elucidated a potential mechanism for CMF22 action in axonemal motility.

Altogether, this work reveals important findings of motility, both at the individual and multicellular level to enhance current understand of protozoan biology, social microbiology, and conserved mechanisms of flagellum motility.

The dissertation of HoangKim Tran Nguyen is approved.

Beth A. Lazazzera

Peter J. Bradley

Alexander Van der Bliek

Kent L. Hill, Committee Chair

University of California, Los Angeles

2014

DEDICATION

The dissertation is dedicated to my biggest cheerleaders, my family. My parents have continually been a source of love and support through both good times and bad. I thank my brother, Brian, for inspiring me to keep my head up, take leaps, and remind me that it's never the end that counts, but the journey that is most important. I would like to thank my Wushu family, both Northern and Southern California: Quan Doan, Mary-Ann Cao, Boshen Jia, Nancy Yu, Kolina Yokoyama, Reid Yokoyama, Linda Baek, Eric Nguyen and Kent Chen. I thank you all for your belief in me and for being proud in my accomplishments, no matter how big or small. Finally, I would like to thank so many others that have helped me on this journey.

TABLE OF CONTENTS

Chapter 1: Introduction 1

Chapter 2: Forward Genetics and Targeted Screens to Identify Genes Required for Social Motility in *T. brucei* 37

Chapter 3: CMF22 is Required for Propulsive Motility in *T. brucei* 82

Chapter 4: Cryo-electron Tomography of *T. brucei* Flagellum Reveals High-Resolution 3D Structural Analysis of the Axoneme and Identifies Structural Defects Caused by the Loss of CMF22 137

Chapter 5: The Role of the CMF22 IQ and AAA domains in *T. brucei* Motility 167

Chapter 6: Future Directions 207

Chapter 7: Conclusion and Perspectives 222

Appendix A: Independent Analysis of the Flagellum Surface and Matrix Proteomes Provides Insight into Flagellum Signaling in Mammalian-infectious *Trypanosoma brucei* 232

LIST OF FIGURES AND TABLES

Chapter 1

Figure 1-1: Geographical distribution of Human African Trypanosomiasis 18

Figure 1-2: An overview of trypanocidal drugs used to treat HAT 19

Figure 1-3: The life-cycle of *Trypanosoma brucei* 20

Figure 1-4: Scanning electron micrograph image of procyclic-form *T. brucei* 21

Figure 1-5: The *T. brucei* flagellum 22

Figure 1-6: 3D ultrastructure of the flagellum 23

Figure 1-7: Location of N-DRC proteins within the complex 24

Chapter 2

Figure 2-1: Cell-cell communication benefits *T. brucei* 61

Figure 2-2: *T. brucei* social motility on a surface 62

Figure 2-3: Social motility in *T. brucei* 63

Figure 2-4: RNAi library screen to isolate motility mutants 64

Figure 2-5: Proof of concept of the RNAi library screen for social motility genes 65

Figure 2-6: Pilots 1 and 2 of the RNAi library screen to identify social motility mutants 66

Figure 2-7: Enrichment screen for social motility mutants 67

Figure 2-8: cAMP signaling is required for normal social motility 68

Figure 2-9: Candidate *T. brucei* cNMP-binding proteins 69

Figure 2-10: Social motility on candidate cNMP-binding proteins 70

Figure 2-11: Individual cNMP mutants (heterogenous) have reduced mRNA levels 71

Figure 2-12: Social motility and knockdown of clones of cNMP3 and cNMP4 72

Chapter 3

Figure 3-1: CMF22 is broadly conserved among organisms with motile flagella 109

Figure 3-2: CMF22 is associated with the flagellum skeleton 111

Figure 3-3: CMF22 is localized to the axoneme 112

Figure 3-4: CMF22 localizes to the axoneme of nascent flagella 113

Figure 3-5: CMF22 knockdown disrupts motility 114

Figure 3-6: Time-lapse series showing the reverse beat in CMF22-UKD following tetracycline induction 115

Figure 3-7: HA-tagged CMF22 rescues the motility defect of CMF22-knockdown cells 116

Figure 3-8: CMF22 is required for propulsive motility 117

Figure 3-9: CMF22-HA is less stably associated with the axoneme in N-DRC mutants 118

Figure 3-S1: CMF22 and basal body co-staining 119

Figure 3-S2: CMF22 knockdown does not affect axoneme ultrastructure 120

Figure 3-S3: Removal of tetracycline restores wild-type motility in CMF22-UKD cells 121

Figure 3-S4: CMF22 knockdown cells exhibits both reverse and forward beats 122

Table 3-1: CMF22 orthologues from 115 diverse eukaryotes 123

Chapter 4

Figure 4-1: Cryo-electron tomography of the *T. brucei* flagella 153

Figure 4-2: The *T. brucei* flagellum has extensive features to interact with the adjacent microtubule 154

Figure 4-3: Conserved and unique MIPs of *T. brucei* 155

Figure 4-4: Doublet specific features of the *T. brucei* axoneme 156

Figure 4-5: Connections of the N-DRC to axonemal protein complexes 157

Figure 4-6: The *T. brucei* N-DRC structure 158

Chapter 5

Figure 5-1: The IQ motif and AAA domain of CMF22 have conserved residues 189

Figure 5-2: CMF22 point mutants are expressed with minimal growth defects 191

Figure 5-3: K662A point mutants have aberrant translocation 192

Figure 5-4: K662A + Tet mutants have defective propulsive motility 193

Figure 5-5: CMF22-HA in the K662A mutants is stably associated with the axoneme 194

Figure 5-S1: Various IQ motif point mutants of CMF22 have normal average motility and translocation 195

Figure 5-S2: Uninduced cell lines are capable of translocation 196

Figure 5-S3: Average velocity does not reveal significant differences 197

Figure 5-S4: The K662A mutant has defective motility and is unable to form radial projections 198

Chapter 6

Figure 6-1: BioID tagging of CMF22 to identify interacting proteins 216

Figure 6-2: BCCP tagging of CMF22 for sub-localization by CryoET 217

Figure 6-3: Co-immunoprecipitation of the 900 kDa soluble CMF22-HA complex 218

Figure 6-4: CMF22-HA co-immunoprecipitation using the S1 fraction of tetracycline-induced trypanin mutants and eluted using 8M urea 219

VITA

EDUCATION

University of California, Los Angeles (09/2008 - 07/2014)

Ph.D., Department of Microbiology, Immunology, and Molecular Genetics (MIMG)

Dissertation: Understanding mechanisms of motility in *Trypanosoma brucei*

University of California, Davis (09/2003 – 06/2007)

Bachelor of Science in Microbiology, Minor in English

Graduated with Honors

AWARDS

Cellular and Molecular Biology (CMB) Training Grant Award

University of California, Los Angeles (2009-2012)

- A highly competitive NIH grant for funding students with research opportunities through financial support, integrative coursework, annual research reports, seminar programs, and retreats in the areas of cellular, biochemical, and molecular sciences

Eugene V. Cota-Robles Fellowship

University of California, Los Angeles (2008-2009, 2013-2014)

-A merit-based four-year fellowship program funded by the University of California Office of the President, the UCLA Graduate Division and the home department for students entering and continuing in a Ph.D. program with an emphasis on students interested in research and teaching

Department of Microbiology Citation Award of Excellence

University of California, Davis (2007)

-A merit-based award given to the top two students in the Department of Microbiology at UC Davis for competitive coursework and outstanding research

PUBLICATIONS

Nguyen HT, Sandhu JS, Langousis G, Hill KL. *CMF22 is a broadly conserved axonemal protein and is required for propulsive motility in Trypanosoma brucei.* Eukaryotic Cell 2013 Sep;12(9):1202-13. doi: 10.1128/EC.00068-13. Epub 2013 Jul 12. PMID: 23851336

Zhang MA, Rego D, Moshkova M, Kebir H, Chruscinski A, **Nguyen H**, Akkermann R, Stanczyk FZ, Prat A, Steinman L, Dunn SE. *Peroxisome proliferator-activated receptor (PPAR)α and -γ regulate IFNγ and IL-17A production by human T cells in a sex-specific way.* Proc Natl Acad Sci U S A. 2012 Jun 12;109(24):9505-10. Epub 2012 May 30. PMID: 22647601

Lopez MA, **Nguyen HT**, Oberholzer M, Hill KL. *Social parasites*. Curr Opin Microbiol. 2011 Dec;14(6):642-8. Epub 2011 Oct 21. Review. PMID:22020108

Oberholzer M, Langousis G, **Nguyen HT**, Saada EA, Shimogawa MM, Jonsson ZO, Nguyen SM, Wohlschlegel JA, Hill KL. *Independent analysis of the flagellum surface and matrix proteomes provides insight into flagellum signaling in mammalian-infectious Trypanosoma brucei.* Mol Cell Proteomics. 2011 Oct;10(10):M111.010538. Epub 2011 Jun 19. PMID:21685506

Dunn SE, Bhat R, Straus DS, Sobel RA, Axtell R, Johnson A, **Nguyen K**, Mukundan L, Moshkova M, Dugas JC, Chawla A, Steinman L. *Peroxisome proliferator-activated receptor delta limits the expansion of pathogenic Th cells during central nervous system autoimmunity*. J Exp Med. 2010 Aug 2;207(8):1599-608. doi: 10.1084/jem.20091663. Epub 2010 Jul 12. PMID: 20624891

RESEARCH EXPERIENCE

Graduate Student Researcher, UCLA, Dr. Kent Hill Laboratory
06/2009 – Present

- Directed individual and collaborative research projects using molecular biology, biochemistry, and techniques in structural biology to understand the mechanism of flagellar motility in the parasitic protozoan *Trypanosoma brucei*.
- Simultaneously managed several projects: optimizing a screening approach using an RNAi library to identify genes required for social motility, identification and characterization of a protein essential for trypanosomal motility (CMF22), and novel high-resolution structural analysis of flagella from a human pathogen.
- Published a first-author paper, two successfully-funded research proposals, a review, and grants to fund research
- Supervised and mentored 2 undergraduates as well as 1 graduate rotating student in basic laboratory techniques

Research Assistant, Stanford University, Dr. Lawrence Steinman Laboratory
10/2007 - 04/2008

- Processed human / murine blood and isolated T cells to determine the role of PPAR delta in autoimmunity and identify sex-specific differences in cytokine production, culminating in authorship of two published papers
- Assisted with maintenance, breeding and genotyping of mice required for laboratory research and scored EAE mice for multiple sclerosis studies
- Performed immunological assays (ELISAs, RT-PCR, T cell-proliferation assays) to detect cytokine production

Undergraduate Student Researcher, Dr. Kazuhiro Shiozaki Laboratory
06/2005 - 06/2007

- Designed and performed a multicopy suppressor screen in *S. pombe* to identify additional interactors with Cdc42p, a protein required for cell cycle regulation

PRESENTATIONS / POSTERS

Investigating the mechanism of axonemal motility in Trypanosoma brucei. (talk)
Parasitology Meeting, UCLA
Los Angeles, CA (November 2013)

CMF22, a flagellar cytoskeleton protein, is required for propulsive motility in Trypanosoma brucei. (Poster)
Southern California Eukaryotic Pathogen Symposium, University of California, Riverside
Riverside, California (November 14, 2012, October 30, 2013)

The cAMP signaling pathway is required for collective migration in Trypanosoma brucei. (talk and poster)
The 9th Global COE International Symposium "Cell Migration in Biology and Medicine", Kyushu University
Fukuoka, Japan (January 21, 2012)

Identification of genes regulating social behavior in Trypanosoma brucei. (poster)
Kinetoplastid Molecular Cell Biology Meeting
Woods Hole, Massachusetts (April 8-12, 2011)

Identification of genes regulating social behavior in Trypanosoma brucei. (talk)
Parasitology Meeting, UCLA
Los Angeles, CA (June 15, 2011)

Identification of genes regulating social behavior in Trypanosoma brucei. (poster)
Molecular Biology Institute Retreat
Lake Arrowhead, CA (October 15-17, 2010)

Chapter 1

Introduction

African Sleeping Sickness

Epidemiology and disease

Human African Trypanosomiasis (HAT) is a devastating disease in sub-Saharan Africa and is considered one the world's most neglected diseases (1). The causative agent of HAT, *Trypanosoma brucei,* is a protozoan parasite and is a threat to approximately 60 million people. There are two subspecies, *Trypanosoma brucei gambiense* and *Trypanosoma brucei rhodesiense* that cause disease in humans (Figure 1-1). *T. brucei gambiense* causes "West African Sleeping Sickness", which is endemic to central Africa and is the causative agent for 97% of all HAT cases. *T brucei rhodesiense* causes "East African Sleeping Sickness", which is the more acute form of the disease and is found in eastern and southeastern Africa. Additionally, a third sub-species, *Trypanosoma brucei brucei*, as well as other African trypanosomes, e.g. *T. congolense,* cause Nagana, a wasting disease in livestock. Lost agricultural gross domestic product due to Nagana totals to almost $4.75 billion, thus, in addition to the human health burden, African trypanosomes present a tremendous economic burden on an already impoverished area (Food and Agriculture Organization of the United Nations).

Trypanosomes are transmitted from one mammalian host to another through the bite of the tsetse fly of the genus *Glossina*. When an infected fly takes a bloodmeal, parasites are transmitted from the fly to the mammalian host. Parasites subsequently proliferate in the bloodstream, lymph nodes, and systemic organs including the spleen, heart, liver, eyes, and endocrine glands. During this haemolymphatic stage (1-3 weeks

post-infection), HAT is characterized by symptoms that include headache, malaise, weight loss, fatigue, and characteristic waves of fever (2). These waves coincide with waves of parasitemia as parasites undergo antigenic variation, a parasite-derived mechanism to evade the host immune system by periodic switching of the surface glycoprotein (3, 4). In addition, infected patients often develop enlarged spleens, livers, anemia and lymphoadenopathy (2). Weeks to months after infection, *T. brucei* parasites cross the blood-brain barrier and enter the central nervous system (CNS) (2). This second stage, or late stage is called the neurological stage and is characterized by meningoencephalitis. Symptoms at this stage include a disruption of the sleep/wake cycle, mental disturbances, motor system disturbances, sensory system disruption and abnormal reflexes (2). Without treatment, infection almost invariably results in coma and death.

Treatment

There is no vaccine to prevent HAT infection, current therapies are out-dated, toxic, and there is now trypanotolerance to these drugs (5). A summary of the current drugs used to treat HAT is shown in Figure 1-2 (6). For treatment during the haemolymphatic stage, pentamide is administered intramuscularly or intravenously to those infected with *T. b. gambiense*. For *T. b. rhodisiense,* suramin is administered to those infected. Although suramin is effective at this early stage, it has been known to cause bone marrow toxicity and neurological complications (2). In addition these early-stage drugs, two other drugs are frontline therapies for late-stage HAT infections. To treat *T. b. rhodesiense*, an arsenic-based compound, melarsoprol, is administered

intravenously. Although melarsoprol is the drug of choice and is the only therapy available for late-stage *T. b. rhodesiense* infection, it is painful and highly toxic, with 5% of patients dying from toxicity of the treatment (7). For treatment of late-stage *T. b. gambiense* infection melarsoprol is also used, as well as eflornithine and nifurtomox-eflornithine combination therapy (NECT). Eflornithine and NECT, however, are not effective against *T. b. rhodesiense* infections. There are now a few novel drugs in various stages of clinical trials to treat HAT (6). The nitroheterocyclic drug fexinidazole is at phase 2 of clinical trials since it was proven to be effective as well as non-toxic in animals models of African Trypanosomiasis and is a promising candidate for treatment of late-stage *T. b. gambiense* HAT. Another treatment for late-stage *T. b. gambiense* is the oxaboroles class of drugs. This drug was able to clear parasites from the CNS in a murine model and is currently at stage 1 of clinical trials. In addition to developing new drugs for treatment of HAT, researchers have also tried a different approach by improving melarsoprol drug delivery by enhancing solubility so that toxicity is reduced. Although a number of new therapies to treat HAT are in the pipeline, it is evident that this neglected disease requires much more attention and research to combat this devastating disease in an already poverty-stricken region.

T. brucei life cycle

Development within the tsetse fly host

The *T. brucei* life cycle requires both the insect vector and mammalian host for completion. Within each host, the parasite goes through a series of developmental

changes to mature into a form that allows for survival and colonization in the next host (Figure 1-3) (8-10). When the tsetse fly takes a bloodmeal from an infected mammalian host, bloodstream-form trypomastigotes develop into actively dividing procyclic-form trypomastigotes within the fly gut lumen. Procyclic-form *T. brucei* subsequently migrate to the ectoperitrophic space, proventriculus, and then foregut where they differentiate into another developmental form, the mesocyclic epimastigote form. These slender epimastigotes have increased motility and migrate to the salivary glands. In the salivary gland, shortened epimastigote forms attach to the salivary gland epithelium through extensions of the flagellar membrane (8, 9, 11, 12). Once attached, epimastigotes differentiate into bloodstream-transmissible metacyclic trypomastigotes that are now primed for survival in the mammalian host.

Development within the mammalian host

One major adaptation to become bloodstream-transmissible is the shedding of the major surface protein of procyclic-form cells, procyclin, and expression of the antigenically distinct variable surface glycoproteins (VSGs) (4, 13). After transmission by a fly, these bloodstream-adapted parasites proliferate in the blood as actively dividing slender metacyclic trypomastigotes. During this stage, metacyclics evade the host immune response through antigenic variation, a mechanism in which a small percentage of *T. brucei* parasites can switch the surface glycoprotein antigens while antibodies are targeting the surface antigen of the population (3). Slender, dividing metacyclics proliferate in the bloodstream, infiltrate systemic organs, and ultimately cross the blood brain barrier into the CNS. In the meantime, a population of these

dividing metacyclics differentiate to short, stumpy non-dividing cells that are uniquely primed for survival in the tsetse fly host (14-16). The developmental cycle of *T. brucei* is intricately fine-tuned for survival in both the mammalian host and in the testse fly vector.

Host-pathogen interaction

Although there are multitudes parasite-derived signals, it is the crosstalk between parasite-derived and host-derived signals that allow for *T. brucei* survival in both hosts. *T. brucei* is extracellular at all stages of its life cycle. In the testse fly vector, there are a number of host factors that contribute to parasite development and efficient transmission. For example, the surface protein EP-procyclin expression is reversibly induced by cold shock (16). This is presumably coordinated with the *T. brucei* life cycle where temperature drops from 37 °C to 28 °C when the fly takes a bloodmeal and metacyclic stage cells enter the colder tsetse fly host. Additionally, stumpy form cells are primed in the mammalian host to resist the external proteolytic environment of the tsetse fly (15).

There is also evidence of communication between *T. brucei* and the mammalian host. One of the most notable examples is the development of the VSG coat on metacyclic parasites acquired in the tsetse fly before becoming mammalian-transmissible. The VSG coat protects parasites from immune destruction by switching to a different isoform faster than antibody can be produced for each isotype (17). The *T. brucei* flagellum itself contains a repertoire of virulence factors. The losses of glycosylphosphatidylinositol-phospholipase C (GPI-PLC), calflagins, and metacaspase 4 (MCA4) all reduce parasite virulence in a *T. brucei* mouse infection model (18-20).

Additionally, a *T. brucei* adenylate cyclase (ESAG4) activates protein kinase A in host macrophages to inhibit the trypanotoxic tumor necrosis factor (TNF) and prolong survival in infected mice (21).

Another example of the host-pathogen communication is apparent in the diversity of protein families with stage-specific isoforms, such as transferrin receptors. Trasferrin is taken up by a heterodimeric transferrin receptor in which the genes for these receptors are expressed on telomeric expression sites along the VSG gene. Although there are up to 20 of these expression sites, only one is active at a time. Additionally, there are different isoforms of these transferrin receptors that have variable binding affinities for different transferrins from different animal hosts. It has been suggested that the ability for *T. brucei* to switch between different transferrin receptor genes has enabled the parasite to occupy various host environments (22). African trypanosomes experience a multitude of differing environments within each host and must therefore sense the host environment to make appropriate adaptations for survival. Profound developments in the studies of *T. brucei* pathogen interaction within both the tsetse fly host and mammalian hosts have been advanced through the use of *T. brucei* as a model organism.

T. brucei **is an exemplary model organism for the study of parasite pathogenesis and flagellum biology.**

The first observation of *T. brucei* was made at the end of the nineteenth century by Plimmer and Bradford in 1899 and over the century, *T. brucei* has been an important

organism for the study of parasite pathogenesis and transmission. Recent advances have made *T. brucei* an exemplary model organism for studies in pathogenesis and ciliary function. Homologous recombination is highly efficient in *T. brucei,* making reverse genetics such as inducible RNA intereference (RNAi), targeted gene knockdowns and inducible expression of recombinant proteins possible (23). In addition, the recent creation of genetic library makes it feasible to do forward genetics in *T. brucei* using a library of RNAi mutants both in procyclic-form and bloodstream-form *T. brucei* (24, 25). *T. brucei* is therefore an incredible genetically tractable model organism with a diverse range of experimental tools for investigating pathogenesis and flagellum biology.

The flagellum

T. brucei is an early-diverging eukaryote. Phylogenetic reconstruction based on small subunit ribosomal RNA predicts that Salivarian trypanosomes branched about 300 million years ago (26). One of the most prominent features of *T. brucei* is the flagellum. The flagellum of *T. brucei* is conserved in deep-branching eukaryotes and across broad evolutionary distances (27). It is suggested that the last eukaryotic common ancestor had a motile flagellum, hinting at its importance (28).

The eukaryotic flagellum is a key structure that is conserved among all eukaryotic groups and is important for motility, sensation, adhesion and mating (29, 30). *T. brucei* is a microscopic parasite about 20 micrometers long and is tapered at both ends (Figure 1-4). The flagellum of the parasite emerges at the flagellar pocket, is attached along the length of the cell body, and extends past the cell body at the anterior end (8). Although

this organelle is important for sensing, it is classically associated with mechanisms of motility in *T. brucei* (31). The flagellum is surrounded by a distinct plasma membrane that is contiguous with the cell body plasma membrane and is attached to the cell body by an array of transmembrane crosslinks call the flagellum attachment zone (FAZ). The core structure of the *T. brucei* flagellum is conserved with the motile eukaryotic flagella in which there is a 9 outer doublet microtubules arranged symmetrically around a central pair of microtubules (Figure 1-5). This axoneme also includes radial spokes that connect the central pair to each of the doublet microtubules. The nexin-dynein regulatory complex (N-DRC), a protein complex that sits at the base of radial spokes and doublet microtubules regulates signals between the central pair, the radial spokes, and adjacent doublet microtubules.

The *T. brucei* flagellum is critical for a variety of roles. These include motility, host cell attachment, endocytosis/ immune evasion, sensory perception, cell morphogenesis, cell division, and cytokinesis (31, 32). The *T. brucei* flagellum has both unique and conserved features and is therefore an excellent model organism with dual roles: the unique features of the flagellum can be exploited for novel therapeutic targets while studies of conserved components of the flagellum provides a foundation for further studies in heritable ciliary diseases (Figure 1-5).

Unique features of the *T. brucei* flagellum

Paraflagellar rod

A unique feature of flagellum in trypanosomatids, euglenoids, and dinoflagellates is the lattice-like structure that is adjacent to the axomeme of *T. brucei* called the paraflagellar rod (PFR) (33). This paracrystalline filament emerges from the flagellar pocket and extends alongside the axoneme all the way to the distal tip of the flagellum (Figure 1-5, green lattice structure). The PFR is composed of major proteins PFR-1 and PFR-2 as well as numerous other minor proteins which include the PFR-associated adenylate kinases ADK-A and ADK-B, and cAMP phosphodiesterases PDEB1 and PDEB2 (34-39). Although the precise role of the PFR is not known, it has been shown that the PFR is required for normal motility. RNAi knockdown of PFR-2 in *T. brucei* and PFR-1 and PFR-2 in *Leishmania* resulted in a paralysis and reduced flagellar velocity, respectively (40, 41). Recently, 20 additional PFR proteins were identified in a screen for proteins that function in motility (37). Several of these proteins localize to the PFR and contain EF-hand domains or IQ motifs, both of which have the capacity for Ca^{2+} binding, suggesting an additional sensing role of the PFR.

Flagellar membrane

T. brucei is a motile parasite that encounters it's environment at the flagellum tip, therefore it is not surprising that the flagellar membrane is a scaffold for a variety of sensory proteins. In a paper I've included in Appendix B, we have purified the flagellum surface of bloodstream-form *T. brucei* to discover that the flagellum surface is enriched for *T. brucei* specific proteins (42). Among the 158 surface proteins identified, 16% was specific to *T. brucei* when compared against a dataset that included 8 ciliated organisms and 4 non-ciliated organisms. In comparison, kinetoplastic-specific proteins comprised

only 5% of the flagellum matrix proteome and 1% of the flagellum skeletal proteome. This flagellum surface proteome also identified proteins from major signaling cascades such as cyclic nucleotide signaling, Ca^{2+} signaling, and proteins that potentially function in transporting solutes across the cell membrane. The surface of the flagellum is a host-pathogen interface that is replete with kinetoplastid specific proteins involved in signaling and can be exploited for therapeutic intervention.

Conserved features of axonemal motility

Axoneme

The axoneme is composed of the 9 outer doublet microtubules, the central pair of singlet microtubules, outer and inner dynein arms that provide the mechanical force for bending, radial spokes that connect the singlet microtubules to outer doublet microtubules, and the N-DRC that is a central hub in regulating motility dynamics. These additional structures on the doublet microtubules (inner dynein arms, outer dynein arms, N-DRC, radial spokes) are arranged in a periodicity of 96 nanometers along the length of the axoneme (Figure 1-6A) (43). The availability of genome sequences has allowed for comparison of the *T. brucei* axoneme to other eukaryotic organisms with motile flagella. These studies have demonstrated that the components of the axoneme are well conserved between *T. brucei* and the motile flagella of diverse eukaryotic groups (44-49). Additionally, these proteins play regulatory roles in flagellar beating as demonstrated by RNAi knockdown of these axonemal proteins.

Motility

The *T. brucei* flagellum is attached along the cell length and wraps around the cell body in a left-handed helix. In this way, the beating movement of the flagellum causes the entire cell body to spiral like a corkscrew to swim. In fact, the word "trypanon" is a Greek word for "auger cell," which describes the corkscrew-like movement of the parasite as it moves through liquid environments. Like other flagellated microbes that have corkscrew motility such as spirochetes or treponemes, this spiraling movement is suggested to be more efficient in viscous environments and to possibly burrow through tight junctions of the blood brain barrier (50). Forward motility in *T. brucei* parasites initiates at the anterior tip of the cell and the wave is propagated towards the posterior end. The flagellum is attached to the cell body so as the cell moves, the flagellum appears to "undulate" when live parasites are examined under light microscopy.

T. brucei are rapid swimmers that have a forward motility at around 3-20 micrometers per second and can swim extended periods of time in one direction. Like most motile microbes, the swimming pattern of *T. brucei* is observed to be longs runs followed by tumbling, often a change in direction and back to a run (51). Motility is achieved through coordination of the dynein motor power strokes around and along the length of the axoneme. The central pair, radial spokes, I1 inner dynein arms, and the dynein regulatory complex are all involved in regulating axonemal motility (52-56). Several seminal studies in *Chlamydomonas reinhardtii* have revealed a general mechanism for motility coordination. External signals are transduced from the central

pair to the radial spokes then to the inner dynein arms (57). The intermediate chain-light chain complex of the I1 inner dynein arm (I1 ICLC) and the nexin-dynein regulatory complex are suggested to transmit these signals to the outer dynein-inner dynein (OID) linker to distribute the signals (55, 58, 59).

Nexin-dynein regulatory complex (N-DRC)

The N-DRC has is considered a regulatory hub for coordinating axonemal motility. The N-DRC sits at the base of the radial spokes on the doublet microtubules and is thought to transmit signals between radial spokes and outer dynein arms as well as mechanical/chemical signals between adjacent outer doublet microtubules (Figure 1-6, gold structure) (57, 58, 60). Minus end-directed motor proteins on the A-tubule of the outer doublet microtubules called dyneins walk unidirectionally on the B-tubule of the adjacent outer doublet microtubule to generate sliding forces (61). However, this sliding movement is restricted by the N-DRC and sliding forces are translated into bending of the flagellum (62-64). In order for flagellar bending to be propagated along the axoneme, dynein activity must be coordinated around the circumference of the flagellum as well as along the axoneme since paralysis would result if all dyneins are active simultaneously (53). Therefore, the N-DRC, a reversible inhibitor of dynein activity, is a focal point of axonemal dynein regulation and is critical for motility. However, little is known about the regulatory mechanism of the N-DRC.

The N-DRC was first discovered through suppressor mutant analysis to isolate suppressors of the motility phenotype in radial spoke and central pair mutants (65-67). These mutants were able to suppress the paralysis defect observed in radial spoke and

central mutants, suggesting the presence of a complex, termed the “dynein regulatory complex” (DRC) that inhibits dynein activity. Electron micrograph (EM) analysis of *drc* mutants in comparison to wild-type axonemes revealed a crescent-shaped structure between radial spoke 2 and the inner dynein arms (68-70). Recent cryo-electron tomography studies of *drc* mutants in *C. reinhardtii* have determined that this DRC structure overlaps with previously described nexin links, such that the two structure are now considered a single complex, the N-DRC (60). The N-DRC from C. reinhardtii is predicted to be a 1.4-1.5 megadalton complex and is comprised of an estimated 11 or more subunits, DRC1-11 (71). Structurally, the DRC is divided into a 300-350 kDa base plate, which attaches to the A-tubule of one outer doublet microtubule, a 350 kDa proximal lobe and a 120 kDa distal lobe (Figure 1-6B). The lobes extend outward to contact the B-tubule of the neighboring outer doublet microtubule. Heuser *et al.* performed tomographic averaging of 24 tomograms of intact, frozen-hydrated axonemes from wild-type and 5 different strains of *drc* mutants. By correlating published data on proteins missing in each mutant, with structural deficiencies observed in each mutant, Heuser *et al.* proposed a model for the sub-cellular localization of several DRC subunits within the N-DRC complex. It was revealed that DRC1 and DRC2 are likely within the base plate, DRC5 and DRC6 (as well as other polypeptides) are localized to the distal lobe of the B-tubule connector, and DRC3, 4, and 7 are within the central region of the linker (Figure 1-7) (60). However, the identity of proteins comprising approximately one-third of the total mass (500 kDa) of the N-DRC, including the entire proximal lobe, were unaccounted for, suggesting that additional DRC subunits remain to be identified.

Models of motility

There are three overlapping models that have been proposed for the regulation of flagellar beating. In the sliding control model, the linear arrangement of the dynein motors along the length of the outer doublet microtubule suggests that there is sequential activation and termination of dynein activity as microtubules slide relative to one another (72-75). The geometric clutch model hypothesizes that ciliary bending is due to changes in increased or decreased probability that a dynein arm will form a cross-bridge with the adjacent outer doublet microtubule, depending on transverse forces that force microtubules apart during bending (74, 76-79). In the last model called the distributor model, mechanical and enzymatic interactions involving the central pair, the radial spokes, a newly discovered calmodulin spoke complex (CSC) at the base of radial spokes, and the N-DRC are regulated by asymmetric contacts with the radial spokes during bending. Strain and tension is sensed and the information is transmitted from the radial spokes to the CSC and DRC to activate and/or inhibit different subsets of the dynein arms (58, 80, 81). The models are not mutually exclusive.

Effectors of motility

It is predicted that there are 800-1000 proteins within the *T. brucei* flagellum, but most of these proteins have unknown domains and functions. It is probable that a subset of these proteins would function as effectors, or proteins that can sense external signals and transmit these signals for coordinated flagellum motility. Which signals and how signals are transduced in the axoneme have been an area of extreme interest.

Regulatory components within the central pair and radial spokes have been identified using the model organism *Chlamydomonas reinhardtii*. The phosphorylation state of the intermediate chain IC138 was revealed to be critical for regulating microtubule sliding (56). Dymek and Smith has shown that dynein activity is responsive to changes in calcium concentration, most likely through the calmodulin spoke complex at the base of radial spokes (82).

Identification of key effectors for motility was attempted using another trypanosomatid, *Crithidia oncopelti*. Holwill and colleagues determined that Ca^{2+} ion concentration influences flagellar wave direction. Tip-to-base beating is predominant at low Ca^{2+} ion concentrations, but this distal beating switches to reverse base-to-tip beating at high Ca^{2+} ion concentrations (83). Additionally, nucleotide signaling has the potential to confer regulatory roles in flagellar beating. Upon ATP binding, protein motors called dyneins provide a mechanical force to drive flagellar motility (84). Although the response to Ca^{2+} or nucleotides as well as the identification of other Ca^{2+}-binding proteins in the flagellum have been described in many flagellated protozoans, effectors have not yet been identified in *T. brucei* (85, 86).

The N-DRC is predicted to be an integral hub for coordinating axonemal motility. One of first N-DRC subunits identified, trypanin, is a protein required for regulating the flagellar beat in *T. brucei* and *C. reinhardtii* (87, 88). The homolog of trypanin is also critical for normal ciliary motility for ear development in zebrafish (89). Another N-DRC subunit identified in *T. brucei* that co-migrates with trypanin in sucrose gradients was CMF70, and like trypanin, this protein is also required for normal flagellar beating (90).

Recent work by Lin *et al.* used two-dimensional electrophoresis and MALDI-TOF mass spectrometry to identify 8 N-DRC proteins with phosphorylated isoforms. In a seminal study in 2011, Lin and colleagues identified 5 more N-DRC proteins in addition to the 7 known N-DRC subunits. Among these 12 N-DRC associated proteins, 8 of these proteins and 2 other components that may regulate N-DRC function were found to have phosphorylated isoforms using a phosphoproteomic approach (91). This study identified DRC7, FAP61, DRC3, FAP206, FAP230, DRC2, FAP252, and DRC1 as proposed N-DRC subunits that are post-translationally modified by phosphorylation, however, some of these proteins have not been independently validated as part of the N-DRC.

This dissertation will discuss efforts to define molecular pathways that regulate motility in *Trypanosoma brucei* with the hopes of augmenting our current understanding of conserved mechanisms of eukaryotic motility as individual cells and as groups for discovering major tenets of social microbiology.

FIGURES

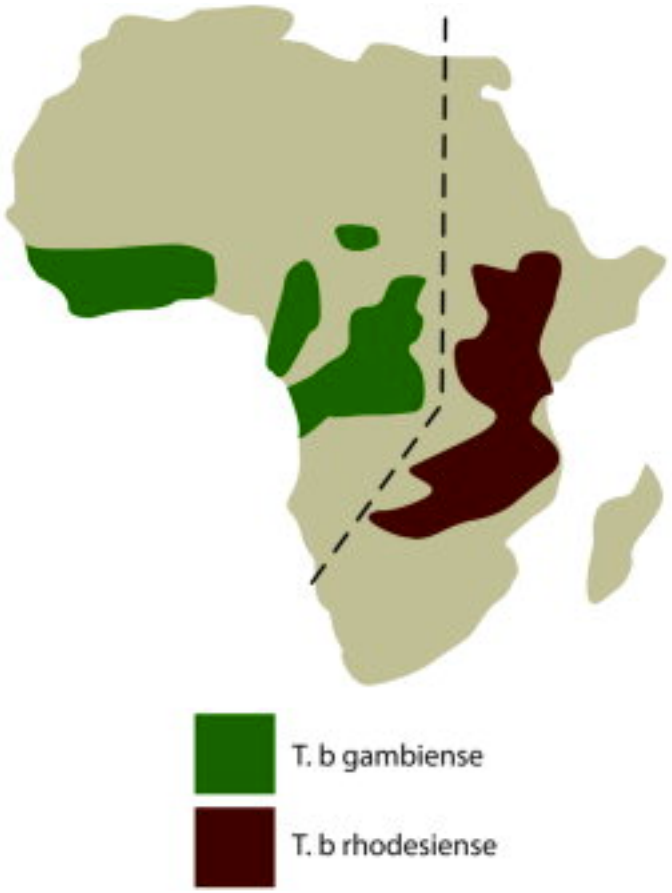


Figure 1-1. Geographical distribution of Human African Trypanosomiasis (HAT). Commonly termed “African Sleeping Sickness,” HAT is endemic to sub-Saharan Africa. Illustrated here is the geographical distribution of *T. b. gambiense*, and *T. b. rhodesiense*. The dotted black line divides the region between the causative agents for West African Sleeping Sickness (*T .b. gambiense*) and East African Sleeping Sickness (*T. b. rhodesiense*). Reprinted with permission from (1).

Table 1. Overview of trypanocidal drugs

Drug	Species	Indication	Year of first use	Structure [half life]	Comments
Pentamidine isethionate	*T b gambiense*	Stage 1	1940	Aromatic diamine [9·4 hours by IM] [6·4 hours by IV]	
Suramin sodium	*T b gambiense* *T b rhodesiense*	Stage 1	Early 1920s	Sulphonated naphtylamine [50 days]	
Melarsoprol (Mel B)	*T b gambiense* *T b rhodesiense*	Stage 2	1949	Trivalent organic arsenical (biological activity) [35 hours]	Increase treatment failure (resistant strains?)
Eflornithine	*T b gambiense*	Stage 2	1981	DL-alpha-difluoromethylornithine [3 hours]	Difficult use
Nifurtimox	*T b gambiense* *T b rhodesiense ?*	Stage 2	1977	5′-nitrofurane [3·5 hours]	Not registered for HAT Case series only Toxicity and action on *T b rhodesiense* poorly documented

IM=intramuscular, IV=intravenous

Figure 1-2. An overview of trypanocidal drugs used to treat Human African Trypanosomiasis. Listed are the drugs used, the targeted *T. brucei* species of each drug, the stages of infection that are susceptible to the drugs (stage 1 is the haemolymphatic stage and stage 2 is the neurological stage), and the half-life of each drug. Reprinted with permission from (6).

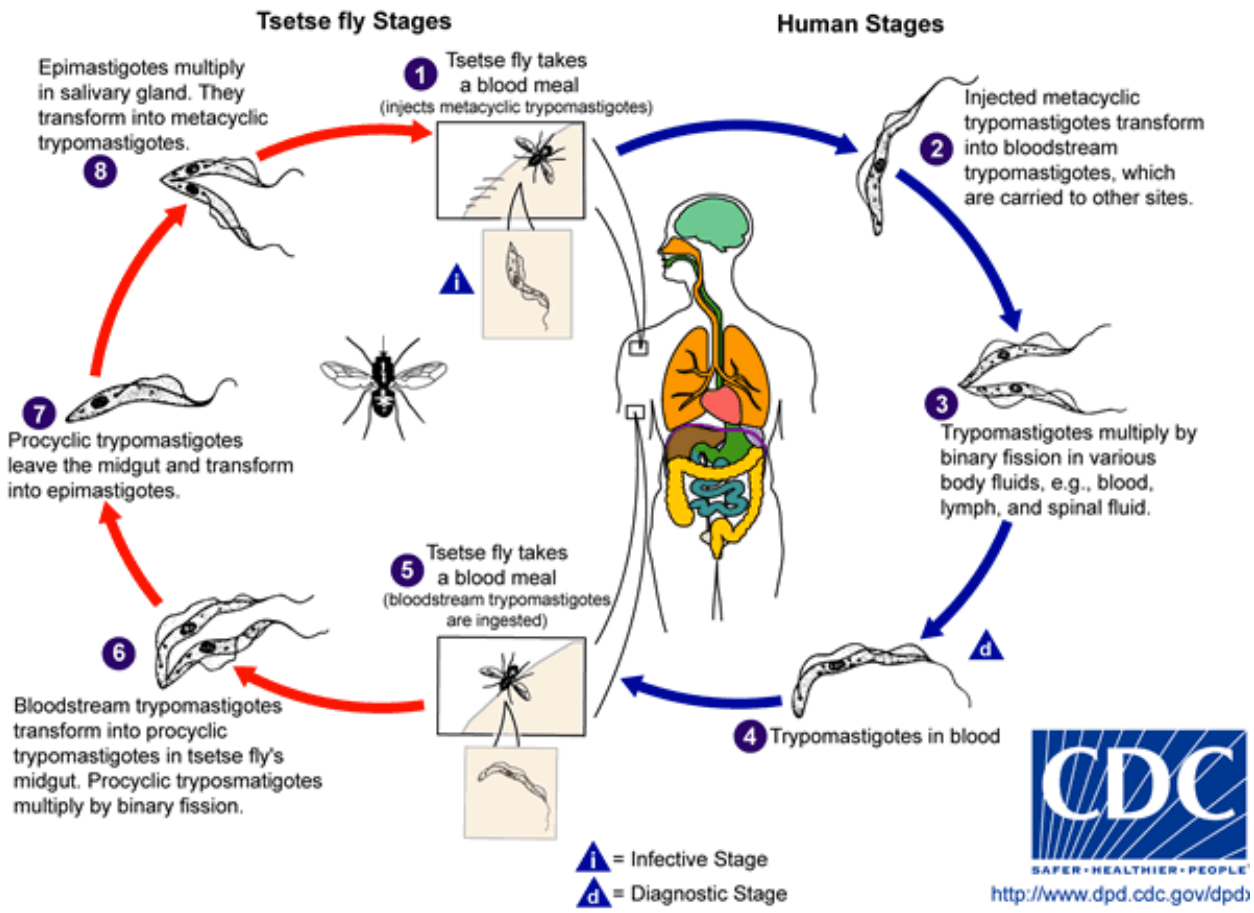


Figure 1-3. The life-cycle of *Trypanosoma brucei. T. brucei* are obligate parasites that reside in two hosts: the tsetse fly (left) and the mammalian host (right). Within each host, the parasite undergoes a series of developmental transformations to be transmissible to the next host. Image reproduced from http://www.cdc.gov/dpdx/trypanosomiasisAfrican/index.html

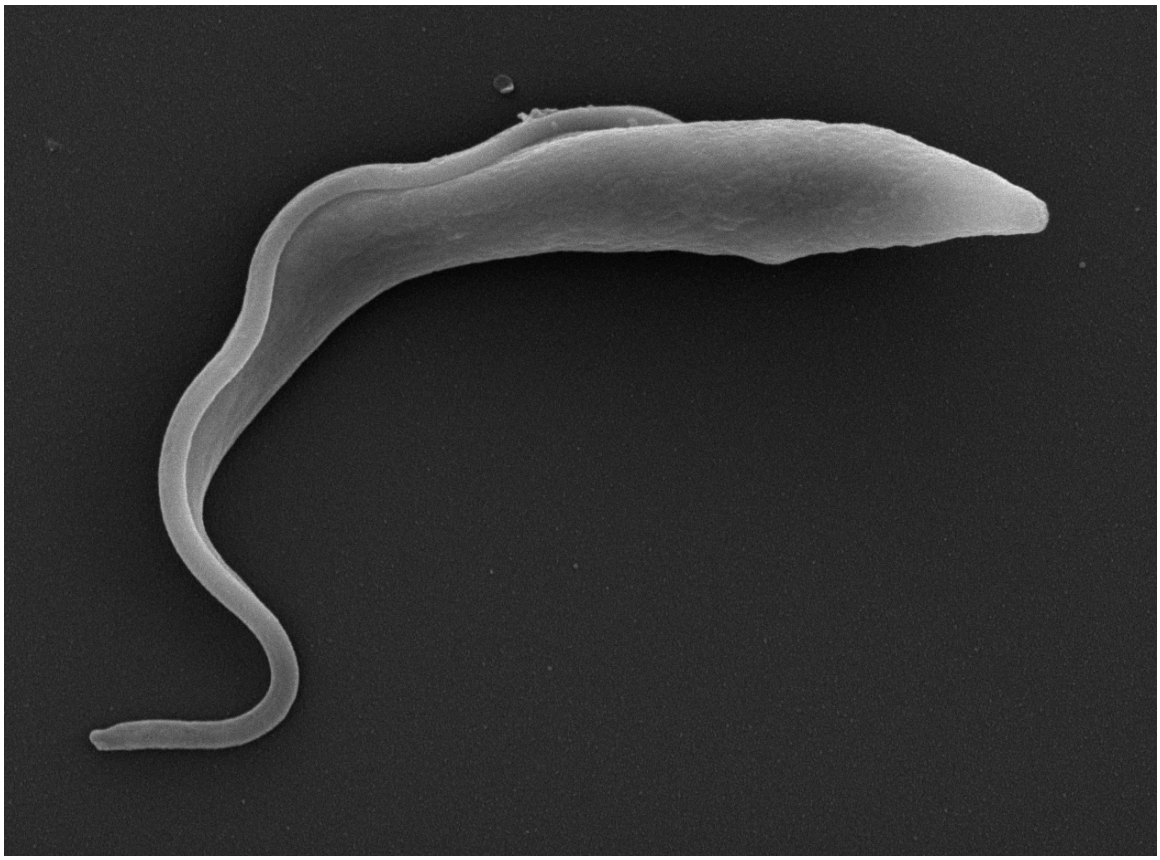


Figure 1-4. Scanning electron micrograph image of a procyclic-form *Trypanosoma brucei*. The flagellum is attached along the length of the cell body and extends past the cell body to culminate in a tip. Image captured by Michelle Thayer.

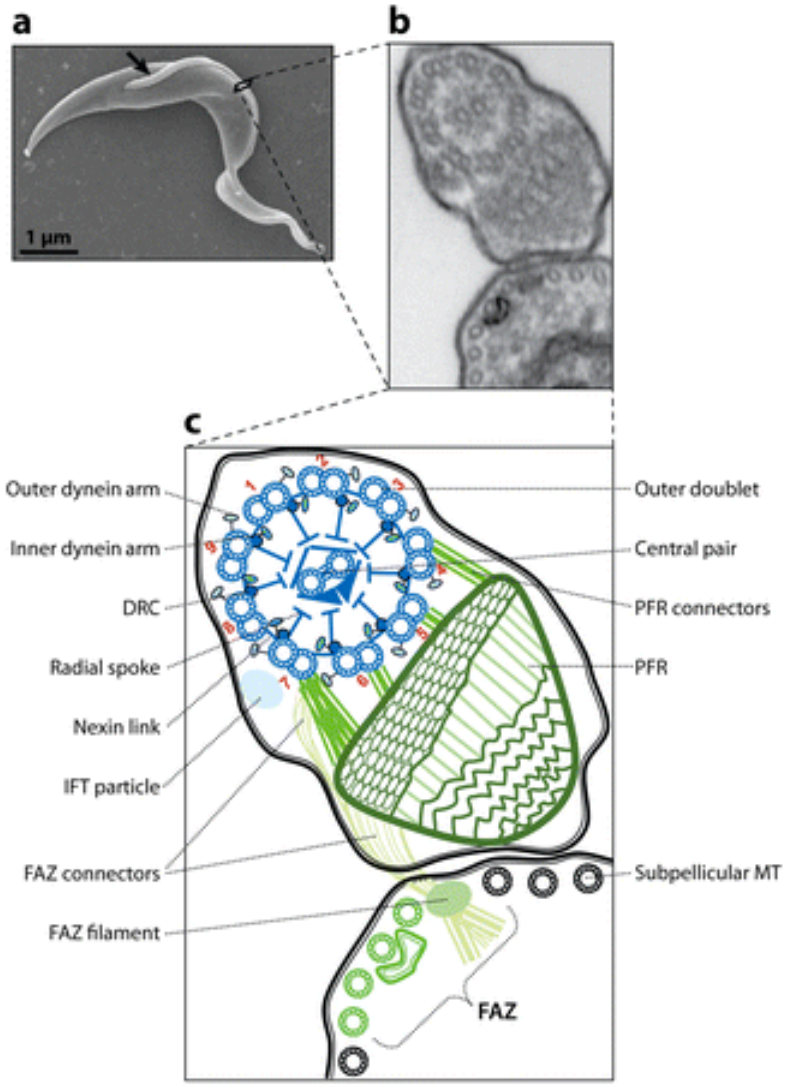


Figure 1-5. The *Trypanosoma brucei* flagellum. (a) Scanning electron micrograph of a procyclic-form *T. brucei* cell. (b) Transmission electron micrograph depicting a cross section of the flagellum with the cell body in the lower right corner. (c) Cartoon schematic of panel *b.* Depicted in blue are the outer doublet microtubules, outer and inner dynein arms, central spoke, radial pairs and nexin-dynein regulatory complex (dark blue circles). Structures unique to trypanosomes and closely related organisms are shown in green while conserved structures are in blue. Figure reproduced from (32).

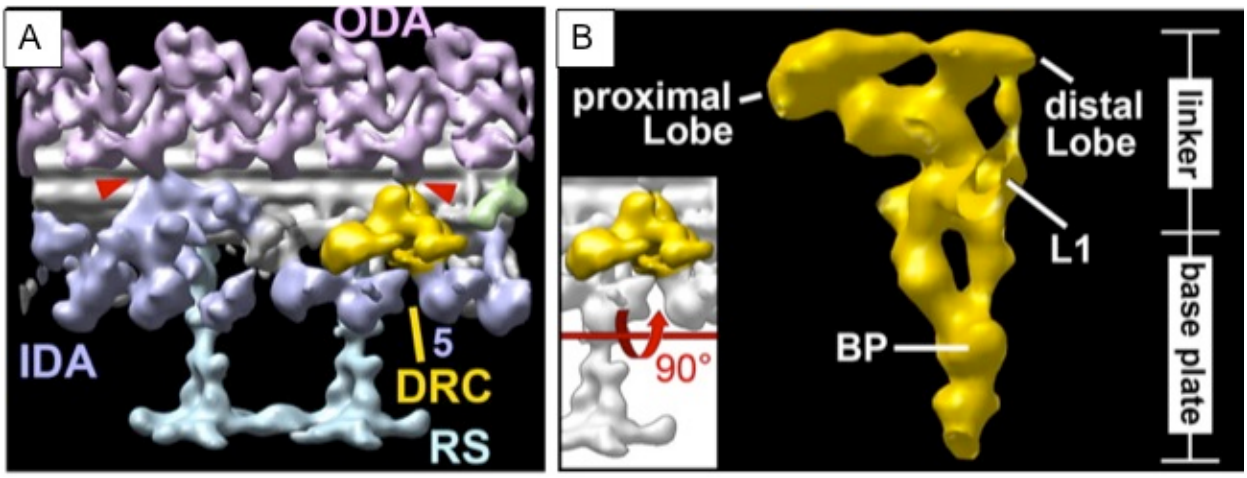


Figure 1-6. 3D ultrastructure of the flagellum. (6A) Depicted is one 96 nanometer repeat of the *C. reinhardtii* flagellum, with the N-DRC labeled in gold. (6B) Simplified surface-rendering of the N-DRC with the inset explaining the orientation seen in the larger view. Figure adapted from (60).

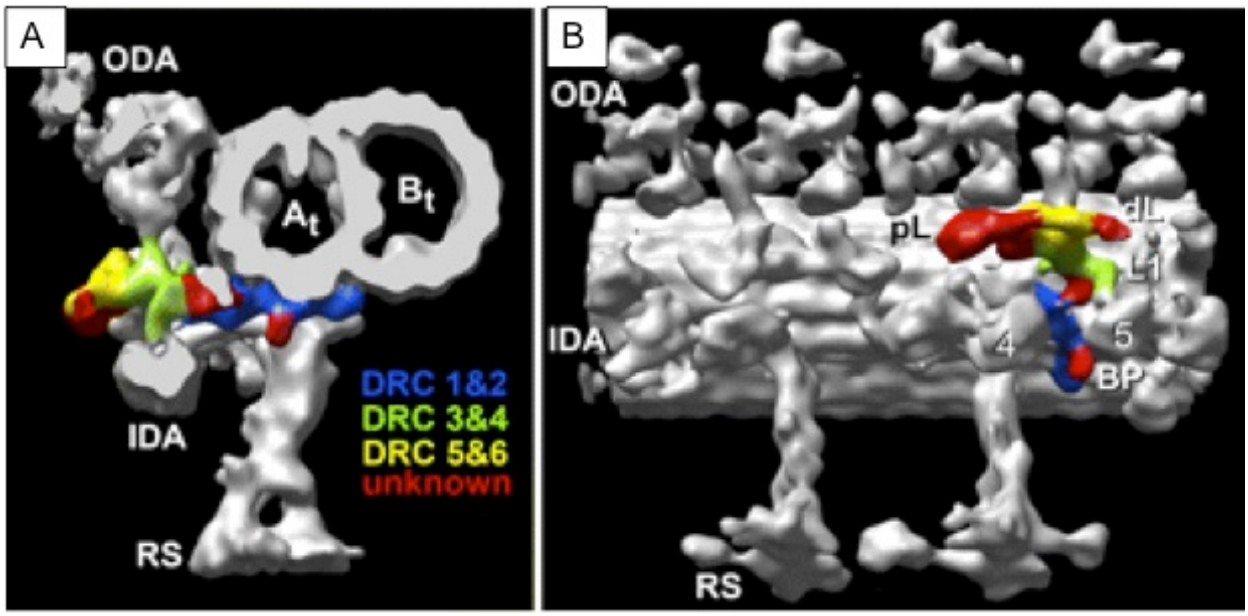


Figure 1-7. Location of N-DRC proteins within the complex. Isosurface rendering was performed on various *drc* mutants to identify proposed locations of subunits using previously published data on missing subunits and structural data on the presence of absence of specific N-DRC features in mutants. (6A) Side view and (6B) front view of proposed locations within the N-DRC. Figure adapted from (60).

REFERENCES

1. Kennedy, P. G. 2008. The continuing problem of human African trypanosomiasis (sleeping sickness). Ann Neurol 64:116-26.
2. Kennedy, P. G. E. 2013. Clinical features, diagnosis, and treatment of human African trypanosomiasis (sleeping sickness). Lancet Neurology 12:186-194.
3. Borst, P., and G. A. Cross. 1982. Molecular basis for trypanosome antigenic variation. Cell 29:291-303.
4. Pays, E., H. Coquelet, P. Tebabi, A. Pays, D. Jefferies, M. Steinert, E. Koenig, R. O. Williams, and I. Roditi. 1990. Trypanosoma brucei: constitutive activity of the VSG and procyclin gene promoters. The EMBO journal 9:3145-51.
5. Baker, N., H. P. de Koning, P. Maser, and D. Horn. 2013. Drug resistance in African trypanosomiasis: the melarsoprol and pentamidine story. Trends Parasitol 29:110-8.
6. Legros, D., G. Ollivier, M. Gastellu-Etchegorry, C. Paquet, C. Burri, J. Jannin, and P. Buscher. 2002. Treatment of human African trypanosomiasis--present situation and needs for research and development. Lancet Infect Dis 2:437-40.
7. Pepin, J., and F. Milord. 1994. The treatment of human African trypanosomiasis. Adv Parasitol 33:1-47.
8. Van Den Abbeele, J., Y. Claes, D. van Bockstaele, D. Le Ray, and M. Coosemans. 1999. *Trypanosoma brucei* spp. development in the tsetse fly:

characterization of the post-mesocyclic stages in the foregut and proboscis. Parasitology 118:469-78.

9. Vickerman, K. 1985. Developmental cycles and biology of pathogenic trypanosomes. Br Med Bull 41:105-14.

10. Hendry, K. A., and K. Vickerman. 1988. The requirement for epimastigote attachment during division and metacyclogenesis in Trypanosoma congolense. Parasitol Res 74:403-8.

11. Tetley, L., and K. Vickerman. 1985. Differentiation in Trypanosoma brucei: host-parasite cell junctions and their persistence during acquisition of the variable antigen coat. J Cell Sci 74:1-19.

12. Vickerman, K., L. Tetley, K. A. Hendry, and C. M. Turner. 1988. Biology of African trypanosomes in the tsetse fly. Biol Cell 64:109-19.

13. Roditi, I., H. Schwarz, T. W. Pearson, R. P. Beecroft, M. K. Liu, J. P. Richardson, H. J. Buhring, J. Pleiss, R. Bulow, and R. O. Williams. 1989. Procyclin gene expression and loss of the variant surface glycoprotein during differentiation of *Trypanosoma brucei*. Journal of Cell Biology 108:737-46.

14. McLintock, L. M., C. M. Turner, and K. Vickerman. 1993. Comparison of the effects of immune killing mechanisms on Trypanosoma brucei parasites of slender and stumpy morphology. Parasite Immunol 15:475-80.

15. Nolan, D. P., S. Rolin, J. R. Rodriguez, J. Van Den Abbeele, and E. Pays. 2000. Slender and stumpy bloodstream forms of Trypanosoma brucei display a differential response to extracellular acidic and proteolytic stress. Eur J Biochem 267:18-27.

16. Engstler, M., and M. Boshart. 2004. Cold shock and regulation of surface protein trafficking convey sensitization to inducers of stage differentiation in Trypanosoma brucei. Genes & development 18:2798-811.

17. Barry, J. D., and R. McCulloch. 2001. Antigenic variation in trypanosomes: enhanced phenotypic variation in a eukaryotic parasite. Adv Parasitol 49:1-70.

18. Webb, H., N. Carnall, L. Vanhamme, S. Rolin, J. Van Den Abbeele, S. Welburn, E. Pays, and M. Carrington. 1997. The GPI-phospholipase C of Trypanosoma brucei is nonessential but influences parasitemia in mice. J Cell Biol 139:103-14.

19. Emmer, B. T., M. D. Daniels, J. M. Taylor, C. L. Epting, and D. M. Engman. 2010. Calflagin inhibition prolongs host survival and suppresses parasitemia in Trypanosoma brucei infection. Eukaryotic cell 9:934-42.

20. Proto, W. R., E. Castanys-Munoz, A. Black, L. Tetley, C. X. Moss, L. Juliano, G. H. Coombs, and J. C. Mottram. 2011. Trypanosoma brucei metacaspase 4 is a pseudopeptidase and a virulence factor. J Biol Chem 286:39914-25.

21. Salmon, D., S. Bachmaier, C. Krumbholz, M. Kador, J. A. Gossmann, P. Uzureau, E. Pays, and M. Boshart. 2012. Cytokinesis of Trypanosoma brucei bloodstream forms depends on expression of adenylyl cyclases of the ESAG4 or ESAG4-like subfamily. Mol Microbiol 84:225-42.

22. Bitter, W., H. Gerrits, R. Kieft, and P. Borst. 1998. The role of transferrin-receptor variation in the host range of Trypanosoma brucei. Nature 391:499-502.

23. Wirtz, E., S. Leal, C. Ochatt, and G. A. Cross. 1999. A tightly regulated inducible expression system for conditional gene knock-outs and dominant-negative genetics in *Trypanosoma brucei*. Mol. Biochem. Parasitol. 99:89-101.

24. Morris, J. C., Z. Wang, M. E. Drew, and P. T. Englund. 2002. Glycolysis modulates trypanosome glycoprotein expression as revealed by an RNAi library. Embo J 21:4429-38.

25. Baker, N., S. Alsford, and D. Horn. 2011. Genome-wide RNAi screens in African trypanosomes identify the nifurtimox activator NTR and the eflornithine transporter AAT6. Molecular and biochemical parasitology 176:55-7.

26. Steverding, D. 2008. The history of African trypanosomiasis. Parasit Vectors 1:3.

27. Fritz-Laylin, L. K., S. E. Prochnik, M. L. Ginger, J. B. Dacks, M. L. Carpenter, M. C. Field, A. Kuo, A. Paredez, J. Chapman, and J. Pham. 2010. The Genome of Naegleria gruberi Illuminates Early Eukaryotic Versatility. Cell 140:631-642.

28. Mitchell, D. R. 2007. The evolution of eukaryotic cilia and flagella as motile and sensory organelles. Adv Exp Med Biol 607:130-40.

29. Takeda, S., and K. Narita. 2012. Structure and function of vertebrate cilia, towards a new taxonomy. Differentiation 83:S4-11.

30. Wilson, N. F. 2008. Gametic cell adhesion and fusion in the unicellular alga Chlamydomonas. Methods Mol Biol 475:39-51.

31. Langousis, G., and K. L. Hill. 2014. Motility and more: the flagellum of Trypanosoma brucei. Nat Rev Microbiol 12:505-18.

32. Ralston, K. S., Z. P. Kabututu, J. H. Melehani, M. Oberholzer, and K. L. Hill. 2009. The Trypanosoma brucei flagellum: moving parasites in new directions. Annual Review of Microbiology 63:335-62.

33. Vickerman, K. 1962. The mechanism of cyclical development in trypanosomes of the Trypanosoma brucei sub-group: an hypothesis based on ultrastructural observations. Trans R Soc Trop Med Hyg 56:487-95.

34. Maga, J. A., and J. H. LeBowitz. 1999. Unravelling the kinetoplastid paraflagellar rod. Trends in Cell Biology 9:409-13.

35. Oberholzer, M., G. Marti, M. Baresic, S. Kunz, A. Hemphill, and T. Seebeck. 2007. The Trypanosoma brucei cAMP phosphodiesterases TbrPDEB1 and TbrPDEB2: flagellar enzymes that are essential for parasite virulence. Faseb J 21:720-31.

36. Portman, N., and K. Gull. 2009. The paraflagellar rod of kinetoplastid parasites: from structure to components and function. International Journal for Parasitology 40:135-48.

37. Portman, N., S. Lacomble, B. Thomas, P. G. McKean, and K. Gull. 2008. Combining RNA Interference Mutants and Comparative Proteomics to Identify Protein Components and Dependences in a Eukaryotic Flagellum. Journal of Biological Chemistry 284:5610-5619.

38. Pullen, T. J. 2004. Protein Targeting of an Unusual, Evolutionarily Conserved Adenylate Kinase to a Eukaryotic Flagellum. Molecular biology of the cell 15:3257-3265.

39. Ginger, M. L., E. S. Ngazoa, C. A. Pereira, T. J. Pullen, M. Kabiri, K. Becker, K. Gull, and D. Steverding. 2005. Intracellular positioning of isoforms explains an unusually large adenylate kinase gene family in the parasite Trypanosoma brucei. J Biol Chem 280:11781-9.

40. Bastin, P., T. Sherwin, and K. Gull. 1998. Paraflagellar rod is vital for trypanosome motility. Nature 391:548.

41. Santrich, C., L. Moore, T. Sherwin, P. Bastin, C. Brokaw, K. Gull, and J. H. LeBowitz. 1997. A motility function for the paraflagellar rod of Leishmania parasites revealed by PFR-2 gene knockouts. Molecular and Biochemical Parasitology 90:95-109.

42. Oberholzer, M., G. Langousis, H. T. Nguyen, E. A. Saada, M. M. Shimogawa, Z. O. Jonsson, S. M. Nguyen, J. A. Wohlschlegel, and K. L. Hill. 2011. Independent analysis of the flagellum surface and matrix proteomes provides insight into flagellum signaling in mammalian-infectious Trypanosoma brucei. Mol Cell Proteomics 10:M111 010538.

43. Ibanez-Tallon, I. 2003. To beat or not to beat: roles of cilia in development and disease. Human molecular genetics 12:27R-35.

44. Baron, D. M., K. S. Ralston, Z. P. Kabututu, and K. L. Hill. 2007. Functional genomics in Trypanosoma brucei identifies evolutionarily conserved components of motile flagella. J Cell Sci 120:478-91.

45. Dawe, H. R., H. Farr, and K. Gull. 2007. Centriole/basal body morphogenesis and migration during ciliogenesis in animal cells. J Cell Sci 120:7-15.

46. Dawe, H. R., H. Farr, N. Portman, M. K. Shaw, and K. Gull. 2005. The Parkin co-regulated gene product, PACRG, is an evolutionarily conserved axonemal protein that functions in outer-doublet microtubule morphogenesis. J Cell Sci 118:5421-30.

47. Branche, C., L. Kohl, G. Toutirais, J. Buisson, J. Cosson, and P. Bastin. 2006. Conserved and specific functions of axoneme components in trypanosome motility. J Cell Sci 119:3443-55.

48. Ralston, K. S., A. G. Lerner, D. R. Diener, and K. L. Hill. 2006. Flagellar Motility Contributes to Cytokinesis in Trypanosoma brucei and Is Modulated by an Evolutionarily Conserved Dynein Regulatory System. Eukaryotic Cell 5:696-711.

49. Broadhead, R., H. R. Dawe, H. Farr, S. Griffiths, S. R. Hart, N. Portman, M. K. Shaw, M. L. Ginger, S. J. Gaskell, P. G. McKean, and K. Gull. 2006. Flagellar motility is required for the viability of the bloodstream trypanosome. Nature 440:224-7.

50. Jahn, T. L., and E. C. Bovee. 1968. Locomotion of Blood Protists, p. 393-436. *In* D. Weinman and M. Ristic (ed.), Infectious Blood Diseases of Man and Animals, vol. 1. Academic Press, NY.

51. Rodriguez, J. A., M. A. Lopez, M. C. Thayer, Y. Zhao, M. Oberholzer, D. D. Chang, N. K. Kisalu, M. L. Penichet, G. Helguera, R. Bruinsma, K. L. Hill, and J. Miao. 2009. Propulsion of African trypanosomes is driven by bihelical waves with alternating chirality separated by kinks. Proc Natl Acad Sci U S A 106:19322-7.

52. Witman, G. B., J. Plummer, and G. Sander. 1978. Chlamydomonas flagellar mutants lacking radial spokes and central tubules. Structure, composition, and function of specific axonemal components. J Cell Biol 76:729-47.

53. Smith, E. F., and W. S. Sale. 1992. Regulation of dynein-driven microtubule sliding by the radial spokes in flagella. Science 257:1557-9.

54. Piperno, G., K. Mead, and W. Shestak. 1992. The inner dynein arms I2 interact with a "dynein regulatory complex" in Chlamydomonas flagella. J Cell Biol 118:1455-63.

55. Smith, E. F. 2002. Regulation of flagellar dynein by the axonemal central apparatus. Cell Motil Cytoskeleton 52:33-42.

56. Bower, R., K. VanderWaal, E. O'Toole, L. Fox, C. Perrone, J. Mueller, M. Wirschell, R. Kamiya, W. S. Sale, and M. E. Porter. 2009. IC138 defines a subdomain at the base of the I1 dynein that regulates microtubule sliding and flagellar motility. Mol Biol Cell 20:3055-63.

57. Nicastro, D., C. Schwartz, J. Pierson, R. Gaudette, M. E. Porter, and J. R. McIntosh. 2006. The molecular architecture of axonemes revealed by cryoelectron tomography. Science 313:944-8.

58. Porter, M. E., and W. S. Sale. 2000. The 9 + 2 axoneme anchors multiple inner arm dyneins and a network of kinases and phosphatases that control motility. J Cell Biol 151:F37-42.

59. Kamiya, R. 2002. Functional diversity of axonemal dyneins as studied in Chlamydomonas mutants. Int Rev Cytol 219:115-55.

60. Heuser, T., M. Raytchev, J. Krell, M. E. Porter, and D. Nicastro. 2009. The dynein regulatory complex is the nexin link and a major regulatory node in cilia and flagella. Journal of Cell Biology 187:921-33.

61. Sale, W. S., and P. Satir. 1977. Direction of active sliding of microtubules in Tetrahymena cilia. Proc Natl Acad Sci U S A 74:2045-9.

62. Satir, P. 1968. Studies on cilia. 3. Further studies on the cilium tip and a "sliding filament" model of ciliary motility. J Cell Biol 39:77-94.

63. Summers, K. E., and I. R. Gibbons. 1971. Adenosine triphosphate-induced sliding of tubules in trypsin-treated flagella of sea-urchin sperm. Proc Natl Acad Sci U S A 68:3092-6.

64. Warner, F. D. 1976. Ciliary inter-microtubule bridges. . Journal of Cell Science 20:101-114.

65. Brokaw, C. J., D. J. Luck, and B. Huang. 1982. Analysis of the movement of Chlamydomonas flagella:" the function of the radial-spoke system is revealed by comparison of wild-type and mutant flagella. J Cell Biol 92:722-32.

66. Huang, B., Z. Ramanis, and D. J. Luck. 1982. Suppressor mutations in Chlamydomonas reveal a regulatory mechanism for Flagellar function. Cell 28:115-24.

67. Piperno, G., K. Mead, M. LeDizet, and A. Moscatelli. 1994. Mutations in the "dynein regulatory complex" alter the ATP-insensitive binding sites for inner arm dyneins in Chlamydomonas axonemes. J Cell Biol 125:1109-17.

68. McIntosh, R., D. Nicastro, and D. Mastronarde. 2005. New views of cells in 3D: an introduction to electron tomography. Trends Cell Biol 15:43-51.

69. Mastronarde, D. N., E. T. O'Toole, K. L. McDonald, J. R. McIntosh, and M. E. Porter. 1992. Arrangement of inner dynein arms in wild-type and mutant flagella of Chlamydomonas. J Cell Biol 118:1145-62.

70. Gardner, L. C., E. O'Toole, C. A. Perrone, T. Giddings, and M. E. Porter. 1994. Components of a "dynein regulatory complex" are located at the junction

between the radial spokes and the dynein arms in Chlamydomonas flagella. J Cell Biol 127:1311-25.

71. Bower, R., D. Tritschler, K. Vanderwaal, C. A. Perrone, J. Mueller, L. Fox, W. S. Sale, and M. E. Porter. 2013. The N-DRC forms a conserved biochemical complex that maintains outer doublet alignment and limits microtubule sliding in motile axonemes. Mol Biol Cell.

72. Riedel-Kruse, I. H., A. Hilfinger, J. Howard, and F. Julicher. 2007. How molecular motors shape the flagellar beat. HFSP J 1:192-208.

73. Charles, J. B. 2008. Thinking about flagellar oscillation. Cell Motility and the Cytoskeleton 9999:NA.

74. Lindemann, C. B., and K. A. Lesich. 2010. Flagellar and ciliary beating: the proven and the possible. Journal of cell science 123:519-28.

75. Mitchison, T. J., and H. M. Mitchison. 2010. Cell biology: How cilia beat. Nature 463:308-9.

76. Morita, Y., and C. Shingyoji. 2004. Effects of imposed bending on microtubule sliding in sperm flagella. Curr Biol 14:2113-8.

77. Hayashi, S., and C. Shingyoji. 2008. Mechanism of flagellar oscillation-bending-induced switching of dynein activity in elastase-treated axonemes of sea urchin sperm. J Cell Sci 121:2833-43.

78. Lindemann, C. B. 2007. The geometric clutch as a working hypothesis for future research on cilia and flagella. Ann N Y Acad Sci 1101:477-93.

79. Brokaw, C. J. 2008. Thinking about flagellar oscillation. Cell Motil Cytoskeleton.

80. Heuser, T., C. F. Barber, J. Lin, J. Krell, M. Rebesco, M. E. Porter, and D. Nicastro. 2012. Cryoelectron tomography reveals doublet-specific structures and unique interactions in the I1 dynein. Proc Natl Acad Sci U S A 109:E2067-76.

81. Smith, E. F., and P. Yang. 2004. The radial spokes and central apparatus: mechano-chemical transducers that regulate flagellar motility. Cell Motil Cytoskeleton 57:8-17.

82. Heuser, T., E. E. Dymek, J. Lin, E. F. Smith, and D. Nicastro. 2012. The CSC connects three major axonemal complexes involved in dynein regulation. Mol Biol Cell 23:3143-55.

83. Holwill, M. E., and J. L. McGregor. 1976. Effects of calcium on flagellar movement in the trypanosome Crithidia oncopelti. J Exp Biol 65:229-42.

84. King, S. M. 2012. Integrated control of axonemal dynein AAA(+) motors. J Struct Biol 179:222-8.

85. Ridgley, E., P. Webster, C. Patton, and L. Ruben. 2000. Calmodulin-binding properties of the paraflagellar rod complex from Trypanosoma brucei. Molecular and Biochemical Parasitology 109:195-201.

86. Wu, Y., J. Deford, R. Benjamin, M. G. Lee, and L. Ruben. 1994. The gene family of EF-hand calcium-binding proteins from the flagellum of *Trypanosoma brucei*. Biochem J 304:833-41.

87. Ralston, K. S., and K. L. Hill. 2006. Trypanin, a Component of the Flagellar Dynein Regulatory Complex, Is Essential in Bloodstream Form African Trypanosomes. PLoS Pathogens 2:873-882, e101 doi:10.1371/journal.ppat.0020101.

88. Rupp, G., and M. E. Porter. 2003. A subunit of the dynein regulatory complex in Chlamydomonas is a homologue of a growth arrest-specific gene product. J Cell Biol 162:47-57.

89. Colantonio, J. R., J. Vermot, D. Wu, A. D. Langenbacher, S. Fraser, J. N. Chen, and K. L. Hill. 2009. The dynein regulatory complex is required for ciliary motility and otolith biogenesis in the inner ear. Nature 457:205-9.

90. Kabututu, Z. P., M. Thayer, J. H. Melehani, and K. L. Hill. 2010. CMF70 is a subunit of the dynein regulatory complex. Journal of Cell Science 123:3587-95.

91. Lin, J., D. Tritschler, K. Song, C. F. Barber, J. S. Cobb, M. E. Porter, and D. Nicastro. 2011. Building blocks of the nexin-dynein regulatory complex in Chlamydomonas flagella. J Biol Chem 286:29175-91.

Chapter 2

Forward Genetics and Targeted Screens to Identify Genes Required for Social Motility in *T. brucei*.

Chapter 2 describes work done to identify genes regulating a novel behavior recently discovered in *T. brucei* termed “social motility” (1). The introduction will encompass current knowledge of social behavior in microbiology and a detailed description of this behavior in *T. brucei*. The introduction contains excerpts from a review published in *Current Opinion in Microbiology* in 2011 entitled “Social Parasites” by Dr. Miguel Lopez, Dr. Michael Oberholzer, Dr. Kent Hill and myself. Results will include two screening approaches: a forward genetics screen using an RNA interference (RNAi) library and a targeted cAMP effector screen to identify genes required for social motility in *T. brucei*.

Introduction

Social behaviors are most widely recognized in the communication and cooperation observed in metazoans, ranging from navigation strategies and group hierarchies in insect communities to complex social networking in humans and other primates. However, communication and cooperation among individuals in a group also occurs at the cellular level, as illustrated in collective motility of migrating cells during wound healing, tissue morphogenesis and tumor metastases. Moreover, cell-cell communication and cooperative behavior is not restricted to higher animals and recent years have seen a surge in the study and understanding of social interactions and their underlying mechanisms in microbial systems.

Social interactions among microbes give rise to multicellular groups having emergent behaviors that are not possible in single cells (2-9). For example, quorom

sensing enables synchronization of gene expression and cellular activities to allow a population to act as a group (2). Surface-associated behaviors such as biofilm formation and swarming motility allow microbes to establish communities with enhanced protection against external agonists and promote colonization and penetration of biotic and abiotic surfaces (10-14). Cell-cell signaling during sporulation in myxobacteria and slime molds directs group motility behaviors and developmental programs in which cellular differentiation gives rise to multicellular forms having distinct cell types with specialized functionalities, thereby enhancing survival through division of labor (15, 16). In extreme cases, multispecies biofilms and microbial mats constitute complex microbial ecosystems where numerous microbes communicate, cooperate and battle with each other (17). Ultimately, the goal is to enhance survival and proliferation of the organism and when the microbe is a pathogen, this has dire consequences for the host (6, 18, 19).

In the bacterial world, cell-cell communication is the rule and considering social behavior as a ubiquitous property of bacteria has transformed our view and understanding of microbiology (2-4). Social behaviors are also well-documented in eukaryotic microbes (6, 7, 20, 21). However, despite the tremendous influence that the paradigm of ‘sociomicrobiology’ has had on our understanding of microbiology, one group of microbes, the parasitic protozoa, seem to have been left without an invitation to the party. Studies of the organisms generally consider them as individual cells in suspension cultures or animal models of infection, while social interactions are largely unstudied.

Parasitic protozoa are etiological agents of several major human maladies, including malaria, epidemic dysentery, Leishmaniasis and African sleeping sickness, that affect over half a billion people worldwide. Parasites also limit economic development in some of the poorest regions on the planet and are thus major contributors to the global human health and economic burden. Parasites have complex life cycles requiring transmission through multiple hosts, survival in diverse environments and a wide variety of cellular differentiation events. Hence, there are numerous facets of parasite biology that may benefit from, or may even depend upon, social interactions.

Cell-cell signaling and cell density-dependent behavior

The protozoan parasite *T. brucei* is the etiologic agent of African trypanosomiasis, which causes widespread mortality and morbidity of humans and livestock in sub-Saharan Africa. These parasites are transmitted to the bloodstream of a mammalian host through the bite of a tsetse fly vector. In the mammalian host, *T. brucei* must balance competing objectives of promoting parasite proliferation and limiting pathologic consequences to preserve the host as nutrient source (Figure 2-1). In addition, as a vector-borne pathogen, *T. brucei* must ready itself for survival in the tsetse vector and must maintain sufficient parasite density in the bloodstream to permit transmission during a tsetse blood meal (22, 23). Parasitemia is controlled partly via host immune defenses, but *T. brucei* is an expert at evading these defenses and thus benefits from differentiation of proliferating ‘slender’ form parasites into growth-arrested ‘stumpy’ forms (24-26). Differentiation into non-dividing stumpy forms is irreversible in

the bloodstream and premature commitment to this pathway would jeopardize maintenance of the infection (24-27). Control is provided via a postulated quorum sensing-type system in which a soluble, parasite-derived ‘stumpy induction factor’ (SIF) accumulates as parasite cell density increases and triggers parasite differentiation only after a sufficient parasitemia has been achieved (24, 25). The nature of SIF and the SIF signaling pathway are not known, but cyclic nucleotide signaling has been suggested to be involved (25, 26). Stumpy-form parasites are pre-adapted for survival in the tsetse midgut, while slender forms are not. Thus, SIF-dependent slender-to-stumpy differentiation limits maximum parasite density in the mammalian host and simultaneously modulates parasite preparation for survival in the next host, optimizing probability of transmission (23, 24).

Recent work has provided insight into slender-to-stumpy differentiation and its contribution to *T. brucei* disease progression and transmission. Previously, studies were limited by subjective parameters for distinguishing slender from stumpy-form parasites. MacGregor *et al.* (22) used a stumpy-specific marker, PAD (28) to conduct a quantitative analysis of trypanosome population dynamics during chronic infection in mice. They demonstrated that stumpy forms dominate the parasite population throughout late stages of infection. The quantitative nature of the approach enabled mathematical modeling, which provided overwhelming support for a quorum sensing mechanism. Moreover, the authors were able to make specific predictions for the cell types that produce SIF and define kinetic parameters for its production, activity and turnover. These data will facilitate efforts to identify the SIF molecule(s). Because SIF is produced only by a subset of cell types in the population, the system has the capacity to

make qualitative as well as quantitative assessments of population dynamics. Interestingly, the findings also have implications for immune evasion strategies employed by *T. brucei*, because stumpy forms do not undergo antigenic variation (29). Overall, the results emphasize the importance of parasite–parasite communication as a crucial element in disease progression and transmission.

Life on a surface and social motility in *T. brucei*

Most microbes are associated with surfaces in their natural environments and engage in surface-induced social behaviors, such as biofilm formation and various forms of social motility (6, 7, 9, 13, 14). These group activities facilitate surface colonization, defense and efficient use of nutrients (12, 14, 30). *T. brucei* is extracellular in both hosts and spends most of its lifecycle in direct contact with host tissue surfaces. Within the tsetse in particular, parasite movement across, and colonization of tissue surfaces are crucial for development and transmission (31-33). Currently, *T. brucei* is studied almost exclusively in suspension cultures and little is known about how life on a surface influences parasite behavior.

With bacteria and fungi, cultivation on semisolid agarose matrices has proven valuable for studies of social behavior (6, 13, 14). Oberholzer *et al.* thus employed semisolid agarose matrices to study surface behavior of procyclic-form (insect life cycle stage) *T. brucei* (1). They discovered a novel group behavior, termed social motility, in which parasites assembled into multicellular communities with emergent properties that are not evident in single cells. Initially, parasites collect into small groups that move *en masse* across the agarose surface and grow larger through recruitment of other cells

(Figure 2-2). At the periphery of the inoculation site, groups of parasites collect in nodes of high cell density and then advance outward, forming radial projections (Figure 2-3). The number and spacing of radial projections is generally consistent from one group to the next and patterns formed resemble those generated during surface colonization by swarming bacteria (13, 14). The events of *T. brucei* social motility occur in defined stages as summarized schematically in Figure 2-3A.

Several features of *T. brucei* social motility indicate cell–cell communication governs the behavior. First, coordination among individuals to enable group movement is striking, for example, in some cases, group movements occur only when other parasites are detected nearby, suggesting cell–cell communication within and between groups. Additionally, individual cells within each radial projection are highly motile and can freely move out and back from lateral edges, yet the group advances only at its leading edge. This indicates that polarized migration of the group is governed by parasites 'choosing' to move in a specific direction and suggests that parasite-derived signals may govern spacing of adjacent projections. In support of this idea, radial projections continue to advance unless they encounter a separate group of parasites, in which case movement is halted or diverted to avoid contact (Figure 2-3B). Adjacent projections alter their course in parallel, indicating that signaling between groups controls group movement. The zone of avoidance is a direct function of parasite number, suggesting that a diffusible substance(s) is responsible, as has been reported for swarming motility in bacteria (34, 35). Overall, the work demonstrates the capacity of protozoan parasites to engage in group activities and reveals a level of complexity and cooperativity to trypanosome behavior that was not previously recognized. The findings

also offer a convenient assay for studying environmental sensing in these organisms, which is an understudied problem.

The rest of this chapter details two approaches used to identify genes required for social behavior in *T. brucei*. The first method is a forward genetics screen using an RNA interference library created by the Paul Englund lab and the second is a targeted screen for cAMP effectors to investigate genes that regulate social motility. The preliminary results from each of these screens are discussed below.

Forward genetics using an RNA interference library

The laboratory of Paul Englund developed an RNA interference (RNAi) library using DNA from procyclic-form *T. brucei* strain 927 cells (36). A sonicator was used to shear the DNA into ~1 kilobase fragments, and using adaptor oligonucleotides, these fragments were inserted into a tetracycline-inducible RNAi vector (pZJMβ). The quality of the library was assessed by re-transforming *E. coli* with the pZJMβ library and 92% of plasmids contained inserts. Additionally, it is estimated that the library contains a 5-fold coverage of the entire genome and the insert can be identified using a nested-PCR strategy.

This pZJMβ RNAi library has had several successes in identifying novel regulators in a diverse multitude of functions in *T. brucei*. This library has revealed important genes for glycoprotein expression, tubericidin resistance, kinetoplast segregation, and mitochondrial membrane potential (36-39). These genes were all identified using a phenotypic assay to screen the RNAi mutant. Due to the number of

successes using this library, we attempted to use this library in conjunction with the social motility assay to identify key regulators in social motility in *T. brucei*.

A targeted approach to identify cyclic mononucleotide (cNMP) binding effectors in the cAMP pathway in *T. brucei*.

Mechanisms that regulate social behavior are diverse, however, all signaling pathways require the ability to sense, transduce and communicate signals to confer a response within the group. There are diverse classes of molecules that have been shown to regulate social behavior in other microbial systems such as acyl-homoserine lactones, nod factors, competence factors, Rho GTPases, Rac, and cyclic adenosine monophosphate (cAMP) (2, 40). For example, in bacteria, c-di-GMP regulates biofilm formation, swarming motility and adherence to tissue surfaces (14, 41, 42). cAMP also modulates fruiting body formation in the slime mold *Dictystelium discoidium*, demonstrating that although there is versatility of this class of molecules in regulating various functions of social behavior, the signaling mechanisms can be conserved between diverse organisms.

The eukaryotic flagellum (or cilia), including the *T. brucei* flagellum, has been implicated to be a major signaling center for sensation and transduction of extracellular signals (43-47). Components of the cAMP pathway have been previously been localized to the flagellum (48-51). The lab performed proteomics of the flagellum membrane in both procyclic-form and bloodstream-form *T. brucei* parasites (52, 53). In both proteomic preparations, components of the cAMP pathway were identified. The cAMP pathway is of interest because it is a major signaling molecule for diverse functions such

as cytokinesis, differentiation, and pathogenesis in *T. brucei* and could potentially function in cell-cell signaling as well (54, 55).

In brief, key players in the cAMP pathway include enzymes that make cAMP from adenosine monophosphate (AMP) called adenylate cyclases (ACs), enzymes that break down cAMP called phosphodiesterases (PDEs), and effector proteins that bind cAMP to generate a response (56). ACs are unique in *T. brucei* in that there exists a highly expanded family of approximately 60 members and have structures that architecturally resemble membrane-bound type I receptor guanalyl cyclases of mammalian systems (57). Trypanosomal ACs have a single transmembrane domain with a catalytic domain at the C-terminus and a variable extracellular N-terminal domain. Like the mammalian receptor guanalyl cyclases, these diverse and genetically expanded ACs may function as receptors for *T. brucei*. This hypothesis is supported by the identification of procyclic-form and bloodstream-form specific ACs (49, 50, 52). ESAG4 is specifically expressed in BSF parasites and functions in parasite viability as well as in modulating the host immune response (49, 50). On the other end of the cAMP pathway, PDEs in *T. brucei* have also been localized to the flagellum and function in parasite viability (48). The data hint at the importance of the cAMP pathway within a well-established signaling organelle of the parasite that potentially regulates cell-cell signaling.

Components of cAMP pathway (ACs and PDEs) were therefore investigated for their role in social motility in *T. brucei*. Dr. Miguel Lopez knocked down several ACs that were preferentially expressed in procyclic-stage *T. brucei* cells. He identified that knockdown of one specific AC, annotated as AC6, resulted in a “hypersocial” phenotype

in which an average of 14 projections were consistently formed in the AC6 knockdown mutants (Figure 2-8C). In addition, replacing one allele at the AC6 locus with an RNAi-immune wild-type copy of AC6 rescues the AC6 “hypersocial” phenotype while using a catalytically inactive mutant copy of AC6 does not rescue the “hypersocial” phenotype (Lopez et al, unplublished data). Dr. Michael Oberholzer discovered that knockdown of *T. brucei* phosphodiesterase B1 (PDEB1), however, results in no radial projection formation (Figure 2-8D). To supplement this finding, wild-type procylic-form *T. brucei* cells innoculated on semi-solid agarose in the presence of a phosphodiesterase inhibitor resulted in an absence of radial projections (Oberholzer et al, unpublished data). Together, these findings suggest that the cAMP pathway is required for social motility.

In mammalian sperm, several scaffolding proteins that anchor cAMP-binding effector proteins called protein kinase A (PKA) are localized to the fibrous sheath of mammalian sperm (58). In *T. brucei*, PKA is also localized to the flagellum, however, the *T. brucei* PKA is not regulated by cAMP and the functional role of *T. brucei* PKA has not yet been identified (59).

RESULTS

RNAi library screen to identify social motility mutants

A schematic of our strategy to screen the mutant library is shown in Figure 2-4. The heterogeneous pool of mutants from the pZJMβ RNAi library was grown to log

phase and the library was sorted in 96-well plates so that each well contained a single parasite. The cells were then clonally expanded over several weeks and frozen. These expanded plates were thawed and batches of these plates were tested using the social motility assay.

In an initial proof-of-concept to test the stringency of our format, a preliminary experiment using wild-type cells that exhibit 1-9 radial projections, “hyper-social” mutants that develop 10+ radial projections, and “SoMo (-)” mutants that do not form radial projections was done (Figure 2-5). These are mutants of the cAMP pathway and a description of these mutants will be discussed in the targeted approach. These mutants were mixed so that 25% of the population were wild-type cells, 25% were “hyper-social” and 50% were “SoMo (-)” cells. The heterogeneous population was induced with tetracycline for 3 days and sorted into 96-well plates. These plates were frozen and batches were clonally expanded to test using the social motility assay. This proof-of-concept pilot screened 72 clones and the results were as follows (Figure 2-5): 16% were had a wild-type phenotype (1-9 radial projections), 24% were “hyper-social” (10+ radial projections), and 35% were “SoMo (-)”. The percentages observed are close to expected ratios therefore this screening strategy was used for additional pilots with the RNAi mutant library.

In the first pilot screen, 196 clones were thawed but only 40% of cells survived the thawing process. Of the remaining 40%, none of the clones had social motility defects and all clonal lines had between 1-9 radial projections. One conclusion from this preliminary screen was that survival was too low. There are two major factors that could

have contributed to the low survival efficiency. One reason is that there could be lethal phenotypes associated with RNAi knockdown and these were not removed prior to screening. The second reason could be that cells were not frozen in logarithmic phase and therefore crashed upon thawing. To improve the low survival rate, we did a second pilot screen with modifications. We induced the heterogenous mutant library with tetracycline prior to sorting to eliminate cells with lethal RNAi effects. In addition, we consolidated only mutants that had normal growth rates at multiple steps and maintained cells at logarithmic phase before freezing. With these changes, 96 clones were screened for a second pilot. The survival after thawing clonal lines was improved from 40% in the first screen to 87% in the second screen. Although this screen also did not yield any clones with social motility defects, the high mortality rate and variability was vastly improved (Figure 2-6).

The *T. brucei* genome is about 10,000 genes and with fragments of approximate 660 bp, it was calculcated that at least 45,000 clones would need to be screened for a 90% probability of knocking down one specific gene. The next step was to make this screen high-throughput. In collaboration with the UCLA MSSR Facility, the use of robots could efficiently plate hundreds of clones at a time with respect to dilutions and plating. All clonal cells lines would be need to be plated at a certain dilution and differential dilutions is possible using robots at the UCLA MSSR Facility. In addition, these robots can also pipette a fixed aliquot of cells from hundreds of different cell lines. Unfortunately our assay format was not conducive to high-throughput screening. The use of the social motility assay relies on a macroscopic phenotype that requires a larger format than a read-out in a 96-well plate. Additionally, the assay conditions can vary

from plate to plate and experiments in triplicate are required to rule out false positives. At this stage in assay development, the social motility assay is far too variable and labor-intensive for productive high-throughput screening. To address this issue, time-lapse microscopy can be used to identify critical developmental changes in colony formation. This would allow for a microscopic or fluorescent-based assay for effective screening.

Targeted cAMP-binding effector screen

In an effort to expand the current study of how the cAMP pathway regulates social motility in *T. brucei*, putative cyclic nucleotide (cAMP or cGMP) binding proteins collectively called cNMP-binding proteins were identified using the Simple Modular Architecture Research Tool (SMART). Using the well-conserved "cNMP-binding motif" as the search parameter in the *T. brucei* genome, 10 putative cNMP-binding proteins were identified. Four additional proteins were identified using Pfam, a protein family database, and homology to closely related *Trypanosoma cruzi* cAMP binding motif. In total, 14 putative cNMP-binding proteins were identified and gene-specific knockdowns were performed in *T. brucei* (Figure 2-9). Unique DNA sequences for the open reading frame (ORF) of each of the 14 genes were generated and inserted by restriction sites into a tetracycline-inducible RNAi-knockdown vector (60). Knockdown of cNMP9 and 10 were previously generated by Jason Melehani and Dr. Michael Oberholzer, respectively. Each of these vectors containing gene-specific inserts were transfected into procyclic form *T. brucei* 29-13 cells. The cells were selected for using the drug phleomycin to create a heterogenous pool of knockdown mutants for each candidate gene. Each

heterogenous pool was then tested using the social motility assay (Figure 2-10). The assay was performed at least 7 times for each candidate and numbers of radial projections were assessed for each knockdown mutant. In addition, wild-type 29-13 cells, a phosphodiesterase (PDE) mutant, and an adenylate cyclase (AC) mutant were used as controls. Jason Melehani and Dr. Michael Oberholzer assessed cNMP9 and cNMP10 before this screen was performed. Clones of these cell lines were found to have normal social motility (data not shown). To ask if these heterogenous mutant pools were sufficiently knocked down, a few candidates were tested for gene-specific knockdown using a northern blot. Figure 2-11 demonstrates that even in the heterogenous mutant pools of cNMP2 and cNMP5, there was tetracycline-inducible RNA depletion.

Assessment of specific cNMP candidates

As illustrated in Figure 2-10, a few candidates had promising results. Knockdown of cNMP12 had no radial projections, however, upon closer investigation of the domain and homology of this protein to the *C. reinhardtii* genome, it was revealed that cNMP12 had homology to RSP11, a radial spoke protein with a cNMP-binding domain. Other promising candidates are cNMP2, cNMP3, and cNMP4 for a slightly higher number of radial projections in comparison to social motility of wild-type cells. In addition, cNMP4 has additional lipid-binding C2 domains that are of interest if this protein functions as part of a signaling pathway for transmembrane-bound ACs. The heterogenous pools of cNMP3 and cNMP4 were sub-cloned and each of these sub-clones were tested using the social motility assay (Figure 2-12A). Clones of cNMP3 had normal wild-type motility,

however, the clones of cNMP4 had a possible “hypersocial” phenotype with an average of 11 radial projections. Clone 4 had the most “hypersocial” phenotype and was assessed by qRT-PCR for the level of knockdown. In two independent experiments, clone 4 only had 35% knockdown (Figure 2-12B). In a preliminary experiment to compare the number of radial projections in tetracycline-induced mutants with uninduced conditions, knockdown of cNMP4 did not have increased number of radial projections in comparison to uninduced cells, however, the number of experiments done was not enough to be evaluated for statistical significance (data not shown).

Discussion

Two approaches were used to investigate signaling pathways required for social motility in *T. brucei*. In the first method, an unbiased screen was performed using a mutant library. Through a proof-of-concept screen and two preliminary screens, the approach was optimized. However, using the social-motility assay was not an efficient method for screening thousands of clones. More microscopic methods of screening are necessary and time-lapse microscopy can be used to identify essential elements of colony formation. In addition, if microscopic changes could be found and combined with a fluorescent-base assay, the optimized screen would be an efficient and comprehensive method to identify genes required for social motility.

In a combinatorial approach, the mutant library can be enriched prior to screening. The pZJMβ library can be plated on a large semi-solid agarose plate and

through enrichment of hyper-social mutants that migrate faster than the rest of the population (at the tips of the radial projections), it is possible pre-select for a small population of “hyper-social” mutants (Figure 2-7A). Similarly, “SoMo (-)” mutants that cannot form radial projections can be enriched through isolation of cells from the center of the colony and re-plating these isolates (Figure 2-7B). Furthermore, motility assays can be used to eliminate mutants with motility defects. These populations can be clonally expanded and screened using the aforementioned screening strategy.

In the second method, a more targeted and biased approach was used to identify cAMP effectors that potentially regulate social behavior. There were several promising when these candidates were knocked down and assessed using the social motility assay. The candidate cNMP12 was not considered for further investigation because it is most likely a radial spoke protein. Mutants of the core components of the axoneme, such as radial spoke proteins, typically have structural defects and these often result in immotility. The social motility defect observed in Figure 2-10 is therefore probably due to a general motility defect rather than social motility defect. Another candidate, cNMP4, seemed to have a “hypersocial” phenotype under tetracycline-induction. However, preliminary results were not significant and this putative cNMP candidate needs to be assessed using a better knockdown line as well as additional experiments in uninduced conditions.

Like the unbiased screening approach, an enrichment method can be also be used to find cAMP effectors. CpdA, a phosphodiesterase inhibitor, was used to demonstrate that in addition to gene knockdowns, biochemical inhibition can also be

used to inhibit social motility (unpublished data). If the RNAi mutant library was plated on semi-solid agarose supplemented with CpdA, mutants downstream of phosphodiesterase inhibition such as mutants of cAMP-binding would be able form radial projections. By plating enough cells, and multiple rounds of enrichment at the tips of the radial projections, it would be possible to identify cAMP effectors.

PKA exists as an inactive heterotetramer with two catalytic subunits attached to two regulatory subunits. Upon binding of cAMP to the regulatory subunits, the catalytic subunits are released and can subsequently be phosphorylated (56). In a closely related parasite, *T. cruzi*, PKA has been identified and the *T. cruzi* PKA regulates stage differentiation in the parasite (61, 62). Downstream effectors of the *T. cruzi* PKA has been identified and they include a variety of signaling molecules such as kinases, cAMP-specific phosphodiesterases, hexokinases, ATPases, and an aquaporin (62). The *T. brucei* PKA, however, binds cGMP rather than cAMP, therefore this *T. brucei* specific PKA may function differently from the conserved cAMP pathway (59).

Although PKA is one of the most common cAMP effectors, there are other cAMP-binding effectors that bind cAMP directly for downstream function. Such examples include ion channels, metabolic enzymes (lipases, phosphorylase kinases) and chemotactic receptors (63). The *T. brucei* cAMP signaling system may diverge from the conserved pathway through the use of unknown cAMP-binding proteins to transduce cAMP signals. Recently, cAMP effectors were identified in a genome-scale RNAi screen for resistance to the phosphodiesterase inhibitor, CpdA (55). In this study, the screen identified four cAMP Response Proteins (CARPs). CARP1 is kinetoplastid-specific and

has a predicted cyclic nucleotide binding-like domain whereas CARP2 and CARP3 are conserved hypothetical proteins that are found in the eukaryotic flagellar proteome or are associated with flagellar function. In our studies, CARP1 is cNMP1, a protein containing a putative cNMP-binding domain and was also found in a proteome of the *T. brucei* flagellum skeleton (unpublished data). The preliminary data from social motility assays of the heterogenous knockdown cell line of cNMP1, however, did not show a social motility defect (Figure 2-10). Although cAMP binding has not been experimentally verified for CARP1/cNMP1, the putative cNMP-binding domain hints at a possible role in cAMP signaling. Furthermore, since the function of CARP1/cNMP1 is still unknown, more in-depth analysis of this gene using clones with a high level of knockdown and assessing other CARPs may reveal a role for these genes in the regulation of social motility.

In summary, investigating the role of social behavior in *T. brucei* enhances our general understanding of social interactions in pathogenic protozoa, and more globally, cell-cell communication. As described above, ubiquitous mechanisms of sensing, communication and transduction within microbiology seem to be conserved in *T. brucei* and pivotal facets of these mechanisms can be examined using *T. brucei* as a model organism. Additionally, the social motility assay provides an excellent framework for interrogating other signaling pathways. In the near future, findings revealed by this approach may lead to parasite-specific signaling pathways that can be exploited for therapeutic intervention.

MATERIALS AND METHODS

Nomenclature and Gene ID

T. brucei Gene IDs are taken from TriTrypDB v.5 are as follows:

cNMP1: Tb927.11.16210, cNMP2: Tb927.11.2380, cNMP3: Tb927.11.2140, cNMP4: Tb927.10.5240, cNMP5: Tb927.1.1530, cNMP6: Tb927.7.4640, cNMP7: Tb927.7.2320, cNMP8: Tb927.8.2130, cNMP9: 927.3.5020, cNMP10: Tb927.11.4610, cNMP11: Tb927.11.15730, cNMP12: Tb427tmp.01.5260, cNMP13: Tb927.9.10890, cNMP14: Tb927.4.670.

Cell Lines and Culture Methods

T. brucei cells were grown in Cunningham's semi-defined medium (SM) supplemented with 10% heat-inactivated fetal calf serum (FCS) as previously described (64). Procyclic 29-13, a 427 strain that expresses T7 RNA polymerase and the tetracycline repressor, (60) were used as wild-type controls for all experiments and were maintained in SM medium supplemented with 10% FCS, 15 mg/mL G418 and 50 mg/mL hygromycin (64). Transfection and selection were done as previously described (64). Clonal lines were established through limiting dilution. The pZJMβ RNAi library was a kind gift from the Englund Lab and was maintained in SM medium supplemented with 10% FCS, 15 mg/mL G418, 50mg/mL hygromycin and 2.5 μg/mL phleomyclin.

pZJMβ RNAi Screening

The pZJMβ RNAi library was thawed and maintained in logarithmic phase (~5x10^6 cells/mL) for 3-5 days before sorting. In pilot #2, the library was induced with 1 μg/mL tetracycline before sorting. 100 μL pre-warmed SM media with 10% FCS, G418, hygromycin and phleomycin were added to ten 96-well plates then the pZJMβ RNAi was sorted into wells so that each well contained a single cell for a total of 960 wells at the Janis V. Giorgi Cytometry Core Facility (UCLA). Cells were passaged three times and healthy clones were consolidated into multiple 12-well plates. For pilot #2, an additional consolidation step was performed before cells were passaged. Each 12-well plate was thawed and the social motility assay was performed on 12 clones at a time.

Social Motility Assay

Cultivation on SM plates with 0.4% semi-solid agarose was performed as previously described (1). Growth of colonies was monitored up to 6 days using a Pentax Optio A30 point-and-shoot 10 megapixel camera.

Database Searches

Candidate cNMP-binding proteins were identified using the SMART database (65). A keyword search using the term “cNMP binding” was performed against the *T. brucei* genome to identify cNMP1-10. The Pfam database was used to find cNMP11-13 and cNMP14 was identified as an ortholog of the *T. cruzi* GAF-domain containing hypothetical protein, TcCLB.507053.90.

RNAi Cell Lines

RNAi plasmids were constructed in the p2T7^{Ti}B plasmid (66). Approximately 500 base pair fragments of each candidate cNMP ORF was selected using parameters described previously (67, 68) and designed using the RNAit algorithm as described in (69, 70). Primers used for each cNMP gene are listed as follows:

cNMP1 F: ATGGATCCCAGTGAATAATTGAAAGATGTGAAGCG

cNMP1 R: ATAAGCTTGGTGGCGAGAAAGAAGAGAAAAG

cNMP2 F: ATGGATCCAGGGTATTAACGCATATTTCAGG

cNMP2 R: ATAAGCTTTTTCCATGGATAACCTCAAGTG

cNMP3 F: ATGGATCCCAAATGAAGGGTTGTGGTTGTG

cNMP3 R: ATAAGCTTGTTCACCGTTGCACATTTTG

cNMP4 F: ATGGATCCCGTATGCATGACATCTCTTAAGTC

cNMP4 R: ATAAGCTTAACGCAGAGACGAAAGGAAA

cNMP5 F: ATGGATCCAATGGACGATATCGTATGACTTG

cNMP5 R: ATAAGCTTAATTTGCTTGGAACCTGCAT

cNMP6 F: ATGGATCCGATCGCCTCGCATAGGGTGTAG

cNMP6 R: ATAAGCTTCGGAGAGACCACAACACATCAG

cNMP7 F: ATGGATCCTACGCGATGTGTCACACTAACG

cNMP7 R: ATAAGCTTCGTCCGAAACAGGAGGTAAG

cNMP8 F: ATGGATCCGGCAAGCGCACCTCTTGATTG

cNMP8 R: ATAAGCTTCCACCCACACATATCCCAATTCC

cNMP11 F: ATGGATCCCTCAAGGGAAGCAGGACGG

cNMP11 R: ATAAGGCTTAGCACAGCGATGAGGAAAATAAG

cNMP 12 F: ATGGATCCAGCGCATCTGCAGCAGTTAAATAAG

cNMP12 R: ATAAGCTTAAGGTAAGGGCAACGTGGACATC

cNMP 13 F: ATGGATCCCAAGGCAGAACTTCGCCTTCG

cNMP13 R: ATAAGCTTGGGATGGGCGTCTATATCAAGAGC

cNMP 14 F: ATGGATCCGGCACCATGTAAACTATTCAAATATTTG

cNMP 14 R: ATAAGCTTAACATCCACAGCAGCCATAC

The amplicons were cloned into the p2T7^{Ti}B plasmid using cut sites *BamHI* and *HindIII* (underlined) and all DNA plasmids were verified by direct sequencing. Each plasmid was linearized with *NotI* and constructs containing gene-specific inserts were transfected into 29-13 cells. After 18-24 hours later, transfected cells were selected for using 2.5 μg/mL phleomyclin. RNAi was induced by adding 1 μg/mL tetracycline.

Northern Blots:

Total RNA was extracted from logarithmic phase cells using the Qiagen RNeasy Miniprep kit. Northern blots were performed on RNA samples (5ug/lane) for cNMP2, cNMP4, and cNMP5 knockdown cell lines as previously described in (71) except that

DIG-labeled probes (DIG Nucleic Acid Detection Kit, Roche) were used. Probes unique to each gene was used in accordance with manufacturer's instructions. Primers for probes are as follows:

cNMP2 F: CAAGGCAGAGGTTCTCAAGG, cNMP2 R: AACAACAATGGGACGAGGAG

cNMP4 F: TTGCACCGTCGTCACATTAT, cNMP4 R: CGTTTATGCTATCAAGCGCA

cNMP5 F: CAGTGCGGGTCTTTCTTCTC, cNMP5 R: CATTCCACGCAGTACATCCA

FIGURES

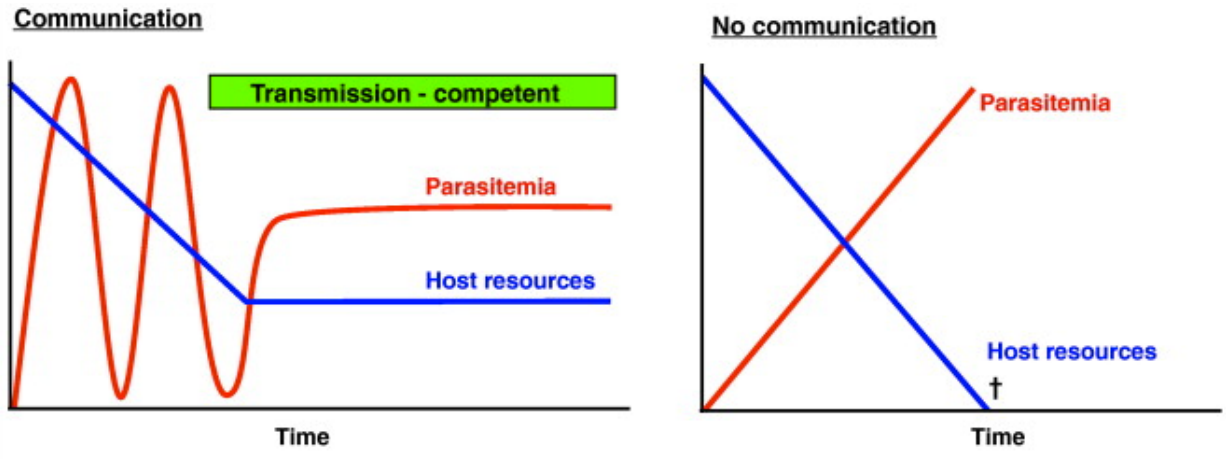


Figure 2-1. Cell–cell communication benefits *T. brucei*. Parasite–parasite communication (chart on left) via cell density-dependent signaling controls *T. brucei* differentiation from proliferating forms that are adapted for survival in the bloodstream to growth-arrested, transmission competent forms that are adapted for survival in the tsetse vector. By linking differentiation to population density, the parasite avoids depletion of host nutrients and prevents premature commitment to a developmental form that is not optimized for survival in the mammalian host. Without density-dependent cell–cell communication (chart on right), continued parasite proliferation would deplete host resources and thus reduce chances for transmission. Reprinted with permission from (72).

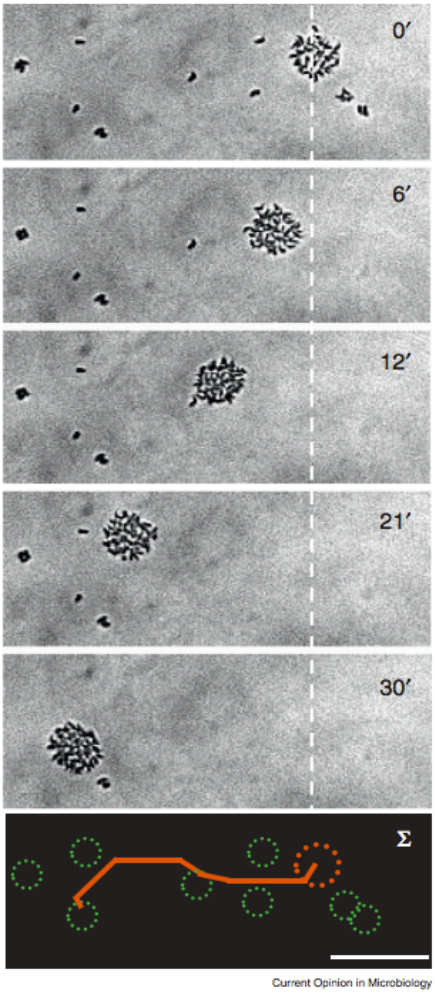


Figure 2-2. *T. brucei* social motility on a surface. *T. brucei* cells assemble into small groups that migrate *en masse* across the surface and enlarge through recruitment of other cells. Panels are time-lapse images showing movement of a group of parasites (top right of panel) across the surface of a semisolid agarose plate, with dashed white line indicating starting position of the group. Bottom panel shows summary. Elapsed time is indicated in minutes. Scale bar is 100 μm. Reprinted with permission from (72).

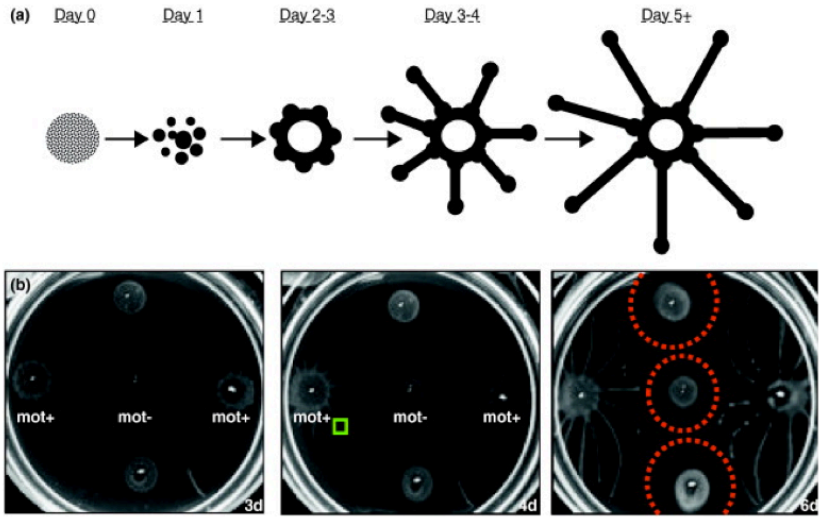


Figure 2-3. Social motility in *T. brucei*. When cultivated on semi-solid surfaces, *T. brucei* engages in complex social interactions that culminate in the formation of characteristic colony patterns. **(A)** Schematic diagram of the main steps of social motility in *T. brucei*, with parasites represented in black. Initially, individual parasites (Day 0) form small groups (Day 1). These groups move *en masse* across the surface and grow through recruitment of additional parasites. Groups assemble at the periphery of the inoculation site, concentrating in nodes (Days 2–3). From these nodes, parasites advance outward, forming radial projections (Days 3–5) that are regularly spaced and advance at the leading edge only (Days 5+). **(B)** Suspension cultures of wild type (mot +) or motility mutant (mot −) parasites were inoculated on semi-solid agarose and imaged at 3, 4 or 6 days (3 d, 4 d, 6 d) post inoculation. Social motility requires active parasite motility, as motility mutants (mot -) fail to undergo social motility. Projections can sense neighboring cells and halt or redirect their movements to avoid contact, resulting a zone of avoidance (dotted red circles in panel B6d). Reprinted with permission from (72).

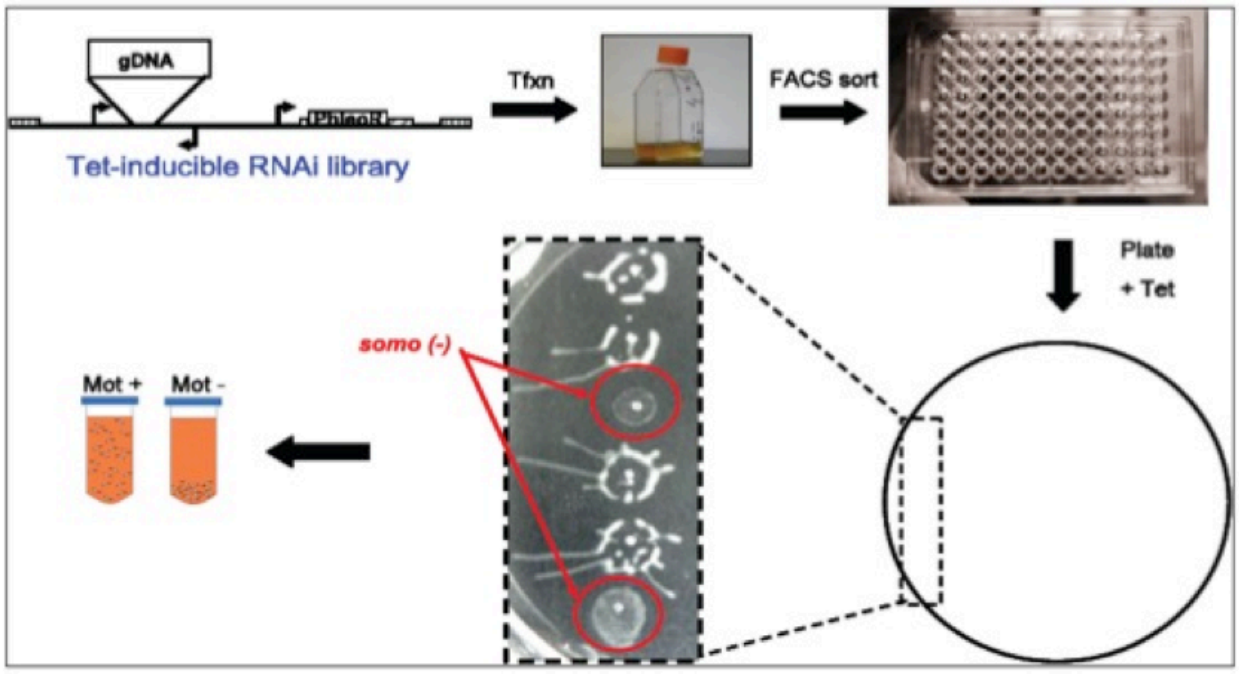


Figure 2-4. RNAi library screen to isolate social motility mutants. Trypanosomes have been transfected with an RNAi library to generate a heterogeneous population of mutants. The population is sorted to single cells in a 96-well plate format. In the second pilot, the population was induced with tetracycline for RNAi knockdown prior to sorting. Lethal or slow growing cells are eliminated and clonal RNAi lines are assayed for social motility. General motility mutants are expected to be recovered and these are distinguished from those specifically defective in social motility by assaying motility in suspension culture.

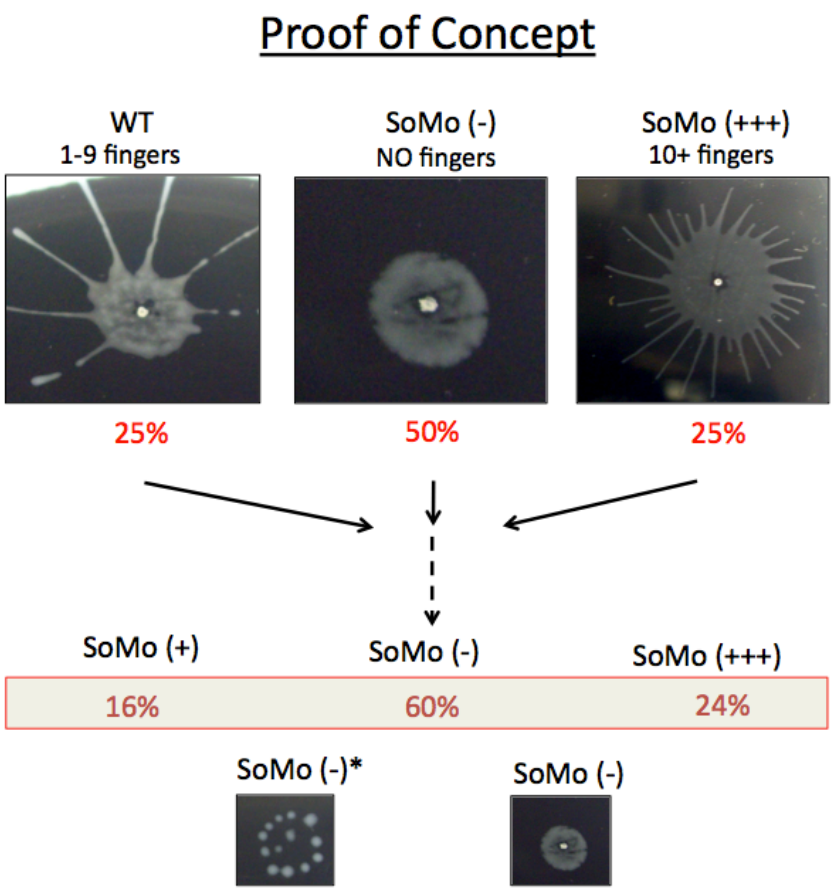


Figure 2-5. Proof of concept of the RNAi library screen for social motility genes. Wild-type procyclic cells that form 1-9 projections (fingers) when plated on semi-solid agarose was mixed with SoMo (-) mutants that do not generate projections, and "hyper-social" mutants (SoMo +++) that generate 10 or more projections were mixed at a 25%, 50%, and 25%, respectively. The screen was performed as illustrated in Figure 4. Observed phenotypes for wild-type, SoMo (-) and SoMo (+++) populations was 16%, 60%, and 24% respectively.

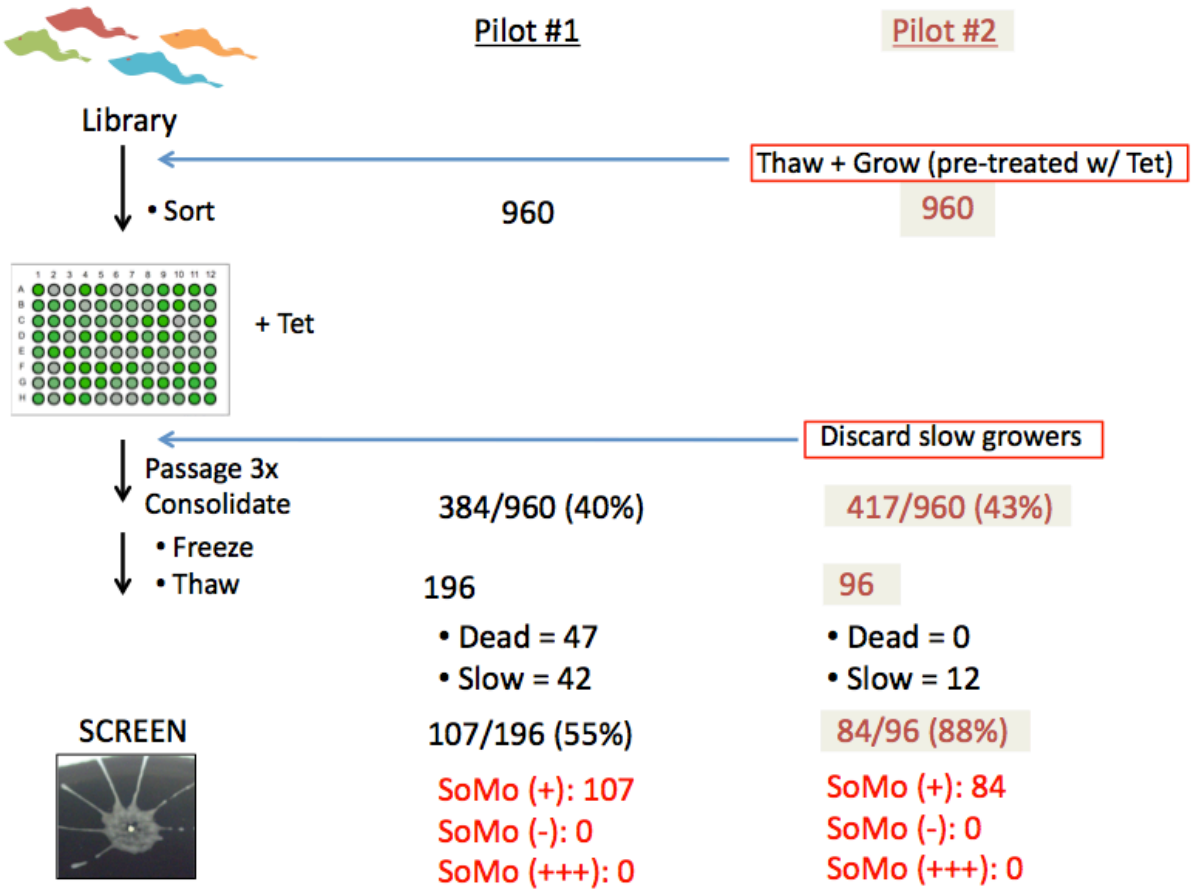


Figure 2-6. Pilots 1 and 2 of the RNAi library screen to identify social motility mutants. In Pilot #1 (middle column), the library was sorted to one cell per well and induced with tetracycline, passaged three times, consolidated, and frozen in 12-well plates. Of the 196 mutants thawed, 47 mutants could not be recovered and 42 had viability defects. 107 were screened and none had social motility defects (radial projections less than 1 or greater than 10). In pilot #2 (right column), cells were pre-treated with tetracycline and slow growers discarded to eliminate growth-related variability. 96 clonal lines were screened and 12 had viability defects. Of the 84 screened, no lines had social motility defects.

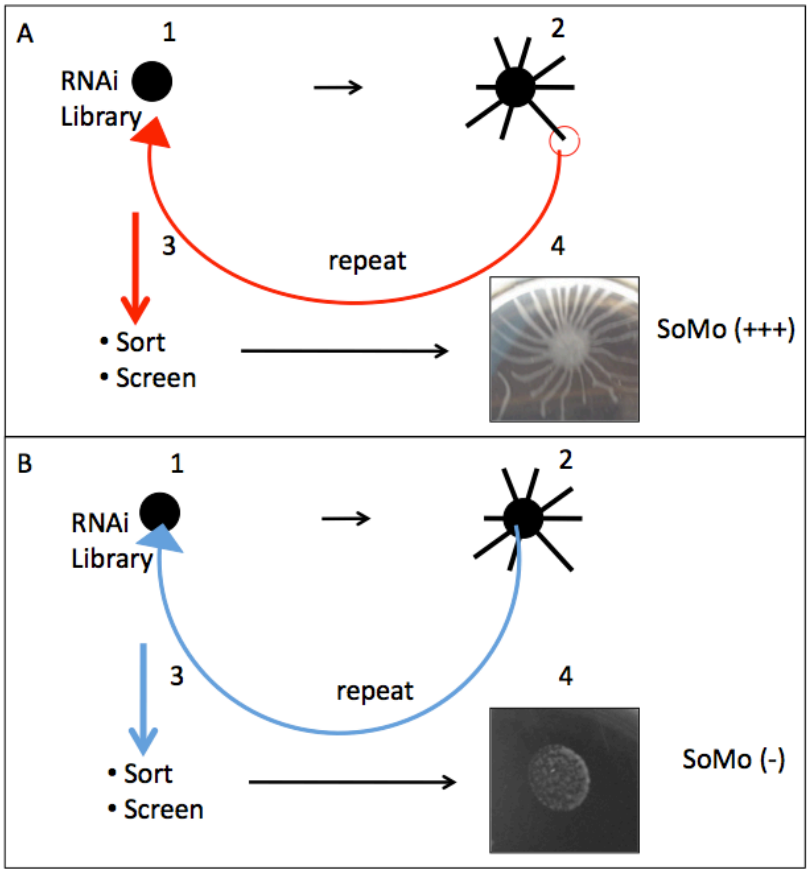


Figure 2-7. Enrichment screen for social motility mutants. (A) The RNAi library is plated on a semi-solid agarose plate (1) and permitted to form radial projections (2). The cells from the tips of the radial projections would be re-plated on semisolid agarose and after multiple rounds of re-plating, the pool of mutants would be sorted and screened (3) to find “hyper-social” mutants (4). (B) The same enrichment screen can be used to isolate SoMo (-) mutants from the center of the radial projections.

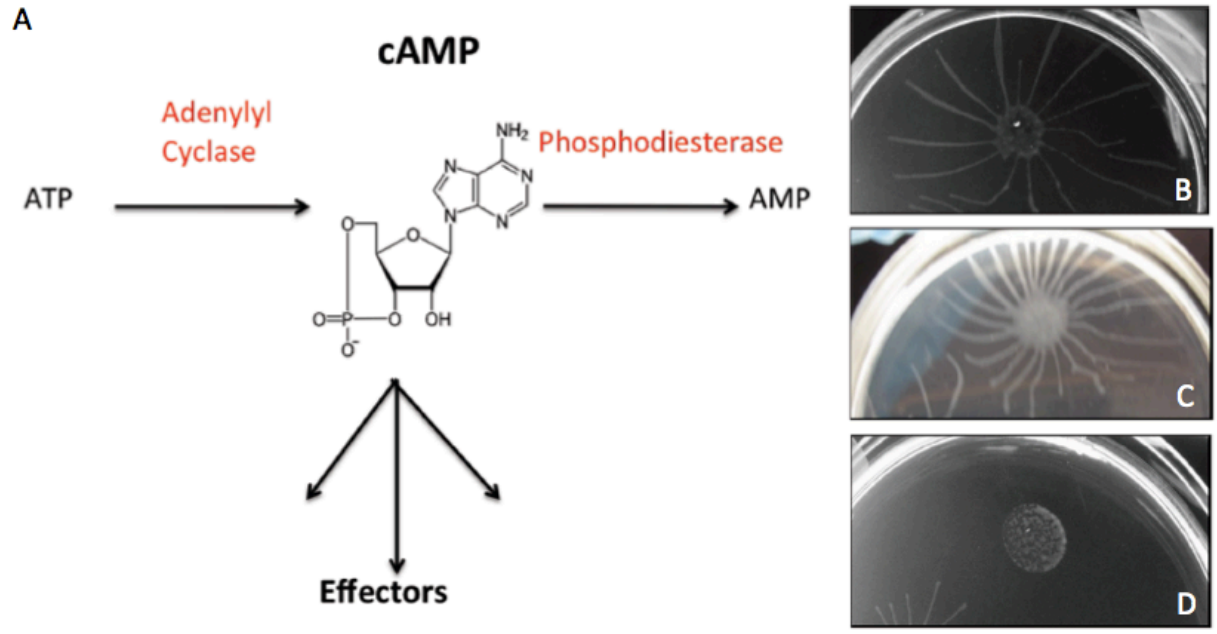


Figure 2-8. cAMP signaling is required for normal social motility. (A) A simplified diagram of the cyclic adenosine monophosphate (cAMP) pathway demonstrates how cAMP is generated and broken down by adenylyl cyclases and phosphodiesterases, respectively, to drive many signaling processes (effectors). (B) Wild-type procyclic 29-13 cells with a normal number of radial projections. (C) RNAi knockdown of an adenylyl cyclase results in “hyper-social” motility while (D) RNAi knockdown of a flagellar phosphodiesterase causes loss of radial projections. These results suggest that the cAMP pathway is a key component in regulating social behavior in *T. brucei*.

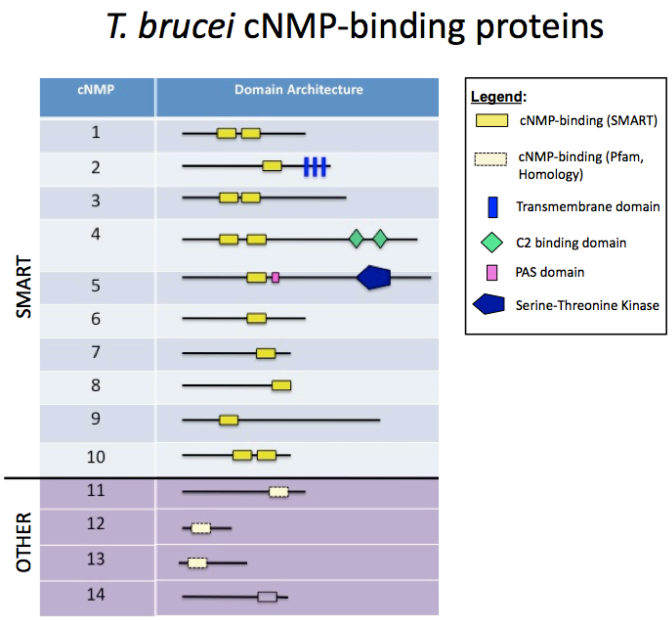


Figure 2-9. Candidate *T. brucei* cNMP-binding proteins. The SMART database was used to search the *T. brucei* genome for cNMP-binding proteins. The database identified 10 putative cNMP-binding proteins (cNMP 1-10) and homology searches as well as searching the Pfam database yielded 4 more cNMP-binding proteins (cNMP 11-14). Other domains such as transmembrane, C2-binding, PAS and serine-threonine kinase domains are illustrated.

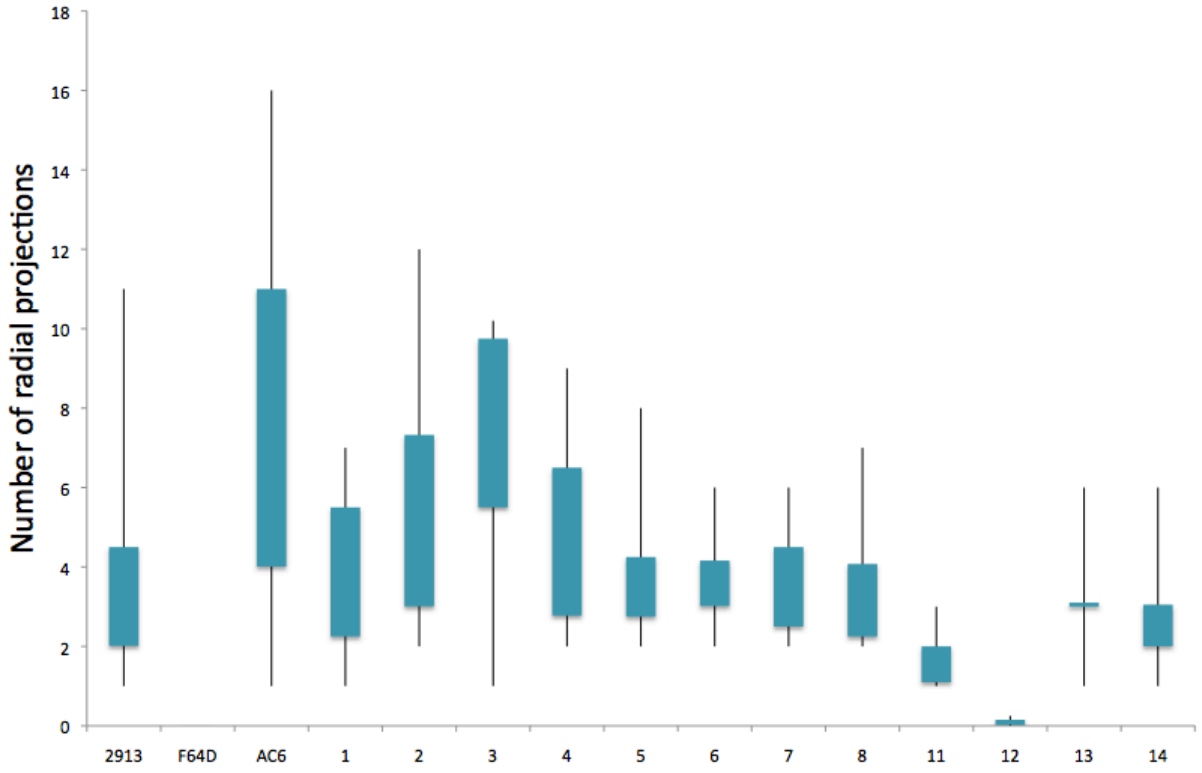


Figure 2-10. Social motility on candidate cNMP-binding proteins. The social motility assay was performed on heterogenous populations of each cNMP knockdown mutant and the number of radial projections was assessed. The social motility assay was also performed on wild-type (WT), the phosphodiesterase knockdown mutant (PDEB) and the adenylyl cyclase mutant (AC) as a control. Knockdowns of cNMP9 and cNMP10 were assessed previously by J. Melehani and M. Oberholzer and were found to have normal social motility.

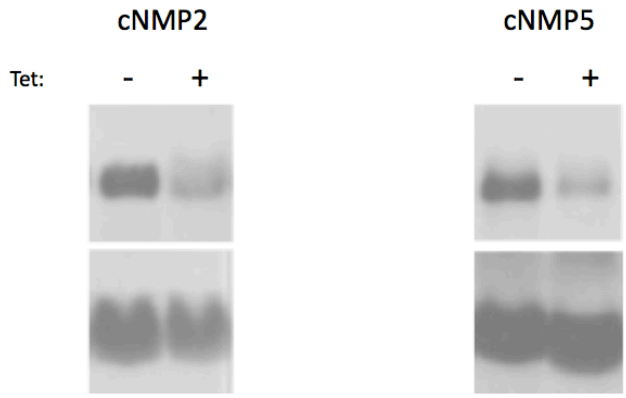


Figure 2-11. Individual cNMP mutants (heterogenous) have reduced mRNA levels. Mutant pools of cNMP2 and cNMP5 were induced with tetracycline for RNAi knockdown and a probe specific for cNMP2 and cNMP5 was used in combination with DIG-labeling to assess mRNA levels. In both panels, the mRNA levels in the heterogeneous pools were reduced (+ Tet lanes).

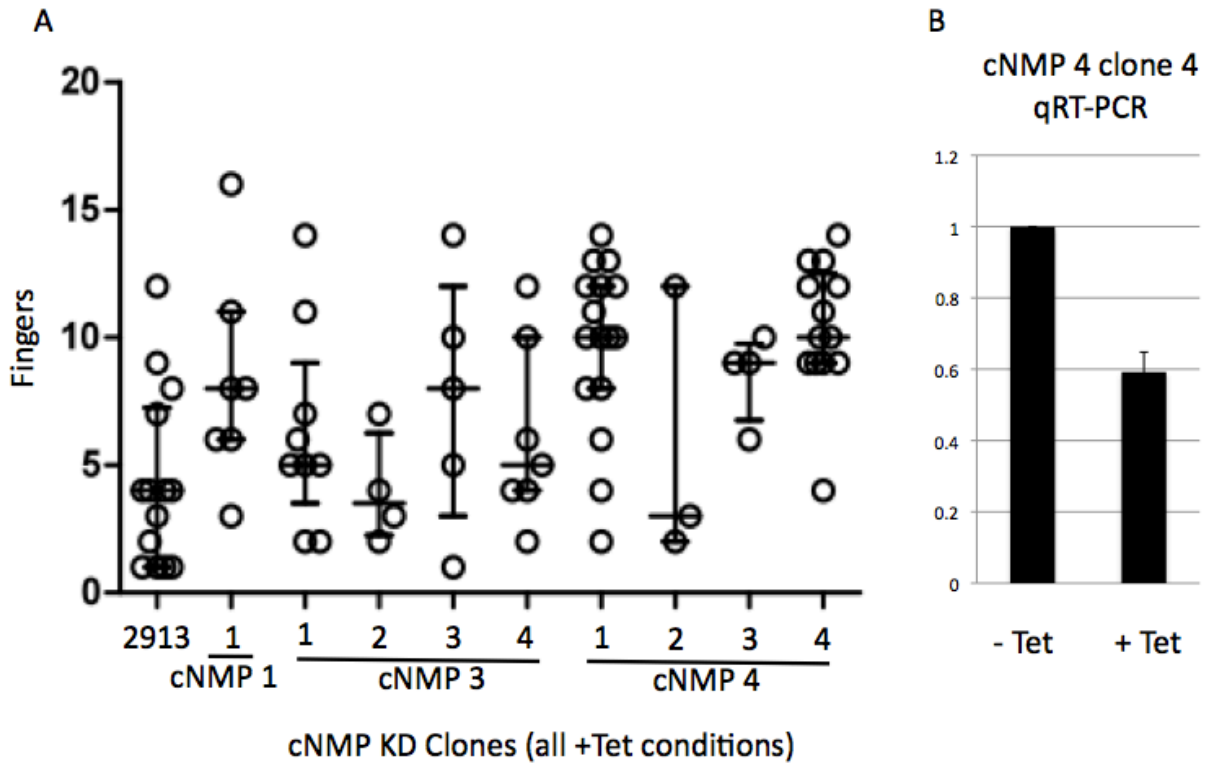


Figure 2-12. Social motility and knockdown of clones of cNMP3 and cNMP4. (A) Social motility was performed on clones of cNMP1, cNMP3 and cNMP4 under RNAi induced conditions. (B) Knockdown of cNMP4 clone 4 was quantitated by qRT-PCR and +Tet conditions show approximately 35% knockdown.

REFERENCES

1. Oberholzer, M., M. A. Lopez, B. T. McLelland, and K. L. Hill. 2010. Social motility in african trypanosomes. PLoS Pathog 6:e1000739.
2. Bassler, B., and R. Losick. 2006. Bacterially Speaking. Cell 125:237-246.
3. Shapiro, J. A. 1998. Thinking about bacterial populations as multicellular organisms. Annual Review of microbiology 52:81-104.
4. Parsek, M. R., and E. P. Greenberg. 2005. Sociomicrobiology: the connections between quorum sensing and biofilms. Trends Microbiol 13:27-33.
5. Nadell, C. D., J. B. Xavier, and K. R. Foster. 2009. The sociobiology of biofilms. FEMS Microbiol Rev 33:206-24.
6. Blankenship, J. R., and A. P. Mitchell. 2006. How to build a biofilm: a fungal perspective. Curr Opin Microbiol 9:588-94.
7. Shaulsky, G., and R. H. Kessin. 2007. The cold war of the social amoebae. Current Biology 17:R684-92.
8. Kearns, D. B. 2010. A field guide to bacterial swarming motility. Nat Rev Microbiol 8:634-44.
9. Velicer, G. J., and M. Vos. 2009. Sociobiology of the myxobacteria. Annu Rev Microbiol 63:599-623.
10. Kozubowski, L., and J. Heitman. 2012. Profiling a killer, the development of Cryptococcus neoformans. FEMS Microbiol Rev 36:78-94.

11. Calderone, R. A., and W. A. Fonzi. 2001. Virulence factors of Candida albicans. Trends Microbiol 9:327-35.
12. Butler, M. T., Q. Wang, and R. M. Harshey. 2010. Cell density and mobility protect swarming bacteria against antibiotics. Proc Natl Acad Sci U S A 107:3776-81.
13. Harshey, R. M. 2003. Bacterial motility on a surface: many ways to a common goal. Annu Rev Microbiol 57:249-73.
14. Verstraeten, N., K. Braeken, B. Debkumari, M. Fauvart, J. Fransaer, J. Vermant, and J. Michiels. 2008. Living on a surface: swarming and biofilm formation. Trends Microbiol 16:496-506.
15. Firtel, R. A., and R. Meili. 2000. Dictyostelium: a model for regulated cell movement during morphogenesis. Curr Opin Genet Dev 10:421-7.
16. Kaiser, D. 2003. Coupling cell movement to multicellular development in myxobacteria. Nat Rev Microbiol 1:45-54.
17. Decho, A. W., R. S. Norman, and P. T. Visscher. 2010. Quorum sensing in natural environments: emerging views from microbial mats. Trends Microbiol 18:73-80.
18. Fraser, G. M., and C. Hughes. 1999. Swarming motility. Curr Opin Microbiol 2:630-5.
19. Pacheco, A. R., and V. Sperandio. 2009. Inter-kingdom signaling: chemical language between bacteria and host. Curr Opin Microbiol 12:192-8.
20. Ramage, G., S. P. Saville, D. P. Thomas, and J. L. Lopez-Ribot. 2005. Candida biofilms: an update. Eukaryot Cell 4:633-8.

21. Verstrepen, K. J., and G. R. Fink. 2009. Genetic and epigenetic mechanisms underlying cell-surface variability in protozoa and fungi. Annual Review of Genetics 43:1-24.

22. MacGregor, P., N. J. Savill, D. Hall, and K. R. Matthews. 2011. Transmission stages dominate trypanosome within-host dynamics during chronic infections. Cell Host Microbe 9:310-8.

23. Pollitt, L. C., P. MacGregor, K. Matthews, and S. E. Reece. 2011. Malaria and trypanosome transmission: different parasites, same rules? Trends Parasitol 27:197-203.

24. Matthews, K. R. 2011. Controlling and coordinating development in vector-transmitted parasites. Science 331:1149-53.

25. Vassella, E., B. Reuner, B. Yutzy, and M. Boshart. 1997. Differentiation of African trypanosomes is controlled by a density sensing mechanism which signals cell cycle arrest via the cAMP pathway. J Cell Sci 110 (Pt 21):2661-71.

26. Matthews, K. R. 2005. The developmental cell biology of Trypanosoma brucei. J Cell Sci 118:283-90.

27. Matthews, K. R., J. R. Ellis, and A. Paterou. 2004. Molecular regulation of the life cycle of African trypanosomes. Trends Parasitol 20:40-7.

28. Dean, S., R. Marchetti, K. Kirk, and K. R. Matthews. 2009. A surface transporter family conveys the trypanosome differentiation signal. Nature 459:213-7.

29. Vickerman, K. 1985. Developmental cycles and biology of pathogenic trypanosomes. Br Med Bull 41:105-14.

30. Kaiser, D. 2007. Bacterial swarming: a re-examination of cell-movement patterns. Curr Biol 17:R561-70.

31. Roditi, I., and M. J. Lehane. 2008. Interactions between trypanosomes and tsetse flies. Curr Opin Microbiol 11:345-51.

32. Sharma, R., E. Gluenz, L. Peacock, W. Gibson, K. Gull, and M. Carrington. 2009. The heart of darkness: growth and form of Trypanosoma brucei in the tsetse fly. Trends Parasitol 25:517-24.

33. Vickerman, K., L. Tetley, K. A. Hendry, and C. M. Turner. 1988. Biology of African trypanosomes in the tsetse fly. Biol Cell 64:109-19.

34. Be'er, A., H. P. Zhang, E. L. Florin, S. M. Payne, E. Ben-Jacob, and H. L. Swinney. 2009. Deadly competition between sibling bacterial colonies. Proc Natl Acad Sci U S A 106:428-33.

35. Caiazza, N. C., R. M. Shanks, and G. A. O'Toole. 2005. Rhamnolipids modulate swarming motility patterns of Pseudomonas aeruginosa. J Bacteriol 187:7351-61.

36. Morris, J. C., Z. Wang, M. E. Drew, and P. T. Englund. 2002. Glycolysis modulates trypanosome glycoprotein expression as revealed by an RNAi library. Embo J 21:4429-38.

37. Drew, M. E., J. C. Morris, Z. Wang, L. Wells, M. Sanchez, S. M. Landfear, and P. T. Englund. 2003. The adenosine analog tubercidin inhibits glycolysis in Trypanosoma brucei as revealed by an RNA interference library. J Biol Chem 278:46596-600.

38. Zhao, Z., M. E. Lindsay, A. Roy Chowdhury, D. R. Robinson, and P. T. Englund. 2008. p166, a link between the trypanosome mitochondrial DNA and flagellum, mediates genome segregation. Embo J 27:143-54.

39. Verner, Z., Z. Paris, and J. Lukes. 2010. Mitochondrial membrane potential-based genome-wide RNAi screen of Trypanosoma brucei. Parasitol Res 106:1241-4.

40. Vedula, S. R., A. Ravasio, C. T. Lim, and B. Ladoux. 2013. Collective cell migration: a mechanistic perspective. Physiology (Bethesda) 28:370-9.

41. Ferreira, R. B., L. C. Antunes, E. P. Greenberg, and L. L. McCarter. 2008. Vibrio parahaemolyticus ScrC modulates cyclic dimeric GMP regulation of gene expression relevant to growth on surfaces. J Bacteriol 190:851-60.

42. Borlee, B. R., A. D. Goldman, K. Murakami, R. Samudrala, D. J. Wozniak, and M. R. Parsek. 2010. Pseudomonas aeruginosa uses a cyclic-di-GMP-regulated adhesin to reinforce the biofilm extracellular matrix. Mol Microbiol 75:827-42.

43. Berbari, N. F., A. K. O'Connor, C. J. Haycraft, and B. K. Yoder. 2009. The primary cilium as a complex signaling center. Current Biology 19:R526-35.

44. Satir, P., and S. T. Christensen. 2007. Overview of structure and function of mammalian cilia. Annu Rev Physiol 69:377-400.

45. Corbit, K. C., P. Aanstad, V. Singla, A. R. Norman, D. Y. Stainier, and J. F. Reiter. 2005. Vertebrate Smoothened functions at the primary cilium. Nature 437:1018-21.

46. Bloodgood, R. A. 2010. Sensory reception is an attribute of both primary cilia and motile cilia. Journal of cell science 123:505-9.

47. Satir, P., D. R. Mitchell, and G. Jekely. 2008. How did the cilium evolve? Curr Top Dev Biol 85:63-82.

48. Oberholzer, M., G. Marti, M. Baresic, S. Kunz, A. Hemphill, and T. Seebeck. 2007. The Trypanosoma brucei cAMP phosphodiesterases TbrPDEB1 and TbrPDEB2: flagellar enzymes that are essential for parasite virulence. Faseb J 21:720-31.

49. Salmon, D., S. Bachmaier, C. Krumbholz, M. Kador, J. A. Gossmann, P. Uzureau, E. Pays, and M. Boshart. 2012. Cytokinesis of Trypanosoma brucei bloodstream forms depends on expression of adenylyl cyclases of the ESAG4 or ESAG4-like subfamily. Mol Microbiol 84:225-42.

50. Salmon, D., G. Vanwalleghem, Y. Morias, J. Denoeud, C. Krumbholz, F. Lhomme, S. Bachmaier, M. Kador, J. Gossmann, F. B. Dias, G. De Muylder, P. Uzureau, S. Magez, M. Moser, P. De Baetselier, J. Van Den Abbeele, A. Beschin, M. Boshart, and E. Pays. 2012. Adenylate cyclases of Trypanosoma brucei inhibit the innate immune response of the host. Science 337:463-6.

51. Paindavoine, P., S. Rolin, S. Van Assel, M. Geuskens, J. C. Jauniaux, C. Dinsart, G. Huet, and E. Pays. 1992. A gene from the variant surface glycoprotein expression site encodes one of several transmembrane adenylate cyclases located on the flagellum of Trypanosoma brucei. Mol Cell Biol 12:1218-25.

52. Saada, E. A., Z. P. Kabututu, M. Lopez, M. M. Shimogawa, G. Langousis, M. Oberholzer, A. Riestra, Z. Jonsson, J. A. Wohlschlegel, and K. L. Hill. 2014. Insect stage-specific receptor adenylate cyclases are localized to distinct subdomains of the Trypanosoma brucei flagellar membrane. Eukaryot Cell.

53. Oberholzer, M., G. Langousis, H. T. Nguyen, E. A. Saada, M. M. Shimogawa, Z. O. Jonsson, S. M. Nguyen, J. A. Wohlschlegel, and K. L. Hill. 2011. Independent analysis of the flagellum surface and matrix proteomes provides insight into flagellum signaling in mammalian-infectious Trypanosoma brucei. Mol Cell Proteomics 10:M111 010538.

54. Laxman, S., and J. A. Beavo. 2007. Cyclic nucleotide signaling mechanisms in trypanosomes: possible targets for therapeutic agents. Mol Interv 7:203-15.

55. Gould, M. K., S. Bachmaier, J. A. Ali, S. Alsford, D. N. Tagoe, J. C. Munday, A. C. Schnaufer, D. Horn, M. Boshart, and H. P. de Koning. 2013. Cyclic AMP effectors in African trypanosomes revealed by genome-scale RNA interference library screening for resistance to the phosphodiesterase inhibitor CpdA. Antimicrob Agents Chemother 57:4882-93.

56. Lefkimmiatis, K., and M. Zaccolo. 2014. cAMP signaling in subcellular compartments. Pharmacol Ther.

57. Ginger, M. L., E. S. Ngazoa, C. A. Pereira, T. J. Pullen, M. Kabiri, K. Becker, K. Gull, and D. Steverding. 2005. Intracellular positioning of isoforms explains an unusually large adenylate kinase gene family in the parasite Trypanosoma brucei. J Biol Chem 280:11781-9.

58. Cao, W., G. L. Gerton, and S. B. Moss. 2006. Proteomic profiling of accessory structures from the mouse sperm flagellum. Mol Cell Proteomics 5:801-10.

59. Shalaby, T., M. Liniger, and T. Seebeck. 2001. The regulatory subunit of a cGMP-regulated protein kinase A of Trypanosoma brucei. European Journal of Biochemistry 268:6197-206.

60. Wirtz, E., S. Leal, C. Ochatt, and G. A. Cross. 1999. A tightly regulated inducible expression system for conditional gene knock-outs and dominant-negative genetics in *Trypanosoma brucei*. Mol. Biochem. Parasitol. 99:89-101.

61. Gonzales-Perdomo, M., P. Romero, and S. Goldenberg. 1988. Cyclic AMP and adenylate cyclase activators stimulate Trypanosoma cruzi differentiation. Exp Parasitol 66:205-12.

62. Bao, Y., L. M. Weiss, V. L. Braunstein, and H. Huang. 2008. Role of protein kinase A in Trypanosoma cruzi. Infect Immun 76:4757-63.

63. Seebeck, T., K. Gong, S. Kunz, R. Schaub, T. Shalaby, and R. Zoraghi. 2001. cAMP signalling in Trypanosoma brucei. International Journal for Parasitology 31:491-8.

64. Oberholzer, M., M. A. Lopez, K. S. Ralston, and K. L. Hill. 2009. Approaches for functional analysis of flagellar proteins in African trypanosomes. Methods in Cell Biology 93:21-57.

65. Schultz, J., F. Milpetz, P. Bork, and C. P. Ponting. 1998. SMART, a simple modular architecture research tool: identification of signaling domains. Proc Natl Acad Sci U S A 95:5857-64.

66. LaCount, D. J., S. Bruse, K. L. Hill, and J. E. Donelson. 2000. Double-stranded RNA interference in *Trypanosoma brucei* using head-to-head promoters. Mol. Biochem. Parasitol. 111:67-76.

67. Benz, C., D. Nilsson, B. Andersson, C. Clayton, and D. L. Guilbride. 2005. Messenger RNA processing sites in Trypanosoma brucei. Mol Biochem Parasitol 143:125-34.

68. Rusconi, F., M. Durand-Dubief, and P. Bastin. 2005. Functional complementation of RNA interference mutants in trypanosomes. BMC Biotechnology 5:6.

69. Redmond, S., J. Vadivelu, and M. C. Field. 2003. RNAit: an automated web-based tool for the selection of RNAi targets in Trypanosoma brucei. Mol Biochem Parasitol 128:115-8.

70. Ralston, K. S., N. K. Kisalu, and K. L. Hill. 2011. Structure-function analysis of dynein light chain 1 identifies viable motility mutants in bloodstream-form Trypanosoma brucei. Eukaryot Cell 10:884-94.

71. Merchant, S., and L. Bogorad. 1986. Regulation by copper of the expression of plastocyanin and cytochrome c552 in Chlamydomonas reinhardi. Mol Cell Biol 6:462-9.

72. Lopez, M. A., H. T. Nguyen, M. Oberholzer, and K. L. Hill. 2011. Social parasites. Curr Opin Microbiol 14:642-8.

Chapter 3

CMF22 is Required for Propulsive Motility in *T. brucei*.

Motility in *T. brucei* is driven by a single flagellum that is attached along the length of the cell body. Chapter 3 focuses on a protein that was identified in an *in silico* screen to be well conserved in diverse eukaryotes with motile flagella [18]. This chapter entitled, “CMF22 is required for propulsive motility in *T. brucei*” is my first-author publication and was published in *Eukaryotic Cell.* It was written by myself, Jaspreet Sandhu, Gerasimos Langousis, and Kent L. Hill. Experiments for this publication were done by Jaspreet Sandhu and myself. Phylogenetic comparisons were performed by Gerasimos Langousis.

INTRODUCTION

The flagellum (also called cilium) is a prominent eukaryotic organelle that functions in motility, environmental sensing, adhesion and mating (1, 2). In humans, flagellar motility is essential for normal development and physiology (3). Defective motility, due to flagellar paralysis or dysregulated beating, results in a variety of diseases including primary ciliary dyskinesia, *situs inversus*, hydrocephalus, respiratory malfunction and male factor infertility (4). In addition, motile flagella provide the primary mode of locomotion for many pathogenic protozoa, including *Trypanosoma spp.*, *Leishmania spp.*, *Giardia lamblia*, and *Trichomonas vaginalis*, which cause immense morbidity throughout the developing world (5-7). For example, *Trypanosoma brucei spp.* depend on a motile flagellum to complete their lifecycle, enabling infections of humans and livestock that result in significant loss of life and economic hardship in sub-Saharan

Africa (8, 9). Therefore, the motile flagellum is a critical component in a range of heritable and infectious diseases.

Flagella are present in all major eukaryotic groups and are built upon a microtubule axoneme that may be motile or non-motile (10-12). Motile flagella exhibit structural elaborations that are not seen in immotile flagella and in most organisms share a canonical “9+2” axoneme structure, which consists of nine outer doublet microtubules arranged symmetrically around a pair of singlet microtubules. Outer doublets provide a scaffold for assembly of dynein motors and regulatory complexes, with adjacent doublets connected via nexin links. Projections extending outward from each of the central pair microtubules form a sheath-like structure that envelopes the central pair (13). Radial spokes extend inward from each outer doublet microtubule and terminate adjacent to the sheath of the central pair microtubules. Recent cryoelectron tomography studies have defined additional axonemal substructures, such as microtubule inner proteins (14) and novel interdoublet linkages (15). Structural variations are present in some organisms, but the general architecture of the 9+2 axoneme described above is conserved across broad evolutionary distances, consistent with the idea that the last eukaryotic common ancestor had a motile axoneme (16).

Because of the importance of flagellum motility to human health and disease, there is great interest in identifying essential functional and structural components of these organelles, as these represent candidate disease genes and/or therapeutic targets. Moreover, such efforts offer insight into flagellum biology and motility

mechanisms by defining fundamental building blocks needed for assembly and operation of motile axonemes. The deep evolutionary origins of the eukaryotic axoneme, together with availability of complete genome sequences from many divergent eukaryotes, has made it possible to identify candidate motility genes based on phylogenetic distribution (17-20). These approaches take advantage of the fact that proteins crucial for axoneme motility are conserved in most organisms with motile flagella, but are absent in organisms that lack motile flagella. Proteins identified may be conserved across diverse taxa or may represent lineage-specific elaborations, depending upon how the analysis is developed (21). As with any genomic approach, direct analyses of resultant candidates must then be conducted to interrogate the predicted role in axoneme motility.

Previously, we performed an *in silico* screen to identify genes that are broadly conserved in organisms with motile flagella and absent in organisms that lack a motile flagellum (19). We identified a cohort of fifty genes postulated to serve as core Components of Motile Flagella (CMF), i.e. having axonemal motility functions conserved across diverse taxa. Several CMF genes encode proteins with known or implicated functions in axoneme motility through independent studies. These include subunits of the nexin-dynein regulatory complex (trypanin, CMF44, CMF46, CMF70) (22-26), protofilament ribbon proteins (CMF2, CMF3, CMF4, CMF19) (27-29), dynein subunits (CMF39, CMF73) (30, 31) and the trypanosome orthologue of the “move backwards only 2”, MBO-2, gene product (CMF8) (32, 33). However, a large number of CMF proteins have not yet been subjected to direct, in-depth analysis. Among the cohort of

CMF proteins, CMF22 piqued our interest because its amino acid sequence contains IQ and AAA sequence motifs, which have potential to confer regulatory roles via Ca^{2+} and nucleotide signaling, respectively (34, 35). Each of these is of interest in the context of flagellum function, because calcium ions and nucleotides both function in regulation of flagellum beating (36, 37). Here we report in-depth analysis of CMF22 in the African trypanosome *T. brucei*, which has emerged as a powerful experimental system for functional analysis of flagellar proteins (38). We employ expanded phylogenetic analysis, together with biochemical and gene knockdown approaches to demonstrate that CMF22 is an axonemal protein required for regulation of flagellar beating.

RESULTS

The original identification of CMF genes surveyed ten organisms and represented a limited number of eukaryotic clades (19). We therefore expanded our analysis with CMF22 to include 115 organisms and incorporate representatives from each of the five major clades that encompass most eukaryotic diversity (39, 40). Within this set, we included members of the chromalveolate and rhizaria clades that were not represented previously. Using reciprocal best BLAST, we identified CMF22 orthologues in 85 out of 86 organisms with motile flagella, 0 out of 4 with only immotile flagella and 3 out of 25 with no flagella (Table 3-1). Notably, a CMF22 orthologue was identified in representatives from all five clades for which there is a complete genome sequence of a ciliated organism available (Fig 3-1A). Together, these results indicate that CMF22 was likely present in the last eukaryotic common ancestor and are consistent with a central role for CMF22 in axonemal motility.

Analysis of the CMF22 primary amino acid sequence revealed the presence of sequence motifs with the potential for regulatory input/output, namely an IQ motif near the N-terminus and an ATPase Associated with a variety of cellular Activities (AAA) motif near the C-terminus (Fig 3-1B). The presence and position of the IQ and AAA domains are conserved in CMF22 orthologues from diverse organisms (Fig 3-1B), supporting a requirement for these sequence motifs for CMF22 function. Although the SMART predicting algorithm detected a weak hit for the IQ motif in the *Bigelowiella natans* orthologue, individual alignment shows that all the conserved residues (IQxxxRGxxxR) are present (data not shown). The combined phylogenetic distribution and domain structure of CMF22 support a role in axonemal motility, with potential for regulatory function. We therefore investigated this idea directly through biochemical and functional analysis of the CMF22 protein in *T. brucei*.

CMF22 is an axonemal protein

To determine the location of CMF22, we utilized *in situ* tagging (41) to place a 3xHA epitope at the protein's C-terminus. Anti-HA antibodies specifically recognized a single protein of approximately 110 kDa in total cell lysates from the CMF22-HA tagged cell line (Figure 3-2A, 3-2B). This size is consistent with the size predicted for the CMF22 protein (102 kDa). To determine if CMF22-HA is associated with the flagellum, cells were extracted with detergent to separate detergent-soluble proteins (S1) from insoluble cytoskeletons (P1). Cytoskeletons were further extracted with 0.5 M NaCl to solubilize the subpellicular cytoskeleton (S2), leaving an insoluble flagellum skeleton

(P2) that includes the axoneme, paraflagellar rod (PFR), basal body and flagellum attachment zone (FAZ) (42). The entire cellular pool of CMF22 fractionated with the axonemal marker trypanin in the flagellum skeleton fraction, even when using high salt extraction (1M NaCl) (Fig 3-2B). Notably, these high-salt extraction conditions solubilize most outer arm dyneins as well as much of the central pair apparatus and portions of the PFR (38).

The biochemical fractionation pattern observed for CMF22 is consistent with an axonemal protein, but would also be observed for protein components of the basal body, PFR or FAZ. To distinguish between these possibilities, we used immunofluorescence to examine the distribution of CMF22 in the cell. CMF22-HA was found to be distributed along the entire length of the flagellum (Figure 3-3) and clearly distinct from the basal body (Figure 3-S1). CMF22-HA staining was adjacent to, but not coincident with, PFR staining along most of the flagellum (Figure 3-3A-D, I). Moreover, at the proximal end of the flagellum, where the flagellum emerges from the cell body, CMF22-HA staining extended beyond the end of the PFR and nearly all the way to the kinetoplast (Figure 3-3J, open arrowheads). Thus, CMF22 is not part of the PFR. At the distal end of the flagellum, CMF22-HA extended all the way to the flagellum tip, beyond the cell body (Figure 3-3A-D, filled arrowhead, I), demonstrating CMF22 is not part of the FAZ, which stops at the end of the cell body (43). Finally, CMF22-HA overlapped and was interspersed with the axonemal marker trypanin along the entire length of the flagellum, including the proximal end of the axoneme (Figure 3-3H, K, L, Figure 3-4). This staining pattern differs from the side-by-side staining pattern observed for CMF22

and PFR. A similar pattern was also observed in dividing cells where the newly forming flagellum is seen posterior to the old flagellum (Figure 3-4). Therefore, the combined biochemical, immunofluorescence and phylogenetic data demonstrate that CMF22 is an axonemal protein.

CMF22 is required for propulsive motility

To investigate CMF22 function, we used tetracycline (Tet)-inducible RNAi to target the CMF22 3'UTR, so as to allow subsequent rescue experiments (see below) (44, 45). Northern blots using RNA from CMF22-UTR-knockdown parasites, hereafter referred to as "CMF22-UKD", showed a single CMF22 mRNA of approximately 3.7 kb that was dramatically reduced within 72 hr of Tet induction (Fig, 3-5A). Knockdown of CMF22 resulted in a modest growth defect (Fig 3-5B), with a doubling time of 14.6 hours for the knockdown compared to 10.1 hours for control cells. This is consistent with prior preliminary analysis of a CMF22 open reading frame knockdown (19). We did not observe any obvious morphological or flagellum defects in the knockdown, based on light microscopy, nor did we observe any obvious ultrastructural defect in the flagellum, based on transmission electron microscopy (Supplementary Figure 3-2). To test the requirement of CMF22 for cell motility, CMF22-UKD parasites were analyzed using high resolution, single cell video microscopy, as well as automated particle tracking and motility trace analysis (44). A motility defect was immediately evident in CMF22-UKD cells when analyzed using automated particle tracking (Figure 3-5C, D) and high-resolution video microscopy (Supplemental Movie 3-1 and 3-2). Knockdown cells retained a vigorously beating flagellum, but beating was unproductive, as the cells were

incapable of translocation, while uninduced controls were motile and moved readily in and out of the field of view (Supplemental Movie 3-1 and 3-2).

To determine the penetrance of the motility phenotype and quantify the impact on cell movement, we employed motility trace analysis and automated particle tracking (44, 46). CMF22-UKD parasites were significantly slower than uninduced controls (2.15 um/s for the knockdown vs 4.48 um/s for controls, $p < 0.0001$). Cell speed provides a reasonable assessment of cell motility, but has limitations because it does not filter out Brownian motion, which will contribute to speed calculation. We therefore measured mean squared displacement as a function of time interval to assess the impact of CMF22 knockdown on propulsive cell movement. Using this approach we found propulsive cell movement to be essentially absent in the CMF22 knockdown (Fig 3-7, top panels). Thus, CMF22 knockdown resulted in a defective flagellar beat that was incapable of driving propulsive motility. The defect was reversed following removal of tetracycline (Supplementary Figure 3-3).

Despite the block in propulsive motility, the flagellum of CMF22 knockdown cells continued to beat. Close examination of flagellum beating using high-speed video microscopy revealed defective coordination of axonemal beating along the length of the flagellum. Beating was erratic and variable in any given cell and from cell to cell, making it difficult to assign a uniform description, but prominent features included erratic movement of the flagellum tip, coupled with sharp bending in the cell's anterior end (Supplemental Movie 3-2 and 3-4). Base-to-tip beats were common (Fig 3-7, +Tet, and

Supplemental Movie 3-4), which contrasts to control cells where the dominant beat is tip-to-base (47, 48) (Fig. 3-7, -Tet, Supplemental Movie 3-1 and 3-3). Tip-to-base beats could be observed in knockdown cells (Figure 3-S3), although not as clearly or as consistently as in control cells, and generally did not appear to propagate along the whole cell (Supplemental Movie 3-5 and 3-8). Thus, it appears erratic and reverse flagellar beating combine to block propulsive cell movement.

Maintaining CMF22 expression in the knockdown restores motility

We next asked whether the motility defect in the knockdown was specific to loss of CMF22 expression. For this, we took advantage of the fact that RNAi targets the 3' UTR of CMF22, allowing us to express CMF22 under inducing conditions by changing the 3' UTR (44, 45). We used in situ tagging (41) to replace the CMF22 3' UTR with the alpha tubulin 3' UTR, while simultaneously incorporating an HA tag at one CMF22 allele in the knockdown. With this method, an HA-tagged copy of the gene is generated that is immune to RNAi and is expressed from the endogenous CMF22 locus (44). We refer to this cell line as "UTR-knockdown-RNAi-immune" (UKD-Ri). Immunoblotting with anti-HA antibodies showed a single band in lysates from UKD-Ri cells (Figure 3-8A). The alpha tubulin 3'UTR is smaller than the CMF22 3' UTR, therefore CMF22-HA mRNA is smaller than endogenous CMF22 mRNA and this size difference enabled us to distinguish between the endogenous and RNAi-immune CMF22 mRNA in Northern blots. A probe specific for the CMF22 ORF hybridized to a single mRNA in the UKD parental line and two mRNAs in the UKD-Ri cell line, corresponding to endogenous and HA-tagged mRNAs (Figure 3-8B). Abundance of the endogenous mRNA (Figure 3-8B, open

arrowhead) was dramatically reduced upon RNAi induction, while the HA-tagged mRNA (Figure 3-8B, filled arrowhead) was unaffected. Thus, CMF22-UKD-Ri cells retain CMF22 expression even under RNAi induction and this cell line was used to test for rescue of the motility phenotype.

RNAi knockdown of endogenous CMF22 had a minimal effect on growth of CMF22-UKD-Ri cells (Figure 3-8C), with a doubling time of 11.5 hours compared to 10.5 hours for -Tet controls. Importantly, UKD-Ri cells retained propulsive motility even upon knockdown of endogenous CMF22, as demonstrated by motility trace (Figure 3-8D, E), movies of individual cells (Supplemental Movies 3-6 and 3-7) and mean squared displacement analyses (Figure 3-6, bottom panels). The slope of the MSD curve was slightly less under induced conditions, but propulsive motility was clearly restored. Therefore, the motility defect in CMF22-KD cells is attributed specifically to the loss of CMF22. Moreover, the ability of HA-tagged CMF22 to support propulsive motility demonstrates that the localization of the HA-tagged protein reflects the location of the endogenous protein.

Stability of CMF22-HA interaction with the axoneme is reduced in NDRC knockdowns

The phylogenetic distribution, biochemical fractionation and localization of CMF22, together with the phenotype of CMF22 knockdowns, demonstrate an important role in axonemal motility. Consistent with these findings, a recent study found that the CMF22 orthologue in *Chlamydomonas reinhardtii* showed reduced abundance in

axonemes from nexin-dynein regulatory complex (NDRC) mutants, suggesting it may be associated with the NDRC (49). The fractionation and localization of CMF22, together with the phenotype of CMF22 knockdowns are consistent with this idea. To test for a potential interaction of CMF22 with the NDRC, we asked whether co-fractionation of CMF22 with axonemes was altered in trypanosomes deficient in NDRC subunits trypanin or CMF70. In control cells, CMF22 fractionates exclusively with 1% NP40-extracted cytoskeleton pellets and 1M NaCl-extracted axoneme pellets (Figure 3-2). As shown in figure 3-9, Tet-inducible knockdown of trypanin or CMF70 resulted in nearly half of the cellular pool of CMF22 being solubilized with 1% NP40 (Figure 3-9). Therefore, an intact NDRC is required for stable association of CMF22 with the axoneme. In the reciprocal experiment, stable association of trypanin with 1M NaCl-extracted axonemes was not altered by CMF22 knockdown (Figure 3-9).

DISCUSSION

Axonemal motility is essential for human development and physiology, as well as for the motility of pathogens that cause tremendous human suffering worldwide (4, 5). Therefore, defining core components of motile axonemes enhances understanding of eukaryotic biology and provides insight into mechanisms of inherited and infectious diseases in humans. In this study, we use phylogenetic, biochemical and functional analysis to demonstrate that CMF22 is a broadly conserved component of the motile axoneme and is required for wild type flagellum beating in *T. brucei*. Ablation of CMF22 expression by RNAi results in altered flagellar beating, including erratic and reverse beating, and completely blocks directional cell motility.

CMF22 is represented in each of the five major eukaryotic clades for which there is a representative having a motile flagellum and a completely sequenced genome (Figure 3-1). This distribution indicates CMF22 arose early in eukaryotic evolution as a core component of the machinery that drives flagellar motility. CMF22 function has not been directly studied in other organisms. However, CMF22 mRNA is among the most abundant transcripts in human sperm (96^{th} percentile) and exhibits five-fold reduced expression in patients with male factor infertility, which is characterized by abnormal sperm morphology and motility (50). These findings support the phylogenetic analyses by indicating a role for CMF22 in flagellar motility in organisms as diverse as trypanosomes and humans. We did not identify a CMF22 orthologue in *Plasmodium falciparum*, which elaborates a motile flagellum during gametocytogenesis (51). *P. falciparum* axonemes are not well-studied, but exhibit unusual features relative to the canonical structure (52). Our analysis suggests that *P. falciparum* has either dispensed with the need for CMF22, or that the gene sequence has diverged sufficiently to preclude detection based on sequence similarity.

Identification of CMF22 orthologues in three organisms reported to lack a flagellum, *Chlorella variabilis, Ostreococcus tauri,* and *Aureococcus anophagefferens,* at first seems contrary to its overall restriction to organisms with motile flagella, but further analysis indicates otherwise. *Ostreococcus* and *Chlorella* are both green algae with no flagellated stage yet described. However, as noted previously (20, 53), these organisms retain genes for several flagellum proteins, including NDRC subunits trypanin

and CMF70, the dynein subunit LC1, the dynein-NDRC assembly factor CCDC39 and MBO2. *Aureococcus* is in a different lineage (Chromalveolates) and no flagellated stage is yet described. Again however, orthologues of flagellar genes are present such as centriolar Pix proteins (54) and in our own analysis, we found LC1, IFT88, BBS5, and trypanin (data not shown). The presence of “flagellar” genes in these organisms has been suggested to indicate they might possess a cryptic flagellated stage, for example a cryptic gamete stage (55), or that ‘flagellar’ genes have been retained for other functions, or even that they have recently lost flagella and there has not been enough time for genomic loss (20). In any case, given the presence of several genes for flagellum proteins, it is not entirely surprising to find that CMF22 is retained in these organisms.

CMF22 knockdown completely blocks propulsive cell motility, but does not cause flagellar paralysis. Rather, the CMF22 knockdown exhibits an abnormal beating pattern characterized by erratic beating and frequent reversals of waveform propagation. The knockdown does not show any indication of defective flagellum assembly or major defects in growth that accompany gross disruptions of axoneme structure in *T. brucei* (23, 56-59). Indeed, TEM analysis did not reveal any obvious defect in axoneme ultrastructure. These data argue for a role in flagellar beat regulation, rather than a structural role or a direct role in generating forces that power microtubule sliding. Two proteins previously shown to function in beat regulation in *T. brucei* are trypanin and CMF70, which function as part of the NDRC (26). The CMF22 knockdown exhibits erratic flagellar beating, as observed in CMF70 knockdowns, but does not exhibit the

continuous cell tumbling that characterizes trypanin knockdowns (23, 25). Also, despite frequent reversals of flagellar wave propagation, CMF22 knockdowns do not exhibit significant backward cell motility, such as that described in outer arm dynein mutants with reverse wave propagation (46, 58). The absence of backward cell locomotion in CMF22 knockdowns may be due to reverse (base-to-tip) beats occurring simultaneously with forward (tip-to-base) beats, which counter each other and block propulsive motility. Thus, CMF22 appears to function in beat regulation, but its precise role is distinct from that of previously described flagellar mutants that lead to altered flagellum beating in *T. brucei*.

Given the flagellum beating defect of the CMF22 knockdown, together with biochemical and immunofluorescence data, we expect CMF22 to reside within an axonemal sub-complex that is crucial to motility regulation. Canonical sub-complexes of motile axonemes are inner and outer arm dynein motors, radial spokes, the nexin-dynein regulatory complex (NDRC) and the central pair apparatus (60). The entire cellular pool of CMF22 remains with insoluble axonemes after extraction with 1M NaCl, which solubilizes outer arm dyneins and much of the central pair apparatus (38). Thus, it is unlikely that CMF22 is a subunit of outer arm dynein complexes or the central pair apparatus. In support of this conclusion, CMF22 is retained in organisms that lack outer dyneins, *Physcomitrella*, and in organisms that lack the central pair apparatus, *Thalasiossira* (20, 61, 62). Notably, NDRC subunits trypanin and CMF70 are likewise conserved in *Physcomitrella* and *Thalasiossira*, the latter of which also lacks radial spokes and inner arm dyneins (20). Altogether, these data suggest that CMF22 can

function independently of the central pair apparatus, radial spokes or any single subset of axonemal dyneins and point to the NDRC or one of the novel axonemal sub-complexes recently identified by cryoelectron microscopy (14) as the site of CMF22 action. Current efforts are aimed at distinguishing between these possibilities. During preparation of this manuscript, Bower et al. (49) reported that the CMF22 orthologue in *Chlamydomonas reinhardtii* is a candidate NDRC subunit, because it shows reduced abundance in axonemes from *drc* mutants. Our data support and extend the important *Chlamydomonas* studies through fractionation, localization and functional analysis of the *T. brucei* CMF22 protein and are consistent with an NDRC function for CMF22. As reported for *C. reinhardtii*, we observed that CMF22 is less stably associated with the axoneme in cells deficient in other NDRC components, which is a hallmark of NDRC subunits (63, 64). Availability of the CMF22 knockdown allowed us to also ask the reciprocal question, namely whether or not NDRC subunits are impacted by loss of CMF22. We found that association of trypanin with salt-extracted axonemes is not affected by CMF22 knockdown. Bower and colleagues (49) suggested that FAP82, the *C. reinhardtii* CMF22 orthologue, may correspond to one of the NDRC distal densities that contact the B-tubule of the adjacent outer doublet (65). The finding that CMF22 knockdown does not alter trypanin fractionation supports this model and structural studies are underway to directly test this idea.

A notable feature of CMF22 is the protein's domain architecture, which includes an N-terminal IQ motif and a C-terminal AAA domain. IQ motifs function as binding sites for calmodulin and other EF hand proteins (66). AAA domains are nucleotide binding

domains that function in regulation and ATP hydrolysis in a variety of cellular contexts (67). The presence and position of each of these domains is conserved in CMF22 orthologues from diverse organisms (Figure 3-1B), indicating there is selective pressure to retain them and supporting the notion that they are important for protein function. The CMF22 AAA domain lacks the glutamate residue in the Walker B motif that is critical for catalysis (68), so it probably does not hydrolyze ATP. However, it might still function in regulation of motility through nucleotide binding.

The CMF22 IQ motif is of particular interest because it links CMF22 to potential functions in Ca^{2+} regulation of flagellar motility, which is conserved across diverse phyla and likely has roots in regulatory mechanisms that appeared early in eukaryotic evolution. Chemotaxis of mammalian sperm as well as flagellated protists is dependent upon modulation of the motility apparatus in response to extracellular cues, using Ca^{2+} as the second messenger (12, 69-73). Targets of Ca^{++} are not well understood, but pioneering studies in *Chlamydomonas* recently identified three axonemal protein complexes that bind calmodulin and are predicted to function in Ca^{++} regulation (74-76). The *Chlamydomonas* CMF22 orthologue, FAP82, was identified in the flagellar proteome (77), but was not identified as part of CaM-binding complexes in *Chlamydomonas* (78). Nonetheless, Ca^{2+} regulated motility is conserved in another trypanosome species, *Crithidia oncopelti*, where direction of flagellar wave propagation is regulated by the concentration of calcium. Forward (tip-to-base) beating predominates at low [Ca^{2+}], <0.1 mM, and reverse (base-to-tip) beating dominates at higher Ca^{2+} concentrations (79, 80). The Ca^{2+} response is observed in demembranated

flagella of *C. oncopelti* (36) indicating that at least some of the targets are axonemal proteins. The axonemal location of CMF22 and frequent reversals of flagellar beating in the CMF22 knockdown are consistent with a role for CMF22 in flagellar beat regulation.

T. brucei and related trypanosomatids are deadly pathogens that cause tremendous human suffering worldwide and the flagellum is central to trypanosome biology, transmission and pathogenesis (81). Distinctive characteristics of *T. brucei* flagellum structure and motility suggest specialized mechanisms for controlling flagellar beating and parasite motility (47, 82-85). In addition to providing insight into fundamental biology of flagella, understanding beat regulation in these organisms thus offers opportunities for discovering novel therapeutic or transmission-blocking strategies. Of the fifty original CMF genes identified in *T. brucei* (19), five have now been demonstrated or implicated to function as part of the NDRC: trypanin, CMF70, CMF46 and CMF44 (22, 23, 25, 26, 56) and, as discussed above, CMF22. While CMF proteins themselves are broadly-conserved, they interact with conserved as well as organism-specific proteins (86, 87). Continued analysis of CMF22 and other CMF proteins therefore offers opportunities to enhance understanding of flagellum motility with relevance to pathogenesis of trypanosomes and related human pathogens.

ACKNOWLEDGMENTS

Funding for the work was provided by grants from the NIH (R01AI052348) and Burroughs Wellcome Fund to KLH. HTN is the recipient of an NIH-NRSA (GM007185) fellowship. JSS is the recipient of a Beckman Scholars Fellowship. GL is the recipient of the Warsaw Fellowship. We thank Jose Rodriguez and Neville Kisalu for assistance on mean square displacement (MSD) analysis and Alvaro Sagasti for use of the X-PRI mono 2s High Speed Camera. We also thank Edwin Saada and Pius Kabututu for technical assistance. We thank Chantal Allamargot (University of Iowa) for electron microscopy. We are grateful to Stephen King for helpful comments and the members of the laboratory for critical reading of the manuscript and comments on the work.

SUPPLEMENTAL MOVIE LEGENDS

Supplemental Movie #1: 30 fps CMF22-UKD –Tet, control cells. Video microscopy shows normal motility of uninduced (-Tet) CMF22-UKD cell line. Notice that the cell rapidly travels across the field of view. Video recorded and played at 30 fps.

Supplemental Movie #2: 30 fps CMF22-UKD +Tet cells. After 72 hours of RNAi induction (+Tet), CMF22-UKD cells exhibit erratic movements in which flagellar beating is impaired and cells are not capable of propulsive motility. Notice in the knockdown (+Tet), erratic movements of the flagellar tip, bent anterior (thin end), and base-to-tip beating. Video recorded and played at 30 fps.

Supplemental Movie #3: 1000fps video of flagellar beating in control cells. Cells maintained –Tet. Videos were recorded at 1000 frames/second and played back at 50 frames/second. Note several tip-to-base beats. Figure 6 (-Tet) shows time-lapse image series taken from frames 100 to 300.

Supplemental Movie #4: 1000fps video of reverse (base-to-tip) flagellar beating in CMF22 Knockdown cells. CMF22-UKD cells were maintained +Tet for 72 hrs. Videos recorded at 1000fps and played at 50 fps. Figure 6 (+Tet) shows time-lapse image series taken from frames 150 to 350.

Supplemental Movie #5. 1000fps video of forward (tip-to-base) flagellar beating in CMF22 knockdown cells. CMF22-UKD cells were maintained +Tet for 72 hrs. Videos recorded at 1000fps and played at 50 fps. Video shows a flagellar beat that moves from tip toward base but then appears to stop and then reverse direction. Supplemental Figure 3 (top panels) shows time-lapse image series taken from frames 110 to 130.

Supplemental Movie #6: 30 fps video of normal cell translocation in CMF22UKD-Ri cells maintained in –Tet. Video shows essentially normal beating and translocation of CMF22-UKD-Ri cells before RNAi induction with Tet.

Supplemental Movie #7: 30 fps video of normal cell translocation in CMF22UKD-Ri cells 72 hours post-induction for RNAi against endogenous CMF22. CMF22UKD-Ri cells were maintained +Tet for 72 hrs. Video was recorded and played at 30 fps. Video shows essentially normal beating and translocation of CMF22-UKD-Ri cells after RNAi knockdown of endogenous CMF22.

Supplemental Movie #8: 1000 fps video of reverse flagellar beating followed by a forward beat in CMF22 Knockdown cells. CMF22-UKD cells were maintained +Tet for 72 hrs. Videos recorded at 1000fps and played at 50 fps. Video shows a forward beat that moves from the tip towards the base of the flagellum (frames 100 to 200) and is immediately followed by a reverse beat that moves back to the tip of the flagellum (frames 300 to 400). Supplemental Figure 3 (bottom) shows time-lapse image series taken from frames 145 to 595

METHODS

Trypanosome transfection and cell maintenance:

Procyclic 29-13 cells (88) were used for all experiments. Cultures were maintained in Cunningham's semi-defined medium (SM), supplemented with 10% heat-inactivated fetal calf serum, 15 mg/mL G418 and 50 mg/mL hygromycin (23).

Transfection and selection were done as previously described (23). Clonal lines were established through limiting dilution. RNAi was induced by adding 1μg/mL tetracycline.

Database searches:

T. brucei CMF22 (XP_828418.1) orthologues were identified in genome databases as reciprocal best BLAST hits using the NCBI BLAST portal as well as species-specific portals when necessary and the *T. brucei* sequence as the original query. Hits were confirmed by individual alignments where there was ambiguity. An organism is listed as having an orthologue if it has a hit and returned *T. brucei* CMF22 as the top hit in a BLAST search against *T. brucei*. Domain identification was done using the SMART database (89) and individual alignments where there was ambiguity. A summary of the organisms used and the corresponding accession numbers of CMF22 orthologues is provided in Table 3-1.

In situ tagging and RNAi knockdown:

In situ tagging of CMF22 was performed using the pMOTag2H vector (41) for direct integration of a tagging cassette at the C-terminus of endogenous *CMF22*. The final 515 bp of the CMF22 ORF were amplified from 29-13 procyclic genomic DNA with forward (5'- ATGGTACCTGAAGAAAGAGGTACTTAAGGGC-3') and reverse (5'-ATCTCGAGTTCCTTCTTCTTGGGTCTCTTCTTAG-3') primers containing a *KpnI* site and an *XhoI* site, respectively. This fragment was ligated into the corresponding sites of pMOTag2H directly upstream of the 3xHA cassette. Subsequently, 655 bp of the 3' UTR immediately downstream of the CMF22 stop codon were amplified with forward (5'-ATGGATCCAGCCCGGAATGTTCCTCAC-3') and reverse (5'-

ATACTAGTGACGCCGGTCGACCTCGAAG-3') primers containing a *BamHI* and a *SpeI* site, respectively. This fragment was then cloned into the corresponding sites directly downstream of the puromycin-resistance cassette. The entire tagging cassette (CMF22ORF-3xHA-igr-PuroR-CMF22 3'UTR) was excised from the resulting plasmid and stably transfected into 29-13 cells.

RNAi plasmids were constructed in the p2T7^{Ti}B plasmid (90). A 405 base pair fragment of the CMF22 3' UTR was selected using parameters described previously (45, 91) and designed using the RNAit algorithm (92) as described in (44, 45). This region was amplified with forward (5'-ATGGATCCAGCCCGGAATGTTCCTCAC-3') and reverse (5'-ATAAGCTTGCTTCGCACCTGTACAACG-3') primers containing a *BamHI* and *HindIII* site, respectively. The resulting amplicon was cloned into the corresponding sites of p2T7^{Ti}B between opposing, tetracycline-inducible T7 promoters. Following linearization with *Not1*, this plasmid was stably transfected into 29-13 cells, to generate a CMF22-3'UTR knockdown (CMF22-UKD) line. All DNA constructs were verified by direct sequencing. The rescue cell line, "UKD-Ri", was generated by stably transfecting the CMF22 C-terminal *in situ* tagging cassette (above) into the CMF22-UKD line. The same CMF22 C-terminal *in situ* tagging cassette (above) was stably transfected into the trypanin-UKD(44) and CMF70-KD (25) cell lines to generate trypanin and CMF70 knockdowns that express tagged CMF22. These cell lines were grown in media without puromycin for a week prior to tetracycline induction.

Cytoskeletal fractionation, western blotting, and immunofluorescence and electron microscopy:

Procyclic 29-13 cells were subjected to detergent fractionation using a two-step fractionation method as previously described (25, 38). Non-ionic 1% Nonidet-P40 (NP40) was used to solubilize the cell and the pellet fraction was subsequently extracted in 0.5 M and 1 M NaCl PMN [10 mM NaPO4 pH 7.4, 1 mM MgCl2, 150 mM NaCl] buffer. Cell lysates and detergent fractionations were analyzed by western blotting as previously described (23). Primary antibody dilutions were as follows: monoclonal anti-HA antibody (HA 11.1 Covance) 1:1000, monoclonal anti-Trypanin antibody (mAb 37.2) 1:5000 (23), monoclonal anti-Tubulin antibody E7 supernatant 1:2500. The monoclonal antibody E7, directed against beta-tubulin, was developed by (93) and obtained from the Developmental Studies Hybridoma Bank maintained by the University of Iowa Department of Biological Sciences.

For immunofluorescence, cells were extracted in PEME buffer (100 mM piperazine-*N*,*N*′-bis(2-ethanesulfonic acid), pH 6.9, 2 mM EGTA, 0.1 mM EDTA, 1 mM $MgSO_4$, 25 µg/ml aprotinin, 25 µg/ml leupeptin) containing 1% NP40 (42). Cell cytoskeletons were fixed in 2% paraformaldehyde, quenched in 0.1M glycine, and subjected to indirect immunofluorescence microscopy as previously described (38). Procyclic 2913 cytoskeletons were used as a negative control and showed no staining (data not shown). The following primary antibody dilutions were used: monoclonal anti-HA antibody (HA11.1, Covance) 1:200, monoclonal anti-PFR antibody (rat αPFR2, a gift from Thomas Seebeck) 1:2500, mouse monoclonal anti-Trypanin antibody (9C7) 1:50,

rat anti-HA antibody clone 3F10 (Roche Applied Science) 1:100, monoclonal anti-tubulin clone YL 1/2 (Millipore) 1:2500. Cytoskeletons were mounted after staining with Vectashield containing DAPI.

For transmission electron microscopy (TEM), log-phase CMF22-UKD cells were uninduced or induced with tetracycline for 72 hours, washed twice with PBS, resuspended in 1 mL fixative (3% paraformaldehyde and 3% glutaraldehyde in 0.1 M Na-cacodylate containing 1% filtered tannic acid), and incubated for one hour. For detergent-extracted cytoskeletons, cells were washed twice in PBS and resuspended in PEME + 1% NP-40 for 10 minutes. Cells were then pelleted and resuspended in 1 mL fixative for one hour (same as above). Fixed cells were pelleted and resuspended in fixative without tannic acid, treated with 1% osmium tetroxide, dehydrated in ethanol, washed three times in Eponate resin, and embedded in Eponate182. After polymerization, cells were sectioned into 80nm thick sections and analyzed using a Jeol 1230 transmission electron microscope at the University of Iowa Central Microscopy Research Facility (94).

Northern blots:

Total RNA was extracted from cells using the Qiagen RNeasy Miniprep kit. Northern blots were performed on RNA samples (5 μg/lane) from each cell line as previously described in (95) with the exception that DIG-labeled probes (DIG Nucleic Acid Detection Kit (Roche)) were used in place of ^{32}P-labeled probes to detect RNA levels. A unique 523 base pair probe corresponding to nt 1398 to 1920 of the CMF22

ORF was used in accordance with manufacturer's instructions. rRNA was crosslinked and visualized under ultraviolet light.

Growth curves and motility assays/videos

Cell growth was monitored using a Z1 Coulter Particle Counter (Beckman Coulter, USA) with curves plotted as cumulative growth and data points are reported as the averages obtained in three independent experiments with duplicate samples taken at each time point. Error bars indicate the standard deviation of the three independent experiments. For motility assays, cells at a density of 3 x 10^6 cells/ml were pipetted into poly-glutamate coated motility chambers (46) at room temperature and imaged on a Zeiss Axioskop II microscope within ten minutes after removal from the incubator. For motility traces, videos were collected using darkfield optics with a 20x objective as described (46). For tetracycline inducible conditions, 1μg/mL tetracycline was added to cultures for 72 hours before video capture. Motility traces were performed as described (46) and average curvilinear velocity was determined using Metamorph software (Molecular Dynamics). A student's unpaired *t*-test was also used to determine significance. To quantify parasite propulsive motility, traces were used to calculate the mean squared displacement of individual cells in the x and y dimensions according to the formula MSD = $<ri(t)^{2>} = <(pi(t) - pi(0))^{2>,}$ where ri is the distance travelled by the parasite over time interval t and pi is the position of the parasite at any given time. The timescale of t ranged from 1 to 30 seconds in increments of 1 second. MSD is calculated for each instance i of a given time interval. Several cell MSDs were then

averaged to obtain an ensemble average. Error bars indicate the standard deviation. For CMF22-UKD, 20 minus Tet parasites were analyzed, compared to 20 plus Tet parasites. For CMF22-UKD-Ri, 20 minus Tet parasites were analyzed, compared to 20 plus Tet parasites. For the tetracycline-removal experiment, CMF22-UKD cells were induced with tetracycline for 72 hours and tetracycline was removed by diluting cells to $1x10^6$ cells/mL in fresh media without tetracycline, with continuous dilution to maintain log phase growth for 5 days. After 5 days of tetracycline removal, motility traces and MSD was performed as described above. For single cell motility videos, cells were imaged using DIC optics with a 100x oil objective. Videos were captured either at 30 frames per second with a COHU CCD camera and imported using Adobe Premiere Elements as described (46), or captured at 1000 frames/second using a X-PRI mono 2s High Speed Camera (AOS Techonologies AG) and the AOS Imaging Studio light V2 software from the manufacturer.

FIGURES

A

Eukaryotic Clades		Organism	Cilia/Flagella Type	CMF22
Unikonts	Fungi	*Allomyces macrogynus*	Motile	Yes
	Sponges	*Amphimedon queenslandica*	Motile	Yes
	Mammals	*Homo sapiens*	Motile	Yes
	Insects	*Drosophila melanogaster*	Motile	Yes
	Platyhelminthes	*Schistosoma mansoni*	Motile	Yes
	Nematodes	*Caenorhabditis elegans*	Immotile	-
	Fungi	*Neurospora crassa*	No Cilia	-
	Amoebas	*Dictyostelium discoideum*	No Cilia	-
Plantae	Green algae	*Chlamydomonas reinhardtii*	Motile	Yes
	Mosses	*Physcomitrella patens*	Motile	Yes
	Angiosperms	*Arabidopsis thaliana*	No Cilia	-
	Red algae	*Cyanidioschyzon merolae*	No Cilia	-
Chromalveolates	Cryptophytes	*Guillardia theta*	Motile	Yes
	Ciliates	*Paramecium tetraurelia*	Motile	Yes
	Oomycetes	*Phytophthora infestans*	Motile	Yes
	Apicomplexa	*Plasmodium falciparum*	Motile	-
	Diatoms	*Thalassiosira pseudonana*	Motile	Yes
	Apicomplexa	*Cryptosporidium parvum*	No Cilia	-
	Diatoms	*Phaeodactylum tricornutum*	No Cilia	-
Excavates	Diplomonads	*Giardia lamblia*	Motile	Yes
	Heterolobosea	*Naegleria gruberi*	Motile	Yes
	Kinetoplastids	*Trypanosoma brucei*	Motile	Yes
Rhizaria	Chlorarachniophyte	*Bigelowiella natans*	Motile	Yes

B

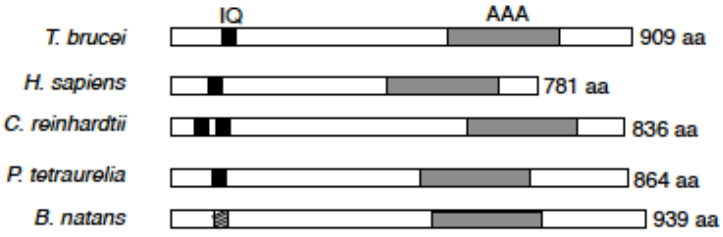


Figure 3-1. CMF22 is broadly conserved among organisms with motile flagella. (A) Representative organisms from each of the indicated eukaryotic clades are shown along with a depiction indicating whether these organisms have a motile flagellum, an immotile flagellum, or no flagellum. The presence or absence of CMF22 orthologues is noted in the right-most column. Only organisms for which the complete genome sequence is available were considered. Groups are based on the work of Keeling et al. (B) The CMF22 domain architecture is conserved in diverse organisms. The schematic

shows the predicted domain architecture for CMF22 orthologues from the indicated organisms. The IQ and AAA motifs were identified using SMART (black and gray boxes) or individual alignments (hash-marked box). The organisms (with their GenBank accession numbers in parentheses) used were as follows: *Trypanosoma brucei* (XP_828418.1), *Homo sapiens* (NP_001257513.1), *Chlamydomonas reinhardtii* (XP_001690665.1), *Paramecium tetraurelia* (XP_001429179.1), and *Bigelowiella natans* (jgi_Bigna1_142761). aa, amino acids.

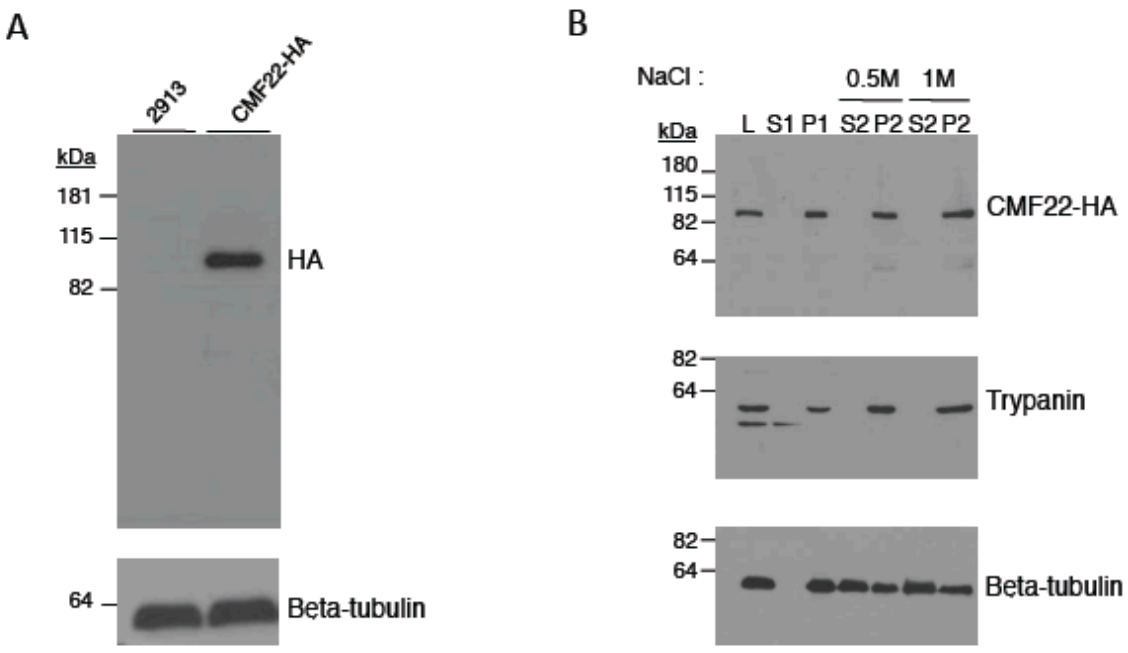


Figure 3-2. CMF22 is associated with the flagellum skeleton. (A) Western blot of total cell lysates from control (2913) or CMF22-HA-tagged (CMF22-HA) cells. Blots were probed with antibodies against the HA epitope or loading control (tubulin). (B) Western blot of whole-cell lysates (lane L) and the indicated subcellular fractions from CMF22-HA cells. Blots were probed with antibodies against the indicated proteins. Fractions correspond to nonionic detergent-soluble (lane S1) and insoluble (lane P1) fractions, as well as soluble (lane S2) and insoluble (lane P2) fractions obtained by extraction of P1 with NaCl at the concentrations indicated at the top. The lower band in the trypanin blot is likely a degradation product.

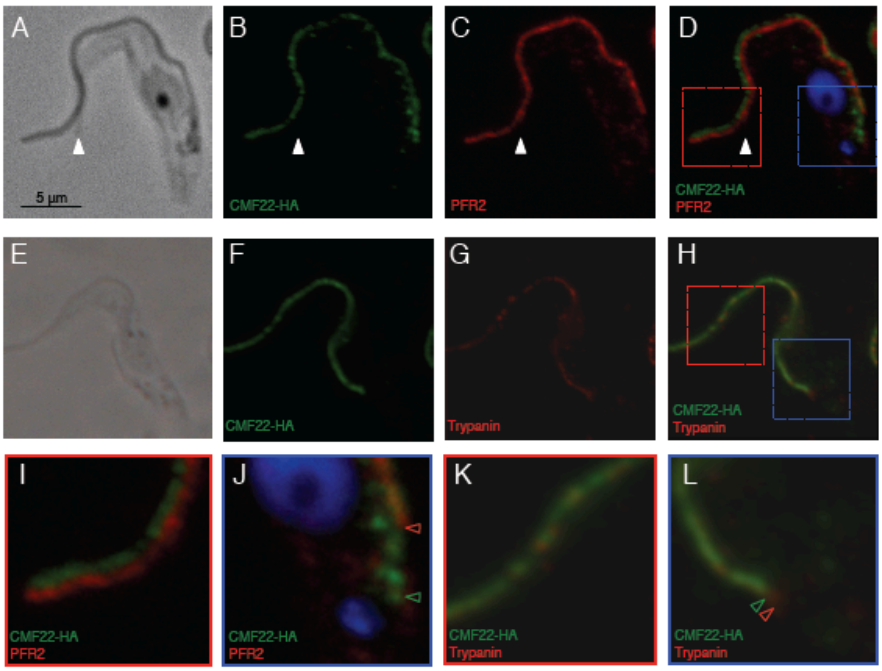


Figure 3-3. CMF22 is localized to the axoneme. Indirect immunofluorescence was performed on detergent-extracted cytoskeletons from CMF22-HA cells. Samples were stained with anti-HA antibodies to detect CMF22-HA and costained with antibodies against markers for the PFR (PFR2) (A to D, I, and J) or axoneme (trypanin) (E to H, K, and L), as indicated. DNA was visualized with DAPI (blue). Phase-contrast, individual fluorescence, and merged fluorescence images are shown. Regions boxed in red and blue in panelDare enlarged in panels I and J, respectively. Regions boxed in red and blue in panel H are enlarged in panels K and L, respectively. The white arrowheads in panels A to D mark the end of the cell body. Red and green arrowheads in panel J mark the proximal end of PFR and CMF22 staining, respectively. Red and green arrowheads in panel L mark the proximal end of trypanin and CMF22 staining, respectively.

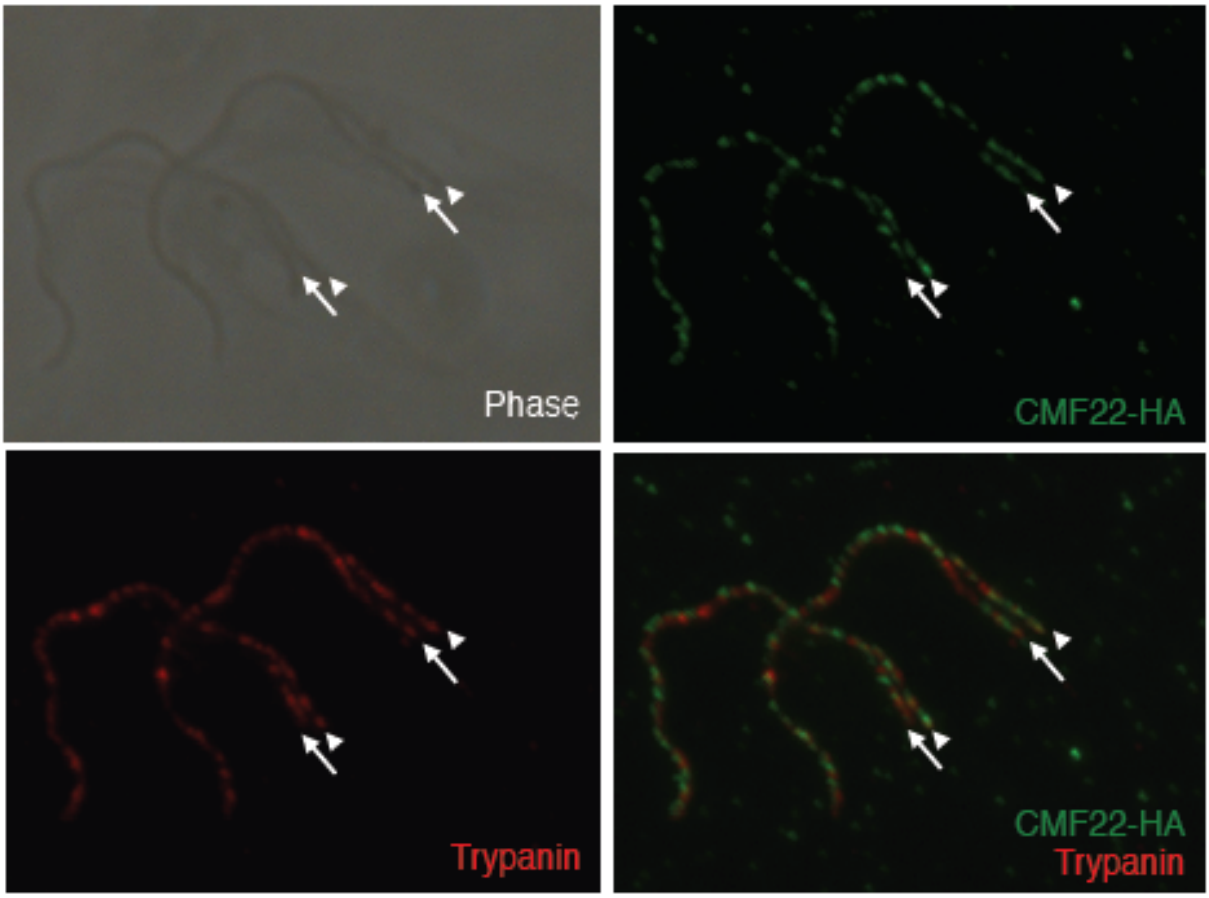


Figure 3-4. CMF22 localizes to the axoneme in nascent flagella. Indirect immunofluorescence was performed on detergent-extracted cytoskeletons from dividing CMF22-HA cells. Samples were stained with anti-HA (green) and anti-trypanin (red) antibodies. The newly emergent daughter flagellum (arrows) is posterior to the old flagellum (arrowheads). Phase-contrast, individual fluorescence, and merged fluorescence images are shown.

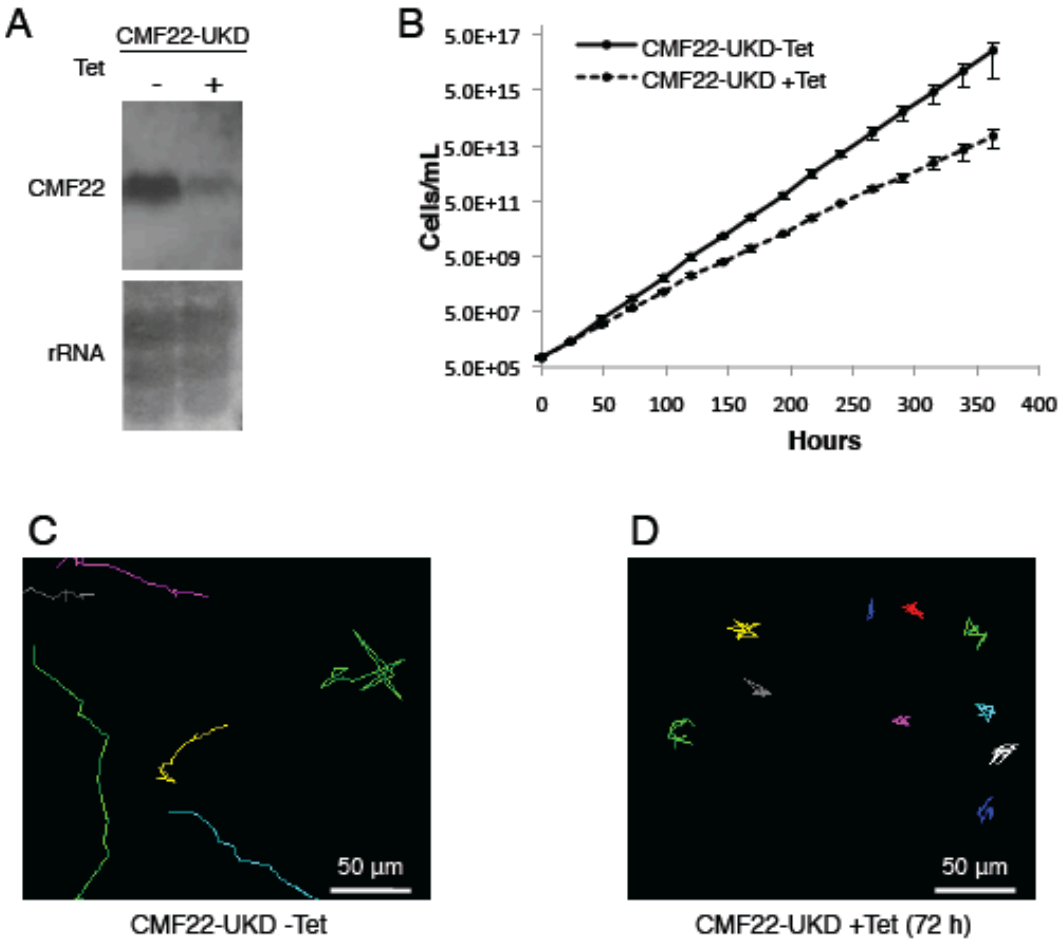


Figure 3-5. CMF22 knockdown disrupts motility. (A) Northern blot of RNA prepared from CMF22-UKD cells grown in the absence (**-**) or presence (**+**) of Tet, as indicated. (Top) Probe with a DNA fragment unique to the CMF22 ORF; (bottom) rRNA as a loading control. (B) Growth curve of CMF22-UKD grown in the absence or presence of Tet for 2 weeks, as indicated. Data are averages of three independent experiments. (C and D) Motility traces of CMF22-UKD grown in the absence or presence of Tet for 72 h, as indicated. Each line traces the movement of an individual trypanosome over a 30-s time interval.

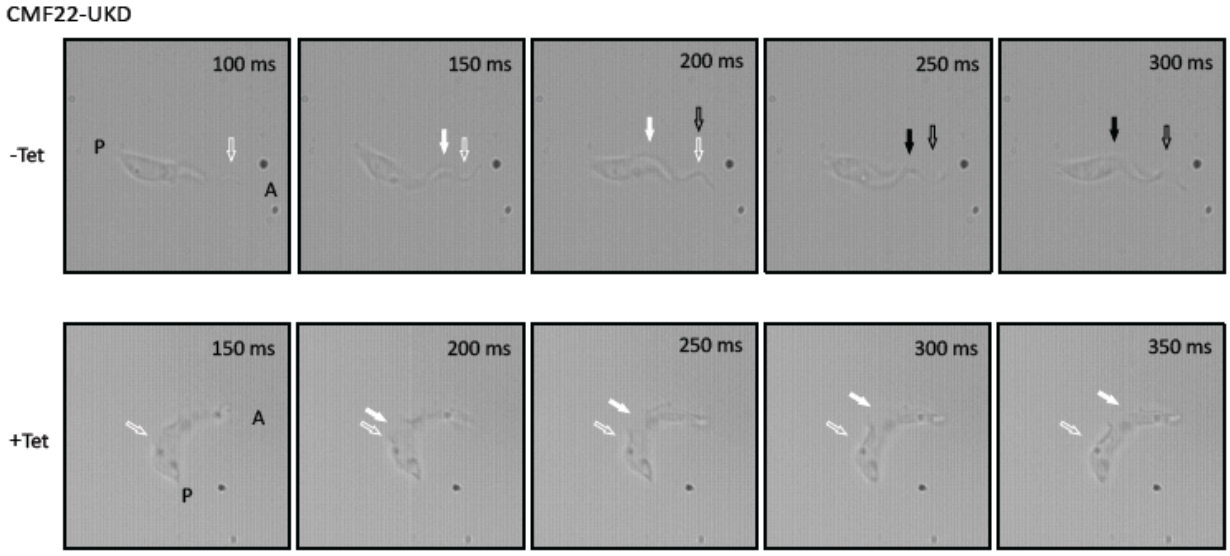


Figure 3-6. Time-lapse series showing the reverse beat in CMF22-UKD following tetracycline induction. (Top) Control cells (CMF22-UKD cells in the absence of Tet) retain a wild-type tip-to-base beat; time-lapse image series taken from frames at 100 to 300 ms of Movie S3 in the supplemental material are shown. (Bottom) After Tet induction for 72 h, CMF22-UKD cells display a flagellar beat that originates at the base of the flagellum and propagates toward the flagellum tip (reverse beat); frames at 150 to 350 ms of Movie S4 in the supplemental material are shown. White arrows, first waveform; black arrows, second waveform; filled arrows, position of the waveform at each time point; unfilled arrows; approximate position where the waveform originates; P, posterior end of the cell; A anterior end of the cell.

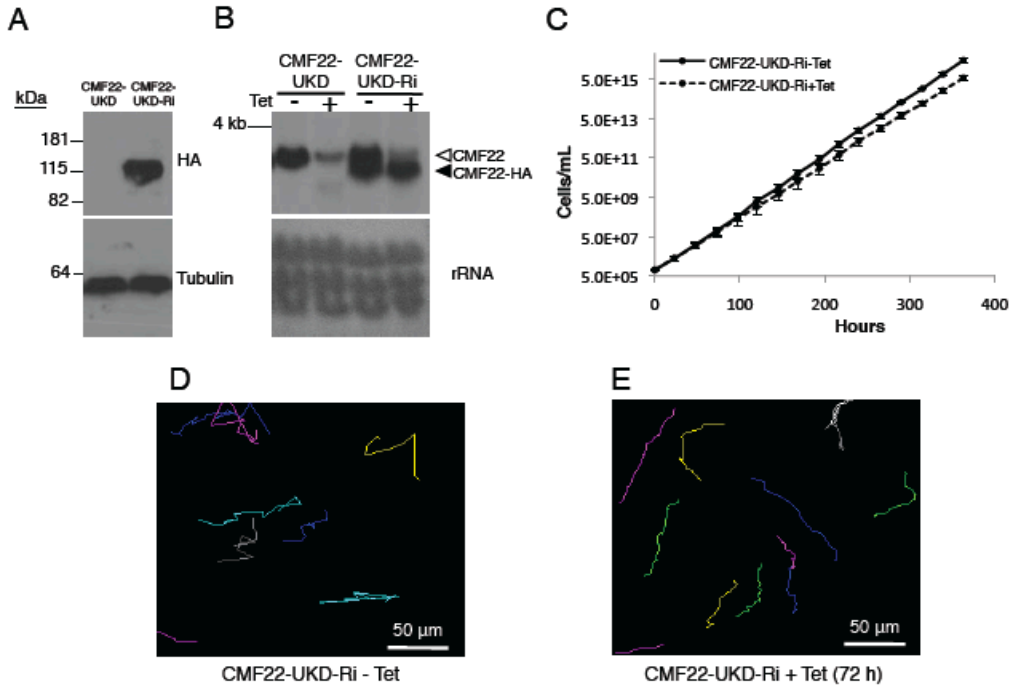


Figure 3-7. HA-tagged CMF22 rescues the motility defect of CMF22-knockdown cells. (A) Western blot of total protein prepared from CMF22-UKD cells or CMF22-UKD-Ri cells probed with anti-HA or antitubulin antibody, as indicated. UKD-Ri cells contain an RNAi-immune HA-tagged CMF22 gene; see the text for details. (B) Northern blot of total RNA prepared from CMF22-UKD or CMF22-UKD-Ri cells grown in the absence or presence of Tet, as indicated. Open arrowhead, endogenous CMF22 mRNA; filled arrowhead, HA-tagged mRNA. Membranes were probed with a DNA fragment specific to the CMF22 ORF (top), and rRNA is shown as a loading control (bottom). (C) Growth curve of CMF22-UKD-Ri cells grown in the absence or presence of Tet, as indicated. (D and E) Motility traces of CMF22-UKD-Ri cells grown in the absence or presence of Tet, as indicated.

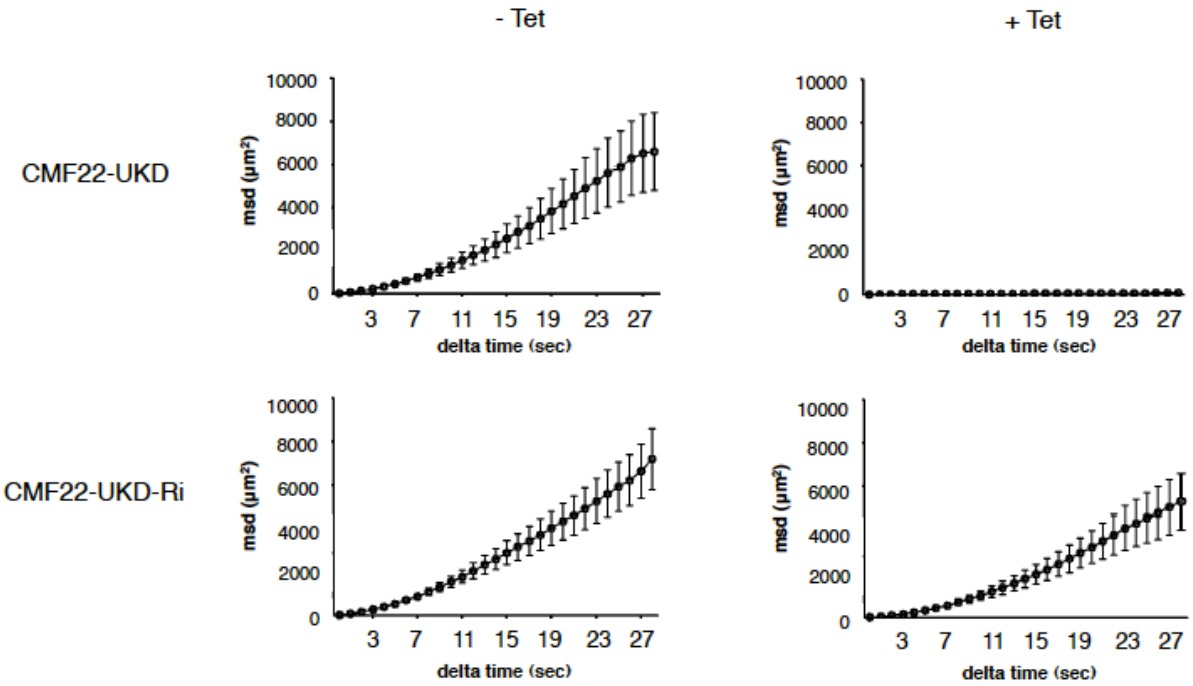


Figure 3-8. CMF22 is required for propulsive motility. MSD is plotted as a function of the time interval (delta time) for CMF22-UKD cells and for CMF22-UKD-Ri cells grown in the absence or presence of Tet, as indicated.

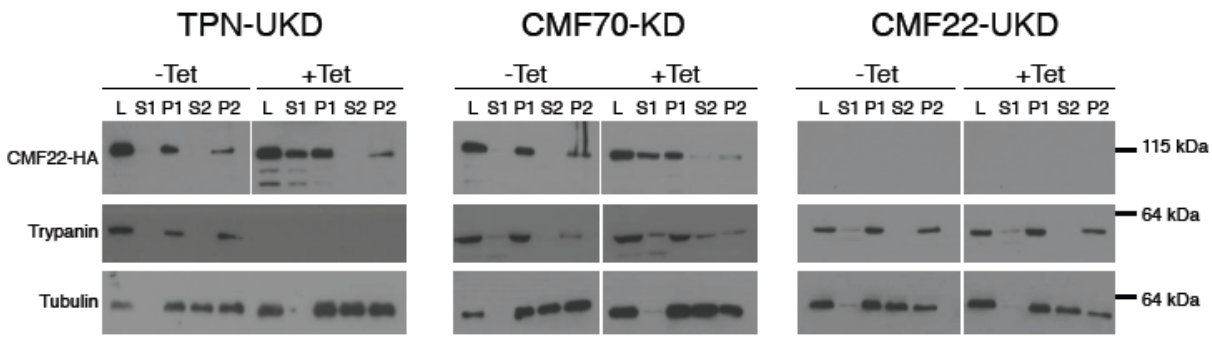


Figure 3-9. CMF22-HA is less stably associated with the axoneme in NDRC mutants. (A) Western blot of the indicated subcellular fractions from trypanin-UTRknockdown, CMF70-knockdown, or CMF22-ORF-knockdown cells probed with anti-HA, anti-trypanin, or anti-tubulin antibody, as indicated. Fractions correspond to whole-cell lysate (lanes L), nonionic detergent-soluble (lanes S1) and insoluble (lanes P1) fractions, as well as soluble (lanes S2) and insoluble (lanes P2) fractions obtained by extraction of P1 with 1 M NaCl. The lower-molecular-mass bands in the anti-HA and anti-trypanin blots are likely degradation products.

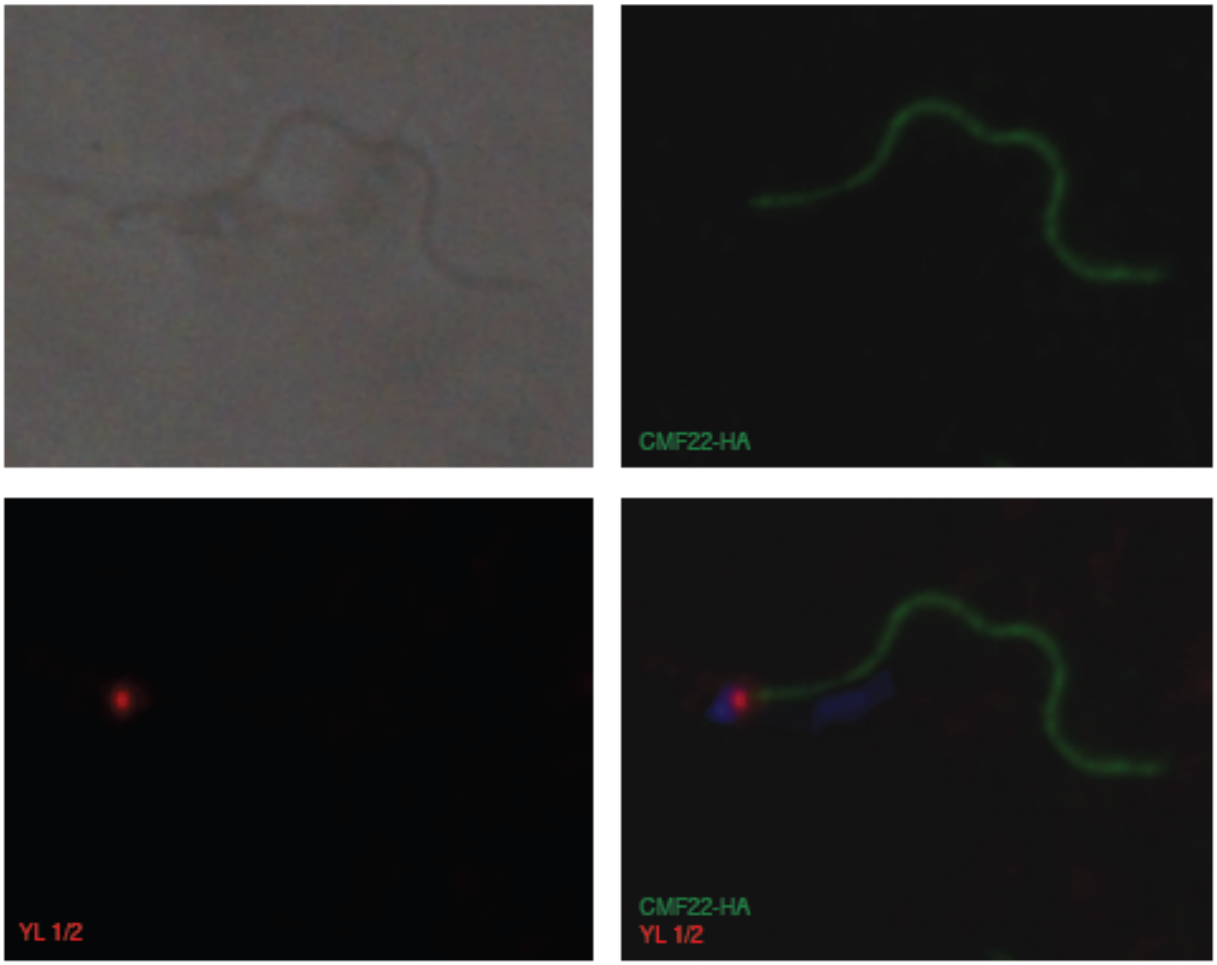


Figure 3-S1. CMF22 and basal body co-staining. Indirect immunofluorescence on detergent-extracted cytoskeletons from CMF22-HA cells. Samples were stained with anti-HA antibodies to detect CMF22-HA (green) and YL 1/2 antibodies as a marker for the basal body (red).The kDNA and nuclear DNA were stained with DAPI (blue).

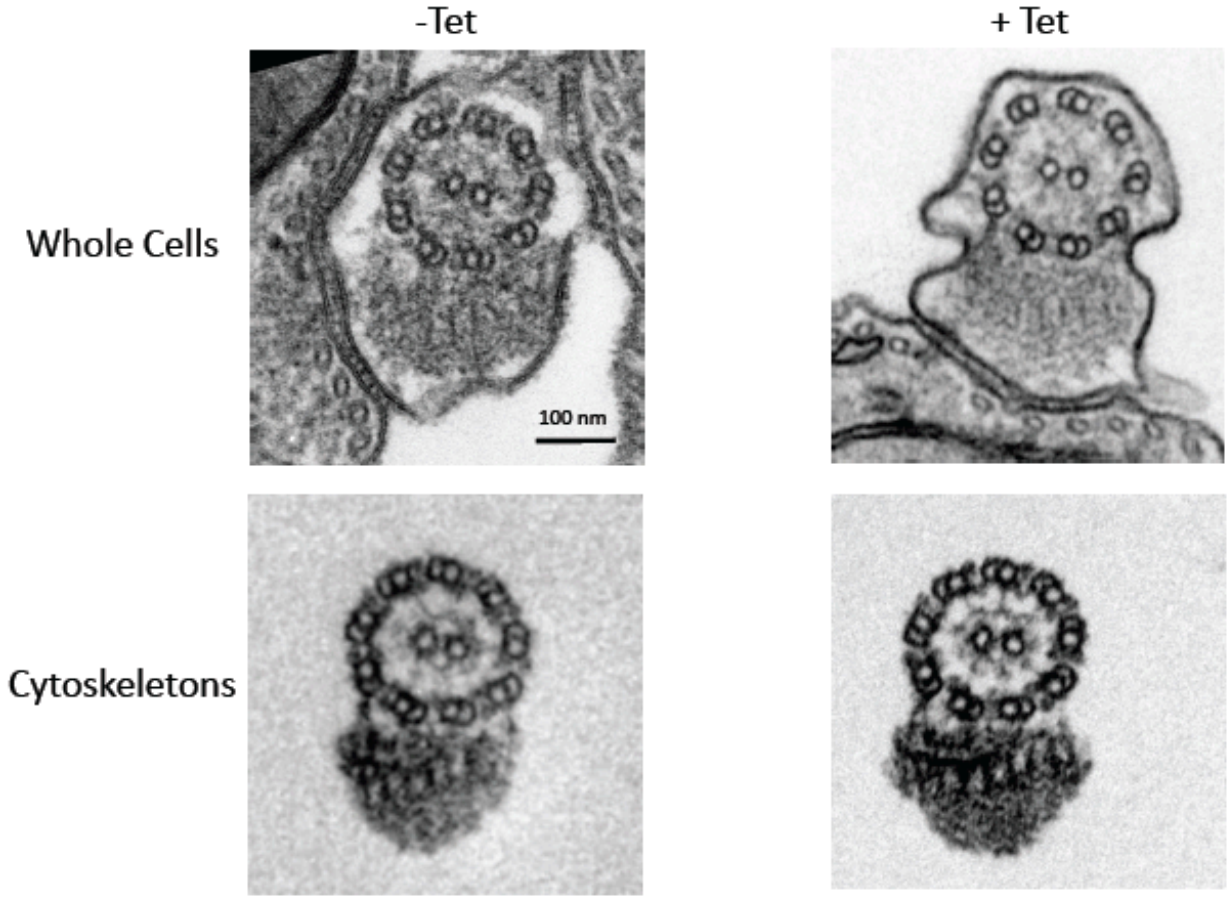


Figure 3-S2. CMF22 knockdown does not affect axoneme ultrastructure. Transmission electron microscopy (TEM) analysis of flagella in CMF22-UKD cells grown in the absence or presence of tetracycline for 72 hours as indicated. Samples are either whole cells (upper panels) or 1% NP40-extracted samples (lower panels).

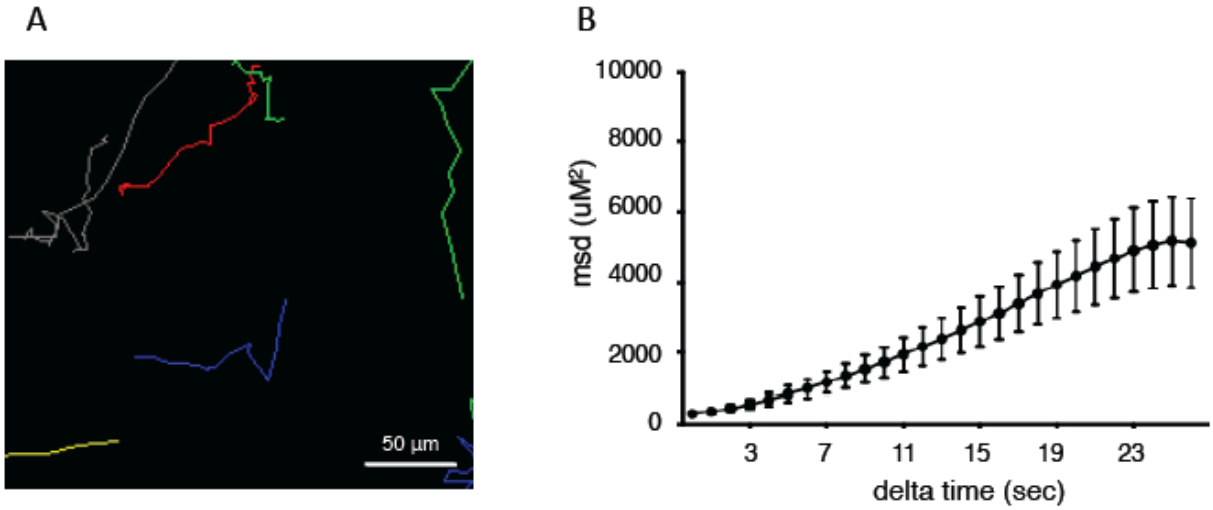


Figure 3-S3. Removal of tetracycline restores wild-type motility in CMF22-UKD cells. CMF22-UKD cells were induced with tetracycline for RNAi knockdown of CMF22 for 72 hours then tetracycline was removed by diluting the culture to $1x10^6$ every 24 hours for 5 days. (A) Motility traces of individual cells at day 5 after tetracycline removal. (B) Mean squared displacement (msd) of CMF22-UKD cells after 5 days tetracycline removal is plotted as a function of time interval.

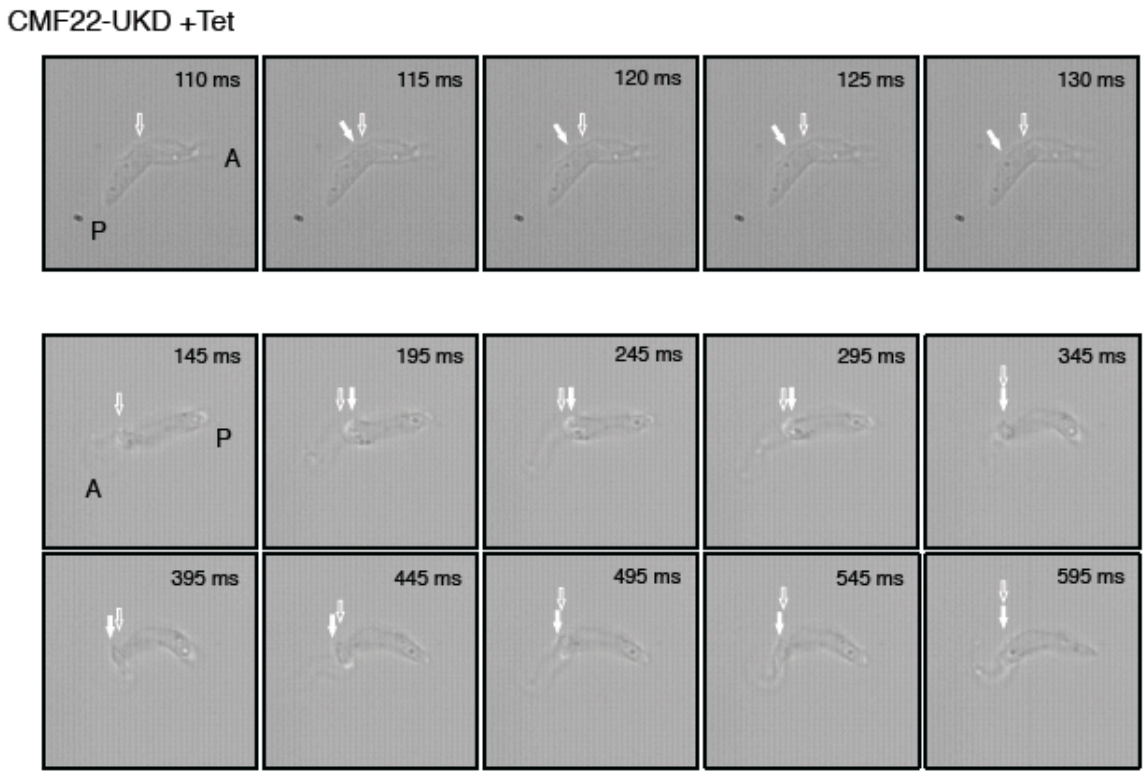


Figure 3-S4. CMF22 knockdown cells exhibits both reverse and forward beats. Time-lapse image series from video microscopy of CMF22-UKD cells 72 hrs post induction. Filled arrow indicates position of wave at each time point. Unfilled arrows indicate approximate position where waveform originated. “P” marks the posterior end of the cell and “A” marks the anterior end of the cell. (Top) Induction with Tet shows a reverse flagellar beat that moves toward the base of the flagellum. Frames 110 to 130 taken from Supplementary Movie 5. (Bottom) A reverse flagellar beat that moves towards the base of the flagellum, then stops and moves toward the tip of the flagellum (bottom panels). Frames 145 to 595 taken from Supplemental Movie 3-8.

Motile Cilia	CMF22 Orthologue
Acyrthosiphon pisum	XP_003242250.1
Aedes aegypti	XP_001658040.1
Ailuropoda melanoleuca	XP_002915532.1
Allomyces macrogynus	AMAG_01639.2
Amphimedon queenslandica	XP_003388958.1
Anolis carolinensis	XP_003215233.1
Anopheles gambiae	XP_320769.4
Apis mellifera	XP_001122486.2
Batrachochytrium dendrobatidis	EGF82441.1
Bigelowiella natans	jgi|Bigna1|142761
Bos taurus	NP_001193476.1
Branchiostoma floridae	XP_002594378.1
Canis familiaris	XP_539921.3
Capitella teleta	ELU03195.1
Chlamydomonas reinhardtii	XP_001690665.1
Ciona intestinalis	XP_002129665.1
Clonorchis sinensis	GAA52427.1
Crassostrea gigas	EKC42060.1
Culex pipiens	XP_001847569.1
Cyanophora paradoxa	ConsensusfromContig8672-snap-gene-0.0
Danaus plexippus	EHJ76815.1
Danio rerio	NP_001073437.2
Drosophila melanogaster	AAM11255.1
Ectocarpus siliculosus	CBN77721.1
Emiliania huxleyi	jgi|Emihu1|235066
Equus caballus	XP_001496552.2
Felis catus	XP_003991344.1
Gallus gallus	XP_421878.2
Giardia lamblia	XP_001707075.1
Guillardia theta	EKX39704.1
Harpegnathos saltator	EFN82410.1
Helobdella robusta	jgi|Helro1|188756
Heterocephalus glaber	EHB01958.1
Homo sapiens	NP_001257513.1
Hydra magnipapillata	XP_002168984.2
Leishmania major	XP_001681896.1
Lottia gigantea	jgi|Lotgi1|61523|0860
Loxodonta africana	XP_003417985.1
Macaca mulatta	EHH17871.1
Meleagris gallopavo	XP_003207414.1
Micromonas pusilla	XP_003061855.1

Motile Cilia	CMF22 Orthologue
Monodelphis domestica	XP_001372750.2
Monosiga brevicollis	XP_001744417.1
Mus musculus	NP_083398.2
Myotis davidii	ELK32629.1
Naegleria gruberi	XP_002678621.1
Nasonia vitripennis	XP_003423849.1
Nematostella vectensis	XP_001637403.1
Oikopleura dioica	CBY14496.1
Oreochromis niloticus	XP_003440019.1
Ornithorhynchus anatinus	XP_001513364.2
Oryctolagus cuniculus	XP_002723285.1
Oryzias latipes	XP_004067899.1
Ovis aries	XP_004001818.1
Oxytricha trifallax	EJY71359.1
Pan troglodytes	XP_003309586.1
Paramecium tetraurelia	XP_001429179.1
Pediculus humanus	XP_002432035.1
Perkinsus marinus	XP_002776859.1
Physcomitrella patens	XP_001767278.1
Phytophthora infestans	XP_002898734.1
Plasmodium falciparum	None
Pongo abelii	XP_002818732.2
Rattus norvegicus	NP_001019488.2
Saccoglossus kowalevskii	NP_001171756.1
Saprolegnia parasitica	SPRG_02274.1
Sarcophilus harrisii	XP_003770307.1
Schistosoma mansoni	XP_002572778.1
Selaginella moellendorffii	XP_002974085.1
Spizellomyces punctatus	SPPG_02701.3
Strongylocentrotus purpuratus	XP_780770.3
Sus scrofa	XP_003133808.1
Taeniopygia guttata	XP_004175065.1
Takifugu rubripes	XP_003974316.1
Tetrahymena thermophila	XP_001015966.1
Tetraodon nigroviridis	CAG08045.1
Thalassiosira pseudonana	XP_002294237.1
Thecamonas trahens	AMSG_00296.2
Toxoplasma gondii	XP_002371250.1
Tribolium castaneum	EFA11364.1
Trichomonas vaginalis	XP_001330039.1
Trichoplax adhaerens	XP_002111442.1
Trypanosoma brucei	XP_828418.1
Trypanosoma cruzi	XP_817318.1
Volvox carteri	XP_002951335.1
Xenopus tropicalis	XP_002932048.1

Immotile Cilia	CMF22 Orthologue
Trichinella spiralis	None
Caenorhabditis elegans	None
Brugia malayi	None
Ascaris suum	None

No Cilia	CMF22 Orthologue
Arabidopsis thaliana	None
Aureococcus anophagefferens	EGB09618.1
Chlorella variabilis	EFN52029.1
Coprinopsis cinerea	None
Cryptococcus neoformans	None
Cryptosporidium parvum	None
Cyanidioschyzon merolae	None
Dictyostelium discoideum	None
Encephalitozoon cuniculi	None
Entamoeba histolytica	None
Glycine max	None
Neurospora crassa	None
Oryza sativa	None
Ostreococcus tauri	XP_003078557.1
Phaeodactylum tricornutum	None
Populus trichocarpa	None
Rhizopus oryzae	None
Saccharomyces cerevisiae	None
Schizosaccharomyces pombe	None
Solanum tuberosum	None
Theileria annulata	None
Ustilago maydis	None
Vitis vinifera	None
Zea mays	None

Table 3-1. CMF22 orthologues from 115 diverse eukaryotes. The TbCMF22 protein (XP_828418.1) was used as the original query to perform reciprocal best BLAST using the NCBI BLAST portal and species specific portals. An orthologue was confirmed only if TbCMF22 was returned as the top hit upon BLAST against the *T. brucei* genome. To get diverse coverage of genomes, multiples species from the same genus were not compared. Our study found 85 orthologues for CMF22 out of 86 organisms with motile cilia, 0 out of 4 organisms with immotile cilia and 3 out of 25 organisms without cilia.

REFERENCES

1. Takeda, S., and K. Narita. 2012. Structure and function of vertebrate cilia, towards a new taxonomy. Differentiation 83:S4-11.
2. Wilson, N. F. 2008. Gametic cell adhesion and fusion in the unicellular alga Chlamydomonas. Methods Mol Biol 475:39-51.
3. Snell, W. J., J. Pan, and Q. Wang. 2004. Cilia and flagella revealed: from flagellar assembly in Chlamydomonas to human obesity disorders. Cell 117:693-7.
4. Fliegauf, M., T. Benzing, and H. Omran. 2007. When cilia go bad: cilia defects and ciliopathies. Nat Rev Mol Cell Biol 8:880-93.
5. Ginger, M. L., N. Portman, and P. G. McKean. 2008. Swimming with protists: perception, motility and flagellum assembly. Nat Rev Microbiol 6:838-50.
6. Bastin, P., T. J. Pullen, F. F. Moreira-Leite, and K. Gull. 2000. Inside and outside of the trypanosome flagellum:a multifunctional organelle. Microbes Infect 2:1865-74.
7. Vincensini, L., T. Blisnick, and P. Bastin. 2011. 1001 model organisms to study cilia and flagella. Biol Cell 103:109-30.
8. Stuart, K., R. Brun, S. Croft, A. Fairlamb, R. E. Gurtler, J. McKerrow, S. Reed, and R. Tarleton. 2008. Kinetoplastids: related protozoan pathogens, different diseases. J Clin Invest 118:1301-10.
9. Hill, K. L. 2003. Biology and mechanism of trypanosome cell motility. Eukaryot Cell 2:200-8.

10. Fritz-Laylin, L. K., S. E. Prochnik, M. L. Ginger, J. B. Dacks, M. L. Carpenter, M. C. Field, A. Kuo, A. Paredez, J. Chapman, and J. Pham. 2010. The Genome of Naegleria gruberi Illuminates Early Eukaryotic Versatility. Cell 140:631-642.
11. Satir, P., and S. T. Christensen. 2006. Overview of Structure and Function of Mammalian Cilia. Annu Rev Physiol.
12. Salathe, M. 2007. Regulation of mammalian ciliary beating. Annu Rev Physiol 69:401-22.
13. Carbajal-Gonzalez, B. I., T. Heuser, X. Fu, J. Lin, B. W. Smith, D. R. Mitchell, and D. Nicastro. 2012. Conserved structural motifs in the central pair complex of eukaryotic flagella. Cytoskeleton (Hoboken).
14. Nicastro, D., C. Schwartz, J. Pierson, R. Gaudette, M. E. Porter, and J. R. McIntosh. 2006. The molecular architecture of axonemes revealed by cryoelectron tomography. Science 313:944-8.
15. Bui, K. H., H. Sakakibara, T. Movassagh, K. Oiwa, and T. Ishikawa. 2009. Asymmetry of inner dynein arms and inter-doublet links in Chlamydomonas flagella. Journal of Cell Biology 186:437-46.
16. Mitchell, D. R. 2007. The evolution of eukaryotic cilia and flagella as motile and sensory organelles. Adv Exp Med Biol 607:130-40.
17. Li, J. B., J. M. Gerdes, C. J. Haycraft, Y. Fan, T. M. Teslovich, H. May-Simera, H. Li, O. E. Blacque, L. Li, C. C. Leitch, R. A. Lewis, J. S. Green, P. S. Parfrey, M. R. Leroux, W. S. Davidson, P. L. Beales, L. M. Guay-Woodford, B. K. Yoder, G. D. Stormo, N. Katsanis, and S. K. Dutcher. 2004. Comparative genomics

identifies a flagellar and basal body proteome that includes the BBS5 human disease gene. Cell 117:541-52.

18. Avidor-Reiss, T., A. M. Maer, E. Koundakjian, A. Polyanovsky, T. Keil, S. Subramaniam, and C. S. Zuker. 2004. Decoding cilia function: defining specialized genes required for compartmentalized cilia biogenesis. Cell 117:527-39.

19. Baron, D. M., K. S. Ralston, Z. P. Kabututu, and K. L. Hill. 2007. Functional genomics in Trypanosoma brucei identifies evolutionarily conserved components of motile flagella. J Cell Sci 120:478-91.

20. Merchant, S. S., S. E. Prochnik, O. Vallon, E. H. Harris, S. J. Karpowicz, G. B. Witman, A. Terry, A. Salamov, L. K. Fritz-Laylin, L. Marechal-Drouard, W. F. Marshall, L. H. Qu, D. R. Nelson, A. A. Sanderfoot, M. H. Spalding, V. V. Kapitonov, Q. Ren, P. Ferris, E. Lindquist, H. Shapiro, S. M. Lucas, J. Grimwood, J. Schmutz, P. Cardol, H. Cerutti, G. Chanfreau, C. L. Chen, V. Cognat, M. T. Croft, R. Dent, S. Dutcher, E. Fernandez, H. Fukuzawa, D. Gonzalez-Ballester, D. Gonzalez-Halphen, A. Hallmann, M. Hanikenne, M. Hippler, W. Inwood, K. Jabbari, M. Kalanon, R. Kuras, P. A. Lefebvre, S. D. Lemaire, A. V. Lobanov, M. Lohr, A. Manuell, I. Meier, L. Mets, M. Mittag, T. Mittelmeier, J. V. Moroney, J. Moseley, C. Napoli, A. M. Nedelcu, K. Niyogi, S. V. Novoselov, I. T. Paulsen, G. Pazour, S. Purton, J. P. Ral, D. M. Riano-Pachon, W. Riekhof, L. Rymarquis, M. Schroda, D. Stern, J. Umen, R. Willows, N. Wilson, S. L. Zimmer, J. Allmer, J. Balk, K. Bisova, C. J. Chen, M. Elias, K. Gendler, C. Hauser, M. R. Lamb, H. Ledford, J. C. Long, J. Minagawa, M. D. Page, J. Pan, W. Pootakham, S. Roje,

A. Rose, E. Stahlberg, A. M. Terauchi, P. Yang, S. Ball, C. Bowler, C. L. Dieckmann, V. N. Gladyshev, P. Green, R. Jorgensen, S. Mayfield, B. Mueller-Roeber, S. Rajamani, R. T. Sayre, P. Brokstein, et al. 2007. The Chlamydomonas genome reveals the evolution of key animal and plant functions. Science 318:245-50.

21. Wickstead, B., and K. Gull. 2007. Dyneins across eukaryotes: a comparative genomic analysis. Traffic 8:1708-21.

22. Rupp, G., and M. E. Porter. 2003. A subunit of the dynein regulatory complex in Chlamydomonas is a homologue of a growth arrest-specific gene product. J Cell Biol 162:47-57.

23. Ralston, K. S., and K. L. Hill. 2006. Trypanin, a Component of the Flagellar Dynein Regulatory Complex, Is Essential in Bloodstream Form African Trypanosomes. PLoS Pathogens 2:873-882, e101 doi:10.1371/journal.ppat.0020101.

24. Colantonio, J. R., J. Vermot, D. Wu, A. D. Langenbacher, S. Fraser, J. N. Chen, and K. L. Hill. 2009. The dynein regulatory complex is required for ciliary motility and otolith biogenesis in the inner ear. Nature 457:205-9.

25. Kabututu, Z. P., M. Thayer, J. H. Melehani, and K. L. Hill. 2010. CMF70 is a subunit of the dynein regulatory complex. Journal of Cell Science 123:3587-95.

26. Lin, J., D. Tritschler, K. Song, C. F. Barber, J. S. Cobb, M. E. Porter, and D. Nicastro. 2011. Building blocks of the nexin-dynein regulatory complex in Chlamydomonas flagella. J Biol Chem 286:29175-91.

27. Ikeda, K., J. A. Brown, T. Yagi, J. M. Norrander, M. Hirono, E. Eccleston, R. Kamiya, and R. W. Linck. 2003. Rib72, a conserved protein associated with the ribbon compartment of flagellar A-microtubules and potentially involved in the linkage between outer doublet microtubules. J Biol Chem 278:7725-34.

28. Norrander, J. M., A. M. deCathelineau, J. A. Brown, M. E. Porter, and R. W. Linck. 2000. The Rib43a protein is associated with forming the specialized protofilament ribbons of flagellar microtubules in Chlamydomonas. Mol Biol Cell 11:201-15.

29. Linck, R. W., and J. M. Norrander. 2003. Protofilament ribbon compartments of ciliary and flagellar microtubules. Protist 154:299-311.

30. Bowman, A. B., R. S. Patel-King, S. E. Benashski, J. M. McCaffery, L. S. Goldstein, and S. M. King. 1999. Drosophila roadblock and Chlamydomonas LC7: a conserved family of dynein-associated proteins involved in axonal transport, flagellar motility, and mitosis. J Cell Biol 146:165-80.

31. Yang, P., and W. S. Sale. 1998. The Mr 140,000 intermediate chain of Chlamydomonas flagellar inner arm dynein is a WD-repeat protein implicated in dynein arm anchoring. Mol Biol Cell 9:3335-49.

32. DiBella, L. M., M. Sakato, R. S. Patel-King, G. J. Pazour, and S. M. King. 2004. The LC7 light chains of Chlamydomonas flagellar dyneins interact with components required for both motor assembly and regulation. Mol Biol Cell 15:4633-46.

33. Tam, L. W., and P. A. Lefebvre. 2002. The Chlamydomonas MBO2 locus encodes a conserved coiled-coil protein important for flagellar waveform conversion. Cell Motil Cytoskeleton 51:197-212.

34. Erzberger, J. P., and J. M. Berger. 2006. Evolutionary relationships and structural mechanisms of AAA+ proteins. Annu Rev Biophys Biomol Struct 35:93-114.

35. Cheney, R. E., and M. S. Mooseker. 1992. Unconventional myosins. Current opinion in cell biology 4:27-35.

36. Sugrue, P., M. R. Hirons, J. U. Adam, and M. E. Holwill. 1988. Flagellar wave reversal in the kinetoplastid flagellate *Crithidia oncopelti*. Biol Cell 63:127-31.

37. Sakato, M., and S. M. King. 2004. Design and regulation of the AAA+ microtubule motor dynein. J Struct Biol 146:58-71.

38. Oberholzer, M., M. A. Lopez, K. S. Ralston, and K. L. Hill. 2009. Approaches for functional analysis of flagellar proteins in African trypanosomes. Methods in Cell Biology 93:21-57.

39. Koonin, E. V. 2010. The Incredible Expanding Ancestor of Eukaryotes. Cell 40:606-608.

40. Keeling, P. J., G. Burger, D. G. Durnford, B. F. Lang, R. W. Lee, R. E. Pearlman, A. J. Roger, and M. W. Gray. 2005. The tree of eukaryotes. Trends in ecology & evolution 20:670-6.

41. Oberholzer, M., S. Morand, S. Kunz, and T. Seebeck. 2006. A vector series for rapid PCR-mediated C-terminal in situ tagging of Trypanosoma brucei genes. Mol Biochem Parasitol 145:117-20.

42. Robinson, D., P. Beattie, T. Sherwin, and K. Gull. 1991. Microtubules, tubulin, and microtubule-associated proteins of trypanosomes. Methods. Enzymol. 196:285-99.

43. Kohl, L., T. Sherwin, and K. Gull. 1999. Assembly of the paraflagellar rod and the flagellum attachment zone complex during the *Trypanosoma brucei* cell cycle. J Eukaryot Microbiol 46:105-109.

44. Ralston, K. S., N. K. Kisalu, and K. L. Hill. 2011. Structure-function analysis of dynein light chain 1 identifies viable motility mutants in bloodstream-form Trypanosoma brucei. Eukaryot Cell 10:884-94.

45. Rusconi, F., M. Durand-Dubief, and P. Bastin. 2005. Functional complementation of RNA interference mutants in trypanosomes. BMC Biotechnology 5:6.

46. Baron, D. M., Z. P. Kabututu, and K. L. Hill. 2007. Stuck in reverse: loss of LC1 in Trypanosoma brucei disrupts outer dynein arms and leads to reverse flagellar beat and backward movement. J Cell Sci 120:1513-20.

47. Walker, P. J., and J. C. Walker. 1963. Movement of trypanosome flagella. J. of Protozoology 10, suppl:32.

48. Kohl, L., and P. Bastin. 2005. The flagellum of trypanosomes. Int Rev Cytol 244:227-85.

49. Bower, R., D. Tritschler, K. Vanderwaal, C. A. Perrone, J. Mueller, L. Fox, W. S. Sale, and M. E. Porter. 2013. The N-DRC forms a conserved biochemical complex that maintains outer doublet alignment and limits microtubule sliding in motile axonemes. Mol Biol Cell.

50. Platts, A. E., D. J. Dix, H. E. Chemes, K. E. Thompson, R. Goodrich, J. C. Rockett, V. Y. Rawe, S. Quintana, M. P. Diamond, L. F. Strader, and S. A. Krawetz. 2007. Success and failure in human spermatogenesis as revealed by teratozoospermic RNAs. Hum Mol Genet 16:763-73.

51. Sinden, R. E. 1983. Sexual development of malarial parasites. Adv Parasitol 22:153-216.

52. Sinden, R. E., A. Talman, S. R. Marques, M. N. Wass, and M. J. Sternberg. 2010. The flagellum in malarial parasites. Curr Opin Microbiol 13:491-500.

53. Blanc, G., G. Duncan, I. Agarkova, M. Borodovsky, J. Gurnon, A. Kuo, E. Lindquist, S. Lucas, J. Pangilinan, J. Polle, A. Salamov, A. Terry, T. Yamada, D. D. Dunigan, I. V. Grigoriev, J. M. Claverie, and J. L. Van Etten. 2010. The Chlorella variabilis NC64A genome reveals adaptation to photosymbiosis, coevolution with viruses, and cryptic sex. Plant Cell 22:2943-55.

54. Woodland, H. R., and A. M. Fry. 2008. Pix proteins and the evolution of centrioles. PLoS One 3:e3778.

55. Grimsley, N., B. Pequin, C. Bachy, H. Moreau, and G. Piganeau. 2010. Cryptic sex in the smallest eukaryotic marine green alga. Mol Biol Evol 27:47-54.

56. Ralston, K. S., A. G. Lerner, D. R. Diener, and K. L. Hill. 2006. Flagellar Motility Contributes to Cytokinesis in Trypanosoma brucei and Is Modulated by an Evolutionarily Conserved Dynein Regulatory System. Eukaryotic Cell 5:696-711.

57. Broadhead, R., H. R. Dawe, H. Farr, S. Griffiths, S. R. Hart, N. Portman, M. K. Shaw, M. L. Ginger, S. J. Gaskell, P. G. McKean, and K. Gull. 2006. Flagellar

motility is required for the viability of the bloodstream trypanosome. Nature 440:224-7.

58. Branche, C., L. Kohl, G. Toutirais, J. Buisson, J. Cosson, and P. Bastin. 2006. Conserved and specific functions of axoneme components in trypanosome motility. J Cell Sci 119:3443-55.

59. Ralston, K. S., and K. L. Hill. 2008. The flagellum of Trypanosoma brucei: new tricks from an old dog. Int J Parasitol 38:869-84.

60. Porter, M. E., and W. S. Sale. 2000. The 9 + 2 axoneme anchors multiple inner arm dyneins and a network of kinases and phosphatases that control motility. J Cell Biol 151:F37-42.

61. Manton, I., K. Kowallik, and H. A. von Stosch. 1970. Observations on the fine structure and development of the spindle at mitosis and meiosis in a marine centric diatom (Lithodesmium undulatum). IV. The second meiotic division and conclusion. J Cell Sci 7:407-43.

62. Bernhard, D., D. D. Leipe, M. L. Sogin, and K. M. Schlegel. 1995. Phylogenetic relationships of the Nassulida within the phylum Ciliophora inferred from the complete small subunit rRNA gene sequences of Furgasonia blochmanni, Obertrumia georgiana, and Pseudomicrothorax dubius. J Eukaryot Microbiol 42:126-31.

63. Huang, B., Z. Ramanis, and D. J. Luck. 1982. Suppressor mutations in Chlamydomonas reveal a regulatory mechanism for Flagellar function. Cell 28:115-24.

64. Piperno, G., K. Mead, and W. Shestak. 1992. The inner dynein arms I2 interact with a "dynein regulatory complex" in Chlamydomonas flagella. J Cell Biol 118:1455-63.

65. Heuser, T., M. Raytchev, J. Krell, M. E. Porter, and D. Nicastro. 2009. The dynein regulatory complex is the nexin link and a major regulatory node in cilia and flagella. Journal of Cell Biology 187:921-33.

66. Yamniuk, A. P., and H. J. Vogel. 2004. Calmodulin's flexibility allows for promiscuity in its interactions with target proteins and peptides. Mol Biotechnol 27:33-57.

67. White, S. R., and B. Lauring. 2007. AAA+ ATPases: achieving diversity of function with conserved machinery. Traffic 8:1657-67.

68. Walker, J. E., M. Saraste, M. J. Runswick, and N. J. Gay. 1982. Distantly related sequences in the alpha- and beta-subunits of ATP synthase, myosin, kinases and other ATP-requiring enzymes and a common nucleotide binding fold. EMBO J 1:945-51.

69. Mizuno, N., M. Taschner, B. D. Engel, and E. Lorentzen. 2012. Structural studies of ciliary components. J Mol Biol 422:163-80.

70. Brokaw, C. J. 1987. Regulation of sperm flagellar motility by calcium and cAMP-dependent phosphorylation. J Cell Biochem 35:175-84.

71. Gibbons, I. R., M. P. Cosson, J. A. Evans, B. H. Gibbons, B. Houck, K. H. Martinson, W. S. Sale, and W. J. Tang. 1978. Potent inhibition of dynein adenosinetriphosphatase and of the motility of cilia and sperm flagella by vanadate. Proc Natl Acad Sci U S A 75:2220-4.

72. King, S. M. 2012. Integrated control of axonemal dynein AAA(+) motors. J Struct Biol 179:222-8.

73. Satir, P. 2011. Coiled-coils and motile cilia. Nature Genetics 43:10-11.

74. Wargo, M. J., E. E. Dymek, and E. F. Smith. 2005. Calmodulin and PF6 are components of a complex that localizes to the C1 microtubule of the flagellar central apparatus. J Cell Sci 118:4655-65.

75. Dymek, E. E., D. Goduti, T. Kramer, and E. F. Smith. 2006. A kinesin-like calmodulin-binding protein in Chlamydomonas: evidence for a role in cell division and flagellar functions. J Cell Sci 119:3107-16.

76. DiPetrillo, C. G., and E. F. Smith. 2010. Pcdp1 is a central apparatus protein that binds Ca(2+)-calmodulin and regulates ciliary motility. The Journal of cell biology 189:601-12.

77. Pazour, G. J., N. Agrin, J. Leszyk, and G. B. Witman. 2005. Proteomic analysis of a eukaryotic cilium. J Cell Biol 170:103-13.

78. Heuser, T., E. E. Dymek, J. Lin, E. F. Smith, and D. Nicastro. 2012. The CSC connects three major axonemal complexes involved in dynein regulation. Mol Biol Cell 23:3143-55.

79. Holwill, M. E., and J. L. McGregor. 1975. Control of flagellar wave movement in Crithidia oncopelti. Nature 255:157-8.

80. Holwill, M. E., and J. L. McGregor. 1976. Effects of calcium on flagellar movement in the trypanosome Crithidia oncopelti. J Exp Biol 65:229-42.

81. Hill, K. L. 2010. Parasites in motion: flagellum-driven cell motility in African trypanosomes. Curr Opin Microbiol 13:459-65.

82. Hughes, L. C., K. S. Ralston, K. L. Hill, and Z. H. Zhou. 2012. Three-dimensional structure of the Trypanosome flagellum suggests that the paraflagellar rod functions as a biomechanical spring. PLoS One 7:e25700.

83. Rodriguez, J. A., M. A. Lopez, M. C. Thayer, Y. Zhao, M. Oberholzer, D. D. Chang, N. K. Kisalu, M. L. Penichet, G. Helguera, R. Bruinsma, K. L. Hill, and J. Miao. 2009. Propulsion of African trypanosomes is driven by bihelical waves with alternating chirality separated by kinks. Proc Natl Acad Sci U S A 106:19322-7.

84. Koyfman, A. Y., M. F. Schmid, L. Gheiratmand, C. J. Fu, H. A. Khant, D. Huang, C. Y. He, and W. Chiu. 2011. Structure of Trypanosoma brucei flagellum accounts for its bihelical motion. Proc Natl Acad Sci U S A 108:11105-8.

85. Heddergott, N., T. Kruger, S. B. Babu, A. Wei, E. Stellamanns, S. Uppaluri, T. Pfohl, H. Stark, and M. Engstler. 2012. Trypanosome motion represents an adaptation to the crowded environment of the vertebrate bloodstream. PLoS Pathog 8:e1003023.

86. Ralston, K. S., Z. P. Kabututu, J. H. Melehani, M. Oberholzer, and K. L. Hill. 2009. The Trypanosoma brucei flagellum: moving parasites in new directions. Annual Review of Microbiology 63:335-62.

87. Lin, J., T. Heuser, B. I. Carbajal-Gonzalez, K. Song, and D. Nicastro. 2012. The structural heterogeneity of radial spokes in cilia and flagella is conserved. Cytoskeleton (Hoboken) 69:88-100.

88. Wirtz, E., S. Leal, C. Ochatt, and G. A. Cross. 1999. A tightly regulated inducible expression system for conditional gene knock-outs and dominant-negative genetics in *Trypanosoma brucei*. Mol. Biochem. Parasitol. 99:89-101.

89. Schultz, J., F. Milpetz, P. Bork, and C. P. Ponting. 1998. SMART, a simple modular architecture research tool: identification of signaling domains. Proc Natl Acad Sci U S A 95:5857-64.

90. LaCount, D. J., S. Bruse, K. L. Hill, and J. E. Donelson. 2000. Double-stranded RNA interference in *Trypanosoma brucei* using head-to-head promoters. Mol. Biochem. Parasitol. 111:67-76.

91. Benz, C., D. Nilsson, B. Andersson, C. Clayton, and D. L. Guilbride. 2005. Messenger RNA processing sites in Trypanosoma brucei. Mol Biochem Parasitol 143:125-34.

92. Redmond, S., J. Vadivelu, and M. C. Field. 2003. RNAit: an automated web-based tool for the selection of RNAi targets in Trypanosoma brucei. Mol Biochem Parasitol 128:115-8.

93. Chu, D. T., and M. W. Klymkowsky. 1989. The appearance of acetylated alpha-tubulin during early development and cellular differentiation in Xenopus. Dev Biol 136:104-17.

94. Hutchings, N. R., J. E. Donelson, and K. L. Hill. 2002. Trypanin is a cytoskeletal linker protein and is required for cell motility in African trypanosomes. Journal of Cell Biology 156:867-877.

95. Merchant, S., and L. Bogorad. 1986. Regulation by copper of the expression of plastocyanin and cytochrome c552 in Chlamydomonas reinhardi. Mol Cell Biol 6:462-9.

Chapter 4

Cryo-electron Tomography of the *T. brucei* Flagellum Reveals High-Resolution 3D Structural Analysis of the Axoneme and Identifies Structural Defects Caused by the Loss of CMF22

This chapter describes the efforts to determine the 3D structure of the *T. brucei* flagellum and to identify structural defects caused by loss of CMF22. I've employed cryo-electron tomography to determine differences between the CMF22-UKD mutant and wild-type procyclic 29-13 cells. In addition to potentially determining the sub-localization of CMF22, these results also revealed novel features of the *Trypanosoma brucei* flagellum. This work is the result of a collaboration with the laboratory of Dr. Hong Zhou in the UCLA Department of Microbiology, Immunology and Molecular Genetics, CnSI (UCLA), and Dr. Huy Bui, a Postdoctoral Fellow at the European Molecular Biology Laboratory in Heidelberg, Germany.

INTRODUCTION

Cilia, or flagella, or are highly conserved, evolutionarily ancient organelles with diverse functions in motility, environmental sensing, adhesion, mating and human development (1-3). In higher eukaryotes such as humans, defects in flagellar motility can cause a number of diseases, termed "ciliopathies", such as primary cilia dyskinesia, *situs inversus*, hydrocephalus, respiratory malfunction and male factor infertility. The first discovery of the association between structural defects of motile cilia and a human genetic disease (primary ciliary dyskinesia) was first demonstrated by Afzelius et al. in 1976 where electron microscopy of sperm from four subjects who produced immotile sperm showed that cilia from these sperm cells were missing the motor proteins (dyneins) required to convert chemical energy from ATP hydrolysis to mechanical

energy for movement (4). This breakthrough was the first of many other discoveries illustrating that structural defects in cilia results in ciliary disorders (5).

The most widely recognized role of flagella/cilia is for cellular motility, for example of mammalian sperm and of pathogenic protozoa such as *Trypanosoma spp., Leishmania spp., Giardia lamblia, and Trichomonas vaginalis* (6-8). Recently, *Trypanosoma brucei* has emerged an attractive model system for studies of flagellar biology due to the development of great molecular tools for molecular genetics (9). There are several advantages that make these parasites attractive model systems. For example, trypanosomes can be rapidly propagated in cell culture, can reach high densities for proteomic analyses, the genome is fully sequenced as well as annotated, and the flagellum skeleton is easily extracted using detergent and high salt (8-11). In addition, reverse genetic approaches such as efficient, inducible RNAi silencing is possible in *T. brucei* (12). The ease of genetic manipulation in *T. brucei* has led to genetic screens, comparative genomics, and proteomics to identify hundreds of putative flagellar proteins (13-16). These approaches have elucidated the highly conserved structure of the *T. brucei* axoneme, however there has been no study to define a high-resolution structural analysis of the *T. brucei* flagellum.

The canonical, eukaryotic motile cilium possess a 9+2 axoneme structure in which 9 “outer doublet” microtubules surround a central pair of singlet microtubules. The outer doublet microtubules also contain substructures for motility that include motor proteins called outer dynein arms (ODA), inner dynein arms (IDA), and radial spokes that project inwards from each outer doublet microtubule to interact with the central pair.

Additionally, the nexin-dynein regulatory complex (N-DRC) sits at the base of radial spokes on each doublet microtubule and is critical for motility regulation (17-21). Motility is achieved by hydrolysis of ATP on the dyneins to provide a mechanical force. These dyneins are coordinated around the circumference of the axoneme and along the length by signals from the central pair and radial spokes. These signals are then regulated through the N-DRC.

Much of the current knowledge of motility coordination is due to technological innovation in the area of high-resolution imaging. These advances have led to more refined structures since the first image of flagella in *Sphagnum* sperm using a metal shadowing whole-mounted, frayed axoneme technique (22). The development of electron tomography and cryo-electron tomography imaging techniques and the use of motility mutants have been made it possible to determine the contribution of protein complexes in coordinating motility. Studies in other model organisms such as *Chlamydomonas reinhardtii*, sea urchin sperm, tetrahymena, chicken chondrocyte cilia, and newt epithelial cilia have refined structures of the outer and inner dynein arms, microtubules doublets, central pair, radial spokes and nexin-dynein regulatory complex among other sub-structures (8). Recently, cryo-electron tomography has also defined novel axonemal substructures such as microtubule inner proteins (MIPs) (23) and novel interdoublet linkages (24). These high-resolution studies of the axoneme have revealed conserved structures across broad evolutionary distances as well as structural variation unique to each organism (25).

High-resolution cryo-electron tomography of *Chlamydomonas reinhardtii*, *Tetrahymena thermophila* and sea urchin sperm has identified many conserved and novel features. Authors compared the axonemal structure of three eukaryotes with diverse waveforms to identify differences that could account for these very different waveforms. The green alga *C. reinhardtii* have two flagella that synchronously beat in "breast-stroke" mode and have asymmetric recovery strokes. The beat in *C. reinhardtii* is planar and perpendicular to the axis of rotation. Another model system for flagellar biology is *Tetrahymena thermophila* in which hundreds of cilia are coordinated in metachronal waves and individually have asymmetric waveform. Finally, sea urchin sperm flagella differ through cyclical, symmetric waves that initiate at the base. Like *C. reinhardtii*, beating of tetrahymena and sea urchin sperm flagella is mostly planar. This comparative study illustrated very diverse molecular architecture in terms of arrangement of protein complexes on the doublet microtubules, microtubule inner proteins (MIPs), dynein structure, and N-DRC structures (25).

The advent of sequencing has led to numerous fully sequenced genomes from diverse eukaryotes. Although there is some controversy regarding the correct eukaryote tree of life, molecular phylogenies as well as morphological and biochemical evidence has suggested that there are five major "supergroups" that encompasses most eukaryotic diversity: Chromalveolates, Plantae, Excavates, Rhizaria, and Unikonts (26, 27). It has been hypothesized that the last common eukaryotic ancestor had a 9 + 2 motile flagellum and every extant branch of eukaryotes includes organisms with motile flagella (28). *C. reinhardtii*, *T. thermophila,* and sea urchin sperm are representative organisms with flagella from eukaryotic clades Plantae, Chromalveolates, and Unikonts

respectively. Thus far, *Bigelowiella natans* is the only flagellated Rhizaria that has been sequenced, however, the genome is not very well annotated therefore studies in this organism have been limited. On the other hand, since the first description 150 years ago, *Trypanosomes* have been a well-studied model organism for flagellar biology yet no high-resolution ultrastructural analysis has been performed on axonemes from this organism. *T. brucei* is a member of the Excavate supergroups that encompasses diverse groups of protists (26). Although it is unclear whether the Excavate supergroup is monophyletic, certain groups within the Excavates are arguably considered early branching lines in eukaryotic evolution, therefore studies in *T. brucei* flagella would add to current knowledge of evolution (26).

T. brucei has a unique beating pattern in which the beat propagates tip-to-base (29) and the beat is driven by bihelical waves with alternating chirality (30). Additionally, *T. brucei* represents a unique model system for studying eukaryotic flagella from a human pathogen. In comparison to primary ciliary dyskinesia, a rare autosomal recessive genetic disorder that affects one in 20,000 individuals, eukaryotic pathogens as a group is estimated to cause up to half a billion deaths worldwide (31-33). Thus far, there has been no high-resolution ultrastructural analysis of a eukaryotic human pathogen.

This study aims to define the three-dimenional architecture of the *T. brucei* flagellum as well as delineation of structural defects in *T. brucei* CMF22 (aka DRC11) mutants. CMF22, previously identified as axonemal protein that regulates propulsive motility in *T. brucei,* was hypothesized to be part of the N-DRC protein complex based

on the phylogenetic profile, axoneme location, co-immunoprecipitation with another DRC subunit (DRC4), and the presence of motility defects upon RNAi knockdown (34, 35). Additionally, this protein is lost in DRC2 and DRC4 mutants but not vice versa suggesting that CMF22 may be part of the outer lobes, which is a major contact for neighboring microtubules (21, 34). Antibodies to the CMF22 ortholog in *C. reinhardtii* has also shown decreased expression in *drc* mutants, however, there is no known mutant of CMF22 (35). CMF22 also has interesting domain structures that include the IQ motif and AAA domain, suggesting a potential signaling component for this protein. High-resolution structural analysis of this first mutant of the N-DRC lobe can therefore provide insight into mechanisms of axonemal motility.

RESULTS

T. brucei is missing dynein c and outer-inner dynein connector between the DRC and ODA

T. brucei flagella were prepared by detergent extraction to remove membranes and the subpellicular cytoskeleton was depolymerized using 150mM KCl, leaving the flagellum skeleton, axoneme plus PFR, intact. To purify the flagellum skeleton from cell body contaminants, the flagellum skeleton fraction was placed over buffer containing 30% sucrose and gently centrifuged. The top layer was concentrated and plunge frozen on carbon grids and tilt series were collected using dual-axis tilt tomography with *Batchtomography* software from FEI (36). Tilt series were used to assemble tomograms as described in (36). Substructures within the axoneme are arranged in a

repeating unit that repeats each 96nm along the length of each outer doublet microtubule. To obtain a high-resolution structure of the *T. brucei* repeating unit, subtomogram volumes encompassing the 96-nm repeat were extracted from six individual tomograms and 581 subtomograms were averaged to reconstruct the 3D structure of the *T. brucei* repeating unit (37).

One major observation is that the *T. brucei* flagellum has 2-headed ODA, similar to *Tetrahymena* and sea urchin sperm (Figure 4-1A, teal), and differing from the 3-headed ODA of *C. reinhardtii*. Additionally, the *T. brucei* axoneme has 3 full-length radial spokes (Figure 4-1A, blue). In contrast, *C. reinhardtii* has only two full-length spokes and a shortened “radial spoke stand-in” at the position of the third radial spoke. Compared to *Tetrahymena* and sea urchin sperm, *C. reinhardtii* seems to have the most divergent ultrastructure (25). Notably, among the inner dynein arms (IDAs), dynein c of the IDAs is present in all organisms for which there is a high-resolution 3D structure, but is missing on all outerdoublet microtubules in *T. brucei* (Figure 1B, red dashed circle). Dynein c groups with the IAD3 phylogenetic group (38). Phylogenetic analysis of *T. brucei* inner arm dynein genes has revealed that diversity of the gene of IAD3 group genes is quite restricted. *C. reinhardtii* has 6 genes within the IAD3 phylogenetic group, while*T. brucei* only has one (38). The limited diversity of IAD3 heavy chain genes may account for the lack of dynein c. Another interesting observation is that *C. reinhardtii* dynein c is required for flagellar beating at high viscosity (39). *T. brucei* are motile swimmers and efficiently swim in high viscosity (30). Therefore, the absence of dynein c suggests that cooperation among individual dyneins to drive axonemal beating may differ substantially among different organisms to swim in highly viscous environments.

C. reinhardtii axonemes have an important structure that connects the N-DRC to the outer dynein arms called the outer-inner dynein (OID) linker. This structure has been suggested to regulate both ODAs and IDAs to coordinate flagellar beating since mutants of this linker had an altered waveform (40). This structure, however, is missing in *T. brucei* axonemes as well as in *Tetrahymena* and sea urchin sperm (Figure 4-5C). Again, it appears that *C. reinhardtii* differs from *T. brucei*, *Tetrahymena*, and sea urchin sperm at the ultrastructure level to coordinate beating.

T. brucei has extensive structures that potentially connect to neighboring microtubules

Interconnections between outer doublets are critical to normal axoneme beating (40). Another feature unique to *T. brucei* is the extensive connections on every doublet microtubule that extend to the neighboring outer doublet (Figure 4-2). In *C. reinhardtii,* besides dyneins themselves, the only interdoublet connection present on all doublets is the N-DRC. *T. brucei,* on the other hand, has an extensive lobe structure on the I1 intermediate chain-light chain (I1 ICLC) complex in comparison to that of other organisms. A side view of the axoneme shows that this I1 ICLC is co-linear with the outer lobes of the N-DRC, a point of contact with the adjacent B-tubule (Figure 4-2B and C, yellow) (21). This extended lobe, in addition to the lobes of the N-DRC, makes the interdoublet connections between neighboring microtubules considerably more extensive than in other organisms. Additionally, *T. brucei* ODA-gamma exhibits a large extension from the N-terminal tail domain that extends significantly toward the

neighboring B-tubule, though it is not clear if this structure makes contact with the neighboring B-tubule (Figure 4-1, black arrow, Figure 4-2, teal).

T. brucei has novel MIP arrangement and a unique ponticulus structure within the B-tubule

Microtubule inner proteins (MIPs) are suggested to function in microtubule stability and molecular assembly of the axoneme (23). The resolution achieved in this study clearly identifies a variety of MIPs in *T. brucei* (Figure 4-3). MIP1b, MIP2a, and MIP3 (25, 41) are clearly visible within the *T. brucei* doublet microtubules (Figure 4-3C). *T. brucei* has additional unique MIPs in the B tubule attached to protofilaments B6-8 as well as a ponticulus, a large structure within the B-tubule that is only present in mature *T. brucei* flagella (Figure 4-3B) (42). This structure can be seen to be connected to the B-tubule at protofilaments B2-4 (Figure 4-3C). This structure is only found in *T. brucei* axonemes (42) and the role of this structure has not yet been identified.

Outer doublet asymmetry in the interdoublet linker and dynein b

Various studies using cryo-electron tomography in *C. reinhardtii* have illustrated structural features that differ between different outer doublet microtubules (43, 44). These include IDA arrangement, doublet specific bridges between adjacent microtubules, lack of ODAs, and specific structures associated with the I1 ICLC inner dynein arm (43, 45). The current study illustrates a similar asymmetry in a sub-structure of the I1 ICLC inner dynein arm that is hypothesized to interact with the adjacent microtubule. Doublets 1-3 have a smaller but protruding density, whereas doublets 4, 5-9 exhibit a larger density that spans a larger surface area closer to the microtubule

(Figure 4-4). There are 4 variations of this interdoublet linker in which doublet microtubules 1-3 are conserved, doublets 5-6 are conserved and doublets 8-9 are conserved. Doublet 4 appears to be unique (Figure 4-4). Interestingly, doublets 8-9 are also missing dynein b. There is poor resolution for doublet microtubule 7 due to the missing wedge effect and is therefore not shown.

A unique N-DRC structure in *T. brucei*

The N-DRC of *T. brucei* is at the same location as observed in *C. reinhardtii, Tetrahymena*, and sea urchin sperm. Compared to *C. reinhardtii* N-DRC (21), the *T. brucei* N-DRC has a smaller proximal lobe and a larger distal lobe (21). The *T. brucei* N-DRC has a large proximal lobe and the length of the lobes that is parallel to the microtubule is quite extensive (Figure 4-1, green). Presumably this results in an increased surface area for binding to the adjacent microtubule. Connections between the N-DRC to other protein complexes on the doublet microtubules are observed to be more extensive in *T. brucei* than reported for other organisms. These connections include contacts between the N-DRC (green) and the MIA complex (grey) (Figure 4-5A), radial spoke 2 (blue) and IDAs 4 and 5 (red) (Figure 4-5C). The N-DRC connections to the MIA complex also appear to be much more extensive in *T. brucei* than in *C. reinhardtii* (21).

The N-DRC is a broadly conserved structure that is a central regulator for coordinating flagellar beat (17-21). The N-DRC is predicted to be a 1.5 megadalton complex and a number of subunits (DRC1-11) have been identified in *T. brucei*, *C. reinhardtii,* and humans (21, 46-49). Some of these subunits have been mapped within

the N-DRC using cryo-electron tomography in various *drc* mutants in *C. reinhardtii*, however many subunits as well as the arrangement of certain subunits within the complex remain unknown (21). CMF22, aka DRC11 is a recently identified N-DRC axonemal protein that is suspected to be an N-DRC subunit (34). An N-DRC assignment for CMF22 is based on co-immunoprecipitation with DRC4 and the observation that CMF22 interaction with the axoneme is reduced in *drc* mutants in *T. brucei* and *C. reinhardtii* (34, 35). Notably, loss of CMF22 did not alter the interaction of DRC2 and DRC4 with the axoneme (34). The location of CMF22 within the N-DRC is unknown, therefore, to determine if the N-DRC structure is affected by loss of CMF22, we used cryo-electron tomography to resolve the 3D structure of the 96-nm repeat unit in axonemes from *T. brucei* CMF22 knockdown cells (CMF22-UKD). For this, 909 subtomograms were extracted from 10 individual flagella tomograms and were averaged to identify structures altered in CMF22-UKD axonemes. In the CMF22-UKD axonemes, a large portion of the proximal lobe and a smaller portion of the distal lobe are missing (Figure 6). In addition, a protrusion on the left side of the N-DRC linker region is altered in the CMF22-UKD axonemes (Figure 6). This data indicates that CMF22 is localized to the N-DRC proximal lobe or is an adaptor protein that is required for assembly of the proximal lobe. The clarity of the CMF22 knockdown structural defect illustrates the strong penetrance of knockdown and demonstrates the value of *T. brucei* RNAi lines for high-resolution structural analysis. Earlier work using cryo-electron tomography of *C. reinhardtii* mutants generated by amiRNA-mediated knockdown of axonemal protein complexes was challenging due to the heterogeneity of the mutant

(50). *T. brucei* is therefore an excellent model system for ultrastructure studies for flagellar biology.

DISCUSSION

Cryo-electron tomography of *T. brucei* axonemes adds to the current knowledge of flagellar biology in that it is the first high-resolution structure for an organism from the Excavate supergroup, which are considered to be deep brancing eukaryotes. Notably, this is also the first high-resolution 3D ultrastructure study of axonemes from a pathogenic organism. Our studies have revealed that the *T. brucei* flagellum has many general features that are more similar to *Tetrahymena* and sea urchin sperm than to *Chlamydomonas reinhardtii*. *T. brucei* has 2-headed ODAs, three full-length radial spokes and a missing OID linker. The *T. brucei* axoneme also has several unique features such as much more extensive network of protrusions that potentially contact the adjacent microtubule, a novel ponticulus, novel MIP arrangement, outer doublet asymmetry, and a unique N-DRC. These novel features may contribute unique features of trypanosome flagellum beating, such as the tip-to-base beating pattern in which the beat is driven by bihelical waves with alternating chirality (30). Possibly, this unique waveform allows this parasite to be uniquely pathogenic and key molecular arrangement of sub-complexes on the *T. brucei* axoneme may modulate this distinct waveform. Further investigation of other pathogenic protozoans with motile flagella can provide insight into conserved mechanisms of eukaryotic pathogenesis through flagellar motility.

Additionally, we have identified the first ever proximal lobe mutant of the N-DRC, demonstrating the importance of this lobe in regulating propulsive motility. Unlike other known mutants of the N-DRC, inner arm dyneins were unaffected by the loss of CMF22. As such, this is the first clear motility defect that can be entirely attributed to perturbation of the N-DRC, as opposed to the N-DRC plus dyneins. Experiments to isolate the sub-complex of CMF22 and the proteins that potentially interact are underway. In a previous experiment, expression of an epitope-tagged CMF22 in another N-DRC mutant, trypanin, results CMF22-HA becoming solubilized (34). RNAi knockdown of trypanin releases a ~900 kDa complex that contains CMF22-HA in the soluble S1 fraction (data not shown). CMF22-HA can be co-immunoprecipitated using anti-HA antibody (not shown), hence mudpit MS/MS mass spectrometry analysis can now be used to define the CMF22 sub-complex.

Additional work using stable isotope labeling by amino acids (SILAC) to identify quantitative differences between different N-DRC mutants and wild-type cells will also be useful to define not only the sub-complex of CMF22, but also which N-DRC proteins are lost in the CMF22 mutant and other N-DRC mutants. Defining these proteins may elucidate the mechanism of motility regulation via CMF22, provide a model of protein-protein interaction required for assembly of the N-DRC, and identify additional N-DRC proteins. This study, along with concurrent cryo-electron tomography studies of other N-DRC mutants will provide a molecular map of the *T. brucei* N-DRC, a central regulator of motility coordination. Identification of human homologs of these core proteins will be useful in evaluating gene products that may be important for the regulation of motility for ciliopathic diseases. A recent study revealed the importance of studying the composition

of the N-DRC. DRC1, a subunit of the N-DRC that is localized to the base plate was shown to be involved in primary ciliary dyskinesia pathogenesis (49). Therefore, the identification of additional N-DRC components advances not only our current knowledge of key regulators, but also a mechanism of how cilia motility fails in ciliary diseases.

MATERIALS AND METHODS

Axoneme preparations:

Procyclic 29-13 wild-type and CMF22-UKD *T. brucei* cells were cultured in Cunningham's SM Medium supplemented with 10% heat-inactivated fetal calf serum, 15 mg/mL G418 and 50mg/mL hygromycin (9). The CMF22-UKD cell line was previously generated in (34). Approximately $4x10^8$ cells from each cell line was used for cryo-electron tomography. Cells were washed three times in PBS and resuspended in extraction buffer [20mM HEPES, 1mM $MgCl_2$, 150mM KCl, 0.5% NP-40, 2x protease inhibitor cocktail (Sigma, EDTA-free), 1x DNase buffer (Turbo DNase, Invitrogen) and 1x Dnase (Turbo DNase, Invitrogen)] at a final concentration of $2x10^6$ cells/μL. Cells were incubated at room temperature for 15 minutes and $CaCl_2$ was added to samples for a final concentration of 1mM. Samples were incubated on ice for 30 mins to solubilize the subpellicular microtubules and centrifuged at 4 °C at 8000 rpm for 10 minutes to isolate insoluble flagella. The supernatant was discarded and the pellet was resuspended in extraction buffer at a final concentration of $4x10^6$ cells/μL. The sample

was carefully overlaid on top of three times the volume of ice-cold 30% (w/v) sucrose supplemented with 10mM HEPES, 5mM $MgSO_4$, and 1mM DTT. The two-layer mixture was centrifuged at 4 °C at 3000 rpm for 5 minutes and half of the upper volume was pipetted into a clean microcentrifuge tube. The sample was washed several times in extraction buffer without detergent and resuspended at a final concentration of $1.6x10^7$ cells/μL.

Quick freezing, cryo-electron tomography, and image analysis:

Samples were plunge frozen and applied on carbon grids with colloidal gold particles as markers for tomographic reconstruction. Cryo-electron tomography and data processing was performed as described in (36). Each tilt series was taken with a defocus of −3 μm from −70° to +70° tilt along alpha and beta tilt axes, with 2° increments at the lower tilt angles (range ± 40°) and 1° increments above +40° and below −40°. Dual axis data sets were achieved by taking single tilt data sets at several points of the grid before manually rotating the grid by 90° and taking the second tilt series at the same locations. For surfaced rendered reconstructions, 6 flagella (581 subtomograms) from wild-type procyclic *T. brucei* cells and 10 flagella (909 subtomograms) from CMF22-UKD cells were averaged as previously described in (25, 51). Segmentation of components (ODA, IDA, RS and N-DRC) was based on axonemes from *C. reinhardtii* (21, 25, 52-54).

FIGURES

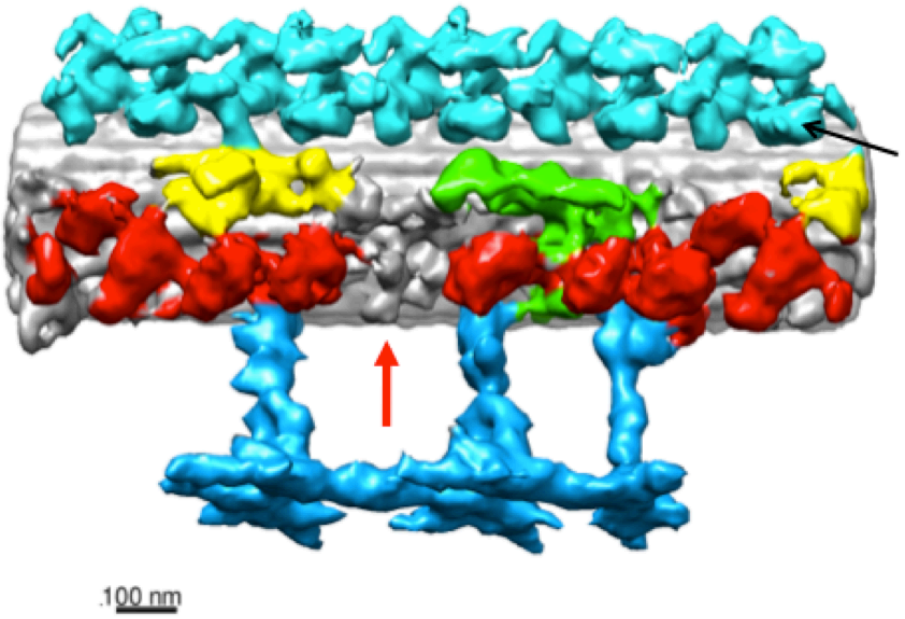


Figure 4-1. Cryo-electron tomography of the *T. brucei* flagella. (A) Cryo-electron tomography of 6 flagella, consisting of 581 tomograms of the 96 nm repeat. Colored as follows: ODA (teal), IDA (red), radial spokes (blue), Intermediate chain-light chain 1 (yellow, left), N-DRC (green). (B) *T. brucei* axonemes are missing inner dynein arm c (red dashed circle, red arrow). *T. brucei* ODA-gamma exhibits a large extension from the N-terminal tail domain that potentially interacts with neighboring microtubules (black dotted circle, black arrow).

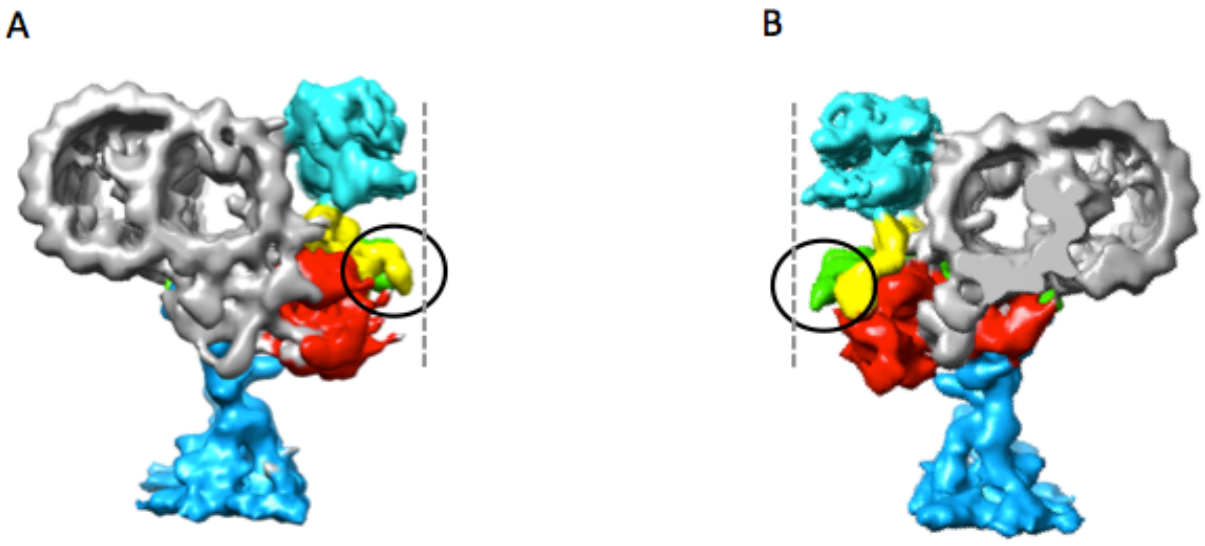


Figure 4-2. The *T. brucei* flagellum has extensive features to interact with the adjacent microtubule. (A) Side view of wild-type axonemes as seen from the left side of Figure 4-1. The *T. brucei* intermediate chain-light chain I1 dynein arm (yellow) has an extended lobe (black circle) that is co-linear with the outer doublet microtubules, depicted by the dashed line. (B) Side view of wild-type axonemes as seen from the right side of Figure 4-1. The N-DRC (green) also extends to the same plane (depicted by the dashed line) as the outer doublet microtubules and may interact with adjacent microtubules. Additionally the large protrusion of the N-terminal tail domain of ODA-gamma is depicted as the teal globular structure almost touching the dashed line.

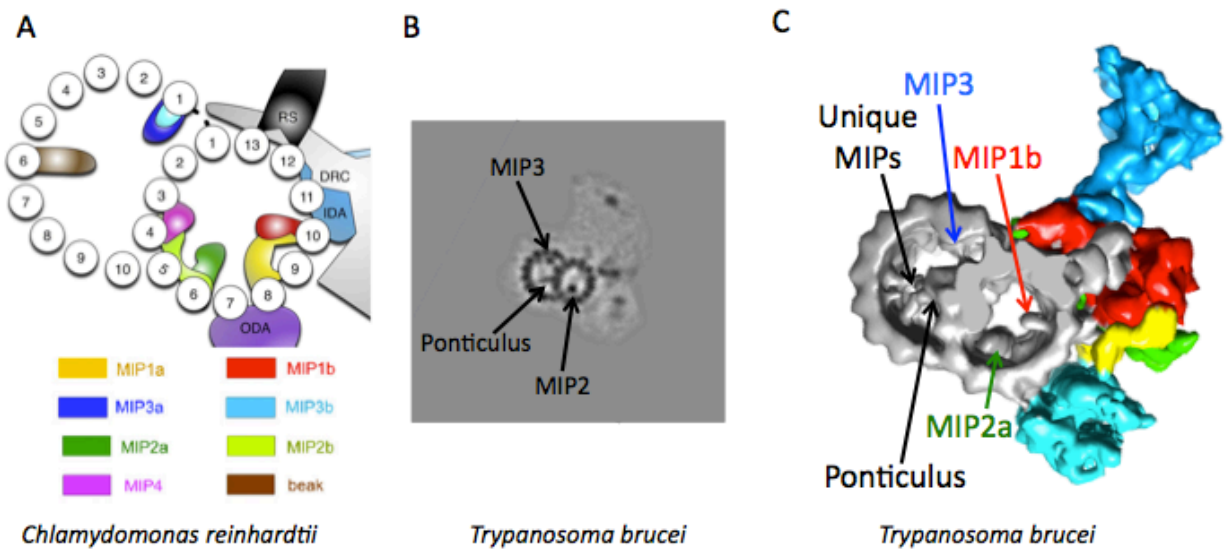


Figure 4-3. Conserved and unique MIPs of *T. brucei*. (A) Schematic of MIPs in *C. reinhardtii* is adapted from (25). (B) Density map of a cross section of the *T. brucei* axoneme shows MIPs within the doublet microtubules. Densities correlate to MIP2 (MIP2a and/or MIP2b), MIP3 (MIP3a and/or MIP3b) and a large density that spans almost through the B-tubule, the ponticulus. (C) Average tomograms and surface rendering of a cross section of the *T. brucei* axoneme illustrate conserved MIPs to *C. reinhardtii* (colored) and unique MIPs to *T. brucei* (black).

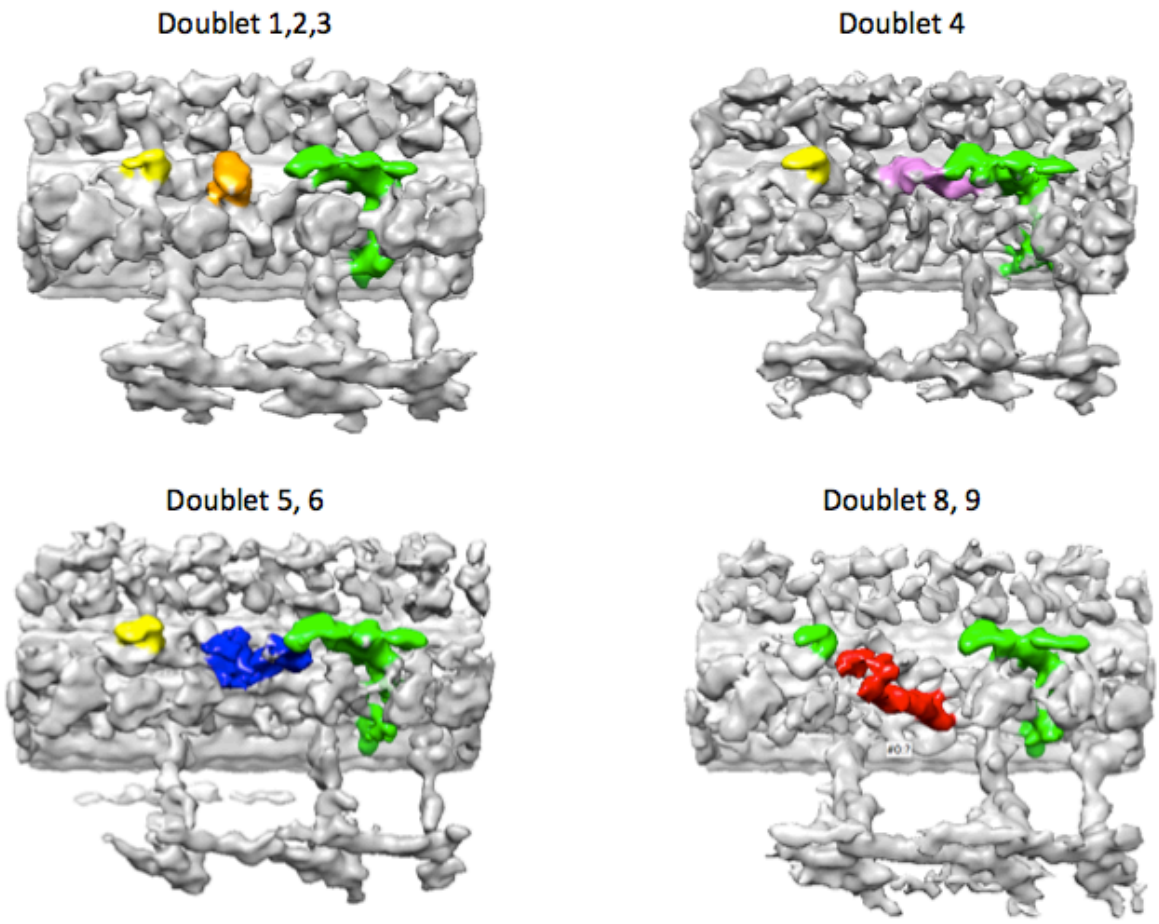


Figure 4-4. Doublet specific features of the *T. brucei* axoneme. Surface rendering of average tomograms of doublet microtubules illustrate doublet specific features of the intermediate chain-light chain I1 inner arm dynein (yellow in doublets 1-6, green in doublets 8-9) and the predicted interdoublet linker (orange for doublets 1-3, purple for doublet 4, blue for doublets 5-6, and red for doublets 8-9).

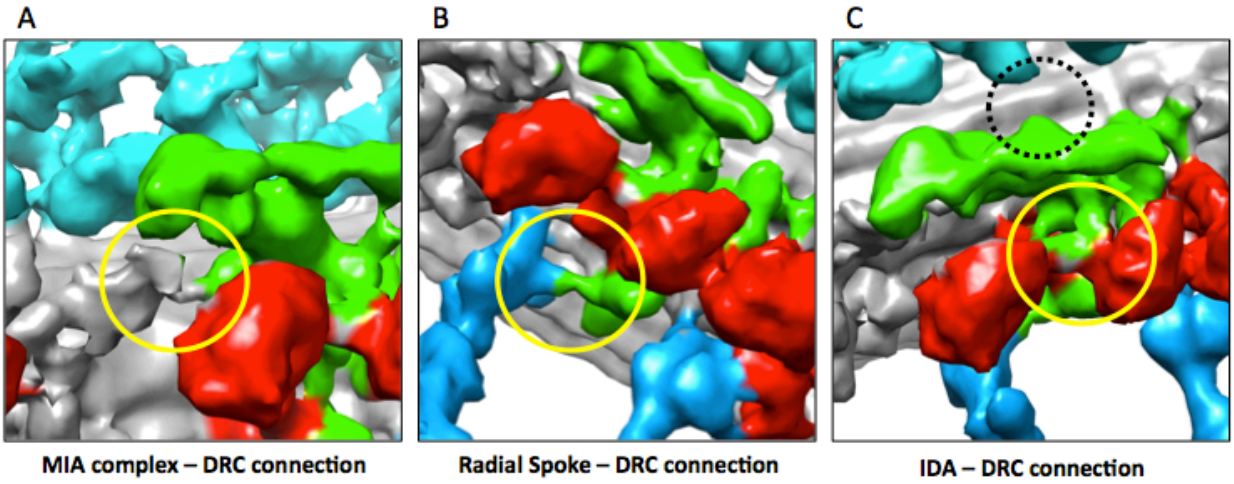


Figure 4-5. Connections of the N-DRC to axonemal protein complexes. (A) The N-DRC (green) has a connection to the predicted MIA complex (grey, yellow circle), (B) radial spoke 2 (blue, yellow circle), and (C) the inner dynein arms 4 and 5 (red, yellow circle). Notably, the N-DRC has no connections with the ODA (dashed circle).

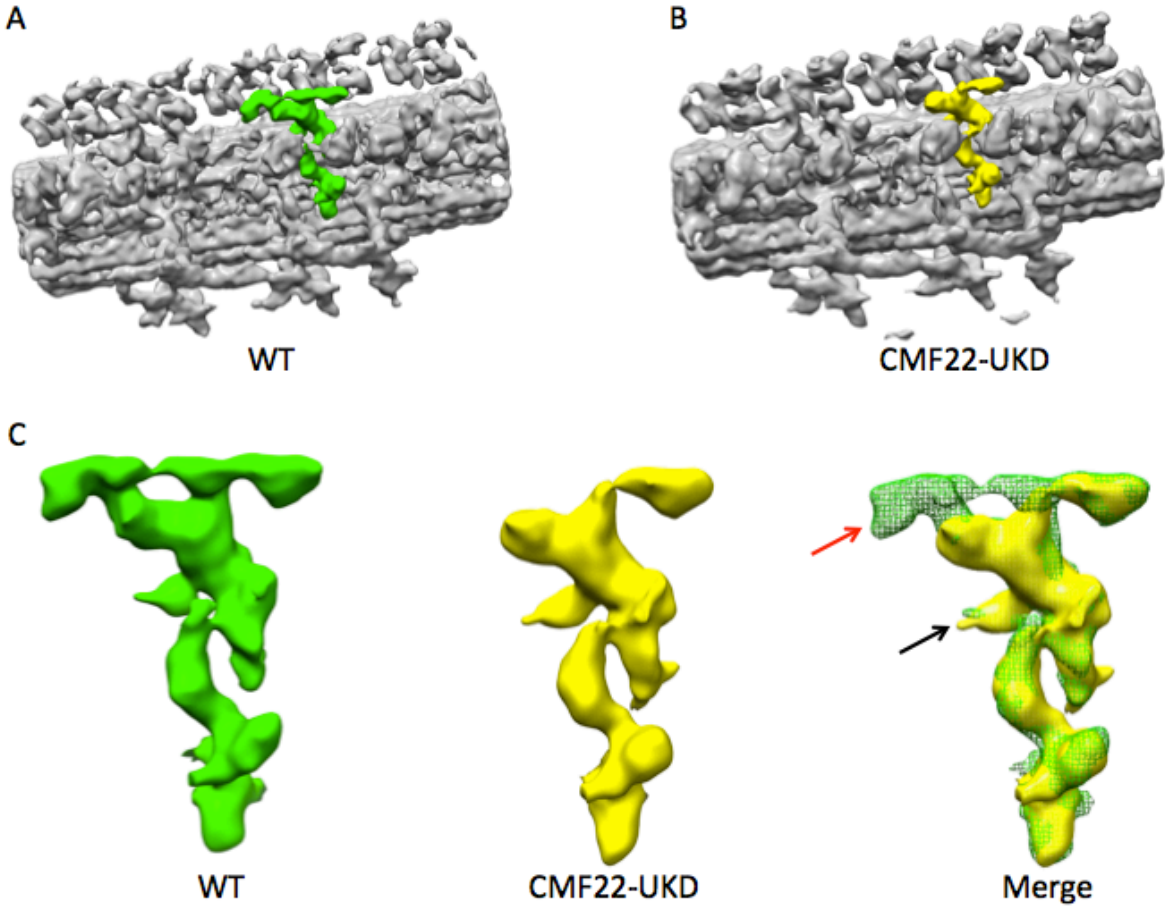


Figure 4-6. The *T. brucei* N-DRC structure. Surface rendering of the wild-type (A) and CMF22-UKD (B) *T. brucei* axoneme reveals the N-DRC in green and yellow, respectively. (C) The N-DRC in wild-type (green) is compared to that of CMF22-UKD (yellow) and the merged image shows the missing proximal lobe (red arrow), part of the distal lobe, and a “nub” that is altered in the CMF22-UKD mutant (black arrow).

REFERENCES

1. Fritz-Laylin, L. K., S. E. Prochnik, M. L. Ginger, J. B. Dacks, M. L. Carpenter, M. C. Field, A. Kuo, A. Paredez, J. Chapman, and J. Pham. 2010. The Genome of Naegleria gruberi Illuminates Early Eukaryotic Versatility. Cell 140:631-642.
2. Takeda, S., and K. Narita. 2012. Structure and function of vertebrate cilia, towards a new taxonomy. Differentiation 83:S4-11.
3. Wilson, N. F. 2008. Gametic cell adhesion and fusion in the unicellular alga Chlamydomonas. Methods Mol Biol 475:39-51.
4. Afzelius, B. A. 1976. A human syndrome caused by immotile cilia. Science 193:317-9.
5. Bisgrove, B. W., and H. J. Yost. 2006. The roles of cilia in developmental disorders and disease. Development 133:4131-43.
6. Ginger, M. L., N. Portman, and P. G. McKean. 2008. Swimming with protists: perception, motility and flagellum assembly. Nat Rev Microbiol 6:838-50.
7. Bastin, P., T. J. Pullen, F. F. Moreira-Leite, and K. Gull. 2000. Inside and outside of the trypanosome flagellum:a multifunctional organelle. Microbes Infect 2:1865-74.
8. Vincensini, L., T. Blisnick, and P. Bastin. 2011. 1001 model organisms to study cilia and flagella. Biol Cell 103:109-30.
9. Oberholzer, M., M. A. Lopez, K. S. Ralston, and K. L. Hill. 2009. Approaches for functional analysis of flagellar proteins in African trypanosomes. Methods in Cell Biology 93:21-57.

10. Broadhead, R., H. R. Dawe, H. Farr, S. Griffiths, S. R. Hart, N. Portman, M. K. Shaw, M. L. Ginger, S. J. Gaskell, P. G. McKean, and K. Gull. 2006. Flagellar motility is required for the viability of the bloodstream trypanosome. Nature 440:224-7.

11. Hart, S. R., K. W. Lau, Z. Hao, R. Broadhead, N. Portman, A. Huhmer, K. Gull, P. G. McKean, S. J. Hubbard, and S. J. Gaskell. 2009. Analysis of the trypanosome flagellar proteome using a combined electron transfer/collisionally activated dissociation strategy. Journal of the American Society for Mass Spectrometry 20:167-75.

12. Wirtz, E., S. Leal, C. Ochatt, and G. A. Cross. 1999. A tightly regulated inducible expression system for conditional gene knock-outs and dominant-negative genetics in *Trypanosoma brucei*. Mol. Biochem. Parasitol. 99:89-101.

13. Gherman, A., E. E. Davis, and N. Katsanis. 2006. The ciliary proteome database: an integrated community resource for the genetic and functional dissection of cilia. Nat Genet 38:961-2.

14. Arnaiz, O., A. Malinowska, C. Klotz, L. Sperling, M. Dadlez, F. Koll, and J. Cohen. 2009. Cildb: a knowledgebase for centrosomes and cilia. Database (Oxford) 2009:bap022.

15. Portman, N., S. Lacomble, B. Thomas, P. G. McKean, and K. Gull. 2008. Combining RNA Interference Mutants and Comparative Proteomics to Identify Protein Components and Dependences in a Eukaryotic Flagellum. Journal of Biological Chemistry 284:5610-5619.

16. Baron, D. M., K. S. Ralston, Z. P. Kabututu, and K. L. Hill. 2007. Functional genomics in Trypanosoma brucei identifies evolutionarily conserved components of motile flagella. J Cell Sci 120:478-91.

17. Porter, M. E., and W. S. Sale. 2000. The 9 + 2 axoneme anchors multiple inner arm dyneins and a network of kinases and phosphatases that control motility. J Cell Biol 151:F37-42.

18. Huang, B., Z. Ramanis, and D. J. Luck. 1982. Suppressor mutations in Chlamydomonas reveal a regulatory mechanism for Flagellar function. Cell 28:115-24.

19. Brokaw, C. J., D. J. Luck, and B. Huang. 1982. Analysis of the movement of Chlamydomonas flagella:" the function of the radial-spoke system is revealed by comparison of wild-type and mutant flagella. J Cell Biol 92:722-32.

20. Gardner, L. C., E. O'Toole, C. A. Perrone, T. Giddings, and M. E. Porter. 1994. Components of a "dynein regulatory complex" are located at the junction between the radial spokes and the dynein arms in Chlamydomonas flagella. J Cell Biol 127:1311-25.

21. Heuser, T., M. Raytchev, J. Krell, M. E. Porter, and D. Nicastro. 2009. The dynein regulatory complex is the nexin link and a major regulatory node in cilia and flagella. Journal of Cell Biology 187:921-33.

22. Manton, I. a. C., B. . 1952. An electron microscope study of the spermatozoid of *Sphagnum*. Journal of experimental botany 3:265-275.

23. Nicastro, D., C. Schwartz, J. Pierson, R. Gaudette, M. E. Porter, and J. R. McIntosh. 2006. The molecular architecture of axonemes revealed by cryoelectron tomography. Science 313:944-8.

24. Bui, K. H., H. Sakakibara, T. Movassagh, K. Oiwa, and T. Ishikawa. 2009. Asymmetry of inner dynein arms and inter-doublet links in Chlamydomonas flagella. Journal of Cell Biology 186:437-46.

25. Pigino, G., A. Maheshwari, K. H. Bui, C. Shingyoji, S. Kamimura, and T. Ishikawa. 2012. Comparative structural analysis of eukaryotic flagella and cilia from Chlamydomonas, Tetrahymena, and sea urchins. J Struct Biol 178:199-206.

26. Keeling, P. J., G. Burger, D. G. Durnford, B. F. Lang, R. W. Lee, R. E. Pearlman, A. J. Roger, and M. W. Gray. 2005. The tree of eukaryotes. Trends in ecology & evolution 20:670-6.

27. Koonin, E. V. 2010. The Incredible Expanding Ancestor of Eukaryotes. Cell 40:606-608.

28. Mitchell, D. R. 2007. The evolution of eukaryotic cilia and flagella as motile and sensory organelles. Adv Exp Med Biol 607:130-40.

29. Walker, P. J. 1961. Organization of function in trypanosome flagella. Nature 189:1017-8.

30. Rodriguez, J. A., M. A. Lopez, M. C. Thayer, Y. Zhao, M. Oberholzer, D. D. Chang, N. K. Kisalu, M. L. Penichet, G. Helguera, R. Bruinsma, K. L. Hill, and J. Miao. 2009. Propulsion of African trypanosomes is driven by bihelical waves with alternating chirality separated by kinks. Proc Natl Acad Sci U S A 106:19322-7.

31. Alvar, J., I. D. Velez, C. Bern, M. Herrero, P. Desjeux, J. Cano, J. Jannin, M. den Boer, and W. H. O. L. C. Team. 2012. Leishmaniasis worldwide and global estimates of its incidence. PLoS One 7:e35671.

32. Haldar, K., S. Kamoun, N. L. Hiller, S. Bhattacharje, and C. van Ooij. 2006. Common infection strategies of pathogenic eukaryotes. Nat Rev Microbiol 4:922-31.

33. Stuart, K., R. Brun, S. Croft, A. Fairlamb, R. E. Gurtler, J. McKerrow, S. Reed, and R. Tarleton. 2008. Kinetoplastids: related protozoan pathogens, different diseases. J Clin Invest 118:1301-10.

34. Nguyen, H. T., J. Sandhu, G. Langousis, and K. L. Hill. 2013. CMF22 is a broadly conserved axonemal protein and is required for propulsive motility in Trypanosoma brucei. Eukaryot Cell 12:1202-13.

35. Bower, R., D. Tritschler, K. Vanderwaal, C. A. Perrone, J. Mueller, L. Fox, W. S. Sale, and M. E. Porter. 2013. The N-DRC forms a conserved biochemical complex that maintains outer doublet alignment and limits microtubule sliding in motile axonemes. Mol Biol Cell.

36. Hughes, L. C., K. S. Ralston, K. L. Hill, and Z. H. Zhou. 2012. Three-dimensional structure of the Trypanosome flagellum suggests that the paraflagellar rod functions as a biomechanical spring. PLoS One 7:e25700.

37. Bui, K. H. a. I. T. 2013. 3D structural analysis of flagella/cilia by cryo-electron tomography. . Methods Enzymol. 524:305-23.

38. Ralston, K. S., Z. P. Kabututu, J. H. Melehani, M. Oberholzer, and K. L. Hill. 2009. TheTrypanosoma brucei Flagellum: Moving Parasites in New Directions. Annual review of microbiology 63:335-362.

39. Yagi, T., I. Minoura, A. Fujiwara, R. Saito, T. Yasunaga, M. Hirono, and R. Kamiya. 2005. An Axonemal Dynein Particularly Important for Flagellar Movement at High Viscosity: IMPLICATIONS FROM A NEW CHLAMYDOMONAS MUTANT DEFICIENT IN THE DYNEIN HEAVY CHAIN GENE DHC9. J Biol Chem 280:41412-20.

40. Oda, T., T. Yagi, H. Yanagisawa, and M. Kikkawa. 2013. Identification of the outer-inner dynein linker as a hub controller for axonemal dynein activities. Curr Biol 23:656-64.

41. Nicastro, D., X. Fu, T. Heuser, A. Tso, M. E. Porter, and R. W. Linck. 2011. Cryo-electron tomography reveals conserved features of doublet microtubules in flagella. Proc Natl Acad Sci U S A 108:E845-53.

42. Vickerman, K. 1969. On the surface coat and flagellar adhesion in trypanosomes. J Cell Sci 5:163-93.

43. Lin, J., T. Heuser, K. Song, X. Fu, and D. Nicastro. 2012. One of the nine doublet microtubules of eukaryotic flagella exhibits unique and partially conserved structures. PLoS One 7:e46494.

44. Bui, K. H., T. Yagi, R. Yamamoto, R. Kamiya, and T. Ishikawa. 2012. Polarity and asymmetry in the arrangement of dynein and related structures in the Chlamydomonas axoneme. J Cell Biol 198:913-25.

45. Heuser, T., C. F. Barber, J. Lin, J. Krell, M. Rebesco, M. E. Porter, and D. Nicastro. 2012. Cryoelectron tomography reveals doublet-specific structures and unique interactions in the I1 dynein. Proc Natl Acad Sci U S A 109:E2067-76.

46. Ralston, K. S., and K. L. Hill. 2006. Trypanin, a Component of the Flagellar Dynein Regulatory Complex, Is Essential in Bloodstream Form African Trypanosomes. PLoS Pathogens 2:873-882, e101 doi:10.1371/journal.ppat.0020101.

47. Rupp, G., and M. E. Porter. 2003. A subunit of the dynein regulatory complex in Chlamydomonas is a homologue of a growth arrest-specific gene product. J Cell Biol 162:47-57.

48. Kabututu, Z. P., M. Thayer, J. H. Melehani, and K. L. Hill. 2010. CMF70 is a subunit of the dynein regulatory complex. Journal of Cell Science 123:3587-95.

49. Wirschell, M., H. Olbrich, C. Werner, D. Tritschler, R. Bower, W. S. Sale, N. T. Loges, P. Pennekamp, S. Lindberg, U. Stenram, B. Carlen, E. Horak, G. Kohler, P. Nurnberg, G. Nurnberg, M. E. Porter, and H. Omran. 2013. The nexin-dynein regulatory complex subunit DRC1 is essential for motile cilia function in algae and humans. Nat Genet 45:262-8.

50. Heuser, T., E. E. Dymek, J. Lin, E. F. Smith, and D. Nicastro. 2012. The CSC connects three major axonemal complexes involved in dynein regulation. Mol Biol Cell 23:3143-55.

51. Bui, K. H., G. Pigino, and T. Ishikawa. 2011. Three-dimensional structural analysis of eukaryotic flagella/cilia by electron cryo-tomography. J Synchrotron Radiat 18:2-5.

52. Ishikawa, T., H. Sakakibara, and K. Oiwa. 2007. The architecture of outer dynein arms in situ. J Mol Biol 368:1249-58.

53. Bui, K. H., H. Sakakibara, T. Movassagh, K. Oiwa, and T. Ishikawa. 2008. Molecular architecture of inner dynein arms in situ in Chlamydomonas reinhardtii flagella. J Cell Biol 183:923-32.

54. Pigino, G., K. H. Bui, A. Maheshwari, P. Lupetti, D. Diener, and T. Ishikawa. 2011. Cryoelectron tomography of radial spokes in cilia and flagella. J Cell Biol 195:673-87.

Chapter 5

The Role of the CMF22 IQ and AAA domains in *T. brucei* Motility

As described in Chapter 2, CMF22 has two domains of interest: an IQ motif for calcium signaling and an ATPase Associated with various cellular Activities (AAA) domain for effector function. Chapter 3 describes efforts to identify if these domains function in regulating propulsive motility and adds insight into a working model on how motility coordination is achieved through CMF22.

Introduction

The eukaryotic flagellum is an evolutionarily ancient organelle with genomic evidence suggesting that the last eukaryotic common ancestor had a motile flagellum (1, 2). The eukaryotic flagellum, also known as cilium, has diverse functions that include motility, environmental sensing, adhesion, and mating (3, 4). Flagella are widely recognized to function in cellular propulsion for many pathogenic protozoa such as *Trypanosoma spp., Leishmania spp., Giardia lamblia,* and *Trichomonas vaginalis* (5-7). In higher eukaryotes such as humans, flagellar motility is required for normal development and physiology (8-10). A number of ciliopathies including primary ciliary dyskinesia, *situs inversus,* hydrocephalus, respiratory malfunction and male factor infertility arise due to motility defects of cilia in human cells (11).

Trypanosoma brucei are vigorous swimmers that move through viscous environments such as blood. An unusual feature of trypanosome motility is that the organism moves with the tip of the flagellum leading, which is reversed in most flagellated organisms. The general mechanism of motility in *T. brucei* is conserved with that of other diverse eukaryotes with motile flagella (12). There has been tremendous

research using *T. brucei* as a model organism for flagellar biology (7, 13). Motility is achieved through coordination of inner and outer dynein motor proteins that provide power for microtubule sliding around and along the length of the canonical 9+ 2 axoneme (12, 14). Current models suggest that dyneins are coordinated by other protein complexes on the axoneme which includes the central pair, radial spokes, and the nexin-dynein regulatory complex (N-DRC), however, how these complexes are coordinated for motility and the effectors to transmit regulatory signals have not yet been identified (15-19).

Decades of work in *Chlamydomonas reinhardtii* have revealed that the N-DRC, a complex that sits at the base of the radial spokes and interacts with inner dynein arms, is a hub of regulating axonemal motility (20-22). Dynein regulation by the N-DRC require proteins with a signaling capacity, however, while many subunits of the N-DRC thus far identified have coiled-coiled domains and motifs for protein-protein interaction, very few have domains predicted to confer regulatory inputs. The N-DRC is a broadly conserved complex in organisms with motile flagella (23-26), therefore, in order to identify effector proteins that regulate N-DRC activity and other core components of motile flagella, our lab performed an *in silico* screen of 10 genomes from diverse eukaryotes to identify genes broadly and uniquely conserved in eukaryotes with motile cilia. This phylogenetic screen identified a cohort of fifty genes, the core Components of Motile Flagella (CMF) genes, that were present in eukaryotes with motile flagella but were absent in organisms that lack flagella (27). This initial study was expanded in a recent work that compared the CMF genes across 115 eukaryotic genomes, leading to the identification of CMF22 as a gene that stood out as being one of the most

conserved CMF genes and contained domains of interest for regulation by Ca^{2+} and ATP (28). CMF22 domain architecture consists of an N-terminal IQ motif and a C-terminal ATPase Associated with various cellular Activities (AAA) domain, both of which make it a promising candidate effector protein for signaling events that allow organisms to alter their motility in response to external signals. The CMF22 protein is therefore of high interest, because very little is known about such effector proteins that control flagellar motility. Our in-depth analysis of CMF22 revealed that CMF22 is a broadly conserved axonemal protein that regulates propulsive motility and may be important for general mechanisms of eukaryotic motility (28). The conserved presence and position of IQ and AAA domains in CMF22 orthologs from diverse eukaryotes with motile flagella indicates these domains are important for CMF22 function and therefore make CMF22 an attractive candidate effector for translating external signals to mechanical forces for motility.

This study aims to analyze the IQ motif and AAA domains of CMF22 to determine their function in regulating motility. Using point mutants of each domain, we identified that the AAA domain may be functional in regulating motility and coordination of motility may be modulated through a key residue important for ATP-binding. Additionally, immunofluorescence and biochemical assays of the AAA point mutant demonstrates that mutation of the residue for ATP-binding does not affect CMF22 localization and therefore the motility defect is not likely to be due to mislocalization of the protein. Altogether, this data suggests CMF22 may modulate axonemal motility through through ATP-binding.

RESULTS

Mutagenesis of the IQ and AAA domains in CMF22

To identify the putative IQ and AAA motifs in *T. brucei* CMF22 (Tb927.11.3360), the protein sequence was run through the SMART and Pfam databases (29). The SMART algorithm identified both the IQ and AAA domains, although the IQ domain (amino acids 229-251) was a weak hit with an e-value of 15.2. The AAA domain, however, was confidently predicted using the SMART algorithm with an e-value of 2.5 e-14 at amino acids 652-783 (data not shown). The Pfam database only predicted an AAA domain at the same site with an e-value of 3.8e-12 and no IQ motif was identified. The SMART database algorithms predicted the IQ motif of TbCMF22 to be LQSAVQAYLTRK at amino acid positions 237-248, the Walker A motif of the AAA domain to be GFHGTGKT at 656-663, and the Walker B motif to be VIYIDN at 709-714. Alignment of these sequences to the consensus sequences for the IQ motif and AAA domain are illustrated in Figure 5-1. Conserved amino acids (red) of the IQ motif are shown to mostly align with the *T. brucei* putative IQ motif except for a key arginine. For the AAA domain, the conserved residues of the consensus sequence perfectly align with the *T. brucei* Walker A motif of CMF22, however, the conserved glutamate residue required for ATP hydrolysis in the consensus sequence is missing in the *T. brucei* AAA domain Walker B motif (Figure 5-1). Notably, closely related kinetoplastids such as *Trypanosoma cruzi*, *Trypanosoma congolense*, and *Leishmania major* do not have the conserved arginine in the IQ motif. Instead, similar to *T. brucei*, they have a glutamine

or a lysine (*L. major*) (Figure 1). In addition, all these kinetoplastids do not have the invariant glutamic acid required for ATP hydrolysis (Figure 5-1).

Using this alignment, mutations were generated for conserved residues of both the IQ motif and the Walker A motif of the AAA domain. For the IQ motif, the hydrophobic amino acid at position 1, conserved glutamine at position 2 and basic charges at position 6 are critical for interaction with calmodulin (30, 31). Therefore, an IQ mutant containing four alanine substitutions at all of the critical interaction points as well as sites surrounding these critical residues was generated and is called the "4A" point mutant (Figure 5-1). Various mutations of this IQ motif were also generated and are illustrated in Figure 5-S1A. To generate the AAA domain mutant, the key lysine of the Walker A motif that is required for nucleotide binding was mutated to an alanine (32), and this mutant is called "K662A". As illustrated in Figure 1, the *T. brucei* Walker B motif lacks the conserved glutamate for ATP hydrolysis, suggesting that ATP hydrolysis may not occur for this protein. Accordingly, no mutation was generated to test this motif.

In a previous study, a CMF22 RNAi knockdown mutant was generated in which the region targeted for knockdown was in the untranslated region. This leaves the open-reading frame region available for mutagenesis (28, 33). The study also described an "RNAi-immune add-back" strategy in which a wild-type copy of gene can be tagged at the endogenous locus and is not targeted for RNAi degradation. Using the same strategy, one can replace the endogenous gene at one allele with a copy of the gene carrying point mutations and a C-terminal tag and leave the other allele untouched. This approach is also tetracycline-inducible so in the uninduced cell lines, there is a mixture

of both endogenous wild-type and mutant protein. However, when cells are induced with tetracycline for RNAi knockdown of the target gene, only mutant protein will be expressed.

To make mutagenesis constructs carrying the point mutations, the full-length CMF22 ORF was cloned into an in situ tagging vector (34) and site-directed mutagenesis was performed (33). Since the CMF22 ORF is a 2.7 kilobase pair fragment, homologous recombination can occur at any region along this length. Transfected cells for both the IQ motif and the AAA domain mutations were each cloned by limiting dilution and genomic DNA was extracted to PCR amplify regions containing the mutation. Primers used were specific to the tagged copy of CMF22 and direct sequencing of each clone for each mutagenesis construct confirmed the presence of desired mutations.

Northern blots were performed on the IQ motif mutant (4A), the AAA domain mutant (K662A), and a previously described RNAi-immune add-back rescue mutant (Ri) in which one allele of the CMF22 RNAi knockdown mutant was replaced with a wild-type, tagged copy of CMF22 (28). As previously shown, the alpha-tubulin 3'UTR is smaller than the CMF22 3'UTR so the tagged copy of CMF22 can be distinguished from endogenous CMF22. Using a probe specific for the CMF22 ORF that hybridizes to both the endogenous and tagged copies of CMF22, there are two bands that appear on a Northern blot (Figure 5-2A). The endogenous copy of CMF22 has a longer 3'UTR and therefore corresponds to the top band (open arrowhead). In the presence of tetracycline, RNA of the endogenous CMF22 in Ri, 4A and K662A cell lines are all

dramatically reduced. RNA levels of the tagged copies of CMF22, whether “wild-type” or point mutants, are not reduced and are unaffected by RNAi induction (closed arrowhead). To ask if the point mutants are expressed, immunoblotting with anti-HA antibodies show a single band at approximately 110kDa in total cell lysates from the Ri cell line, 4A and K662A point mutants but not in the parental line CMF22-UKD (Figure 5-2B). Notably, the K662A mutants seem to express less protein than Ri or 4A cells. Cells were then monitored for growth defects under both uninduced and tetracycline-induced conditions. RNAi knockdown of CMF22 in the AAA point mutant resulted in a mild growth defect (Figure 5-2C) whereas growth of the other mutants were unaffected by RNAi induction.

Both the IQ and AAA point mutants were then tested for their requirement for propulsive cell motility. Motility was analyzed using high resolution, single cell video microscopy and RNAi induced K662A point mutants had an observable motility defect. In comparison to uninduced cells, RNAi induction of K662A point mutants inhibited propulsive motility such that cells moved slower across the field of view and many cells had frequent reverse beats (Supplemental Movies 5-3 and 5-4). The 4A IQ motif mutant, however, was able to translocate in and out of the field of view (Supplemental Movies 5-1 and 5-2). To determine the impact of the motility defect on a population scale, point mutant cell lines were traced using automated particle tracking and motility trace analysis (33) under uninduced and induced conditions. Motility traces of Ri and point mutants in uninduced conditions showed that cells were motile and were capable of translocation (Figure 5-S2). Traces reveal a motility defect in the K662A point mutant but not for cells with point mutants in the IQ motif (Figure 5-S1C, Figure 5-3). The

motility defect, however, was not as pronounced as the CMF22-UKD mutant in that cells were able to minimally translocate in a “zig-zag” pattern (Figure 5-3).

To quantify the impact of the motility defect, mean squared displacement was measured as a function of time interval. In comparison to a previous study in which the CMF22-UTR knockdown resulted in an absence of propulsive motility (28), the K662A point mutant has some ability for propulsive movement when not induced with tetracycline and this level of propulsive motility is similar to that of induced Ri cells and the induced 4A point mutant. In the RNAi induced K662A point mutants, however, propulsive motility is largely reduced (Figure 5-4, red line). In contrast, the 4A point mutant for the IQ motif had normal propulsive motility in both uninduced and induced conditions (Figure 5-4). Although the defect in propulsive motility was evident in the K662A induced cells, a student’s unpaired *t*- test on average motility of all point mutants do not reveal a significant difference ($p>0.05$) (Figure 5-S1B and 5-S3). Using the social motility assay described in Oberholzer *et al.* (35) as a motility assay, 4A and K662A point mutants were cultivated on semi-solid agarose in the presence and absence of tetracycline. As expected for a mutant that has defective propulsive motility, K662A mutants cannot form radial projections in the presence of tetracycline (Figure 5-S4).

To examine if the K662A motility defect was due to mislocalization, biochemical fractionation was performed on the K662A point mutants. Cells from induced K662A and induced Ri cells were first extracted with detergent to separate soluble proteins (S1) from the insoluble cytoskeletons (P1). The P1 pellet was then salt extracted with 1M NaCl to isolate insoluble flagellum skeletons (P2) from the subpellicular cytoskeleton

(S2). Since the K662A point mutant is tagged with a 3xHA epitope, cell equivalents of each of the fractionation steps were blotted with anti-HA to determine if the K662A point mutant has a similar profile to the “wild-type” Ri fractionation pattern at 1M NaCl. The entire cellular pool mutant CMF22 in the K662A point mutant fractionated in the flagellum skeleton (P2) fraction similarly to the wild-type, tagged copy of CMF22 in Ri cells (Figure 5-5A). The distribution of mutant CMF22 in the K662A point mutants was also examined by immunofluorescence. Like wild-type CMF22-HA (Figure 5-5B, left panels), mutant CMF22-HA in the K662A point mutants was localized along the length of the flagellum (Figure 5-5B, right panels). The biochemical and immunofluorescent data suggest that the motility defect in K662A point mutants is not likely due to structural defects associated with mislocalization of the protein.

DISCUSSION

CMF22 was identified as a broadly conserved axonemal protein with an orthologue in each of the five major eukaryotic clades. Previous work has demonstrated that knockdown of CMF22 results in a defect in propulsive motility (28). CMF22 contains putative IQ and AAA domains in which the presence and position of these domains are well conserved in CMF22 orthologues (28). This suggests that there is a selective pressure to retain these domains and therefore must be important for protein function. This study expands on the original characterization of CMF22 by determining whether these domains are required for regulating motility. Using site-directed mutagenesis to substitute key residues with alanine, point mutations of the IQ and AAA domain were generated. Point mutants of the IQ motif had normal motility, however, the AAA domain

mutant with a mutation in the key lysine required for ATP binding revealed a motility defect. This data suggests that the ATP binding through the AAA domain of CMF22 may be functionally required for propulsive motility.

The IQ domain is 25 amino acids long with a consensus sequence of [I, L, V]QxxxRxxxRGxx[R,K] that is widely distributed from yeast to plants (30, 36). The structure of the IQ motif is an amphiphilic seven-turn-α-helix. Calmodulin is suggested to interact with the IQ motif at the hydrophobic amino acid (typically isoleucine, leucine, or valine) at position 1, a conserved glutamine at position 2, basic amino acids (typically arginine) at positions 6 and 11, and in some cases a glycine at position 7 (30). IQ motifs are thought to bind calmodulin in a calcium-independent manner, or apo-CaM (37, 38). In some cases, apo-CaM binds the protein via IQ motifs in both the absence and presence of calcium and is required for function in enzymatic activities (37). However, a subset of these apo-CaM binding proteins such as neuromodulin bind calmodulin in the absence of calcium and have been speculated to sequester intracellular calmodulin under low calcium conditions. In this context, these apo-CaM binding proteins function to concentrate CaM to specific regions of the cell for rapid release in response to calcium (39, 40).

In our study, we have chosen to mutate conserved amino acids rather than make a truncated mutant without the putative IQ motif to avoid misinterpretation of results. Our goal was to assess the functional contribution of this domain without the complication of large structural defects that could result when creating truncation mutants. We mutated the IQ motif at positions 1, 2, 5 and 6 in which the conserved

hydrophobic amino acid followed by a conserved glutamine and the basic amino acid at position 6 were all mutated to alanine. In 2000, Zuhlke et al. created point mutants in the IQ motif of an L-type calcium channel and demonstrated that the mutant with the least capacity to bind calmodulin contained mutations at positions 1, 2, 5, 6, and 7 (31). To mirror this mutation, we made an alanine substitution at position 5 in addition to the conserved amino acids as positions 1, 2, and 6. With this "4A" mutant, we assessed the motility phenotype under uninduced and RNAi induced conditions. In both conditions, the 4A mutant had normal motility. This data suggests that the IQ motif is not functional for axonemal motility of *T. brucei* parasites in suspension cultures and on semi-solid agarose. This data also correlates with weak domain predictions in which the IQ domain was a weak hit. However, as more IQ motifs have been identified, recent work has shown that there are many divergent CaM isoforms that do not match the consensus sequence. Additionally, this domain was only investigated in the context of motility and without physiological relevant cues. It is possible that this IQ motif is a signaling component for regulating motility in more natural environments such as within the tsetse fly insect vector or the mammalian host.

ATPase Associated with various cellular Activity (AAA) proteins are a group of highly divergent proteins in which over 30,000 have been identified throughout all kingdoms of life (41). The AAA+ module of AAA proteins is a 200-250 stretch of amino acids that is comprised of two domains: a core $\alpha\beta\alpha$ nucleotide-binding domain and a smaller α-helical domain for catalysis of ATP (42). AAA proteins are involved in diverse cellular functions such as DNA recombination, DNA replication, DNA repair, protein folding, protein assembly, protein transport, protein degradation, and many others (42).

The core αβα nucleotide-binding domain, also called the Walker A motif of the AAA domain, has a key lysine that is required for ATP binding. This lysine interacts with the β and γ phosphates of ATP (32). This invariant lysine residue has been assessed for over 20 AAA proteins and data from these mutagenesis experiments suggest that given the conservation of the ATPase binding motif across diverse kingdoms, this lysine is so critical for ATP-binding that even conservative amino acid exchanges are not tolerated (41). We therefore mutated the invariant lysine to an alanine and assessed motility of the point mutants for the functional contribution of this invariant lysine and indirectly, ATP-binding. Our studies reveal that this invariant lysine is required for normal propulsive motility since only the K662A mutant results in defective motility. Our findings suggest that ATP-binding at the AAA domain in CMF22 may be required for normal motility.

The Walker B motif of CMF22 in *T. brucei* diverges from the consensus sequence and lacks the invariant glutamate required for priming a water molecule for nucleophilic attack on the γ phosphate group of ATP (43). This suggests that that CMF22 does not hydrolyze ATP but may still function in regulating motility through nucleotide binding. An example of this is in the *Caenorhabditis elegans* adapter protein Uncoordinated protein 53 (UNC-53) that contains a AAA domain. UNC-53 is required for migration of cells and neuronal processes. UNC-53 is an adapter protein that integrates guidance information for cytoskeletal reorganization at the leading edge of motile cells such as mechanosensory neurons, excretory canals, and sex muscles (44-46). The human homologs, neuron navigators (NAV), has been identified and were shown to be

required for neuronal outgrowth (47-49). One of the NAVs, NAV1, requires ATP binding for function. Authors mutated the highly conserved lysine residue of the Walker A motif to abolish nucleotide binding. They found that neurite extensions were reduced in this AAA mutant form of NAV1. Interestingly, similar to CMF22, NAV1 has an asparagine instead of the conserved glutamate in the Walker B motif. This suggests that like NAV1, CMF22 may function through nucleotide binding rather than hydrolysis of ATP.

We noted that the K662A mutant has a propulsive motility defect when half of the potential CMF22 copies are mutated (uninduced) and the ability for propulsive mutant is even more pronounced when all the copies are mutated (induced) (Figure 5-4). The result of the AAA mutation on propulsive motility is complicated by the fact that both the uninduced and RNAi induced cell lines do not express CMF22 as abundantly as the "rescue" cell lines or the IQ motif point mutants (Figure 5-2B). The uninduced K662A point mutants that express both wild-type and mutant CMF22 have the same level of propulsive motility as RNAi -induced Ri and 4A cells. As stated previously, endogenous CMF22 at one allele is knocked down when cells are induced and potentially half the copies of CMF22 mRNA are degraded. In many cases, there is some level of protein regulation and that is why the protein abundance of CMF22 in the Ri + Tet cells seem to be similar to that of the uninduced cell line. This is not always the case and a mutation could possibly affect the stability of a protein. This may be the case for the K662A mutant therefore we cannot definitively state that decreased propulsive motility is due to the mutated lysine in the walker A motif of the CMF22 AAA domain.

In order to assess whether the mutation alone truly results in a motility defect, a critical experiment would be to find a clonal cell line that expresses a similar amount of CMF22 to the “rescue” cell line. If a clonal line of the point mutant with equal protein expression level of CMF22 as the wild-type cells (Ri) has a defect in propulsive motility, the defect can be attributed to the mutation. An alternative method to address the issue of protein abundance is to overexpress the K662A mutant in the CMF22-UKD background so that there is equal or overexpressed CMF22. This cell line would then be compared to overexpression of wild-type CMF22 without the mutation and Ri “add back” cells (that have decreased protein expression). If the invariant lysine affects propulsive motility, then overexpression of the K662A mutant copy of CMF22 would result in defective propulsive motility in comparison to overexpression of wild-type CMF22 and Ri “add back” cells. It is also possible that the K662A point mutation could be linked to protein stability and the contribution of the point mutation or protein abundance on propulsive motility cannot be parsed out.

The K662A mutant may also have a dominant-negative effect. AAA proteins typically exist as homohexamers and function through binding (50). In addition to the issue of protein abundance, another explanation for why the uninduced K662A mutant cell line has decreased propulsive motility is that the K662A point mutant CMF22 may be binding to the wild-type CMF22 and inhibiting function or that the point mutant structurally inhibits oligomerization and therefore CMF22 protein stability. To address this, an experiment using different epitope tags to tag each CMF22 allele and co-immunoprecipitation in the trypanin knockdown cell line may reveal CMF22 dimerization.

To determine if the AAA point mutants phenotype is due to mislocalization, we performed biochemical fractionation and immunofluorescence. Even in high salt extractions, the RNAi-induced K662A point mutant has an identical profile with wild-type CMF22 protein and the entire pool of contents of the mutant CMF22 is in the insoluble flagellum skeleton fraction. Previous work has shown that CMF22 localizes to the axoneme so to determine if the RNAi-induced K662A point mutants mislocalize, we performed immunofluorescence microscopy. Epitope-tagged K662A point mutants localized to the axoneme and was distributed along the length of the entire flagellum. The biochemical and immunofluorescent data suggests that the K662A point mutant CMF22 is not mislocalized and the phenotype is potentially due to the point mutation in the ATP binding site of CMF22.

Altogether, the data suggests that although the IQ domain is not required for motility in this context of this study, the AAA domain may be functional. Expressing point mutants of the ATP-binding site of the AAA domain in which potentially half the copies of CMF22 are mutant reduces propulsive motility to similar levels as induced add-back (Ri) or 4A mutants (Figure 5-4). Additionally, RNAi induction results in expression of only the K662A point mutant and the resulting effect is an even more substantial defect in propulsive motility. Whether the defect is entirely due to the contribution of the point mutant, the decreased protein expression or both remains to be investigated. It is still an important find that nucleotide binding may modulate the function of this protein, and as suggested by previous work, this protein may be localized to a central regulating hub called the N-DRC (28). No candidate effector protein that transduces external cues into a mechanical force at this central hub has been identified and CMF22 may be that

missing link. A recent study has found another protein in the N-DRC, DRC7, has a conserved transglutaminase-like (TGL) peptidase domain (51). It has been demonstrated that proteins with TGL domains interact with AAA-containing proteins and therefore it is possible that CMF22 interacts with DRC7. If the TGL domain is functional in DRC7, it may facilitate interactions with glutamylated tubulin residues on the B-tubule since *T. brucei* flagellar microtubules are extensively glutamylated (19, 51, 52). In addition, glutamylation-deficient *C. reinhardtii* demonstrated that there is interaction between glutamylated tubulin, dynein e, and the N-DRC during microtubule sliding (53, 54). Further investigation of CMF22, the function of both the IQ and AAA domains, and identification of CMF22 interacting partners will provide insight into the current work of flagellar biology and add to our working model of motility in a protozoan pathogen.

SUPPLEMENTAL MOVIE LEGENDS

Supplemental Movie 5-1. **30fps 4A point mutant, -Tet, control cells.** Single-cell video microscopy shows normal motility of the uninduced (-Tet) 4A point mutant cell line. Cells are capable of translocating across the field of view. Video recorded and played at 30 fps.

Supplemental Movie 5-2. **30 fps 4A point mutant, + Tet cells.** 4A point mutants were grown in tetracycline for 72 hours and assessed using single-cell video microscopy. 4A + Tet cells are able to translocate across the field of view and exhibit a normal beating pattern. Video recorded and played at 30 fps.

Supplemental Movie 5-3. 30 fps K662A point mutant, -Tet cells. Uninduced K662A point mutants are capable of translocating across the field of view and exhibit normal beat. Video recorded and played at 30 fps.

Supplemental Movie 5-4. 30 fps K662A point mutant, + Tet cells. After 72 hours of RNAi induction (+Tet), K662A point mutants cannot move across the field of view and exhibit frequent reverse beats. Video recorded and played at 30 fps.

MATERIALS AND METHODS

Trypanosoma brucei cell culture maintenance and transfection:

Procyclic 29-13 *T. brucei* cells that express T7 RNA polymerase and the tetracycline repressor (55) were cultured in Cunningham's semi-defined medium (SM) supplemented with 10% heat-inactivated fetal calf serum (FCS), 15mg/mL G418 and 50 mg/mL hygromycin as previously described (56). Transfection and selection were performed as previously described (56). Clonal cell lines were established through limiting dilution.

Database searches:

IQ and AAA domain identification performed on CMF22 (XP_828418.1) using the SMART (57) and Pfam databases (29).

Mutagenesis Cell Lines:

The full-length CMF22 ORF was cloned into the *in situ* pMOTag2H tagging vector (34) to be used as a template for site-directed mutagenesis. GeneArt Seamless

Cloning and Assembly (Invitrogen, Catalog #A13288) was used and primers for cloning the full-length CMF22 ORF were: (Forward) AAGGGAACAAAAGCTGGGTACCATGTCTTCGTTGACATGT and (Reverse) GCACATCGTAAGGGTACTCGAGTTCCTTCTTCTTGGGTCT. The QuikChange II Site-Directed Mutagenesis Kit (Agilent Technologies) was used to mutate key residues of the IQ and AAA domains of CMF22. Primers for mutagenesis are as follows:

4A IQ motif mutant

(Forward) 5'- ggagggaaagagccgctacagttgcggcaagtgctgcggcagcttacctgacccgaaa -3'
(Reverse) 5'- tttcgggtcaggtaagctgccgcagcacttgccgcaactgtagcggctctttccctcc -3'

K662A AAA domain mutant

(Forward) 5' - gttttcatgggactggagcgacccacctggtgcacg -3'
(Reverse) 5' – cgtgcaccaggtgggtcgctccagtcccatgaaaac -3'

All DNA constructs were verified by direct sequencing. The amplicons containing mutation sites were excised using the *KpnI* and *XhoI* restriction digests and the tagging cassettes was stably transfected into the CMF22-UKD cell line (28). Clonal lines were established through limiting dilution and genomic DNA was isolated from each clonal line. Primers surrounding the mutation site were used to amplify the region and PCR products sequenced for mutation verification. Primers used were the forward primer used to clone the CMF22 ORF into the *in situ* pMOTag2H tagging construct and the reverse primer that spans the sequence for the 3xHA and intergenic tubulin region: CGTTGTCACACTTTGTCGACTATGCGTAATC. Clones with verified mutations were used for further analysis.

Northern blots:

The Qiagen RNeasy Miniprep kit (Qiagen) was used to extract total RNA and northern blots were performed on RNA samples. 5 μg of RNA from each cell line was used for each cell line as previously described in (58) except DIG-labeled probes (DIG Nucleic Acid Detection Kit, Roche) was used to detect RNA levels. A unique probe for nucleotides 1398 to 1920 of the CMF22 ORF and a unique probe for nucleotides 2577 to 3108 of the Tb927.1.1530 gene that is unaffected by CMF22 knockdown for a loading control was used in accordance with manufacturer's instructions.

Growth curves and motility assays/videos:

Cell growth was monitored using a Z1 Coulter Particle Counter (Beckman Coulter, USA) and growth was plotted as cumulative growth. Data points were obtained from the averages of two counts for each time point. Cells were grown to a density of 3 x 10^6 cells/ml for motility assays and pipetted into poly-glutamate coated motility chambers (59) at room temperature. Cells were imaged using a Zeiss Axioskop II microscope within ten minutes of removal from the incubator. 30-second videos using darkfield optics under a 20x objective was collected for motility traces. 1 μg/mL tetracycline was added to cultures for 72 hours prior to video capture for RNAi induction. Traces were performed as previously described (59) and average curvilinear velocity was determined using Metamorph software (Molecular Dynamics). For each cell line, average velocities from 31 cells were used to calculate the mean. A student's unpaired *t*-test was also used to determine significance. Propulsive motility was quantified using motility traces in which the mean squared displacement of individual cells in the x and y

dimensions was calculated according to the formula MSD = $<ri(t)^{2>}$ = $<(pi(t) - pi(0)^{)2>,}$ where ri is the distance travelled by the parasite over time interval t and pi is the position of the parasite at any given time. MSD is calculated for each instance I of a given time interval. MSDs for at least 24 cells were averaged to obtain an ensemble average and error bars indicate standard deviation. For single cell motility videos, cells were imaged using DIC optics with a 100x oil objective and were captured at 30 frames per second with a COHU CCD camera. Videos were imported using Adobe Premiere Elements (59).

Cytoskeletal fractionation, western blotting and immunofluorescence:

Cells were subjected to detergent fractionation using a two-step fractionation method as previously described (56, 60). Cells were solubilized using non-ionic 1% Nonidet-P40 (NP-40) and the pellet was extracted using 1 M NaCl PMN (10mM NaPO4 pH 7.4, 1mM $MgCl_2$, 150mM NaCl] buffer. Detergent extracted samples on cell lysates were analyzed by western blotting as previously described (61). Primary antibody dilutions were as follows: monoclonal anti-HA antibody (HA 11.1 Covance) 1:1000, monoclonal anti-Tubulin antibody E7 supernatant 1:2500. The monoclonal antibody E7 is directed against beta-tubulin was developed by (62) and obtained from the Developmental Studies Hybridoma Bank maintained by the University of Iowa Department of Biological Sciences.

Cells were extracted in PEME buffer (100mM piperazine-*N*,*N*′-bis(2-ethanesulfonic acid), pH 6.9, 2mM EGTA, 0.1mM EDTA, 1mM $MgSO_4$, 25 µg/ml aprotinin, 25 µg/ml leupeptin) containing 1% NP40 for immunofluorescence microscopy

(63). Cytoskeletons were fixed in 2% paraformaldehyde, quenched in 0.1 M glycine and subjected to indirect immunofluorescence microscopy as previously described (56). For a negative control, immunofluorescence microscopy was performed on procyclic 29-13 cytoskeletons and showed no staining (data not shown). Monoclonal anti-HA antibody (HA11.1, Covance) was used at a 1:200 dilution. Cytoskeletons were mounted with Vectashield containing DAPI after staining.

Social Motility Assay:

The assay was performed as described in (35). Procyclic cells were cultivated on SM plates with 0.4% semi-solid agarose and 1 μg/mL tetracycline. Plates were incubated at 28 °C and 4% CO_2 for up to 5 days. A Pentax Optio A30 point-and-shoot 10 megapixel camera was used to monitor and document the growth of colonies.

FIGURES

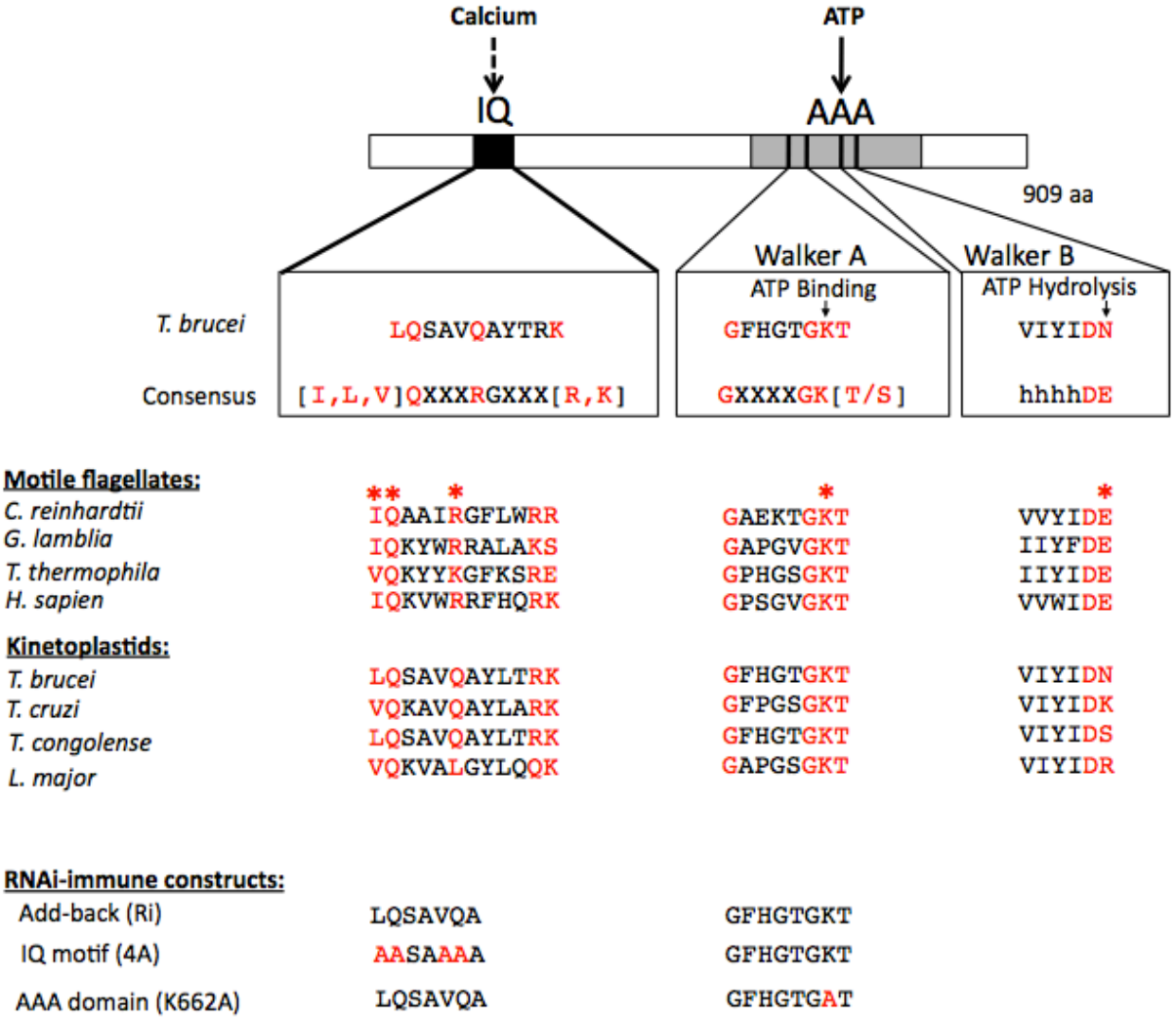


Figure 5-1. The IQ motif and AAA domain of CMF22 have conserved residues. The *T. brucei* CMF22 protein sequence was aligned with the consensus IQ motif and AAA domain (SMART). Conserved residues are shown in red, conserved invariant residues important for calmodulin or ATP binding are marked with an asterisk (30, 32). Additionally, these motifs were aligned to CMF22 orthologues in representative eukaryotic organisms with motile flagella and closely related kinetoplastids. The

organisms (with their GenBank accession numbers in parentheses) used were as follows: *Trypanosoma brucei* (XP_828418.1), *Chlamydomonas reinhardtii* (XP_001690665.1), *Giardia lamblia* (XP_001707075.1), *Tetrahymena thermophila* (XP_001015966.1), *Homo sapiens* (NP_001257513.1), *Trypanosoma cruzi* (XP_817318.1), *Trypanosoma congolense* (CCC94925.1), *Leishmania major* (XP_001681896.1). RNAi immune mutagenesis constructs used in this paper are also listed: Ri (no mutation), 4A (IQ motif mutation), and K662A (mutation of the invariant lysine required for ATP binding).

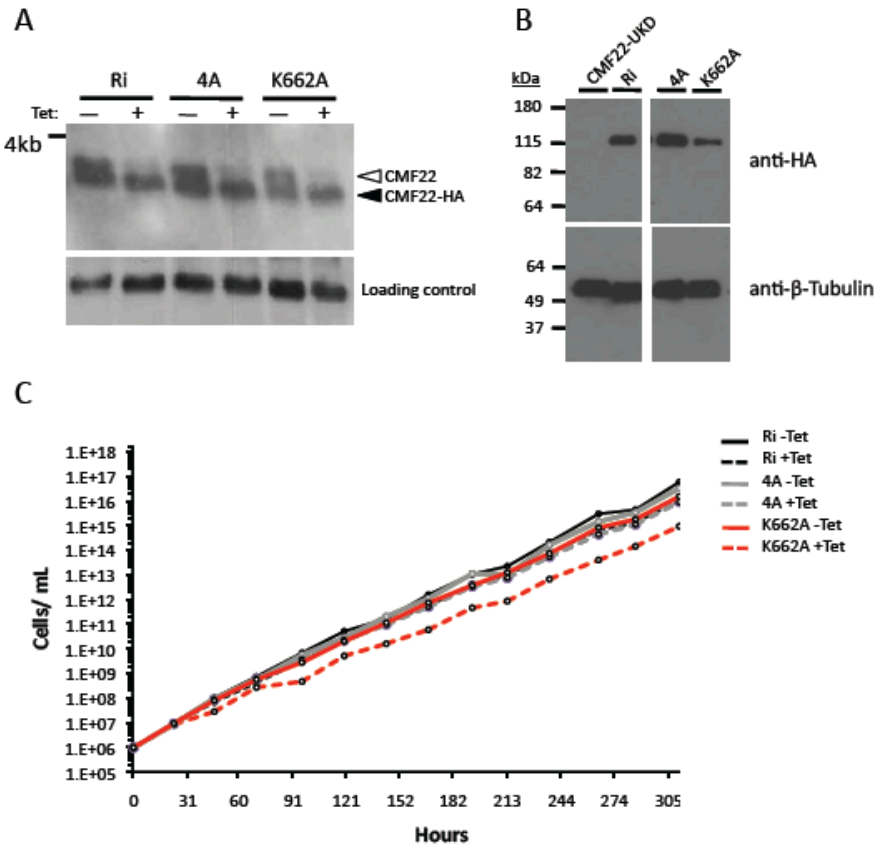


Figure 5-2. CMF22 point mutants are expressed with minimal growth defects. (A) Northern blot of RNA from Ri (no mutation), 4A (IQ point mutant), and K662A (AAA point mutant) cell lines in the absence (-) or presence (+) of Tet, as indicated. Empty arrowhead denotes the endogenous CMF22 while filled arrowhead marks the HA-tagged (mutant) CMF22. CMF22 was probed with a unique probe to the CMF22 ORF and the loading control was a unique probe to an unaffected gene (Tb927.1.1530). (B) Western blot of total cell lysates from parental (CMF22-UKD), RNAi immune add-back (Ri), 4A and K662A mutants. Blots were probed with antibodies against the HA epitope or loading control (beta-tubulin). (C) Growth curve of Ri, 4A and K662A cell lines in the absence (-) and presence (+) of Tet for 306 hours, as indicated.

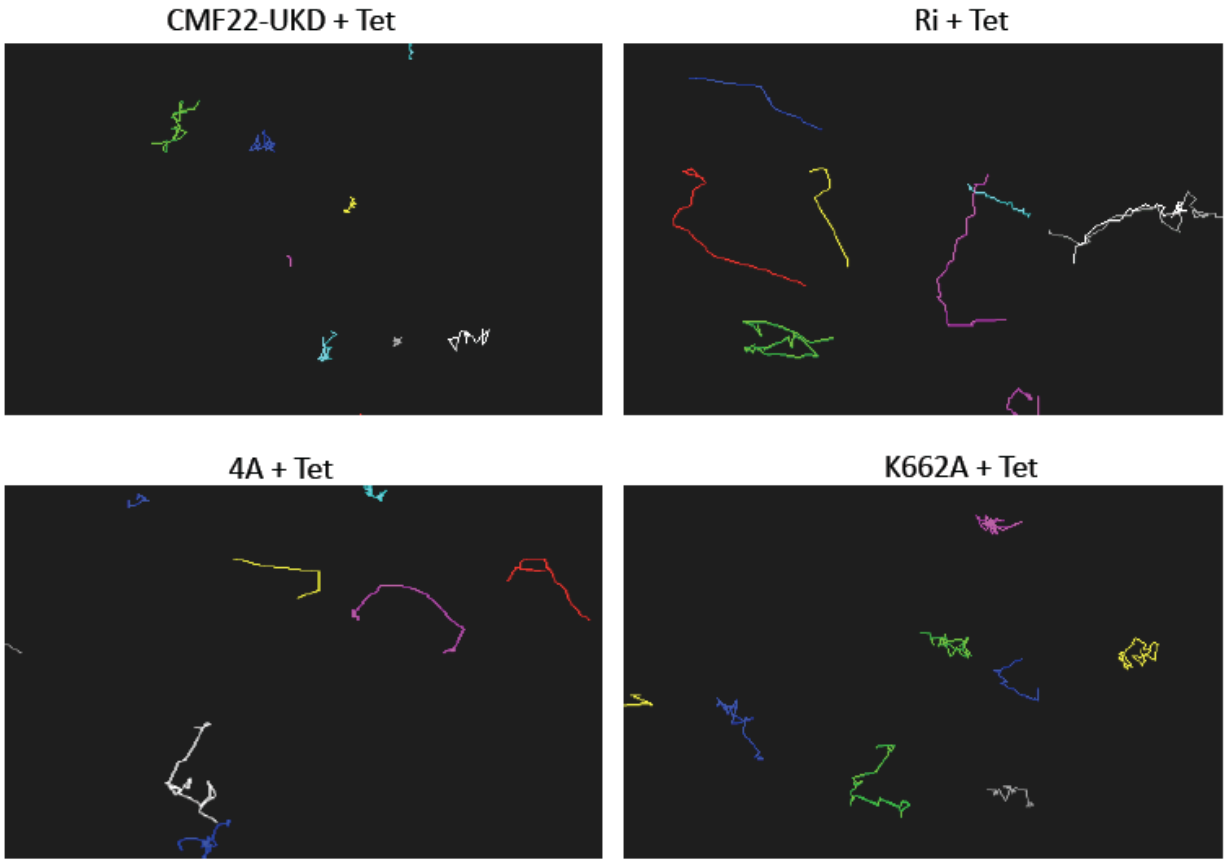


Figure 5-3. K662A point mutants have aberrant translocation. Motility traces of CM22-UKD, Ri, 4A and K662A cell lines in the presence of Tet for 72 hours as indicated. Each line represents the movement of individual parasites over a 30 second time interval.

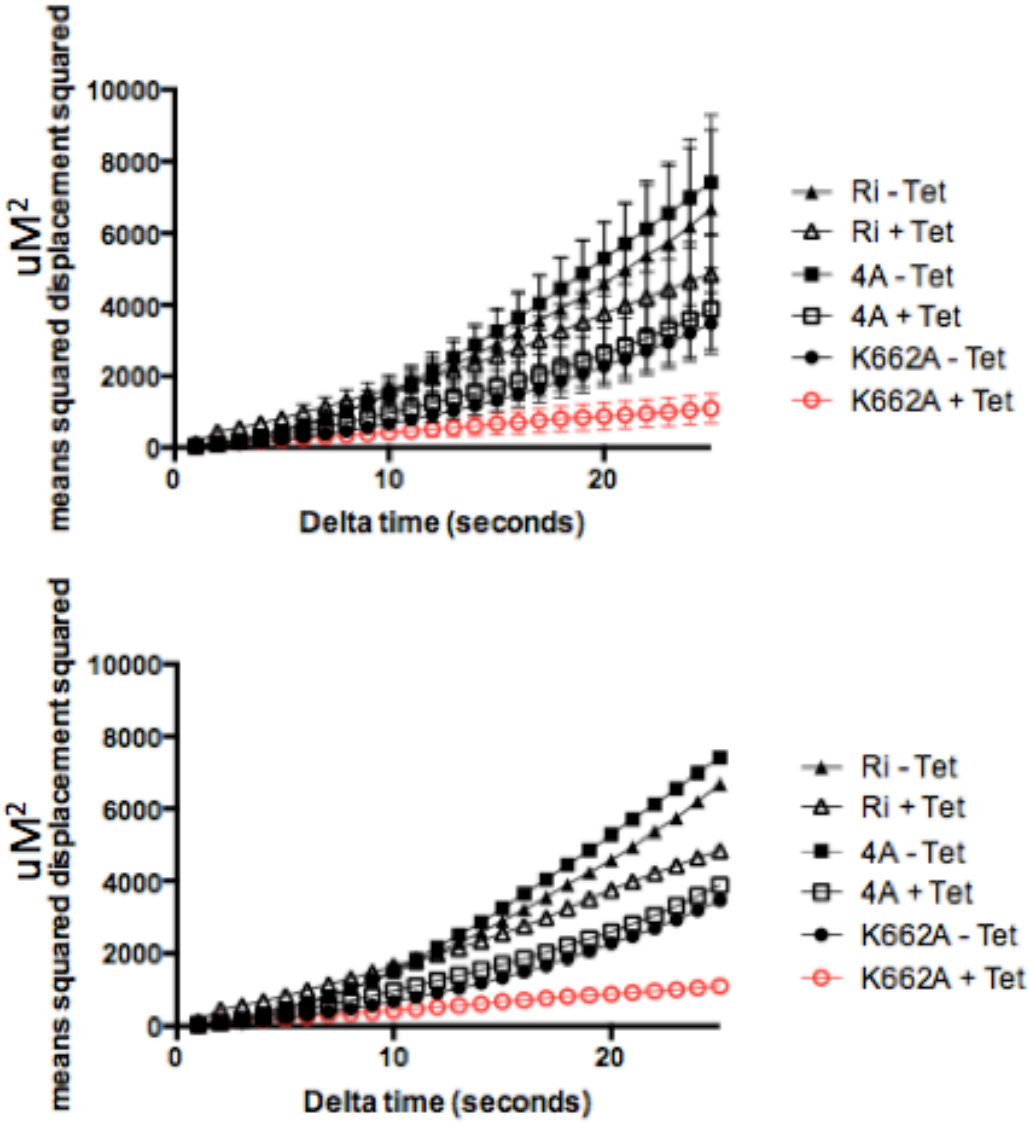


Figure 5-4. K662A + Tet mutants have defective propulsive motility. MSD is plotted as a function of time interval (delta time in seconds) for Ri, 4A and K662A cell lines in the absence and presence of tetracycline for 72 hours, as indicated. K662A mutants induced with tetracycline are illustrated in red. Top graph includes error bars (standard error of mean) and the bottom graph does not.

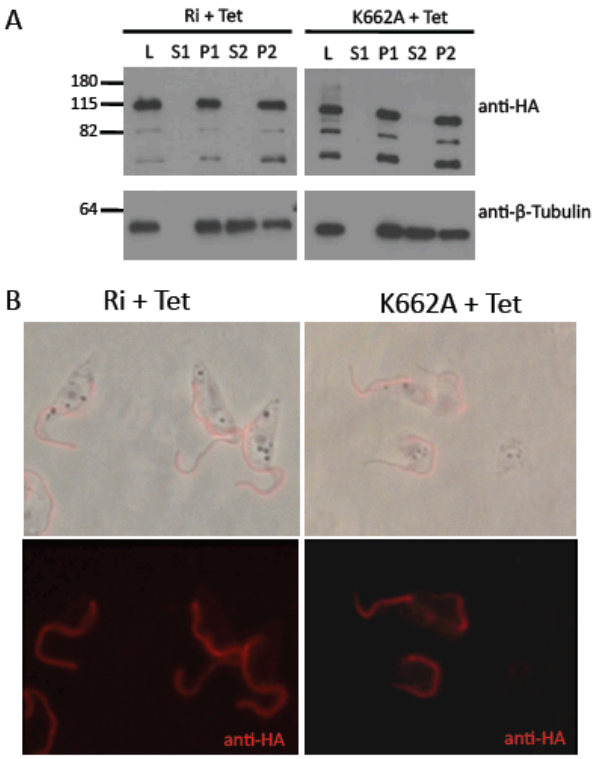


Figure 5-5. CMF22-HA in the K662A mutants is stably associated with the axoneme. (A) Western blot of the indicated subcellular fractions from Ri and K662A cell lines after growth in tetracycline for 72 hours. Blots were probed with anti-HA and anti-beta-tubulin, as indicated. Fractions correspond to whole-cell lysates (L), non-ionic detergent-soluble (S1) and insoluble (P1) fractions, as well as soluble (S2) and insoluble (P2) fractions from 1 M NaCl extraction of the P1 fractions. The lower molecular mass bands in the anti-HA blots are likely degragation products. (B) Indirect immunofluorescence was performed on detergent-extracted cytoskeletons from Ri and K662A cells grown in tetracycline for 72 hours, as indicated. Samples were stained with anti-HA (red) antibodies.

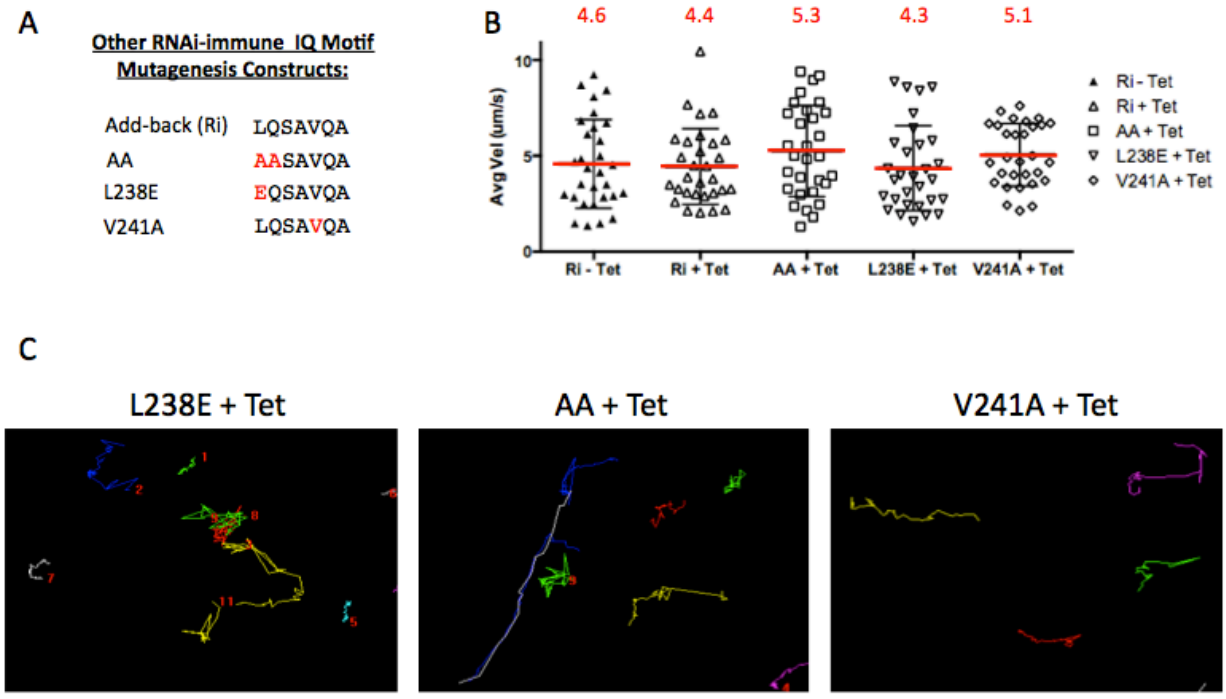


Figure 5-S1. Various IQ motif point mutants of CMF22 have normal average motility and translocation. (A) In addition to the "4A" mutant, three variations of the IQ motif mutants were generated at positions 1, 2, and 5 of the IQ motif, as indicated. (B) Student's unpaired *t*- test of average motility of the point mutants show no significant defect. (C) Motility traces from L238E, AA and V241A point mutants cell lines grown in the presence of tetracycline for 72 hours, as indicated. Each line traces the translocation of a single cell over a 30 second time interval.

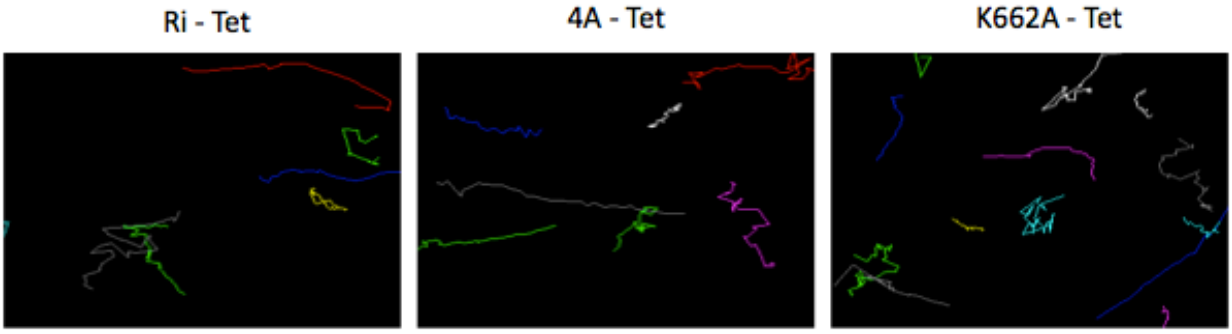


Figure 5-S2. Uninduced cell lines are capable of translocation. Motility traces of Ri, 4A and K662A cells lines grown in the absence of tetracycline, as indicated. Each line traces the translocation of an individual parasite over a 30 second period.

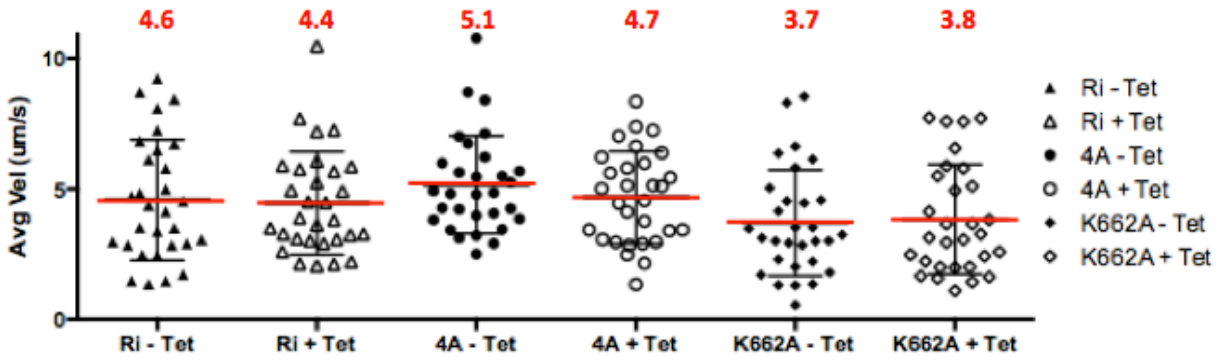


Figure 5-S3. Average velocity does not reveal significant differences. Ri, 4A, and K662A cells were grown in the absence and presence of tetracycline for 72 hours. The "add-back" Ri cell line from Figure 5-S1 is shown as reference. Metamorph software tracked the average velocity of cells and the mean is highlighted in red. A student's unpaired *t*-test reveals no significant difference between all cell lines, both under uninduced and induced conditions. Red bar = mean, as indicated (red).

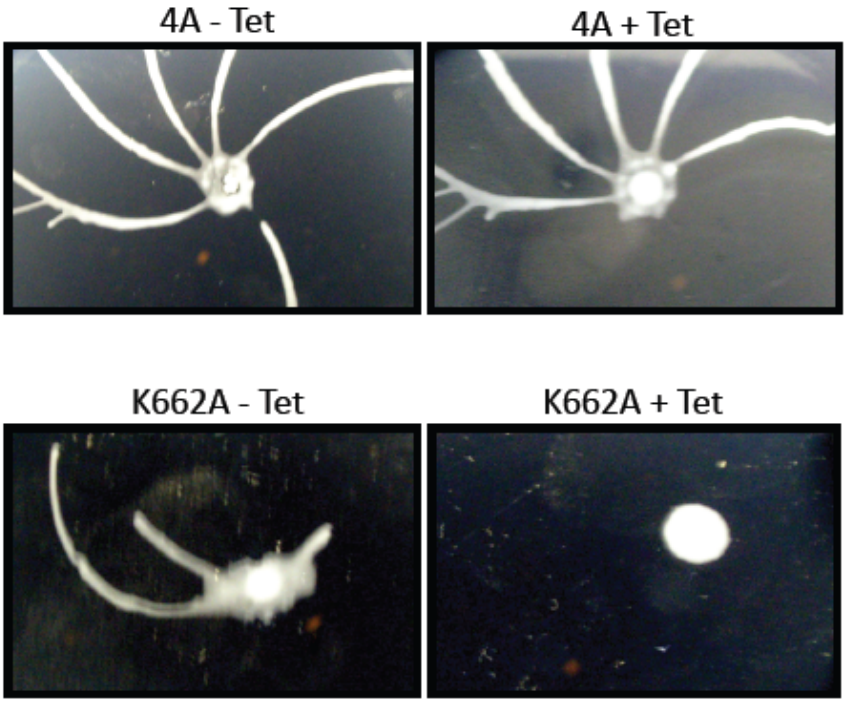


Figure 5-S4. The K662A mutant has defective motility and is unable to form radial projections. 4A and K662A mutants were grown in the presence or absence of tetracycline for 3 days, as indicated. Cells were then assayed for social motility by plating on Cunningham's SM media supplemented with 0.4% semi-solid agarose and 1 μg/mL tetracycline according to standard methods (35). Pictures were taken at day 5 post-plating.

REFERENCES

1. Satir, P. 1995. Landmarks in cilia research from Leeuwenhoek to us. Cell Motil. Cytoskel. 32:90-4.
2. Fritz-Laylin, L. K., S. E. Prochnik, M. L. Ginger, J. B. Dacks, M. L. Carpenter, M. C. Field, A. Kuo, A. Paredez, J. Chapman, and J. Pham. 2010. The Genome of Naegleria gruberi Illuminates Early Eukaryotic Versatility. Cell 140:631-642.
3. Takeda, S., and K. Narita. 2012. Structure and function of vertebrate cilia, towards a new taxonomy. Differentiation 83:S4-11.
4. Wilson, N. F. 2008. Gametic cell adhesion and fusion in the unicellular alga Chlamydomonas. Methods Mol Biol 475:39-51.
5. Ginger, M. L., N. Portman, and P. G. McKean. 2008. Swimming with protists: perception, motility and flagellum assembly. Nat Rev Microbiol 6:838-50.
6. Bastin, P., T. J. Pullen, F. F. Moreira-Leite, and K. Gull. 2000. Inside and outside of the trypanosome flagellum:a multifunctional organelle. Microbes Infect 2:1865-74.
7. Vincensini, L., T. Blisnick, and P. Bastin. 2011. 1001 model organisms to study cilia and flagella. Biol Cell 103:109-30.
8. Snell, W. J., J. Pan, and Q. Wang. 2004. Cilia and flagella revealed: from flagellar assembly in Chlamydomonas to human obesity disorders. Cell 117:693-7.
9. Badano, J. L., N. Mitsuma, P. L. Beales, and N. Katsanis. 2006. The Ciliopathies: An Emerging Class of Human Genetic Disorders. Annu Rev Genomics Hum Genet 7:125-148.

10. Satir, P., and S. T. Christensen. 2006. Overview of Structure and Function of Mammalian Cilia. Annu Rev Physiol.
11. Fliegauf, M., T. Benzing, and H. Omran. 2007. When cilia go bad: cilia defects and ciliopathies. Nat Rev Mol Cell Biol 8:880-93.
12. Langousis, G., and K. L. Hill. 2014. Motility and more: the flagellum of Trypanosoma brucei. Nat Rev Microbiol 12:505-18.
13. Steverding, D. 2008. The history of African trypanosomiasis. Parasit Vectors 1:3.
14. Kohl, L., and P. Bastin. 2005. The flagellum of trypanosomes. Int Rev Cytol 244:227-85.
15. Witman, G. B., J. Plummer, and G. Sander. 1978. Chlamydomonas flagellar mutants lacking radial spokes and central tubules. Structure, composition, and function of specific axonemal components. J Cell Biol 76:729-47.
16. Smith, E. F., and W. S. Sale. 1992. Regulation of dynein-driven microtubule sliding by the radial spokes in flagella. Science 257:1557-9.
17. Piperno, G., K. Mead, and W. Shestak. 1992. The inner dynein arms I2 interact with a "dynein regulatory complex" in Chlamydomonas flagella. J Cell Biol 118:1455-63.
18. Bower, R., K. VanderWaal, E. O'Toole, L. Fox, C. Perrone, J. Mueller, M. Wirschell, R. Kamiya, W. S. Sale, and M. E. Porter. 2009. IC138 defines a subdomain at the base of the I1 dynein that regulates microtubule sliding and flagellar motility. Mol Biol Cell 20:3055-63.
19. Bower, R., D. Tritschler, K. Vanderwaal, C. A. Perrone, J. Mueller, L. Fox, W. S. Sale, and M. E. Porter. 2013. The N-DRC forms a conserved biochemical

complex that maintains outer doublet alignment and limits microtubule sliding in motile axonemes. Mol Biol Cell.

20. Porter, M. E., and W. S. Sale. 2000. The 9 + 2 axoneme anchors multiple inner arm dyneins and a network of kinases and phosphatases that control motility. J Cell Biol 151:F37-42.

21. Nicastro, D., C. Schwartz, J. Pierson, R. Gaudette, M. E. Porter, and J. R. McIntosh. 2006. The molecular architecture of axonemes revealed by cryoelectron tomography. Science 313:944-8.

22. Heuser, T., M. Raytchev, J. Krell, M. E. Porter, and D. Nicastro. 2009. The dynein regulatory complex is the nexin link and a major regulatory node in cilia and flagella. Journal of Cell Biology 187:921-33.

23. Ralston, K. S., and K. L. Hill. 2006. Trypanin, a Component of the Flagellar Dynein Regulatory Complex, Is Essential in Bloodstream Form African Trypanosomes. PLoS Pathogens 2:873-882, e101 doi:10.1371/journal.ppat.0020101.

24. Rupp, G., and M. E. Porter. 2003. A subunit of the dynein regulatory complex in Chlamydomonas is a homologue of a growth arrest-specific gene product. J Cell Biol 162:47-57.

25. Colantonio, J. R., J. Vermot, D. Wu, A. D. Langenbacher, S. Fraser, J. N. Chen, and K. L. Hill. 2009. The dynein regulatory complex is required for ciliary motility and otolith biogenesis in the inner ear. Nature 457:205-9.

26. Wirschell, M., H. Olbrich, C. Werner, D. Tritschler, R. Bower, W. S. Sale, N. T. Loges, P. Pennekamp, S. Lindberg, U. Stenram, B. Carlen, E. Horak, G. Kohler,

P. Nurnberg, G. Nurnberg, M. E. Porter, and H. Omran. 2013. The nexin-dynein regulatory complex subunit DRC1 is essential for motile cilia function in algae and humans. Nat Genet 45:262-8.

27. Baron, D. M., K. S. Ralston, Z. P. Kabututu, and K. L. Hill. 2007. Functional genomics in Trypanosoma brucei identifies evolutionarily conserved components of motile flagella. J Cell Sci 120:478-91.

28. Nguyen, H. T., J. Sandhu, G. Langousis, and K. L. Hill. 2013. CMF22 is a broadly conserved axonemal protein and is required for propulsive motility in Trypanosoma brucei. Eukaryot Cell 12:1202-13.

29. Sonnhammer, E. L., S. R. Eddy, and R. Durbin. 1997. Pfam: a comprehensive database of protein domain families based on seed alignments. Proteins 28:405-20.

30. Terrak, M., L. R. Otterbein, G. Wu, L. A. Palecanda, R. C. Lu, and R. Dominguez. 2002. Crystallization, X-ray characterization and selenomethionine phasing of Mlc1p bound to IQ motifs from myosin V. Acta Crystallogr D Biol Crystallogr 58:1882-5.

31. Zuhlke, R. D., G. S. Pitt, R. W. Tsien, and H. Reuter. 2000. Ca2+-sensitive inactivation and facilitation of L-type Ca2+ channels both depend on specific amino acid residues in a consensus calmodulin-binding motif in the(alpha)1C subunit. J Biol Chem 275:21121-9.

32. Saraste, M., P. R. Sibbald, and A. Wittinghofer. 1990. The P-loop--a common motif in ATP- and GTP-binding proteins. Trends Biochem Sci 15:430-4.

33. Ralston, K. S., N. K. Kisalu, and K. L. Hill. 2011. Structure-function analysis of dynein light chain 1 identifies viable motility mutants in bloodstream-form Trypanosoma brucei. Eukaryot Cell 10:884-94.

34. Oberholzer, M., S. Morand, S. Kunz, and T. Seebeck. 2006. A vector series for rapid PCR-mediated C-terminal in situ tagging of Trypanosoma brucei genes. Mol Biochem Parasitol 145:117-20.

35. Oberholzer, M., M. A. Lopez, B. T. McLelland, and K. L. Hill. 2010. Social motility in african trypanosomes. PLoS Pathog 6:e1000739.

36. Yamniuk, A. P., and H. J. Vogel. 2004. Calmodulin's flexibility allows for promiscuity in its interactions with target proteins and peptides. Mol Biotechnol 27:33-57.

37. Bahler, M., and A. Rhoads. 2002. Calmodulin signaling via the IQ motif. FEBS Lett 513:107-13.

38. Rhoads, A. R., and F. Friedberg. 1997. Sequence motifs for calmodulin recognition. FASEB J 11:331-40.

39. Alexander, K. A., B. M. Cimler, K. E. Meier, and D. R. Storm. 1987. Regulation of calmodulin binding to P-57. A neurospecific calmodulin binding protein. J Biol Chem 262:6108-13.

40. Cimler, B. M., T. J. Andreasen, K. I. Andreasen, and D. R. Storm. 1985. P-57 is a neural specific calmodulin-binding protein. J Biol Chem 260:10784-8.

41. Wendler, P., S. Ciniawsky, M. Kock, and S. Kube. 2012. Structure and function of the AAA+ nucleotide binding pocket. Biochim Biophys Acta 1823:2-14.

42. Snider, J., and W. A. Houry. 2008. AAA+ proteins: diversity in function, similarity in structure. Biochem Soc Trans 36:72-7.

43. Walker, J. E., M. Saraste, M. J. Runswick, and N. J. Gay. 1982. Distantly related sequences in the alpha- and beta-subunits of ATP synthase, myosin, kinases and other ATP-requiring enzymes and a common nucleotide binding fold. EMBO J 1:945-51.

44. Hekimi, S., and D. Kershaw. 1993. Axonal guidance defects in a Caenorhabditis elegans mutant reveal cell-extrinsic determinants of neuronal morphology. J Neurosci 13:4254-71.

45. Hedgecock, E. M., J. G. Culotti, and D. H. Hall. 1990. The unc-5, unc-6, and unc-40 genes guide circumferential migrations of pioneer axons and mesodermal cells on the epidermis in C. elegans. Neuron 4:61-85.

46. Stringham, E., N. Pujol, J. Vandekerckhove, and T. Bogaert. 2002. unc-53 controls longitudinal migration in C. elegans. Development 129:3367-79.

47. Maes, T., A. Barcelo, and C. Buesa. 2002. Neuron navigator: a human gene family with homology to unc-53, a cell guidance gene from Caenorhabditis elegans. Genomics 80:21-30.

48. Merrill, R. A., L. A. Plum, M. E. Kaiser, and M. Clagett-Dame. 2002. A mammalian homolog of unc-53 is regulated by all-trans retinoic acid in neuroblastoma cells and embryos. Proc Natl Acad Sci U S A 99:3422-7.

49. Peeters, P. J., A. Baker, I. Goris, G. Daneels, P. Verhasselt, W. H. Luyten, J. J. Geysen, S. U. Kass, and D. W. Moechars. 2004. Sensory deficits in mice

hypomorphic for a mammalian homologue of unc-53. Brain Res Dev Brain Res 150:89-101.

50. Sakato, M., and S. M. King. 2004. Design and regulation of the AAA+ microtubule motor dynein. J Struct Biol 146:58-71.

51. Zhang, D., and L. Aravind. 2012. Novel transglutaminase-like peptidase and C2 domains elucidate the structure, biogenesis and evolution of the ciliary compartment. Cell Cycle 11:3861-75.

52. Schneider, A., U. Plessmann, and K. Weber. 1997. Subpellicular and flagellar microtubules of Trypanosoma brucei are extensively glutamylated. J Cell Sci 110:431-7.

53. Kubo, T., H. A. Yanagisawa, T. Yagi, M. Hirono, and R. Kamiya. 2010. Tubulin polyglutamylation regulates axonemal motility by modulating activities of inner-arm dyneins. Curr Biol 20:441-5.

54. Kubo, T., T. Yagi, and R. Kamiya. 2012. Tubulin polyglutamylation regulates flagellar motility by controlling a specific inner-arm dynein that interacts with the dynein regulatory complex. Cytoskeleton (Hoboken) 69:1059-68.

55. Wirtz, E., S. Leal, C. Ochatt, and G. A. Cross. 1999. A tightly regulated inducible expression system for conditional gene knock-outs and dominant-negative genetics in *Trypanosoma brucei*. Mol. Biochem. Parasitol. 99:89-101.

56. Oberholzer, M., M. A. Lopez, K. S. Ralston, and K. L. Hill. 2009. Approaches for functional analysis of flagellar proteins in African trypanosomes. Methods in Cell Biology 93:21-57.

57. Schultz, J., F. Milpetz, P. Bork, and C. P. Ponting. 1998. SMART, a simple modular architecture research tool: identification of signaling domains. Proc Natl Acad Sci U S A 95:5857-64.

58. Merchant, S., and L. Bogorad. 1986. Regulation by copper of the expression of plastocyanin and cytochrome c552 in Chlamydomonas reinhardi. Mol Cell Biol 6:462-9.

59. Baron, D. M., Z. P. Kabututu, and K. L. Hill. 2007. Stuck in reverse: loss of LC1 in Trypanosoma brucei disrupts outer dynein arms and leads to reverse flagellar beat and backward movement. J Cell Sci 120:1513-20.

60. Kabututu, Z. P., M. Thayer, J. H. Melehani, and K. L. Hill. 2010. CMF70 is a subunit of the dynein regulatory complex. Journal of Cell Science 123:3587-95.

61. Ralston, K. S., A. G. Lerner, D. R. Diener, and K. L. Hill. 2006. Flagellar Motility Contributes to Cytokinesis in Trypanosoma brucei and Is Modulated by an Evolutionarily Conserved Dynein Regulatory System. Eukaryotic Cell 5:696-711.

62. Chu, D. T., and M. W. Klymkowsky. 1989. The appearance of acetylated alpha-tubulin during early development and cellular differentiation in Xenopus. Dev Biol 136:104-17.

63. Robinson, D., P. Beattie, T. Sherwin, and K. Gull. 1991. Microtubules, tubulin, and microtubule-associated proteins of trypanosomes. Methods. Enzymol. 196:285-99.

Chapter 6

Future Directions

This dissertation explores various mechanisms of motility in *T. brucei* parasites for signaling pathways required for surface-induced behavior and for individual movement. Chapter 2 discusses the novel social behavior of *T. brucei* parasites and efforts to identify genes required for social motility. Chapters 3-5 describe a multitude of experiments performed to characterize CMF22, a broadly conserved protein in diverse eukaryotes with motile flagella/cilia that is found to be required for propulsive motility and complete N-DRC assembly.

The findings described in this dissertation expand our current knowledge of both social microbiology and flagellum biology. However, these discoveries have merely opened the doors for additional progress that will enhance our understanding of motility. This chapter outlines preliminary data and future experiments for the continuation of this work.

Social Motility in *T. brucei*

In Chapter 2, both a forward and reverse genetics screen was performed to identify genes that regulate social motility in *T. brucei*. An RNAi library screen was optimized for high-throughput screening, however the assay itself was deemed to macroscopic and variable for efficient screening. One method to improve the screen would be to use time-lapse microscopy to identify essential precursors of colony formation such as a pattern of movement that must occur for parasites to form radial projections. Another technique would be to link this microscopic phenotype with a fluorescence marker to easily identify mutants.

As outlined in Chapter 2, the inducible RNAi library can be enriched prior to screening. As illustrated in Figure 2-7, the RNAi library would be plated the center of a large, semi-solid agarose plate and allowed to form radial projections. Mutants could be isolated from the center for “SoMo (-)” mutants or from the tips of the radial projections for “hypersocial” mutants. These pre-selected mutants would be innoculated on semi-solid agarose multiple times to enrich for the mutants. These mutants can then be sorted as individual clones and the identity of these mutants can be determined using nested PCR to identify the gene (1).

The second approach was a targeted screen to identify genes that bind cNMP. Unpublished data from the lab has revealed that the cAMP pathway is required for social motility in *T. brucei*. Thus, 14 genes with putative cNMP-binding domains were investigated. Individual knockdown of each of these genes and preliminary social motility assays on the heterogenous knockdown pools of each candidate gene was performed. From this biased screen, cNMP4, seemed to have a “hypersocial” phenotype. The heterogenous pool of cNMP4 knockdown mutants was sub-cloned and the social motility assay was performed to reveal a potential “hypersocial” phenotype. The level of knockdown for cNMP4 was assessed for cNMP4 clone 4 and the level of knockdown was only 35% (Figure 4-12). Additional clones would need to be tested to identify a clone with greater knockdown to see if cNMP4 is required for social motility. Other cNMPs to test would be cNMP1 since Gould *et al.* found that knockdown of cNMP1 (cAMP Response Protein 1, CARP1) allows for resistance to the phosphodiesterase inhibitor CpdA and that this protein is responsive to cAMP. The function of cNMP1/CARP1 is still unknown and may function in social motility.

Another enrichment screen to identify cNMP-binding proteins and downstream cAMP effectors that are required for social motility would be to innoculate the RNAi library on semi-solid agarose plates supplemented with the phosphodiesterase inhibitor CpdA. In this gain-of-function screen, mutants that can bypass the CpdA inhibition and form radial projections can be isolated as social motility mutants that are responsive to cAMP. Like the aforementioned unbiased enrichment screen, these mutants can be sorted as described in Chapter 2 and using nested PCR, the genes required for social motility can be identified.

Additional techniques for genome-wide screening through RNA sequencing was performed by Dr. Michael Oberholzer in which RNA parasites cultivated on semi-solid surfaces were compared to parasites grown in suspension cultures (unpublished data). This approach identified 22 candidate genes that were at least two-fold upregulated on plates. These candidates are currently being evaluated by independent RNA knockdown and tested using the social motility assay as a read-out.

Conserved axonemal motility

CMF22 is an axonemal protein that is required for propulsive motility and association of this protein to the axoneme is reduced in N-DRC mutants (2, 3). To determine if the sub-localization of CMF22 is within the N-DRC and to identify binding partners of CMF22, several approaches were taken. One method was to compare the axonemes of CMF22 knockdown mutant to wild-type axonemes using cryo-electron tomography. Results from this study discussed in Chapter 4 revealed that CMF22 is

required for assembly of the N-DRC proximal lobe. However, this data does not definitively identify the sub-localization of CMF22 since the proximal lobe could consist of other proteins that require CMF22 for assembly. In one approach, called BioID, CMF22 is tagged with a mutated version of the BirA enzyme (BirA*). Three versions of the tagging construct were created and are illustrated in Figure 6-1A. This mutated BirA can biotinylate proteins in close proximity to a protein of interest to co-immunoprecipitate binding partners. In addition, this technique allows for co-immunoprecipitation of skeletal proteins such as CMF22 because it allows for stringent solubilization techniques (4). This proximity-dependent approach has been used in *T. brucei* to identify proteins in the bilobe, a discrete cytoskeletal structure with few known protein components (5). In this approach, we planned to solubilize the axonemes with SDS and pull down biotinylated proteins using streptavidin beads. It is expected that mudpit mass spectrometry will be able to identify the binding partners of CMF22 and that these proteins will be known as well as unknown N-DRC proteins. Thus far, only the *in situ* CMF22 tagging construct containing BirA* at the C-terminus and the N-terminal tetracycline-inducible BirA*-CMF22 was cloned and transfected into *T. brucei* procyclic-form parasites. This resulted in expression Myc-BirA*-CMF22 at approximate 135 kDa (Figure 6-1B). There was no anti-HA labeling for the *in situ* CMF22-BirA* but there was axoneme as well as subpellicular microtubule labeling for the N-terminal tetracycline-inducible BirA*-CMF22. Unfortunately, as illustrated by immunofluorescence, efforts to exogenously biotinylate the N-terminal BirA*-CMF22 have been unsuccessful (Figure 6-1C).

In another approach to localize CMF22, a technique using cryoET with biotin-streptavidin is underway. This approach was developed and pioneered by the Kikkawa group and has been used to successfully localize proteins in the outer-inner dynein linker, the inner junction of doublet microtubules, and radial spokes in *C. reinhardtii* (5-9). The method is a structural labeling method in which proteins of interest are tagged with a biotinylation domain and the protein is then endogenously biotinylated. The addition of the biotin binding partner, streptavidin, is large enough to generate a high signal intensity for visualization by electron microscopy. Because biotin is small but streptavidin is large, the system also has high specificity and precision of localization (6, 10). Current efforts are focused on cloning a biotin carboxyl carrier (BCCP) domain at the C-terminus of CMF22 with a HA epitope tag (Figure 6-2). Thus far, anti-myc shows that CMF22 is localized to the axoneme, however, immunoflourescence using streptavidin did not show endogenous biotinylation (Figure 6-2). Commercial BirA to biotinylate the axoneme was suggested and efforts to optimize this approach is underway.

CMF22 was found to remain in a ~900 kDa complex in the soluble fraction (S1) of another N-DRC mutant, trypanin, when induced with tetracycline (Figure 6-3, right). Since the N-DRC is a 1.5 mDa complex and CMF22 may be localized to the proximal lobe, the 900 kDa complex may be a large portion of the N-DRC. Co-immunoprecipitation of this CMF22 sub-complex is currently underway and the strategy is illustrated in Figure 6-3, left. In one approach, anti-HA beads are being used to co-immunoprecipitate CMF22-HA. Preliminary experiments to attempt to co-immunuprecipitate CMF22-HA using anti-HA beads in the S1 fraction of induced

trypanin-knockdown mutants have been proven difficult since it seems that CMF22 precipitates on beads and even stringent elution methods such as 8M urea does not work (Figure 6-4, beads). To address this issue, two approaches have been taken. One method is to perform on-bead digestion in which proteins are trypsinized on the anti-HA beads themselves. Another technique is to use express BCCP tagged CMF22 in trypanin knockdown mutants and as described previously, perform co-immunoprecipitation of the soluble 900 kDa complex using streptavidin beads. On-bead digestion for streptavidin beads has been performed routinely, therefore if BCCP-tagged CMF22 can be expressed and endogenously biotinylated, the binding partners of CMF22 can be identified.

Finally, stable isotope labeling by amino acids (SILAC) is another approach that can be used to identify which proteins are lost when compared to a wild-type sample. SILAC was performed on CMF22, in addition to other N-DRC mutants by Dr. Michelle Shimogawa and Gerasimos Langousis. Thus far, preliminary SILAC analysis was able to detect reduced amounts of other N-DRC proteins as well as numerous hypothetical proteins with interesting domains in N-DRC mutants when compared to wild-type cells (unpublished data). Promising results for this initial experiment are expected to be informative in reconstructing the molecular architecture of the N-DRC, a central hub for regulating axonemal motility.

Mutations of the IQ and AAA domains were performed in Chapter 5 to determine the contribution of these domains and potentially elucidate the mechanism of motility coordination through CMF22. Results from the mutation experiments have found that in

the context of *T. brucei* motility in suspension cultures, the IQ motif is not required for propulsive motility. On the other hand, mutation of the key lysine required for ATP binding in the AAA domain of CMF22 results in a motility defect. As discussed, the impact of the mutation is not clear since there is also decreased protein abundance in the K662A point mutant. AAA domains typically form ring-like structures, either by oligomerization to form homohexamers or through protein folding of a large protein (11). Sequence analysis of CMF22 predicts that like other AAA proteins, it may form a ring (personal communication). This may explain the possible dominant negative effect of the uninduced K662A point mutant in which uninduced cells do not have propulsive motility like the uninduced “add-back” Ri cells or the uninduced 4A point mutant. Also, if the point mutation alters CMF22 structure so that CMF22 stability is compromised when it cannot oligomerize, this could explain the decreased protein expression. To determine if CMF22 is a dimer, both endogenous CMF22 alleles could be tagged with different epitope tags (anti-HA and anti-Myc) in the trypanin knockdown mutant so that under tetracycline induction, CMF22 would be soluble and can be co-immunprecipitated. Thus, using anti-HA beads to co-immunoprecipitate CMF22, it is expected that if CMF22 is a dimer, the Myc-tagged CMF22 can be detected in this complex using anti-Myc antibodies following the anti-HA pull-down. The experiment should hold true in the vice versa experiment as well. If CMF22, like predicted, is a homohexamer, this ~900 kDa complex could be mostly CMF22 proteins. Additionally, other clones of the K662A mutants are currently being screened to find a clone that has higher levels of protein expression so that the contribution of the point mutant in regulating propulsive motility can be clearly assessed.

Due to the high conservation between *T. brucei* and the canonical eukaryotic axoneme, defining the mechanism of motility through structural analysis and protein-protein interaction will help elucidate broadly conserved mechanisms of motility in other organisms such as humans. As yet, the human homolog of CMF22 has only been associated with teratozoospermia, a disease in which sperm have physiological and motility defects (10). CMF22 may be an undiscovered key player in other ciliopathies and current advances in identifying the mechanism of CMF22 action within the N-DRC as well as in axonemal motility in eukaryotes will be useful in finding conserved mechanisms of motility in flagellar biology.

FIGURES

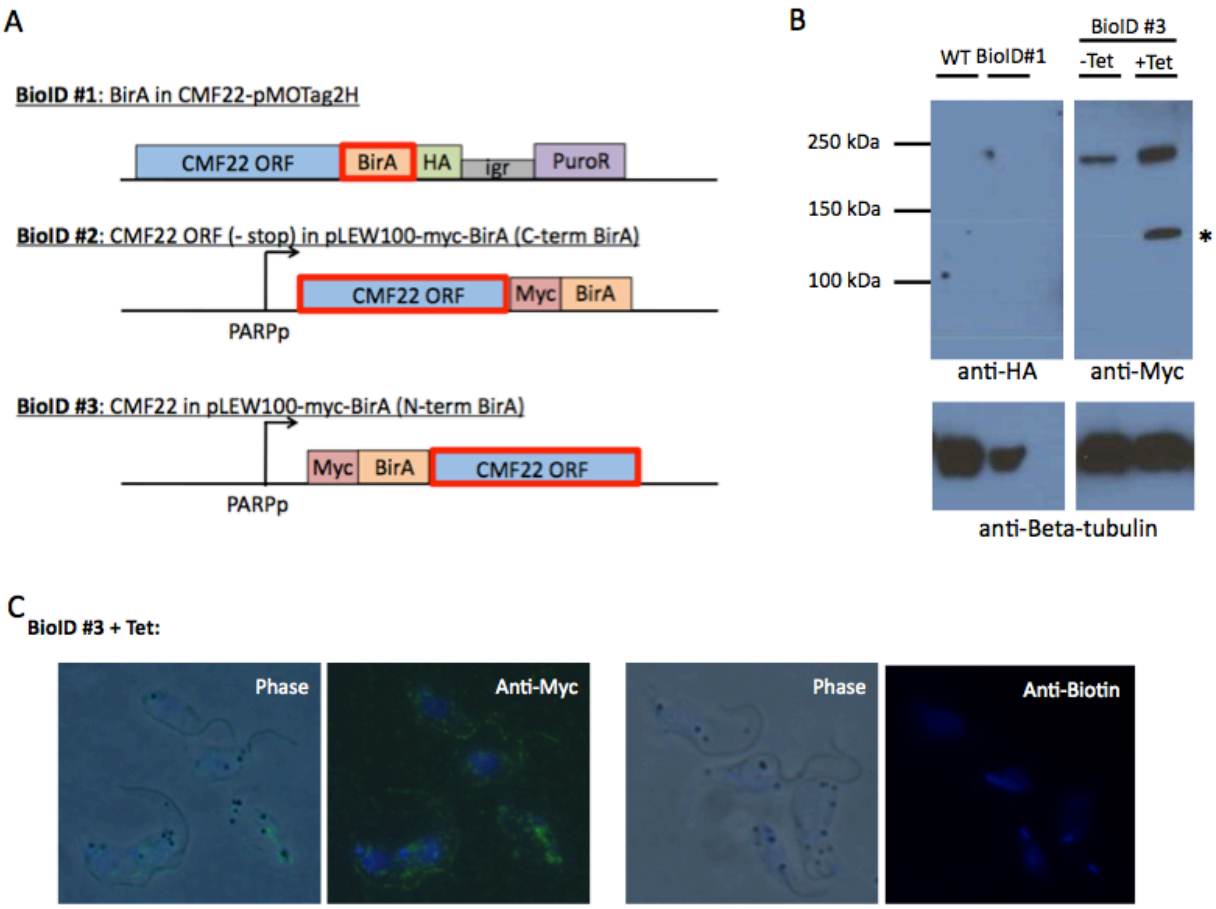


Figure 6-1. BioID tagging of CMF22 to identify interacting proteins. (A) Schematic of BioID constructs created. For BioID #1, BirA* was cloned into the *in situ* tagging pMOTag2H plasmid. For BioID #2 and #3, the CMF22 ORF was cloned into a tetracyline-inducible construct created by (5). (B) BioID #3 expresses Myc-tagged CMF22 at approximately 135 kDa, denoted by the asterisk. (C) Anti-Myc shows Myc-BirA*-CMF22 is localized along the axoneme and in microtubules (left panels), but is not biotinylated (right panels).

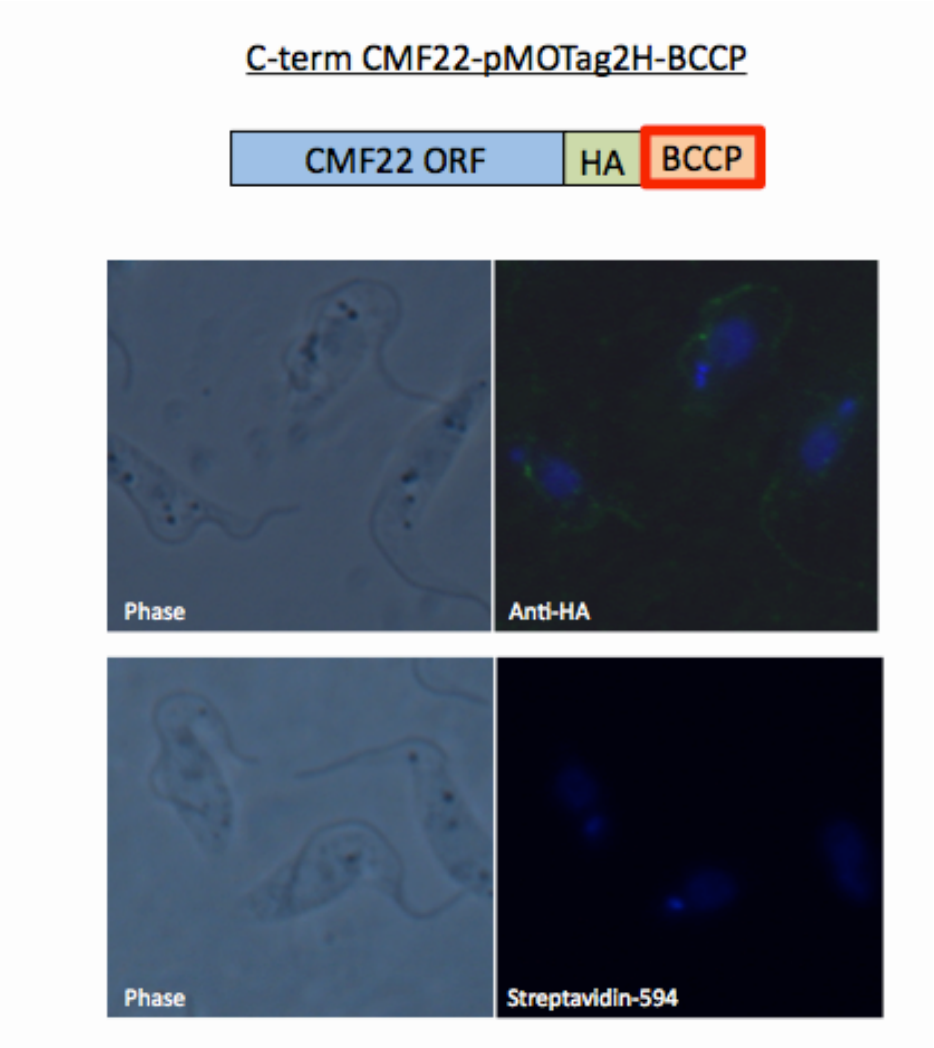


Figure 6-2. BCCP tagging of CMF22 for sub-localization by CryoET. The biotin carboxyl carrier protein domain (BCCP) was added at the C- terminus of CMF22 as shown in the schematic to the left. IFA (right panels) show that CMF22-HA-BCCP is localized to the axoneme in detergent-extracted cells upper right) but streptavidin staining (bottom right) shows that there is no biotinylation.

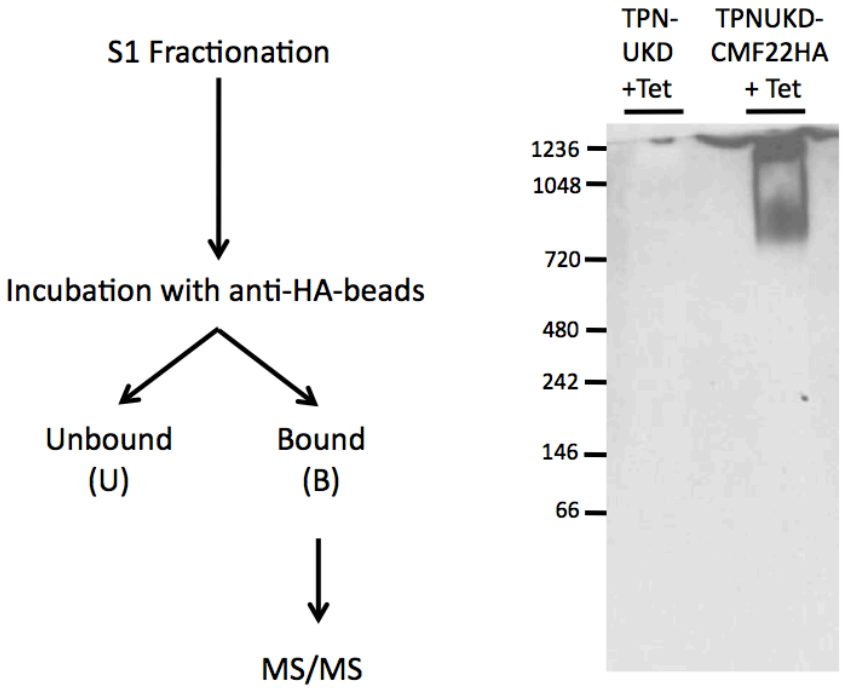


Figure 6-3. Co-immunoprecipitation of the 900kDa soluble CMF22-HA complex. (Left) Schematic of co-immunoprecipitation includes taking the detergent soluble (S1) fraction and incubating the lysate with anti-HA beads. The bound fraction containing the complex is eluted and mudpit MS/MS spectrometry will be used to identify CMF22 binding partners. (Right) S1 fraction of RNAi-induced trypanin mutants were run on a blue native gel and the band in the right lane shows that CMF22-HA is in a ~900 kDa complex.

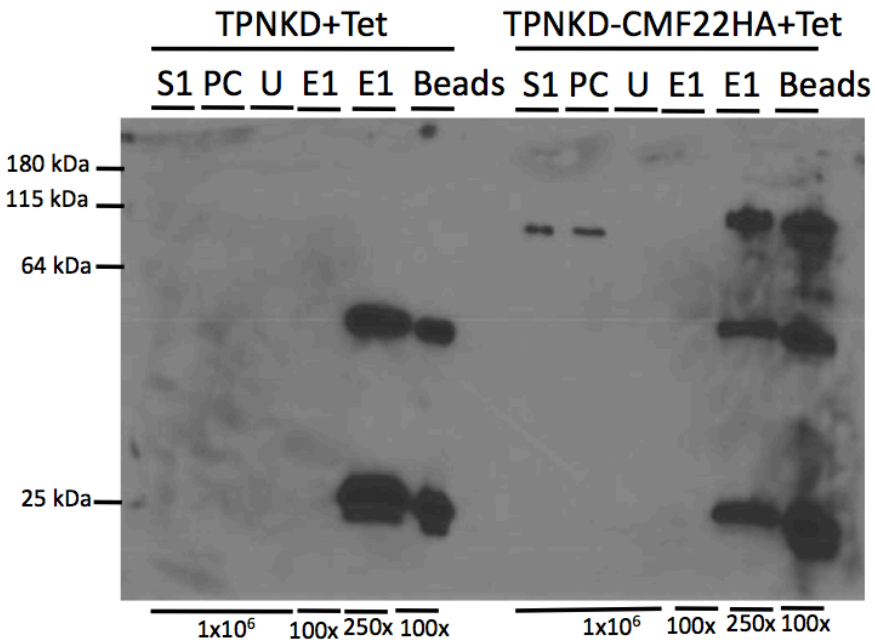


Figure 6-4. CMF22-HA co-immunoprecipitation using the S1 fraction of tetracycline-induced trypanin mutants and eluted using 8M urea. Western blot using anti-HA shows that CMF22-HA (110 kDa band) in the S1 fraction of trypanin mutants + Tet are soluble (S1) and after pre-clearing the lysate (PC), no protein was lost. CMF22-HA and interacting proteins were eluted using 8M urea (E1, E2) and is seen in $2.5x10^8$ cell equivalents (250x) but is also still massively bound to beads (Beads). Bands corresponding to 50 and 25 kDa are likely heavy and light chains of the anti-HA antibody.

REFERENCES

1. Morris, J. C., Z. Wang, M. E. Drew, and P. T. Englund. 2002. Glycolysis modulates trypanosome glycoprotein expression as revealed by an RNAi library. Embo J 21:4429-38.
2. Nguyen, H. T., J. Sandhu, G. Langousis, and K. L. Hill. 2013. CMF22 is a broadly conserved axonemal protein and is required for propulsive motility in Trypanosoma brucei. Eukaryot Cell 12:1202-13.
3. Bower, R., D. Tritschler, K. Vanderwaal, C. A. Perrone, J. Mueller, L. Fox, W. S. Sale, and M. E. Porter. 2013. The N-DRC forms a conserved biochemical complex that maintains outer doublet alignment and limits microtubule sliding in motile axonemes. Mol Biol Cell.
4. Roux, K. J., D. I. Kim, M. Raida, and B. Burke. 2012. A promiscuous biotin ligase fusion protein identifies proximal and interacting proteins in mammalian cells. J Cell Biol 196:801-10.
5. Morriswood, B., K. Havlicek, L. Demmel, S. Yavuz, M. Sealey-Cardona, K. Vidilaseris, D. Anrather, J. Kostan, K. Djinovic-Carugo, K. J. Roux, and G. Warren. 2013. Novel bilobe components in Trypanosoma brucei identified using proximity-dependent biotinylation. Eukaryot Cell 12:356-67.
6. Oda, T., and M. Kikkawa. 2013. Novel structural labeling method using cryo-electron tomography and biotin-streptavidin system. J Struct Biol 183:305-11.
7. Oda, T., T. Yagi, H. Yanagisawa, and M. Kikkawa. 2013. Identification of the outer-inner dynein linker as a hub controller for axonemal dynein activities. Curr Biol 23:656-64.

8. Oda, T., H. Yanagisawa, T. Yagi, and M. Kikkawa. 2014. Mechanosignaling between central apparatus and radial spokes controls axonemal dynein activity. J Cell Biol 204:807-19.

9. Yanagisawa, H. A., G. Mathis, T. Oda, M. Hirono, E. A. Richey, H. Ishikawa, W. F. Marshall, M. Kikkawa, and H. Qin. 2014. FAP20 is an inner junction protein of doublet microtubules essential for both the planar asymmetrical waveform and stability of flagella in Chlamydomonas. Mol Biol Cell 25:1472-83.

10. Platts, A. E., D. J. Dix, H. E. Chemes, K. E. Thompson, R. Goodrich, J. C. Rockett, V. Y. Rawe, S. Quintana, M. P. Diamond, L. F. Strader, and S. A. Krawetz. 2007. Success and failure in human spermatogenesis as revealed by teratozoospermic RNAs. Hum Mol Genet 16:763-73.

11. Snider, J., and W. A. Houry. 2008. AAA+ proteins: diversity in function, similarity in structure. Biochem Soc Trans 36:72-7.

Chapter 7

Conclusion and Perspectives

The eukaryotic flagellum is a highly conserved organelle that functions in motility, sensing, transport, pathogenesis and human development (1, 2). These cellular structures are ubiquitous organelles and are classically associated with motility in a number of organisms. Various genetic and proteomic approaches to define the eukaryotic flagellum have identified hundreds of flagellar proteins, however, the mechanism in which these proteins interact with one another to drive motility is still unknown (3-6). In the model organism *T. brucei*, the flagellum is required for motility, infection and pathogenesis (7, 8). The *T. brucei* flagellum has high conservation to the canonical "9 + 2" axoneme and the genetic amenability of this organism have made *T. brucei* an incredible system for studying flagellum biology.

Social motility in *T. brucei*

The first focus of this dissertation was to examine the novel social behavior exhibited by these parasites. Recent advances in our laboratory have revealed that *T. brucei* are able to communicate with one another to collectively migrate as a group across surfaces (9). The mechanism of how these individual parasites are able to come together to form a group and subsequently form projections that radiate outwards from the site of innoculation is largely unknown. To identify genes required for social behavior, a tetracyline-inducible RNAi library developed by another laboratory was utilized in combination with the social motility assay. This work optimized an approach to use this RNAi library through a proof-of-concept experiment and several pilot experiments to optimize parameters for high-throughput screening. Although the social

motility assay was considered too variable and macroscopic for high-throughput, the method of sorting and growth of these parasites in bulk was optimized. Efforts to identify more microscopic or fluorescent read-outs are underway.

Another targeted approach to identify genes required for social motility was to knockdown genes with putative cNMP-binding domains and test their ability to engage in social behavior. Unpublished data from our laboratory has revealed that the cAMP pathway regulates social motility. Knockdown of certain adenylate cyclases, a family of proteins that generate cAMP, resulted in a “hyper-social” phenotype when these mutants were plated on semi-solid agarose. In contrast, knockdown mutants of phosphodiesterases, proteins that break down cAMP, resulted in parasites that were unable to form radial projections. To identify the mechanism of social motility through the cAMP pathway, this study evaluated the putative proteins that function downstream of the cAMP pathway through binding cAMP or cGMP. Using a search algorithm in both the SMART and Pfam databases, 14 candidates with potential cNMP-binding sites were identified. Individual knockdown of these genes were performed and these candidates are currently being evaluated. Recent work from the Boshart lab that identified other proteins that function downstream of the cAMP pathway and these are also potential candidates for regulating social behavior (10).

Altogether, this dissertation has employed both forward and reverse genetics to identify several candidates that potentially coordinate social behavior. Current efforts are focused on evaluating these candidates genes.

Conserved mechanism of motility

T. brucei is an exemplary model organism for the study of flagellum biology. Highly efficient homologous recombination, the presence of RNAi machinery, and inducible genetic vectors for expression and knockdown/ knockout of genes are just a few of the many diverse molecular tools in *T. brucei* (11). Furthermore, the *T. brucei* is sequenced and annotated, which allows for ease in genetic manipulation. The *T. brucei* flagellum is composed of a canonical “9 + 2” axoneme with core proteins conserved between *T. brucei* and other flagellated eukaryotic model organisms. The availability of complete genomic sequence has allowed for comparison of motility genes across divergent eukaryotic organisms with motile flagella and define key proteins essential for motility. An initial study compared 8 genomes of various eukaryotes with motile flagella against genomes of eukaryotes that lack flagella or have an immotile flagella (5). This study identified 50 genes that are core Components of Motile Flagella (CMF), many of which have been validated as proteins required for axonemal motility in *T. brucei* and other organisms. Investigation of genes broadly conserved in eukaryotes with motile flagella was expanded in Chapter 3 of this dissertation. The study compared the 50 CMF genes in 115 genomes to identify a broadly conserved gene with interesting domains (12). CMF22 was present in almost all organisms that have motile flagella and has an IQ motif at the N terminus as well as an ATPase Associated with various cellular Activities (AAA) domain at the C terminus. Biochemical fractionation and immunofluorescent localization identified CMF22 as an axonemal protein that is localized along the length of the flagellum. RNAi knockdown of CMF22 results in

defective propulsive motility, and normal motility is restored when an RNAi immune copy of the wild-type CMF22 gene is added back into the knockdown construct.

Phylogenetic, localization and biochemical data suggests that CMF22 is part of a microtubule-associated complex that regulates motility, the nexin-dynein regulatory complex (N-DRC). Additionally, Figure 3-8 shows that the association of CMF22-HA to the flagellum is compromised in *drc* mutants Trypanin and CMF70 (13, 14). Complementary work in Bower *et al.* also shows the loss of CMF22 in *drc* mutants in *C. reinhardtii* (15). Altogether, these data strongly suggested that CMF22 is part of the N-DRC. This hypothesis was investigated in Chapter 4 through high-resolution cryo-electron tomography of CMF22-UKD. Findings from Chapter 4 revealed that CMF22 is required for the assembly of the proximal lobe of the N-DRC and since were no disruptions to inner arm dyneins as seen by CryoET, the defect in propulsive motility can be entirely attributed to the loss of CMF22 and the loss of the proximal lobe of the N-DRC. This is an important find since this is the first N-DRC mutant identified that has a defect exclusively in the N-DRC.

In addition to the discovery that CMF22 is required for assembly of the proximal lobe of the N-DRC, this dissertation also presented high-resolution structural analysis of the *T. brucei* flagellum. This is the first high-quality structure of the flagella from an Excavate and the first analysis of flagella from a eukaryotic human pathogen. The flagella in *T. brucei* is critical for pathogenesis and key differences in flagella architecture in comparison to flagella from non-pathogenic eukaryotes may reveal novel features that are required for pathogenesis. Results show key conserved features such

as the outer dynein arms, inner dynein arms, the presence of radial spokes, and the N-DRC. However, there are also differences such as the missing inner dynein arm c, the lack of an inner-outer dyenin linker, a novel interdoublet linker, and more obvious extensions between neighboring microtubules than in other eukaryotic axonemes for which there is a 3D structure. These differences may contribute to the unique waveform of *T. brucei* that increases the parasite's ability to infect or evade host immune responses. Further studies that define contributions of these unique features may elucidate the mechanism of motility in *T. brucei*.

To characterize the contribution of CMF22 and how it possibly interacts with neighboring proteins, the putative domains of CMF22 were investigated in Chapter 5. The IQ motif and AAA domain of CMF22 was mutated to determine if these domains are required for propulsive motility and to potentially understand the mechanism of CMF22 action. Alanine substitutions of the IQ motif and the key lysine required for ATP-binding in the AAA domain were performed to create various mutant constructs. None of the IQ motif mutants had a defect in propulsive motility, however, the AAA mutant was not able to translocate as efficiently as wild-type cells. Therefore, in the context of propulsive motility in suspension cultures, the AAA mutant may be required for propulsive motility. The contribution of decreased protein expression in this AAA domain mutant is unknown and further analysis should be done using an AAA mutant that expresses wild-type levels of CMF22 or overexpression of the AAA mutant for expression of CMF22 at wild-type levels. In addition, determining if CMF22 functions as a dimer may also elucidate the mechanism of CMF22 action.

The findings in this dissertation contribute to our current understanding of novel mechanisms employed by *T. brucei* to communicate and cooperate at the multicellular level through social behavior and move at the individual level. Additionally, the results from CMF22 experiments also expand our understanding of conserved mechanisms of eukaryotic flagellum biology. The insight gained through these works uncovers both unique aspects of parasite biology that can be further exploited for potential therapeutics and conserved tenets of eukaryotic biology for discovering new links between cilia motility and ciliary diseases.

REFERENCES

1. Takeda, S., and K. Narita. 2012. Structure and function of vertebrate cilia, towards a new taxonomy. Differentiation 83:S4-11.
2. Wilson, N. F. 2008. Gametic cell adhesion and fusion in the unicellular alga Chlamydomonas. Methods Mol Biol 475:39-51.
3. Pazour, G. J., N. Agrin, J. Leszyk, and G. B. Witman. 2005. Proteomic analysis of a eukaryotic cilium. J Cell Biol 170:103-13.
4. Portman, N., S. Lacomble, B. Thomas, P. G. McKean, and K. Gull. 2008. Combining RNA Interference Mutants and Comparative Proteomics to Identify Protein Components and Dependences in a Eukaryotic Flagellum. Journal of Biological Chemistry 284:5610-5619.
5. Baron, D. M., K. S. Ralston, Z. P. Kabututu, and K. L. Hill. 2007. Functional genomics in Trypanosoma brucei identifies evolutionarily conserved components of motile flagella. J Cell Sci 120:478-91.
6. Oberholzer, M., G. Langousis, H. T. Nguyen, E. A. Saada, M. M. Shimogawa, Z. O. Jonsson, S. M. Nguyen, J. A. Wohlschlegel, and K. L. Hill. 2011. Independent analysis of the flagellum surface and matrix proteomes provides insight into flagellum signaling in mammalian-infectious Trypanosoma brucei. Mol Cell Proteomics 10:M111 010538.
7. Langousis, G., and K. L. Hill. 2014. Motility and more: the flagellum of Trypanosoma brucei. Nat Rev Microbiol 12:505-18.

8. Ralston, K. S., Z. P. Kabututu, J. H. Melehani, M. Oberholzer, and K. L. Hill. 2009. The Trypanosoma brucei flagellum: moving parasites in new directions. Annual Review of Microbiology 63:335-62.

9. Oberholzer, M., M. A. Lopez, B. T. McLelland, and K. L. Hill. 2010. Social motility in african trypanosomes. PLoS Pathog 6:e1000739.

10. Gould, M. K., S. Bachmaier, J. A. Ali, S. Alsford, D. N. Tagoe, J. C. Munday, A. C. Schnaufer, D. Horn, M. Boshart, and H. P. de Koning. 2013. Cyclic AMP effectors in African trypanosomes revealed by genome-scale RNA interference library screening for resistance to the phosphodiesterase inhibitor CpdA. Antimicrob Agents Chemother 57:4882-93.

11. Oberholzer, M., M. A. Lopez, K. S. Ralston, and K. L. Hill. 2009. Approaches for functional analysis of flagellar proteins in African trypanosomes. Methods in Cell Biology 93:21-57.

12. Nguyen, H. T., J. Sandhu, G. Langousis, and K. L. Hill. 2013. CMF22 is a broadly conserved axonemal protein and is required for propulsive motility in Trypanosoma brucei. Eukaryot Cell 12:1202-13.

13. Ralston, K. S., and K. L. Hill. 2006. Trypanin, a Component of the Flagellar Dynein Regulatory Complex, Is Essential in Bloodstream Form African Trypanosomes. PLoS Pathogens 2:873-882, e101 doi:10.1371/journal.ppat.0020101.

14. Kabututu, Z. P., M. Thayer, J. H. Melehani, and K. L. Hill. 2010. CMF70 is a subunit of the dynein regulatory complex. Journal of Cell Science 123:3587-95.

15. Bower, R., D. Tritschler, K. Vanderwaal, C. A. Perrone, J. Mueller, L. Fox, W. S. Sale, and M. E. Porter. 2013. The N-DRC forms a conserved biochemical complex that maintains outer doublet alignment and limits microtubule sliding in motile axonemes. Mol Biol Cell.

Appendix A

Independent Analysis of the Flagellum Surface and Matrix Proteomes Provides Insight into Flagellum Signaling in Mammalian-infectious *Trypanosoma brucei*

© 2011 by The American Society for Biochemistry and Molecular Biology, Inc.
This paper is available on line at http://www.mcponline.org

Independent Analysis of the Flagellum Surface and Matrix Proteomes Provides Insight into Flagellum Signaling in Mammalian-infectious *Trypanosoma brucei*[*] [S]

Michael Oberholzer‡, Gerasimos Langousis‡**, HoangKim T. Nguyen‡**, Edwin A. Saada‡**, Michelle M. Shimogawa‡**, Zophonias O. Jonsson§‖, Steven M. Nguyen‡, James A. Wohlschlegel§¶‡‡, and Kent L. Hill‡¶‡‡

The flagellum of African trypanosomes is an essential and multifunctional organelle that functions in motility, cell morphogenesis, and host-parasite interaction. Previous studies of the trypanosome flagellum have been limited by the inability to purify flagella without first removing the flagellar membrane. This limitation is particularly relevant in the context of studying flagellum signaling, as signaling requires surface-exposed proteins in the flagellar membrane and soluble signaling proteins in the flagellar matrix. Here we employ a combination of genetic and mechanical approaches to purify intact flagella from the African trypanosome, *Trypanosoma brucei*, in its mammalian-infectious stage. We combined flagellum purification with affinity-purification of surface-exposed proteins to conduct independent proteomic analyses of the flagellum surface and matrix fractions. The proteins identified encompass a broad range of molecular functionalities, including many predicted to function in signaling. Immunofluorescence and RNA interference studies demonstrate flagellum localization and function for proteins identified and provide insight into mechanisms of flagellum attachment and motility. The flagellum surface proteome includes many *T. brucei*-specific proteins and is enriched for proteins up-regulated in the mammalian-infectious stage of the parasite life-cycle. The combined results indicate that the flagellum surface presents a diverse and dynamic host-parasite interface that is well-suited for host-parasite signaling. ***Molecular & Cellular Proteomics 10: 10.1074/mcp.M111.010538, 1–14, 2011.***

The eukaryotic flagellum (synonymous with cilium) is recognized as a major signaling center that acts as a cellular antenna to sense and transduce extracellular signals (1–4). A sensory function for the flagellum is broadly conserved across diverse taxa (5). In metazoans, receptor-guanylate cyclases, ion channels, and G protein-coupled receptors (GPCRs)[1] in the flagellar membrane perceive chemical and mechanical cues that are necessary for normal development, physiology, and reproduction (6–9). Important examples include wingless (Wnt) and hedgehog signaling responses in vertebrates (1, 3, 10, 113). In protists, flagellum-localized ion channels, agglutinins, and receptor-kinases control motility, mating, and response to extracellular growth factors (11–13). Flagella are prominent among pathogenic protozoa, which cause tremendous human suffering worldwide and present a barrier to economic development in some of the poorest regions of the world (14–17). These include the etiological agents of African sleeping sickness, leishmaniasis, malaria, epidemic diarrhea, and trichomoniasis (14–16,18). In most cases these pathogens are obligate parasitic organisms whose survival depends upon their ability to sense and respond to extracellular cues in diverse host environments. The flagellum's motility function in protozoan parasites is self-evident, but its capacity for sensing and responding to external signals is largely unexplored.

African trypanosomes, *e.g. Trypanosoma brucei*, are uniflagellate protozoan parasites that cause African sleeping sickness in humans and related diseases in wild and domestic animals (19). *T. brucei* is transmitted to the bloodstream of a mammalian host through the bite of a tsetse fly vector. To be successful, *T. brucei* must integrate environmental signals that direct parasite movements and developmental transformations within specific host compartments (20–22). For example, entry into the mammalian bloodstream promotes cel-

From the ‡Department of Microbiology, Immunology, and Molecular Genetics, §Department of Biological Chemistry, ¶Molecular Biology Institute, University of California Los Angeles, Los Angeles, CA 90095, USA. ‖Current address Institute of Biology, University of Iceland, Sturlugata 7, 101-Reykjavik, Iceland

Received April 28, 2011, and in revised form, June 8, 2011
Published, MCP Papers in Press, June 19, 2011, DOI 10.1074/mcp.M111.010538

[1] The abbreviations used are: PFR, paraflagellar rod; MudPIT, multidimensional protein identification technology; RNAi, RNA interference; VSG, variable surface glycoprotein; FS, flagellum surface; TM, transmembrane; RSU, protein kinase A regulatory subunit; IFT, intraflagellar transport; HA, hemagglutinin; PBS, phosphate-buffered saline; GRCR, G protein coupled receptor; BIP, intracellular binding protein.

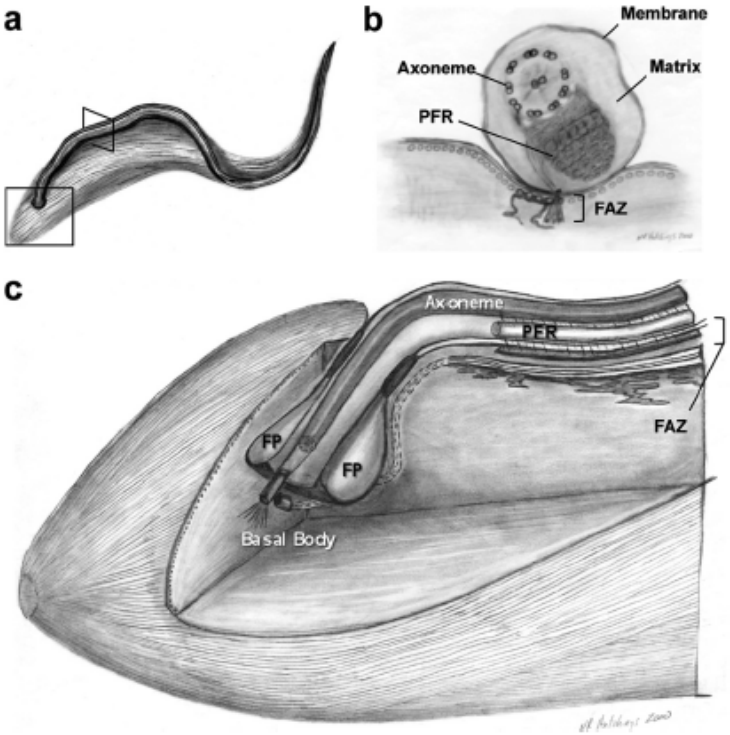


FIG. 1. **Flagellum architecture of *T. brucei*.** Schematic diagrams showing the *T. brucei* cell and flagellum (*A*), together with cross sectional (*B*), and cutaway (*C*) views corresponding to the regions indicated by boxes in panel *A*. Relevant structural features are labeled, including the flagellum membrane, matrix, axoneme, and paraflagellar rod (PFR), as well as the flagellum attachment zone (FAZ), flagellar pocket (FP), and basal body. See text for details. Figure adapted from reference (110), with permission.

lular adaptations that define the bloodstream-form life cycle stage, including changes in metabolism, morphology, and surface protein composition (23). Prominent among these is differentiation of proliferative, "long-slender" forms into cell cycle-arrested, "short-stumpy" forms that are adapted for survival in the tsetse (23, 24). Parasite-host signaling is also reported to contribute to invasion of the central nervous system (25). In the tsetse, bloodstream-forms differentiate into procyclic-forms, which re-enter the cell cycle and establish an infection in the fly midgut. Procyclic-form parasites undergo a defined series of directional migrations and tissue-specific developmental transformations, culminating in flagellum attachment to epithelial cells in the tsetse salivary gland and differentiation into human-infectious forms (26, 27). Except for surface-exposed carboxylate transporters that participate in stumpy-to-procyclic differentiation (24), proteins that perceive signals for directing parasite navigation and tissue-specific development are mostly unknown.

The paradigm of the flagellum as a sensory organelle in other eukaryotes, together with the observation that the trypanosome flagellum interacts directly with host tissues (26, 28), has fueled the hypothesis that the parasite flagellum functions as a signaling organelle for integrating host-derived and parasite-derived signals (20, 22). In *T. brucei*, this idea is supported by the finding that specific proteins from cyclic nucleotide and Ca^{2+} signaling pathways are present in the flagellum (29–34). The *T. brucei* flagellum (Fig. 1) is built around a microtubule-based axoneme plus an extra-axonemal filament, termed the paraflagellar rod (PFR), which runs alongside and is attached to the axoneme (15, 35). The axoneme and PFR are ensheathed by a flagellar membrane whose protein and lipid composition are distinct from the cell surface membrane (36, 37). The lumen of the flagellum, termed the flagellar matrix, is contiguous with the cytoplasm, but selective filters at the base of the flagellum restrict access to the matrix, such that protein composition of the matrix is distinct from that of the cytoplasm (38). The flagellum emerges from the cytoplasm at the cell posterior and is laterally connected to the cell body by cytoskeletal filaments that connect the axoneme and PFR to subpellicular microtubules in the cell body and maintain tight apposition of the flagellar and cell surface membranes (39, 40). These connections form a "flagellum attachment zone" (FAZ) that runs along most of the length of the flagellum, with a small distal portion of the flagellum extending free of the cell body. A specialized membrane domain, termed the flagellar pocket, surrounds the flagellum at the site where it emerges from the cytoplasm at the cell posterior (39, 41, 42). As the sole site of surface protein turnover and macromolecular uptake in trypanosomes, the flagellar pocket is a key portal for host-parasite interaction (41, 42), yet little is known about its protein and lipid compositions.

Lateral attachment of the flagellum to the cell body poses significant challenges for isolating intact flagella from *T. brucei*. Existing procedures employ detergent-extraction and salt-extraction to isolate the insoluble flagellum skeleton,

which contains the axoneme and PFR, but lacks the membrane and matrix (43–45). Thus, although several hundred axonemal and PFR proteins have been identified (31, 43, 46), the protein compositions of the flagellar membrane and matrix in *T. brucei* are largely unknown. This poses a particular limitation for studying flagellum signaling, because signaling capacity is dictated by surface-exposed membrane proteins coupled to soluble components of signaling cascades in the matrix (2).

Here we employ a combined genetic and mechanical approach to isolate intact, membrane-enclosed flagella from *T. brucei* in its mammalian-infectious stage. We used flagellum purification, combined with affinity purification of surface-exposed proteins and multidimensional protein identification technology (MudPIT) to define the flagellum surface and flagellum matrix proteomes. Immunofluorescence and RNA interference (RNAi) studies demonstrate flagellum localization and function for proteins identified and provide insight into mechanisms of flagellum attachment and motility. Our combined studies indicate that the trypanosome flagellum presents a diverse and dynamic signaling platform adapted for host-pathogen interaction.

EXPERIMENTAL PROCEDURES

Cell Lines—Bloodstream-form trypanosomes, 221 single marker cell line (47), were used for all experiments and were cultivated in HMI-9 medium supplemented with 10–15% fetal bovine serum (Invitrogen) as described previously (48). The *fla1* cell line was generated by transfection with the p2T7-Fla1 plasmid (49) using standard procedures (48). Selection for transformants was done using 5 μg/ml Phleomycin (InvivoGen, San Diego, CA).

Surface Biotinylation—Cells were washed twice in ice-cold phosphate-buffered saline (PBS) and resuspended in ice-cold PBS + 0.5 mg/ml sulfosuccinimidyl-2-[biotinamido]ethyl-1,3-dithiopropionate (Sulfo-NHS-SS-biotin; Thermo Scientific). After incubation on ice for 10–30 min with gentle agitation, unreacted Sulfo-NHS-SS-biotin was blocked by addition of Tris to 100 mM final concentration. Biotinylated cells were washed three times in ice-cold PBS + 100 mM Tris.

Purification of Flagella and Flagellar Surface Proteins—Cells harboring the *fla1* tet-inducible RNAi cassette (density 5 × 10^5 cells/ml) were induced for 18 h with 1 μg/ml tetracycline. From this step onward all procedures were performed at 4 °C unless otherwise stated and all solutions were cooled on ice. Induced cells were surface biotinylated as described above. Flagella were removed from the cell bodies by repeated passage (five times) through a 28-G needle. Some (<1%) of the isolated flagella remained motile. The resulting flagella plus cell body mixture was loaded on a 30% sucrose bed and centrifuged for 10 min at 770 × *g*. The supernatant and interface containing isolated flagella were collected and sucrose sedimentation was repeated. Purified flagella were collected by a high-speed spin (15,000 × *g*, 1h) and resuspended in 200 μl PBS, containing 2.5 μg/ml Leupeptin and 0.5 μg/ml Pepstatin. Purified, biotinylated flagella were lysed by addition of Nonidet P-40 to 0.5% final concentration and incubation on ice for 10 min. Soluble proteins (flagellum matrix and membrane) were separated from insoluble proteins (flagellum skeleton) by centrifugation (15,000 × *g*, 30 min). The resulting soluble flagellar proteins (200 μl) were incubated with 50 μl streptavidin beads (Streptavidin Sepharose High Performance, GE Healthcare) for 30 min with agitation. Proteins bound to streptavidin beads were separated from the unbound fraction by centrifugation and washed at room temperature once in buffer A (8 M Urea, 200 mM NaCl, 2% SDS, 100 mM Tris, pH 8), once in buffer B (8 M Urea, 1.2 M NaCl, 0.2% SDS, 100 mM Tris, 10% Ethanol, 10% Isopropanol, pH 8), once in buffer C (8 M Urea, 200 mM NaCl, 0.2% SDS, 100 mM Tris, 10% Ethanol, 10% Isopropanol, pH 8), and twice in buffer D (8 M Urea, 100 mM Tris, pH 8). All fractions were analyzed by Western blotting using standard protocols (see Fig. 3). Antibodies used were anti-BiP 1:10,000 (50), anti-PFR 1:1,000 (45), anti-variable surface glycoprotein VSG 221 1:10,000 (51), anti-biotin 1:2,000 (Jackson Immunoresearch, West Grove, PA). Secondary antibodies were donkey anti-mouse or donkey anti-rabbit HRP coupled 1:2,500 (Bio-Rad, Hercules, CA).

MudPIT Analysis—Streptavidin-bound proteins were digested directly on beads by the sequential addition of lys-C and trypsin proteases (52, 53). Peptide samples were fractionated online using multidimensional chromatography followed by tandem mass spectrometric analysis on a LTQ-Orbitrap mass spectrometer (ThermoFisher) as previously described (53, 54). RawXtract (version 1.8) was used to extract peaklist information from Xcalibur-generated RAW files. Database searching of the MS/MS spectra was performed using the ProLuCID algorithm (version 1.0) and a user assembled database consisting of all protein entries from the TriTrypDB for *T. brucei* strain 927 (version 2.3, 10533 entries) and seven sequences from *T. brucei* strain 427: 453391 (Tb-1.7g), 458439 (Tb-24), 18413545 (ESAG4.a from 221 expression site), 18413551 (ESAG4.b from 221 expression site), 189094632 (VSG-221), 18413541 (ESAG7 from 221 expression site), 18413542 (ESAG6 from 221 expression site) (55). Other database search parameters included: (1) precursor ion mass tolerance of ± 20 ppm, (2) fragment ion mass tolerance of ± 400 ppm, (3) only peptides with fully tryptic ends were considered candidate peptides in the search with no consideration for missed cleavages, and (4) static modification of +57.02156 on cysteine residues. Peptide identifications were organized and filtered using the DTASelect algorithm which uses a linear discriminant analysis to identify peptide scoring thresholds that yield a peptide-level false discovery rate of less than 5% as estimated using a decoy database approach. Proteins were considered present in the analysis if they were identified by two or more peptides using the 5% peptide-level false discovery rate (56–58). Details from mass spectrometric analysis are given in supplemental table S10.

Immunofluorescence Microscopy—Cells or isolated flagella were washed once in PBS and fixed by addition of paraformaldehyde to 0.1% for 5 min on ice. Fixed cells were washed once in PBS and air-dried onto coverslips. The coverslips were incubated for 10 min in −20 °C methanol and 10 min in −20 °C acetone. After a re-hydration step (10–30 min in PBS) the slides were blocked for 1.5 h in blocking solution (PBS + 5% bovine serum albumin (BSA) + 5% Normal donkey serum (Invitrogen)). Coverslips were incubated with primary antibodies diluted in blocking solution for 1.5 h. Antibodies used were anti-biotin 1:2000 (Jackson ImmunoResearch), anti-BiP 1:10,000 (50), anti-hemagglutinin HA.11 1:200–1:1,000 (Covance, Princeton, NJ), anti-PFR 1:500 (45), anti-tyrosinated tubulin YL1/2 1:500 (Chemicon International, Temecula, CA). After three washes in PBS + 0.05% Tween-20 for 10 min each, samples were stained with secondary antibodies diluted in blocking solution for 1.5 h (donkey anti-mouse Alexa Fluor 488, donkey anti-rabbit Alexa Fluor 594, goat anti-rat Alexa Fluor 594 1:500 (Molecular Probes, Eugene, OR)). Cells were washed three times in PBS + 0.05% Tween-20, once in PBS and mounted with Vectashield containing DAPI (Vector Laboratories). Flagellar pocket staining with biotinylated tomato lectin was performed as described (59). Biotinylated tomato lectin was visualized using streptavidin Alexa Fluor 594 (Molecular Probes). Images were taken using a 100x objective on a Zeiss Axioskop II compound microscope and processed using Axiovision (Zeiss, Inc., Jena, Germany) and Adobe Photoshop (Adobe Systems, Inc., Mountain View, CA).

Nonidet P-40 Fractionation of Whole Cells—Cells were washed once in PBS and lysed in ice-cold PBS + 0.5% Nonidet P-40 + protease inhibitors (complete mini, Roche) for 10 min on ice. Lysates were centrifuged for 30 min at 15,000 × *g* at 4 °C and supernatant and pellet fractions were analyzed by Western blotting using standard procedures. Primary antibodies used were anti-HA.11, anti-BiP (as described above) and anti-trypanin 1:1000 (60). Secondary antibodies were donkey anti-mouse or donkey anti-rabbit HRP coupled 1:2500 (Bio-Rad).

In situ Tagging—*In situ* tagging was carried out as previously described (61) to introduce epitope-tagged copies of each gene analyzed into the corresponding endogenous chromosomal locus. In brief, 500–800 bp DNA fragments homologous to the target gene open reading frame or 3′ UTR were PCR-amplified from genomic DNA and cloned upstream of the 3xHA or downstream of the puromycin resistance marker in pMOTag2H. pMOTag2H is an *in situ* tagging plasmid containing a 3xHA epitope tag and a puromycin resistance marker, adapted from (61). All sequences were verified by DNA sequencing at the UCLA Sequencing and Genotyping Core center. The tagging cassettes were excised from the pMOTag2H vector backbone by restriction digestion, then purified and transfected into 221 bloodstream-form *T. brucei* using standard methods (48). Stable transformants were selected using 0.1 μg/ml puromycin.

RNAi—The targets for RNAi against FS179 and RSU (FM458) were identified by the Trypanofan RNAit algorithm (62), then PCR-amplified from genomic DNA using primers listed below: (restriction enzyme cleavage sites are underlined):

FS179-RNAi-f: 5′ CAT*AAGCTT*TCATTGCGTCATTTTGCCTA 3′
FS179-RNAi-r: 5′ CA*TCTAGA*AAGGCTGACGAGATCTTGGA 3′
RSU-RNAi-f: 5′ TGTGAAGCAACCCAACACAT 3′
RSU-RNAi-r: 5′ GTAATGCGAGAGCGGAGTTC 3′

The resulting DNA fragments for RNAi were ligated into the p2T7-Ti/B-RNAi vector, which is a tetracycline-controlled expression vector with opposing T7 promoters (49). Inserts were verified by sequencing at the UCLA genomics center. The p2T7-Ti/B-RNAi vector containing the FS179 or FM458 target sequence was linearized with NotI, ethanol precipitated and transfected into 221 bloodstream form *T. brucei* as described above. Transformants were selected using 5 μg/ml phleomycin.

Imaging and Motility Traces—FS179 RNAi imaging (see Fig. 7*A–C*): Cells were induced for 48 h with 1 μg/ml tetracycline, fixed using 4% PFA and mounted with Vectashield containing DAPI (Vector Laboratories). Images were taken and processed as described above. FM458 RNAi motility traces (see Fig. 7*D*, 7*E*): Cells were induced for 48h with 1 μg/ml tetracycline and motility traces were obtained for induced and uninduced control cells as described previously (48). The movie of the isolated flagellum was recorded and played at 30 frames per second as described previously (48).

Bioinformatic and Protein Comparisons—Protein domains were assessed using the SMART database (63). For homology searches, we employed eight ciliated (*Leishmania major, Trypanasoma cruzi, Plasmodium falciparum, Chlamydomonas reinhardtii, Monosiga brevicollis, Caenorhabditis elegans, Drosophila melanogaster,* and *Homo sapiens*) and four nonciliated (*Dictyostelium discoideum, Saccharomyces cerevisiae, Cyanidioschyzon merolae,* and *Arabidopsis thaliana*) eukaryotic species, including both unicellular and multicellular representatives. Homology searches were performed using NCBI BLAST with default parameters. Proteins with an expect-value of $\leq 1 \times 10^{-10}$ were considered as homologs and identical criteria were applied across all data sets and comparisons. For *T. brucei* flagellum skeleton proteomes, we used the combined, nonoverlapping set of proteins identified in three proteomic analyses of extracted flagellum skeletons from procyclic-form parasites (31, 43, 46). Comparison to the *C. reinhardtii* flagellum proteome was done locally with proteins downloaded from (64). For analysis of molecular function (see Table I), the DAVID Bioinformatics Resource, version 6.7 (65, 66) was used for functional annotation of proteins in TbFSP and TbFMP. Proteins were categorized using annotated Gene Ontology (GO) terms for molecular function (67), using the GOTERM_MF_2 category with a threshold count of 2 and an EASE of 0.1. Expression analysis (see Fig.10) was done using RNA sequencing data from (68).

RESULTS

Purification of Intact, Membrane-enclosed Flagella from T. brucei in its Mammalian-infectious Form—The *T. brucei* flagellum is laterally connected to the cell body along most of its length by filamentous connectors and tightly apposed membrane-membrane contacts (40). These connections present significant challenges for isolating intact flagella. Current approaches employ detergents to remove membranes, together with salt-extraction to disrupt filamentous connectors, followed by centrifugation to isolate flagellum skeletons from solubilized material (43–45). Resultant preparations contain the axoneme and PFR, but are stripped of flagellar membrane and soluble matrix proteins. To obviate the need for detergent and salt-extraction, and thus retain the flagellar membrane, we employed tetracycline-inducible RNAi against *fla1* to disrupt lateral flagellum attachment to the cell body (49). This allowed intact flagella to be separated from cell bodies by shearing, without using detergent (Fig. 2). Importantly, some isolated flagella remained motile without addition of exogenous ATP (Fig. 2*B*, supplemental Movie S1), indicating that they retained an intact flagellum membrane, as well as internal proteins and small molecules necessary for motility. Flagella were purified from cell bodies by sucrose density sedimentation (Fig. 2). To enable purification of surface-exposed proteins, cells were surface biotinylated before flagellum purification (Fig. 2*D*, supplemental Fig. S1). Surface-biotinylation was retained in purified flagella (Fig. 2*E*). The bulbous enlargement at one end of purified flagella contains material from the basal body, kinetoplast, and flagellar pocket (Fig. 2*E*). Thus, purified flagella retain an intact membrane that includes flagellar pocket membrane.

Purified, surface-biotinylated flagella were lysed with nonionic detergent (Nonidet P-40) and lysates were centrifuged to separate the insoluble fraction, containing flagellum skeleton proteins, from the soluble fraction, containing matrix plus membrane proteins. Biotinylated proteins in the soluble fraction were purified by adsorption to streptavidin beads and fractions from the purification were analyzed for total protein, biotin, and specific marker proteins (Fig. 3). Purified flagella were enriched for flagellum markers (PFR) relative to intracellular markers (BiP). Streptavidin-binding quantitatively purified biotinylated proteins and SYPRO-Ruby staining revealed unique protein profiles for the streptavidin-bound and unbound fractions. The bound fraction contained surface proteins (variable surface glycoprotein, VSG (69)), but not abundant intracellular proteins (Binding Protein, BiP (50)), or intraflagellar proteins (PFR (45)) (Fig. 3). These results support

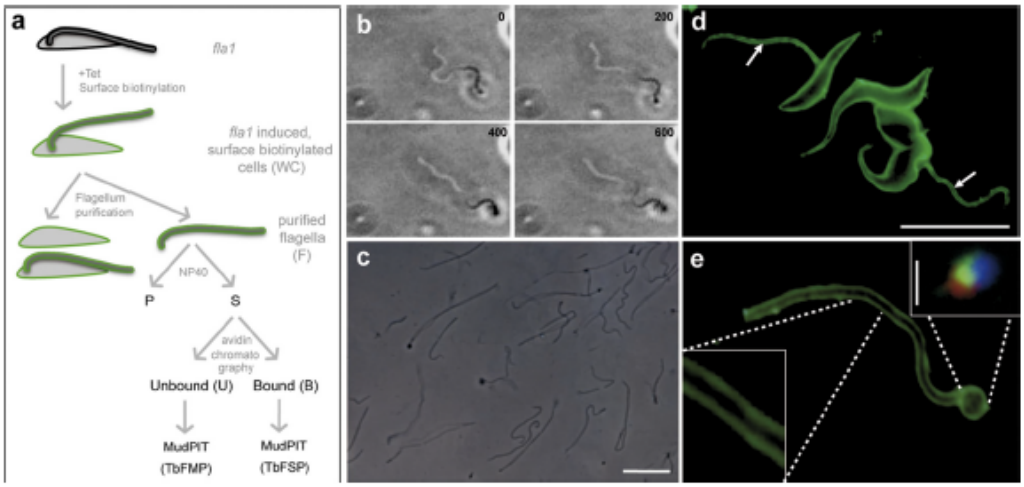


FIG. 2. **Purification of flagellum surface and matrix proteins from bloodstream-form *T. brucei*.** *A*, Schematic diagram illustrating the strategy for flagellum purification and separation of flagellum surface and matrix proteins. Lateral connections between the flagellum and cell body were removed by tetracycline-induced (+Tet) RNAi against Fla1 (49). Induced *fla1* cells were surface biotinylated (*fla1*-induced, surface biotinylated cells) and flagella were removed from the cell body by mechanical shearing, then purified by sucrose sedimentation (purified flagella). Purified, surface-biotinylated flagella were lysed with nonionic detergent (Nonidet P-40) and soluble proteins (S) were separated from insoluble flagellar skeletons (P) by centrifugation. Soluble proteins were applied to streptavidin beads (avidin chromatography). Proteins in the streptavidin-bound (B) and streptavidin-unbound (U) fractions were identified using multidimensional protein identification technology (MudPIT). *B*, Time-lapsed image sequence (from supplemental movie 1, recorded and played at 30 fps), showing that some flagella continued to beat after detachment from cell bodies (timestamps are given in ms). *C*, Phase contrast image of purified flagella (Scale bar 5 μm). *D*, Antibiotin immunofluorescence (*green*) of surface-biotinylated RNAi-induced *fla1* cells showing detached flagella (arrows, scale bar 25 μm). *E*, Anti-biotin immunofluorescence (*green*) of purified flagella shows surface labeling (inset, bottom left). The bulbous structure at one end of the flagellum (inset, *upper right*) includes material from the flagellar pocket (tomato lectin staining, *red*), the basal body (tyrosinated tubulin staining, *green*) and kinetoplast DNA (DAPI staining, *blue*). (scale bar 0.5 μm)

immunofluorescence data (Fig. 2*D* and 2*E*, supplemental Fig. S1) indicating that biotinylation was specific for surface proteins.

Identification of Flagellum Surface and Matrix Proteins by Mass Spectrometry—Proteins in the streptavidin-bound and unbound fractions were identified by MudPIT proteomic analysis. In some cases peptide coverage allowed unambiguous identification of proteins. In other cases, peptides did not distinguish between proteins with very similar sequences. As such, each proteomic data set represents a maximum number and minimum number of total proteins, with the minimum number reflecting groups of proteins whose sequences could not be unambiguously distinguished. From here on, we refer to the minimum number of proteins identified in each fraction. This analysis identified 158 proteins in the bound fraction, termed the *T. brucei* flagellum surface proteome ("TbFSP," supplemental Table S1) and 666 proteins in the unbound fraction, termed the *T. brucei* flagellum matrix proteome ("TbFMP," supplemental Table S3). Proteins in the two data sets encompassed a broad range of predicted functionalities and both data sets included a large number of proteins with no annotated molecular function (Table 1). We next employed several independent analyses to validate the proteomic data sets. Each dataset included suspected contaminants, *e.g.* ribosomal proteins. However, to avoid user bias, no subjective filters were applied to remove these suspected contaminants and analyses were performed on the unfiltered datasets, *i.e.* 158 proteins in TbFSP and 666 proteins in TbFMP. We focused on the flagellum surface proteome because the primary interest was surface-exposed proteins.

Validation of the Flagellum Surface Proteome—As a first step in assessing the quality of the proteomic data sets, we probed each dataset for proteins known to localize to specific flagellum compartments (Fig. 4). The flagellum surface proteome contained most known flagellum membrane proteins and was generally devoid of intraflagellar proteins, *i.e.* flagellum matrix and skeleton proteins (Fig. 4*A*, supplemental Tables S2, S5, and S8). By comparison, the flagellum matrix proteome contained seven of 21 known matrix proteins, nine of 10 known membrane proteins and 62 of 532 flagellum skeleton proteins (Fig. 4*B*, supplemental Tables S4, S8). We also examined each data set for predicted transmembrane (TM) domains, as these are expected to be enriched in the surface proteome. As expected, proteins with predicted TM domains were enriched in the surface proteome (51%) compared with the genome as a whole (19%) (70, 71), the flagellum matrix (20%) or the flagellum skeleton (2%) (Fig. 5). Proteins with a predicted signal peptide were also enriched in the flagellum surface proteome (38%) *versus* the genome (24%) and the matrix (20%) (supplemental Tables S2, S4). By using

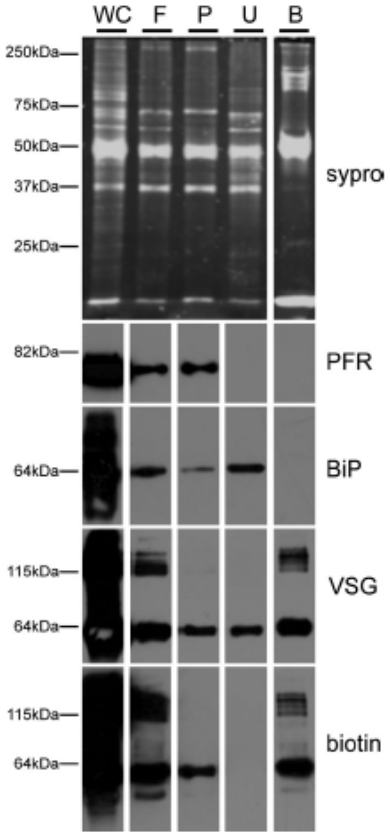


FIG. 3. **Analysis of flagellum purification fractions.** Proteins from the indicated fractions of the purification were analyzed by SDS-PAGE and SYPRO-Ruby staining (*top*) or Western blotting (*bottom*) with antibodies against intracellular (BiP), flagellar skeleton (PFR) and cell surface (VSG) markers. Biotinylated proteins were detected with anti-biotin antibody. Whole cells (WC), purified flagella (F), detergent-insoluble flagellum pellets (P), and the streptavidin-unbound (U) and bound (B) fractions are as indicated in Fig. 2*A*. Flagellum enrichment is indicated by the increased ratio of the flagellar marker PFR to the intracellular marker BiP in the purified flagellum fraction (F) *versus* whole cells (WC). Both PFR and BiP are largely absent from the streptavidin bound fraction (B).

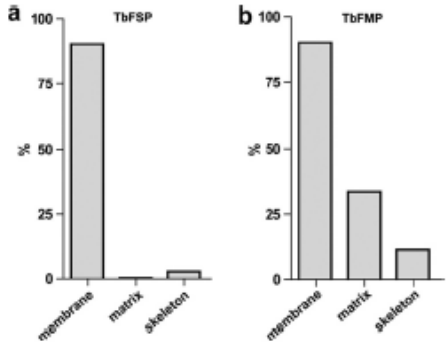


FIG. 4. **The flagellum surface proteome contains known flagellum surface proteins but is generally devoid of intraflagellar proteins.** Chart shows the percentage of known flagellum membrane, matrix, and skeleton proteins that were identified in the flagellum surface proteome (TbFSP) and flagellum matrix proteome (TbFMP). Flagellum skeleton proteins are from (31, 43, 46). Known flagellum membrane and matrix proteins are given in supplemental Tables S5 and table S8, respectively. TbFSP included 9 of 10 (90%) membrane, none of 21 (0%) matrix and 14 of 532 (2.6%) skeleton proteins. TbFMP included 9 of 10 (90%) membrane, 7 of 21 (33%) matrix and 62 of 532 (11.6%) skeleton proteins.

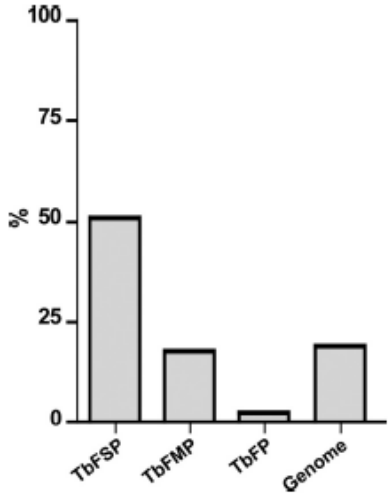


FIG. 5. **The flagellum surface proteome is enriched for transmembrane proteins.** Chart shows the percentage of proteins in the flagellum surface (TbFSP), matrix (TbFMP), and skeleton (TbFP) (31, 43, 46) proteomes that are predicted to contain transmembrane domains. For comparison, the relative number of predicted transmembrane-containing proteins in the *T. brucei* genome (71) is shown. Numbers are 80/158, 118/666, 12/532, and 2133/11425 for TbFSP, TbFMP, TbFP, and genome, respectively.

the minimal number of proteins identified, our analysis is suspected to underestimate the enrichment of TM domains and signal peptides in the flagellum surface proteome, because the genome numbers include redundant and closely related sequences.

We next used epitope-tagging and immunofluorescence microscopy to determine the subcellular location of ten proteins from the flagellum surface proteome. All tagged proteins were detergent-soluble (supplemental Fig. S2 and not shown), consistent with membrane association. Eight of ten tagged proteins localized to one or more subdomains of the flagellum membrane, *e.g.* along the entire length of the flagellum, the flagellar pocket or the flagellum attachment zone (Fig. 6, supplemental Fig. S3 and data not shown). Four of these eight proteins were exclusively located in the flagellum and/or flagellar pocket, one was distributed throughout the whole cell surface and three were also observed in intracellular compartments (summarized in supplemental Table S6). In sum, the flagellum surface proteome includes most experimentally characterized flagellum membrane proteins, is largely devoid of intraflagellar proteins and immunolocalization demon-

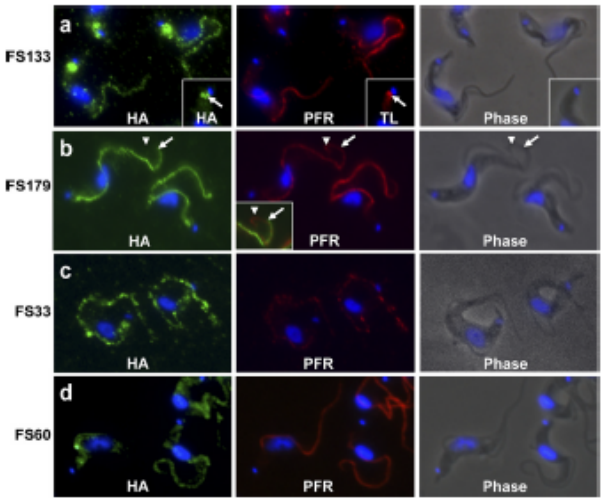


FIG. 6. **Immunofluorescence shows flagellum localization for proteins identified in the flagellum surface proteome.** (*A–D*) Immunofluorescence analysis of bloodstream-form trypanosomes expressing the indicated HA-tagged flagellum surface proteins (FS133, FS179, FS33, or FS60). Cells were co-stained for the HA epitope (*green*), the paraflagellar rod (PFR, *red*) or the flagellar pocket marker tomato lectin (TL, *red*) as indicated. DNA was visualized with DAPI. *A*, FS133 localizes along the flagellum and in the flagellar pocket (inset, *arrows*). *B*, FS179 localizes along the flagellum, but does not extend to the flagellum distal tip, as evidenced by the extension of PFR staining (*arrowhead*) beyond the end of FS179 staining (*arrow*). See inset for merged images. *C*, *D*, FS33 and FS60 localize along the entire length of the flagellum. FS60 was also observed in cytoplasmic puncta (not shown).

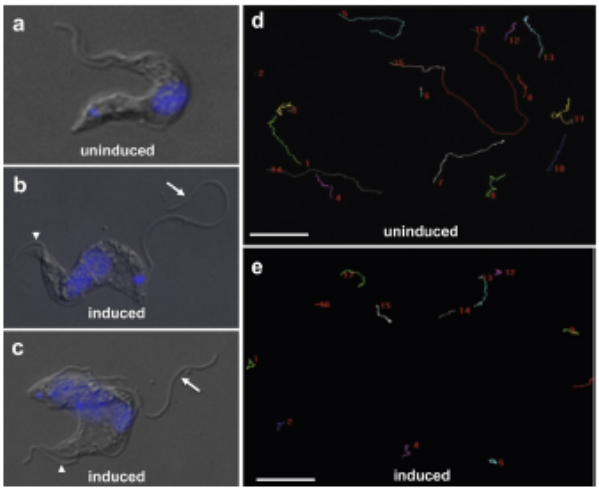


FIG. 7. **RNAi knockdown indicates flagellum function for FS179 and FM458.** *A–C*, Phase contrast images of tetracycline-inducible FS179 RNAi cells grown in the absence (*A*) or presence (*B* and *C*) of tetracycline to induce RNAi. FS179 knockdown causes the daughter flagellum to become detached (arrows in *B* and *C*), while the parental flagellum remains connected to the cell body (arrowheads in b and c). DNA is visualized with DAPI. (d and e) Motility trace analysis of FM458 RNAi cells grown in the absence (*D*) or presence (*E*) of tetracycline to induce RNAi. Each line traces the path of a single cell for 2 min (Scale bar 50 μm).

strates flagellar location for several proteins identified. Thus, the results indicate that the flagellum surface proteome is enriched for flagellum membrane proteins.

RNAi Knockdown Reveals Flagellar Functions for Proteins Identified—We used tetracycline-inducible RNAi to determine whether loss of a particular protein impacted flagellum function. In most cases, RNAi directed against proteins in the flagellum surface proteome did not reveal an obvious phenotype in culture (not shown). One notable exception was FS179, which encodes a putative calcium channel. Immunofluorescence showed that FS179 was localized to the flagellum attachment zone (Fig. 6*B*), suggesting a potential role in flagellum attachment. RNAi knockdown of FS179 caused the flagellum to become detached from the cell body and the daughter flagellum was preferentially affected (Fig. 7*A–C*). This result supports FS179 localization to the flagellum attachment zone and is consistent with previous studies suggesting a requirement for Ca^{2+} in flagellum attachment (40). The flagellar matrix protein FM458 corresponds to the protein kinase A regulatory subunit (RSU) (72) and was of interest based on the importance of protein kinase A and cyclic nucleotide signaling to flagellum function in other organisms (13, 73, 74). RNAi knockdown of FM458 inhibited forward motility, consistent with a role in flagellum function (Fig. 7*D*,7*E*). Interestingly, despite motility defects, bloodstream-form FM458 knockdowns were viable, which contrasts to the lethal phenotype caused by knockdown of flagellum skeleton proteins (29, 43, 60).

Host-Parasite Signaling Capacity of the Flagellum Surface—Prominent within the flagellum surface proteome were proteins known or suspected to function in host-parasite interaction and/or signaling (Fig. 8). For example, VSG, MSP-A, and GPI-PLC, are characterized surface proteins that function in antigenic variation and VSG clearance (69, 75, 76). Likewise, transferrin receptor and glucose transporter function in host nutrient uptake (77, 78), whereas adenylate cyclases and calflagins are predicted to function in host-parasite signaling (30, 33, 34, 79). In addition, many uncharacterized flagellum surface ("FS") proteins have domain architectures that indicate receptor function, with a large extracellular domain suitable for binding host ligands connected to an intracellular signaling module, *e.g.* kinase domains in FS164, FS190, and FS201. In some cases, extracellular domains exhibit homology to characterized ligand-binding motifs, such as the periplasmic binding protein superfamily (receptor-type adenylate cyclases) or EGF-like domain superfamily involved in protein-protein interaction (FS133) (80, 81). Also well-represented among uncharacterized proteins are several classes of ion and metabolite transporters, including ABC-transporters (FS166), P-type ATPase pumps (FS60, FS80, FS163, FS188, FS193, and FS198), ion channels (FS179), amino acid transporters (FS group 108 and 121), glucose transporters (FS192)

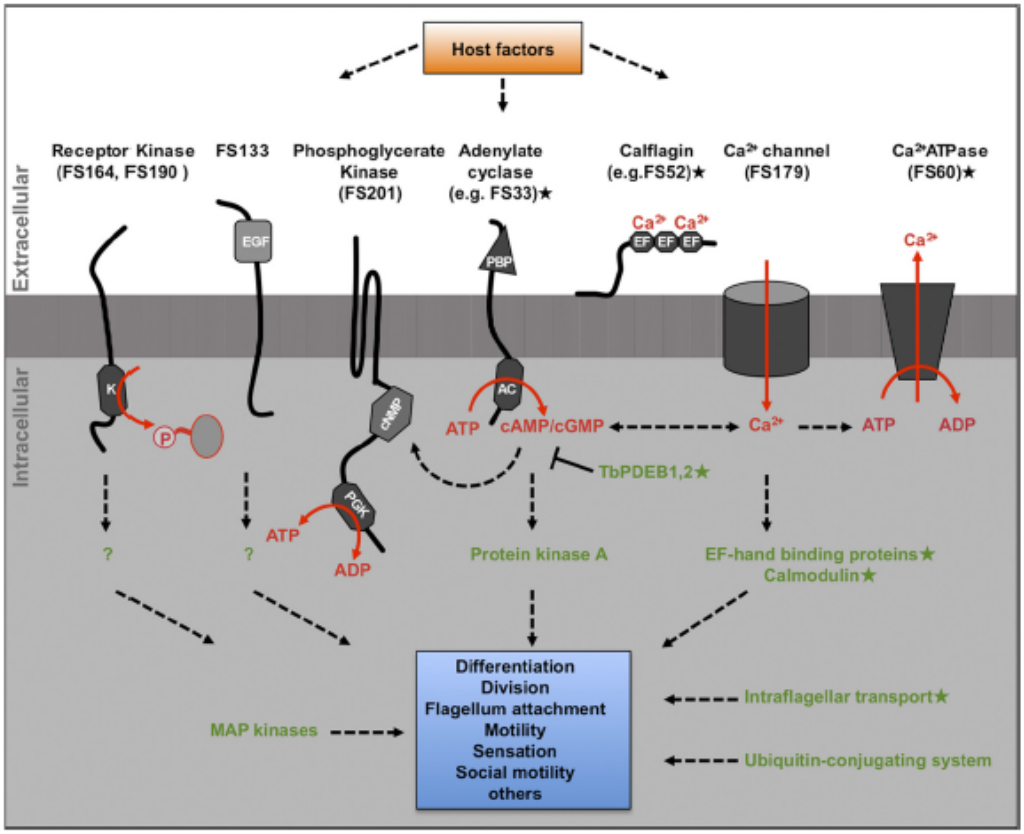


FIG. 8. **The trypanosome flagellum provides a diverse signaling platform.** Diagram shows representative components of signaling pathways identified in the flagellum surface proteome (*black* text) and flagellum matrix proteome (*green* text). These include receptors and transporters for initiating signal transduction (*black* text) and downstream signaling proteins (*green* text). Predicted domain structures are indicated for flagellum surface proteins (K, kinase; EGF, epidermal growth factor domain superfamily; cNMP, cyclic nucleotide binding domain; PGK, phosphoglycerate kinase domain; PBP, periplasmic binding protein domain; AC, adenylate cyclase domain; EF, EF hand calcium-binding domain). Predicted interactions are indicated with dashed lines. Unknown host factors (*orange* box) are predicted to engage signaling pathways, which mediate downstream trypanosome processes (*blue* box). [star] Indicates proteins that have been demonstrated to be flagellar by independent studies (29–33, 93, 96, 97, 111).

and a group of major facilitator proteins (FS group 126) related to the PAD surface receptors that perceive extracellular signals for bloodstream-form to procyclic-form differentiation (24). In sum, the data indicate a diverse flagellar surface protein repertoire that is suitable for mediating a broad range of host-parasite interactions.

The Flagellum Surface is Enriched for T. brucei-specific Proteins—The flagellum surface is postulated to function in detection of extracellular signals and is therefore anticipated to include cell-specific proteins that accommodate environments uniquely encountered by *T. brucei*. The availability of an independent flagellum surface proteome allowed us to test this idea directly by examining the phylogenetic distribution of proteins in the flagellum surface and matrix proteomes (Fig. 9, supplemental table S1 and S3). As reference organisms, we chose eight ciliated (*L. major, T. cruzi, P. falciparum, C. reinhardtii, M. brevicollis, C. elegans, D. melanogaster, H. sapiens*) and four nonciliated (*D. discoideum, S. cerevisiae, C. merolae, A. thaliana*) eukaryotic species, including both unicellular and multicellular representatives. Among the 158 flagellum surface proteins, 16% were specific to *T. brucei*. By comparison, 5% of matrix proteins and 1% of flagellum skeleton proteins were *T. brucei*-specific.

Conserved Flagellum Surface Proteins are not Biased Toward Flagellated Organisms—Proteins required for flagellum structure and motility are broadly conserved among organisms with flagella, but are generally absent in organisms that lack flagella (82–84). To determine if the same bias applied to flagellum surface and matrix proteins, we examined the phylogenetic distribution of "conserved" proteins in each data set, *i.e.* proteins that were encoded in the genome of at least one non-kinetoplastid organism (Fig. 9). As expected (82–84), a large fraction (42%) of conserved flagellum skeleton proteins were restricted to organisms with flagella. In contrast,

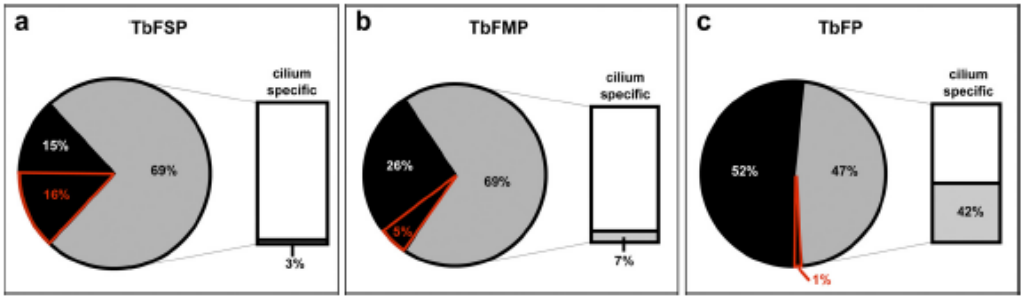


FIG. 9. **The flagellum surface proteome contains many *T. brucei*-specific proteins.** (*A–C*) Pie charts show phylogenetic distribution of proteins in the flagellum surface (TbFSP), flagellum matrix (TbFPM), or flagellum skeleton (TbFP) proteomes. Percentages are shown for proteins that are conserved in at least one nonkinetoplastid organism (*gray*), or are kinetoplastid-specific (*black*), or *T. brucei*-specific (*red* outline). Bar charts show the percentage of conserved proteins, *i.e.* not kinetoplastid-specific, that are restricted to ciliated organisms.

only 3% of conserved flagellum surface proteins and 7% of conserved flagellum matrix proteins were restricted to organisms with flagella.

DISCUSSION

Flagellum Purification—The *T. brucei* flagellum is an essential and multifunctional organelle that is required for cell motility and cell morphogenesis and is postulated to function in immune evasion and host-parasite signaling (15, 20, 35, 85–87). Previous studies of the *T. brucei* flagellum have been limited by the inability to purify intact, membrane-enclosed flagella. Here we combine genetic manipulation and mechanical force to isolate intact flagella from mammalian-infectious *T. brucei*. The quality of the preparation is evidenced by motility of flagella separated from cell bodies, combined with biochemical and microscopic analysis of purified flagella. The flagellum preparation is further validated by independent analyses showing flagellum localization and/or function for several proteins identified in the purified sample. The availability of intact flagellum preparations opens new opportunities for studying unique and conserved features of *T. brucei* flagella. In other organisms, the ability to purify intact flagella has been critical for advancing studies of flagellum biology, including the recent resurgence in awareness of the important roles played by flagella in human health and disease (7, 64, 88). Development of a method for flagellum isolation from *T. brucei* is anticipated to advance efforts to understand flagellum biology in these pathogens and will expand the utility of trypanosomes as an experimental system for studying flagellum biology.

Identification of Flagellum Surface and Flagellum Matrix Proteins—We took advantage of our flagellum purification to conduct a proteomic analysis of surface-exposed flagellum membrane proteins and soluble flagellum matrix proteins. We identified 158 and 666 proteins in the flagellum surface and matrix fractions, respectively, with 87 proteins common between the two datasets. The combined surface and matrix proteomes include 165 proteins for which homologs were identified in a proteomic analysis of intact flagella from *C. reinhardtii* (64) (supplemental Table S7). Gene ontology annotation indicates that proteins identified in the *T. brucei* surface and matrix fractions encompass a wide range of functionalities (Table I). A notable feature of each dataset was the large number of proteins, 52% of the surface and 52% of the matrix proteome, for which gene ontology analyses did not reveal predicted functionality. Previously, pioneering proteomic studies of detergent-extracted flagellum skeletons from procyclic *T. brucei* provided important insights into flagellum biology (31, 43, 46). Novelty of the membrane and matrix proteomes identified in the current study is illustrated by comparison with these previous analyses. There is minimal overlap among the proteomes, with 91% of proteins identified in the surface and matrix proteomes being unique to the current analysis. The combined studies make *T. brucei* one of few organisms for which analysis of the entire flagellum, *i.e.* membrane, matrix, and skeleton, is available and, to our knowledge, provides the first example where an

TABLE I

Predicted molecular function of proteins identified in TbFSP and TbFMP. *Proteins in the flagellum surface proteome (TbFSP) and flagellum matrix proteome (TbFMP) were analyzed for predicted molecular function using the DAVID database for gene ontology and protein domain analysis*

Predicted molecular function	TbFSP (158)	TbFMP (666)
Cyclase activity	17	0
Lyase activity	18	0
Substrate-specific transporter activity	12	0
Transmembrane transporter activity	15	0
Nucleotide binding	31	117
Hydrolase activity	0	117
Protein binding	0	54
Oxidoreductase activity	0	52
Cofactor binding	0	20
Translation factor activity, nucleic acid binding	0	12
Carboxylic acid binding	0	5
Peroxidase activity	0	4
Carbohydrate binding	0	4
No Annotated Function	83	350
Not in DAVID	22	46

independent analysis of surface-exposed flagellar proteins is available.

Analysis of the surface data set is particularly interesting, as it shows enrichment for transmembrane proteins, including several predicted transporters and proteins predicted to initiate host-parasite signaling (see below). The number and predicted functionalities of proteins identified in the flagellum surface fraction indicate that *T. brucei* surface protein diversity is greater than might be inferred from the relatively few previously characterized surface proteins (89). The surface data set has relevance from a therapeutic standpoint because the identified proteins are accessible to small molecules added to live, mammalian-infectious parasites.

Signaling Capacity of the Trypanosome Flagellum—The trypanosome flagellum has been hypothesized to participate in host-parasite signaling, but proteins responsible for detection and transduction of extracellular signals are mostly unknown. Previously, only a handful of flagellar membrane (including the flagellar pocket) and matrix proteins have been identified in *T. brucei* (24, 30, 33, 34, 75, 90–97). In other organisms, flagellum-dependent signaling is dominated by three signal transduction pathways: cyclic nucleotide signaling, Ca^{2+} signaling and phosphorylation cascades initiated by receptor-kinases on the flagellar membrane (2, 8). The *T. brucei* flagellum surface proteome is replete with proteins capable of initiating signal transduction in each of these signaling pathways (Fig. 8), including receptor kinases, receptor adenylate cyclases (30) and proteins predicted to function in Ca^{2+} signaling (33, 36). The surface proteome also includes many proteins predicted to function in transport of solutes across the cell membrane (Table I). The combined data indicate a diverse flagellar surface protein repertoire suitable for mediating a broad range of signaling functions, thus providing molecular support for the hypothesis that the flagellum membrane is an important host-parasite signaling interface.

A role for the *T. brucei* flagellum as a signaling platform is supported by previous work that identified downstream targets of cyclic nucleotide, Ca^{2+} and phospho-signaling pathways anchored to the *T. brucei* flagellum skeleton (Fig. 8) (29, 31, 32, 43). The flagellar matrix fraction included many of these effectors, as well as several other candidate signaling proteins (supplemental Table S3) (Fig. 8). A major effector of cyclic nucleotide signaling that was not identified in previous studies of the *T. brucei* flagellum is the protein kinase A RSU, which binds cyclic nucleotide (72). RSU mediates cyclic nucleotide signaling in diverse organisms (98, 99), although a function has not been defined for this protein in *T. brucei*. We identified RSU in the flagellum matrix fraction (supplemental Table S3). Absence of RSU from detergent-extracted flagellum preparations (31, 43, 46) indicates it is not stably associated with the axoneme or PFR. To test for a requirement of RSU in flagellum function, we used RNAi. RSU knockdown inhibited motility of bloodstream-form cells (Fig. 7*D*,7*E*). The motility defect caused by RSU knockdown supports the identification of RSU in the flagellum matrix and provides experimental evidence for cyclic nucleotide-dependent signaling in regulating flagellum function.

Functional Analysis of Flagellum Surface Proteins Provides Insight into Mechanisms of Flagellum Attachment—One of the most distinctive features of the *T. brucei* flagellum is lateral attachment to the cell body, via regularly-spaced, desmosome-like adhesions between the flagellar and cell surface membranes (40). Immunofluorescence revealed that some proteins in the flagellum surface fraction, *e.g.* FS179 (Fig. 6*B*) and FS105 (supplemental Fig. S3), are restricted to the flagellum-cell body interface and do not extend to the flagellum tip, suggesting a potential role in flagellum attachment. RNAi knockdown of FS179, which encodes a putative Ca^{2+} channel, caused the flagellum to become detached from the cell body, with the daughter flagellum being preferentially affected (Fig. 7*A–7C*). The phenotype was ultimately lethal (supplemental Fig. S4). FS179 knockdown phenocopies flagellum detachment caused by treatment of bloodstream trypanosomes with Ca^{2+} chelators, as reported by Vickerman forty years ago (40). These results indicate a requirement for Ca^{2+} in establishment of flagellum-cell body adhesion in *T. brucei* (40) and suggest that FS179 is critical for maintaining Ca^{2+} homeostasis at the flagellum-cell body interface. In other organisms Ca^{2+} is required for homophilic cell-cell adhesion, including fibrous linkages between the connecting cilium and the periciliary inner segment collar of mammalian photoreceptors (100). Defects in these periciliary attachments cause Usher syndrome in humans (101). Previous analogies have been drawn between mammalian Ca^{2+}-dependent cell-cell adhesions and trypanosome flagellum-cell body adhesions (40). Our findings support this view at the molecular level. Flagellum attachment is essential in *T. brucei,* suggesting that Ca^{2+} channels might be exploited as targets for therapeutic intervention in trypanosomiases. Indeed, Ca^{2+} channels are major targets of the pharmaceutical industry for treating of a variety of human diseases (102) and Ca^{2+} channel blockers have antiprotozoal activity *in vitro* (103).

Matrix-Specific Proteins Include IFT Proteins and Components of the Ubiquitin Conjugating System—Many proteins identified in the flagellum surface fraction were also identified in the flagellum matrix fraction. This result is expected because biotinylation and avidin purification are not 100% efficient. On the other hand, the vast majority (87%) of proteins in the flagellum matrix were exclusive to this fraction. Matrix-specific proteins include components of the intraflagellar transport (IFT) system that are required for flagellum assembly and signaling (104, 105). We identified six IFT complex B proteins, and the IFT anterograde kinesin motor, KIF3A (supplemental Table S8). Notably, none of the IFT proteins were identified in the surface fraction, or in previous proteomic analyses of the flagellum skeleton (31, 43, 46).

Another interesting group of proteins specifically identified in the matrix fraction includes components of the ubiquitin

conjugating system (supplemental Table S9). Ubiquitination is a post-translational protein modification that has essential roles in many cellular processes, including cell-cycle control, protein quality control and signaling (106–108). A recent study identified a functional ubiquitination system in the flagellum of *C. reinhardtii,* where it is postulated to control flagellar resorption and cAMP-dependent signaling in the flagellum during mating (109). Several ubiquitinated proteins were identified, including the polycystin 2 cation channel (CrPKD2) and a cyclic GMP-dependent protein kinase (CrPKG) that both participate in flagellum signaling during mating (109). Polyubiquitin was identified in all three *T. brucei* flagellum fractions (supplemental Tables S9 (31, 43, 46)), indicating ubiquitination of *T. brucei* flagellar proteins. The identification of an ubiquitin-activating enzyme and three ubiquitin conjugating enzymes in the flagellum matrix fraction suggests that ubiquitination might be carried out within the flagellum itself. Although the function of ubiquitination in the *T. brucei* flagellum remains to be determined, we postulate that this pathway participates in regulation of flagellum function as described for *C. reinhardtii* (109).

The Flagellum Surface Presents a Dynamic and Cell-specific Host-Parasite Interface—Phylogenetic analysis revealed that 16% of flagellar surface proteins are *T. brucei*-specific. By comparison, only 5% of proteins in the flagellar matrix and 1% in the flagellum skeleton are *T. brucei*-specific. These results suggest that flagellum surface proteins must accommodate cell-specific functions, such as perception of signals specific to the parasite's extracellular environment. In contrast, composition of the flagellar matrix and skeleton fractions reflect more broadly conserved functions, *e.g.* downstream signal transduction and motility capacity of the organelle. Trypanosomes infect a broad range of organisms and survival in diverse host environments necessitates specialized surface proteins for signaling, nutrient acquisition and protection against host defenses. A cell-specific flagellum surface proteome would provide an interface that is tailored to meet the demands specifically imposed on *T. brucei* in each host. In support of this idea, we found that 21% of flagellum surface proteins are up-regulated by twofold or more in the bloodstream life cycle stage (Fig. 10) (68, 71). This is higher than seen for matrix proteins (10%), flagellum skeleton proteins (3%) or for the genome as a whole (3%) (Fig. 10) (68, 71). Thus, the flagellum surface proteome is a dynamic host-parasite interface that is particularly subject to life cycle stage-specific regulation.

Conserved Flagellum Surface Proteins are not Biased Toward Flagellated Organisms—Comparing the phylogenetic distribution of conserved proteins, *i.e.* those that are not kinetoplastid-specific, in each flagellum sub-fraction revealed an interesting feature of surface and matrix proteins. Namely, conservation of surface and matrix proteins is not biased toward flagellated organisms. This result contrasts markedly from what is observed for conserved flagellum skeleton proteins, which are generally more restricted to flagellated organisms (Fig. 9). The bias toward flagellated organisms reflects the requirement of flagellum skeleton proteins for axoneme structure and motility, which are unique to organisms with flagella (82–84). Flagellum surface and matrix proteins on the other hand, are predicted to be involved in perception and transduction of extracellular signals, *i.e.* processes that are not unique to flagellated organisms. An exception is the group of IFT proteins in the matrix, which are involved in flagellum assembly but represent a small fraction of matrix proteins. The combined phylogenetic analyses indicate that protein composition of the eukaryotic flagellum surface is shaped by selective forces that are a combination of cell-specific demands, imposed by unique extracellular environments, and more broadly conserved signaling needs. This finding has practical implications, as it means comparative genomic approaches, which are useful for identifying flagellum assembly and motility genes (82–84), are not well-suited for identification of genes involved in flagellum signaling.

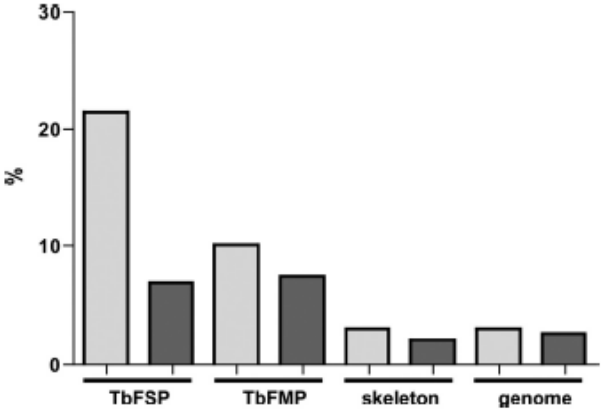


FIG. 10. **Flagellum surface proteins are up-regulated in bloodstream-form cells.** Chart shows the percentage of proteins in each proteomic dataset that are up-regulated in bloodstream-form cells (*light gray* bars) or procyclic-form cells (*dark gray* bars) by twofold or more based on RNA sequencing analysis (68). Proteomic data sets are for the flagellum surface (TbFSP), the flagellum matrix (TbFMP), and the flagellum skeleton (TbFP) proteomes (31, 43, 46).

Acknowledgments—We thank Dr. Zakayi Pius Kabututu for assistance and input for flagellum purification. Prof. G. Cross for the pMOTag2H vector and the 221 cell line; Prof. T. Seebeck and Prof. J. Bangs for antibodies. We also thank colleagues for critical reading of the manuscript.

* This work was supported by the Swiss National Science Foundation (MO), National Institutes of Health (NIH)-AI052348 (KLH), the Burroughs Wellcome Fund (KLH), NIH-NRSA-GM07185 (HTN), the A. G. Leventis Foundation (GL), NIH-NRSA-GM GM07104 (EAS), URC-CARE-GM55052 and UC-LEADS (SMN), Jonsson Cancer Center at UCLA and NIH-GM089778 (JAW).

[S] This article contains supplemental Figs. S1 to S4, Tables, S1 to S10 and Movie S1.

‡‡ To whom correspondence should be addressed: Kent L. Hill, Department of Microbiology, Immunology, and Molecular Genetics,

University of California, Los Angeles, CA 90095, USA. Tel.: (310) 267-0546; E-mail: kenthill@mednet.ucla.edu. James A. Wohlschlegal, Department of Biological Chemistry, David Geffen School of Medicine, University of California, Los Angeles, CA 90095, USA. Tel.: (310) 794-7955; E-mail: jwohl@mednet.ucla.edu.

** These authors contributed equally to the work.

REFERENCES

1. Berbari, N. F., O'Connor, A. K., Haycraft, C. J., and Yoder, B. K. (2009) The primary cilium as a complex signaling center. *Curr. Biol.* **19,** R526–535
2. Christensen, S. T., and Ott, C. M. (2007) Cell signaling. A ciliary signaling switch. *Science* **317,** 330–331
3. Corbit, K. C., Aanstad, P., Singla, V., Norman, A. R., Stainier, D. Y., and Reiter, J. F. (2005) Vertebrate Smoothened functions at the primary cilium. *Nature* **437,** 1018–1021
4. Bloodgood, R. A. Sensory reception is an attribute of both primary cilia and motile cilia. *J. Cell Sci.* **123,** 505–509
5. Satir, P., Mitchell, D. R., and Jékely, G. (2008) How did the cilium evolve? *Curr. Top. Dev. Biol.* **85,** 63–82
6. Badano, J. L., Mitsuma, N., Beales, P. L., and Katsanis, N. (2006) The ciliopathies: an emerging class of human genetic disorders. *Annu. Rev. Genomics Hum. Genet.* **7,** 125–148
7. Fliegauf, M., Benzing, T., and Omran, H. (2007) When cilia go bad: cilia defects and ciliopathies. *Nat. Rev. Mol. Cell Biol.* **8,** 880–893
8. Kaupp, U. B., Kashikar, N. D., and Weyand, I. (2008) Mechanisms of sperm chemotaxis. *Annu. Rev. Physiol.* **70,** 93–117
9. Pan, J., Wang, Q., and Snell, W. J. (2005) Cilium-generated signaling and cilia-related disorders. *Lab. Invest.* **85,** 452–463
10. Rohatgi, R., Milenkovic, L., and Scott, M. P. (2007) Patched1 regulates hedgehog signaling at the primary cilium. *Science* **317,** 372–376
11. Christensen, S. T., Guerra, C. F., Awan, A., Wheatley, D. N., and Satir, P. (2003) Insulin receptor-like proteins in Tetrahymena thermophila ciliary membranes. *Curr. Biol.* **13,** R50–R52
12. Ogura, A., and Takahashi, K. (1976) Artificial deciliation causes loss of calcium-dependent responses in Paramecium. *Nature* **264,** 170–172
13. Pan, J., and Snell, W. J. (2000) Signal transduction during fertilization in the unicellular green alga, *Chlamydomonas*. *Curr. Opin. Microbiol.* **3,** 596–602
14. Dawson, S. C., and House, S. A. (2010) Life with eight flagella: flagellar assembly and division in Giardia. *Curr. Opin. Microbiol.* **13,** 480–490
15. Ralston, K. S., Kabututu, Z. P., Melehani, J. H., Oberholzer, M., and Hill, K. L. (2009) The Trypanosoma brucei flagellum: moving parasites in new directions. *Annu. Rev. Microbiol.* **63,** 335–362
16. Sinden, R. E., Talman, A., Marques, S. R., Wass, M. N., and Sternberg, M. J. (2010) The flagellum in malarial parasites. *Curr. Opin. Microbiol.* **13,** 491–500
17. WHO (2004) Available at http://www.who.int/evidence/bod
18. Bastin, P. The peculiarities of flagella in parasitic protozoa. *Curr. Opin. Microbiol.* **13,** 450–452
19. Brun, R., Blum, J., Chappuis, F., and Burri, C. (2010) Human African trypanosomiasis. *Lancet* **375,** 148–159
20. Maric, D., Epting, C. L., and Engman, D. M. (2010) Composition and sensory function of the trypanosome flagellar membrane. *Curr. Opin. Microbiol.* **13,** 466–472
21. Parsons, M., and Ruben, L. (2000) Pathways involved in environmental sensing in trypanosomatids. *Parasitol. Today* **16,** 56–62
22. Rotureau, B., Morales, M. A., Bastin, P., and Spath, G. F. (2009) The flagellum-MAP kinase connection in Trypanosomatids: a key sensory role in parasite signaling and development? *Cell Microbiol.* **11,** 710–718
23. Fenn, K., and Matthews, K. R. (2007) The cell biology of Trypanosoma brucei differentiation. *Curr. Opin. Microbiol.* **10,** 539–546
24. Dean, S., Marchetti, R., Kirk, K., and Matthews, K. R. (2009) A surface transporter family conveys the trypanosome differentiation signal. *Nature* **459,** 213–217
25. Nikolskaia, O. V., de, A, Lima, A. P., Kim, Y. V., Lonsdale-Eccles, J. D., Fukuma, T., Scharfstein, J., and Grab, D. J. (2006) Blood-brain barrier traversal by African trypanosomes requires calcium signaling induced by parasite cysteine protease. *J. Clin. Invest.* **116,** 2739–2747
26. Tetley, L., and Vickerman, K. (1985) Differentiation in Trypanosoma brucei: host-parasite cell junctions and their persistence during acquisition of the variable antigen coat. *J. Cell Sci.* **74,** 1–19
27. Van Den Abbeele, J., Claes, Y., van Bockstaele, D., Le Ray, D., and Coosemans, M. (1999) Trypanosoma brucei spp. development in the tsetse fly: characterization of the post-mesocyclic stages in the foregut and proboscis. *Parasitology* **118,** 469–478
28. Gluenz, E., Höög, J. L., Smith, A. E., Dawe, H. R., Shaw, M. K., and Gull, K. (2010) Beyond 9+0: noncanonical axoneme structures characterize sensory cilia from protists to humans. *Faseb J.* **24,** 3117–3121
29. Oberholzer, M., Marti, G., Baresic, M., Kunz, S., Hemphill, A., and Seebeck, T. (2007) The Trypanosoma brucei cAMP phosphodiesterases TbrPDEB1 and TbrPDEB2: flagellar enzymes that are essential for parasite virulence. *Faseb J.* **21,** 720–731
30. Paindavoine, P., Rolin, S., Van Assel, S., Geuskens, M., Jauniaux, J. C., Dinsart, C., Huet, G., and Pays, E. (1992) A gene from the variant surface glycoprotein expression site encodes one of several transmembrane adenylate cyclases located on the flagellum of Trypanosoma brucei. *Mol. Cell. Biol.* **12,** 1218–1225
31. Portman, N., Lacomble, S., Thomas, B., McKean, P. G., and Gull, K. (2009) Combining RNA interference mutants and comparative proteomics to identify protein components and dependences in a eukaryotic flagellum. *J. Biol. Chem.* **284,** 5610–5619
32. Ridgley, E., Webster, P., Patton, C., and Ruben, L. (2000) Calmodulin-binding properties of the paraflagellar rod complex from Trypanosoma brucei. *Mol. Biochem. Parasitol.* **109,** 195–201
33. Wu, Y., Deford, J., Benjamin, R., Lee, M. G., and Ruben, L. (1994) The gene family of EF-hand calcium-binding proteins from the flagellum of Trypanosoma brucei. *Biochem. J.* **304,** 833–841
34. Wu, Y., Haghighat, N. G., and Ruben, L. (1992) The predominant calcimedins from Trypanosoma brucei comprise a family of flagellar EF-hand calcium-binding proteins. *Biochem. J.* **287,** 187–193
35. Kohl, L., and Bastin, P. (2005) The flagellum of trypanosomes. *Int. Rev. Cytol.* **244,** 227–285
36. Balber, A. E. (1990) The pellicle and the membrane of the flagellum, flagellar adhesion zone, and flagellar pocket: functionally discrete surface domains of the bloodstream form of African trypanosomes. *Crit. Rev. Immunol.* **10,** 177–201
37. Tyler, K. M., Fridberg, A., Toriello, K. M., Olson, C. L., Cieslak, J. A., Hazlett, T. L., and Engman, D. M. (2009) Flagellar membrane localization via association with lipid rafts. *J. Cell Sci.* **122,** 859–866
38. Hu, Q., Milenkovic, L., Jin, H., Scott, M. P., Nachury, M. V., Spiliotis, E. T., and Nelson, W. J. (2010) A septin diffusion barrier at the base of the primary cilium maintains ciliary membrane protein distribution. *Science* **329,** 436–439
39. Lacomble, S., Vaughan, S., Gadelha, C., Morphew, M. K., Shaw, M. K., McIntosh, J. R., and Gull, K. (2009) Three-dimensional cellular architecture of the flagellar pocket and associated cytoskeleton in trypanosomes revealed by electron microscope tomography. *J. Cell Sci.* **122,** 1081–1090
40. Vickerman, K. (1969) On the surface coat and flagellar adhesion in trypanosomes. *J. Cell Sci.* **5,** 163–193
41. Field, M. C., and Carrington, M. (2009) The trypanosome flagellar pocket. *Nat. Rev. Microbiol.* **7,** 775–786
42. Webster, P., and Russell, D. G. (1993) The flagellar pocket of trypanosomatids. *Parasitol. Today* **9,** 201–206
43. Broadhead, R., Dawe, H. R., Farr, H., Griffiths, S., Hart, S. R., Portman, N., Shaw, M. K., Ginger, M. L., Gaskell, S. J., McKean, P. G., and Gull, K. (2006) Flagellar motility is required for the viability of the bloodstream trypanosome. *Nature* **440,** 224–227
44. Robinson, D. R., and Gull, K. (1991) Basal body movements as a mechanism for mitochondrial genome segregation in the trypanosome cell cycle. *Nature* **352,** 731–733
45. Schlaeppi, K., Deflorin, J., and Seebeck, T. (1989) The major component of the paraflagellar rod of Trypanosoma brucei is a helical protein that is encoded by two identical, tandemly linked genes. *J. Cell Biol.* **109,** 1695–1709
46. Hart, S. R., Lau, K. W., Hao, Z., Broadhead, R., Portman, N., Hühmer, A., Gull, K., McKean, P. G., Hubbard, S. J., and Gaskell, S. J. (2009) Analysis of the trypanosome flagellar proteome using a combined electron transfer/collisionally activated dissociation strategy. *J. Am. Soc. Mass Spectrom.* **20,** 167–175
47. Wirtz, E., Leal, S., Ochatt, C., and Cross, G. A. (1999) A tightly regulated

inducible expression system for conditional gene knock-outs and dominant-negative genetics in Trypanosoma brucei. *Mol. Biochem. Parasitol.* **99,** 89–101
48. Oberholzer, M., Lopez, M. A., Ralston, K. S., and Hill, K. L. (2009) Approaches for functional analysis of flagellar proteins in African trypanosomes. *Methods Cell Biol.* **93,** 21–57
49. LaCount, D. J., Barrett, B., and Donelson, J. E. (2002) Trypanosoma brucei FLA1 is required for flagellum attachment and cytokinesis. *J. Biol. Chem.* **277,** 17580–17588
50. Bangs, J. D., Uyetake, L., Brickman, M. J., Balber, A. E., and Boothroyd, J. C. (1993) Molecular cloning and cellular localization of a BiP homologue in Trypanosoma brucei. Divergent ER retention signals in a lower eukaryote. *J. Cell Sci.* **105,** 1101–1113
51. McDowell, M. A., Ransom, D. M., and Bangs, J. D. (1998) Glycosylphosphatidylinositol-dependent secretory transport in Trypanosoma brucei. *Biochem. J.* **335,** 681–689
52. Tagwerker, C., Flick, K., Cui, M., Guerrero, C., Dou, Y., Auer, B., Baldi, P., Huang, L., and Kaiser, P. (2006) A tandem affinity tag for two-step purification under fully denaturing conditions: application in ubiquitin profiling and protein complex identification combined with in vivocross-linking. *Mol. Cell Proteomics* **5,** 737–748
53. Wohlschlegel, J. A. (2009) Identification of SUMO-conjugated proteins and their SUMO attachment sites using proteomic mass spectrometry. *Methods Mol. Biol.* **497,** 33–49
54. Florens, L., Carozza, M. J., Swanson, S. K., Fournier, M., Coleman, M. K., Workman, J. L., and Washburn, M. P. (2006) Analyzing chromatin remodeling complexes using shotgun proteomics and normalized spectral abundance factors. *Methods* **40,** 303–311
55. Xu, T. V., Venable, J. D., Cociorva, D., Lu, B., Liao, L., Wohlschlegel, J., Hewel, J., and Yates, J. R., 3rd (2006) ProLuCID, a fast and sensitive tandem mass spectra-based protein identification program. *Mol. Cellular Proteomics* **5**
56. Eng, J. K., McCormack, A. L. YJI (1994) An approach to correlate tandem mass spectral data of peptides with amino acid sequences in a protein database. *J. Am. Soc. Mass Spectrom.* **5,** 976–989
57. Tabb, D. L., McDonald, W. H., and Yates, J. R., 3rd (2002) DTASelect and Contrast: tools for assembling and comparing protein identifications from shotgun proteomics. *J. Proteome Res.* **1,** 21–26
58. Cociorva, D. L. T. D., and Yates, J. R. (2007) Validation of tandem mass spectrometry database search results using DTASelect. Curr. Protoc. Bioinformatics **13**
59. Tazeh, N. N., Silverman, J. S., Schwartz, K. J., Sevova, E. S., Sutterwala, S. S., and Bangs, J. D. (2009) Role of AP-1 in developmentally regulated lysosomal trafficking in Trypanosoma brucei. *Eukaryot. Cell* **8,** 1352–1361
60. Ralston, K. S., and Hill, K. L. (2006) Trypanin, a component of the flagellar Dynein regulatory complex, is essential in bloodstream form African trypanosomes. *PLoS Pathog.* **2,** e101
61. Oberholzer, M., Morand, S., Kunz, S., and Seebeck, T. (2006) A vector series for rapid PCR-mediated C-terminal in situ tagging of Trypanosoma brucei genes. *Mol. Biochem. Parasitol.* **145,** 117–120
62. Redmond, S., Vadivelu, J., and Field, M. C. (2003) RNAit: an automated web-based tool for the selection of RNAi targets in Trypanosoma brucei. *Mol. Biochem. Parasitol* **128,** 115–118
63. Schultz, J., Milpetz, F., Bork, P., and Ponting, C. P. (1998) SMART, a simple modular architecture research tool: identification of signaling domains. *Proc. Natl. Acad. Sci. U.S.A.* **95,** 5857–5864
64. Pazour, G. J., Agrin, N., Leszyk, J., and Witman, G. B. (2005) Proteomic analysis of a eukaryotic cilium. *J. Cell Biol.* **170,** 103–113
65. Huang, da W., Sherman, B. T., and Lempicki, R. A. (2009) Systematic and integrative analysis of large gene lists using DAVID bioinformatics resources. *Nat. Protoc.* **4,** 44–57
66. Huang, da W., Sherman, B. T., and Lempicki, R. A. (2009) Bioinformatics enrichment tools: paths toward the comprehensive functional analysis of large gene lists. *Nucleic Acids Res.* **37,** 1–13
67. Ashburner, M., Ball, C. A., Blake, J. A., Botstein, D., Butler, H., Cherry, J. M., Davis, A. P., Dolinski, K., Dwight, S. S., Eppig, J. T., Harris, M. A., Hill, D. P., Issel-Tarver, L., Kasarskis, A., Lewis, S., Matese, J. C., Richardson, J. E., Ringwald, M., Rubin, G. M., and Sherlock, G. (2000) Gene ontology: tool for the unification of biology. The Gene Ontology Consortium. *Nat. Genet.* **25,** 25–29
68. Siegel, T. N., Hekstra, D. R., Wang, X., Dewell, S., and Cross, G. A. (2010) Genome-wide analysis of mRNA abundance in two life-cycle stages of Trypanosoma brucei and identification of splicing and polyadenylation sites. *Nucleic Acids Res.* **38,** 4946–4957
69. Vanhamme, L., Pays, E., McCulloch, R., and Barry, J. D. (2001) An update on antigenic variation in African trypanosomes. *Trends Parasitol.* **17,** 338–343
70. Berriman, M., Ghedin, E., Hertz-Fowler, C., Blandin, G., Renauld, H., Bartholomeu, D. C., Lennard, N. J., Caler, E., Hamlin, N. E., Haas, B., Böhme, U., Hannick, L., Aslett, M. A., Shallom, J., Marcello, L., Hou, L., Wickstead, B., Alsmark, U. C., Arrowsmith, C., Atkin, R. J., Barron, A. J., Bringaud, F., Brooks, K., Carrington, M., Cherevach, I., Chillingworth, T. J., Churcher, C., Clark, L. N., Corton, C. H., Cronin, A., Davies, R. M., Doggett, J., Djikeng, A., Feldblyum, T., Field, M. C., Fraser, A., Goodhead, I., Hance, Z., Harper, D., Harris, B. R., Hauser, H., Hostetler, J., Ivens, A., Jagels, K., Johnson, D., Johnson, J., Jones, K., Kerhornou, A. X., Koo, H., Larke, N., Landfear, S., Larkin, C., Leech, V., Line, A., Lord, A., Macleod, A., Mooney, P. J., Moule, S., Martin, D. M., Morgan, G. W., Mungall, K., Norbertczak, H., Ormond, D., Pai, G., Peacock, C. S., Peterson, J., Quail, M. A., Rabbinowitsch, E., Rajandream, M. A., Reitter, C., Salzberg, S. L., Sanders, M., Schobel, S., Sharp, S., Simmonds, M., Simpson, A. J., Tallon, L., Turner, C. M., Tait, A., Tivey, A. R., Van., Aken, S., Walker, D., Wanless, D., Wang, S., White, B., White, O., Whitehead, S., Woodward, J., Wortman, J., Adams, M. D., Embley, T. M., Gull, K., Ullu, E., Barry, J. D., Fairlamb, A. H., Opperdoes, F., Barrell, B. G., Donelson, J. E., Hall, N., Fraser, C. M., Melville, S. E., and El-Sayed, N. M. (2005) The genome of the African trypanosome Trypanosoma brucei. *Science* **309,** 416–422
71. Aslett, M., *et al.* TriTrypDB: a functional genomic resource for the Trypanosomatidae. Nucleic Acids Res. 38: D457–462
72. Shalaby, T., Liniger, M., and Seebeck, T. (2001) The regulatory subunit of a cGMP-regulated protein kinase A of Trypanosoma brucei. *Eur. J. Biochem.* **268,** 6197–6206
73. Gaillard, A. R., Diener, D. R., Rosenbaum, J. L., and Sale, W. S. (2001) Flagellar radial spoke protein 3 is an A-kinase anchoring protein (AKAP). *J. Cell Biol.* **153,** 443–448
74. Eisenbach, M., and Giojalas, L. C. (2006) Sperm guidance in mammals - an unpaved road to the egg. *Nat. Rev. Mol. Cell Biol.* **7,** 276–285
75. Hanrahan, O., Webb, H., O'Byrne, R., Brabazon, E., Treumann, A., Sunter, J. D., Carrington, M., and Voorheis, H. P. (2009) The glycosylphosphatidylinositol-PLC in Trypanosoma brucei forms a linear array on the exterior of the flagellar membrane before and after activation. *PLoS Pathog.* **5,** e1000468
76. LaCount, D. J., Gruszynski, A. E., Grandgenett, P. M., Bangs, J. D., and Donelson, J. E. (2003) Expression and function of the Trypanosoma brucei major surface protease (GP63) genes. *J. Biol. Chem.* **278,** 24658–24664
77. Salmon, D., Geuskens, M., Hanocq, F., Hanocq-Quertier, J., Nolan, D., Ruben, L., and Pays, E. (1994) A novel heterodimeric transferrin receptor encoded by a pair of VSG expression site-associated genes in T. brucei. *Cell* **78,** 75–86
78. Tetaud, E., Barrett, M. P., Bringaud F., and Baltz, T. (1997) Kinetoplastid glucose transporters. *Biochem. J.* **325,** 569–580
79. Emmer, B. T., Daniels, M. D., Taylor, J. M., Epting, C. L., and Engman, D. M. (2010) Calflagin inhibition prolongs host survival and suppresses parasitemia in Trypanosoma brucei infection. *Eukaryot. Cell* **9,** 934–942
80. Felder, C. B., Graul, R. C., Lee, A. Y., Merkle, H. P., and Sadee, W. (1999) The Venus flytrap of periplasmic binding proteins: an ancient protein module present in multiple drug receptors. *AAPS PharmSci.* **1,** E2
81. Campbell, I. D., Baron, M., Cooke, R. M., Dudgeon, T. J., Fallon, A., Harvey, T. S., and Tappin, M. J. (1990) Structure-function relationships in epidermal growth factor (EGF) and transforming growth factor-alpha (TGF-alpha). *Biochem. Pharmacol* **40,** 35–40
82. Li, J. B., Gerdes, J. M., Haycraft, C. J., Fan, Y., Teslovich, T. M., May-Simera, H., Li, H., Blacque, O. E., Li, L., Leitch, C. C., Lewis, R. A., Green, J. S., Parfrey, P. S., Leroux, M. R., Davidson, W. S., Beales, P. L., Guay-Woodford, L. M., Yoder, B. K., Stormo, G. D., Katsanis, N., and Dutcher, S. (2004) Comparative genomics identifies a flagellar and basal body proteome that includes the BBS5 human disease gene. *Cell* **117,** 541–552
83. Avidor-Reiss, T., Maer, A. M., Koundakjian, E., Polyanovsky, A., Keil, T.,

Subramaniam, S., and Zuker, C. S. (2004) Decoding cilia function: defining specialized genes required for compartmentalized cilia biogenesis. *Cell* **117,** 527–539
84. Baron, D. M., Ralston, K. S., Kabututu, Z. P., and Hill, K. L. (2007) Functional genomics in Trypanosoma brucei identifies evolutionarily conserved components of motile flagella. *J. Cell Sci.* **120,** 478–491
85. Bastin, P. (2010) The peculiarities of flagella in parasitic protozoa. *Curr. Opin. Microbiol.* **13,** 450–452
86. Rodriguez, J. A., Lopez, M. A., Thayer, M. C., Zhao, Y., Oberholzer, M., Chang, D. D., Kisalu, N. K., Penichet, M. L., Helguera, G., Bruinsma, R., Hill, K. L., and Miao, J. (2009) Propulsion of African trypanosomes is driven by bihelical waves with alternating chirality separated by kinks. *Proc. Natl. Acad. Sci. U.S.A.* **106,** 19322–19327
87. Engstler, M., Pfohl, T., Herminghaus, S., Boshart, M., Wiegertjes, G., Heddergott, N., and Overath, P. (2007) Hydrodynamic flow-mediated protein sorting on the cell surface of trypanosomes. *Cell* **131,** 505–515
88. Smith, J. C., Northey, J. G., Garg, J., Pearlman, R. E., and Siu, K. W. (2005) Robust method for proteome analysis by MS/MS using an entire translated genome: demonstration on the ciliome of Tetrahymena thermophila. *J. Proteome Res.* **4,** 909–919
89. Borst, P., and Fairlamb, A. H. (1998) Surface receptors and transporters of Trypanosoma brucei. *Annu. Rev. Microbiol.* **52,** 745–778
90. Mussmann, R., Engstler, M., Gerrits, H., Kieft, R., Toaldo, C. B., Onderwater, J., Koerten, H., van Luenen, H. G., and Borst, P. (2004) Factors affecting the level and localization of the transferrin receptor in Trypanosoma brucei. *J. Biol. Chem.* **279,** 40690–40698
91. Vanhollebeke, B., De Muylder, G., Nielsen, M. J., Pays, A., Tebabi, P., Dieu, M., Raes, M., Moestrup, S. K., and Pays, E. (2008) A haptoglobin-hemoglobin receptor conveys innate immunity to Trypanosoma brucei in humans. *Science* **320,** 677–681
92. Engstler, M., Weise, F., Bopp, K., Grünfelder, C. G., Günzel, M., Heddergott, N., and Overath, P. (2005) The membrane-bound histidine acid phosphatase TbMBAP1 is essential for endocytosis and membrane recycling in Trypanosoma brucei. *J. Cell Sci.* **118,** 2105–2118
93. Luo, S., Rohloff, P., Cox, J., Uyemura, S. A., and Docampo, R. (2004) Trypanosoma brucei plasma membrane-type Ca(2+)-ATPase 1 (TbPMC1) and 2 (TbPMC2) genes encode functional Ca(2+)-ATPases localized to the acidocalcisomes and plasma membrane, and essential for Ca(2+) homeostasis and growth. *J. Biol. Chem.* **279,** 14427–14439
94. Ziegelbauer, K., Multhaup, G., and Overath, P. (1992) Molecular characterization of two invariant surface glycoproteins specific for the bloodstream stage of Trypanosoma brucei. *J. Biol. Chem.* **267,** 10797–10803
95. Vanhamme, L., Paturiaux-Hanocq, F., Poelvoorde, P., Nolan, D. P., Lins, L., Van, Den, Abbeele, J., Pays, A., Tebabi, P., Van, Xong, H., Jacquet, A., Moguilevsky, N., Dieu, M., Kane, J. P., De, Baetselier, P., Brasseur, R., and Pays, E. (2003) Apolipoprotein L-I is the trypanosome lytic factor of human serum. *Nature* **422,** 83–87
96. Absalon, S., Blisnick, T., Kohl, L., Toutirais, G., Doré, G., Julkowska, D., Tavenet, A., and Bastin, P. (2008) Intraflagellar transport and functional analysis of genes required for flagellum formation in trypanosomes. *Mol. Biol. Cell* **19,** 929–944
97. Franklin, J. B., and Ullu, E. Biochemical analysis of PIFTC3, the Trypanosoma brucei orthologue of nematode DYF-13, reveals interactions with established and putative intraflagellar transport components. *Mol. Microbiol.* **78,** 173–186
98. Howard, D. R., Habermacher, G., Glass, D. B., Smith, E. F., and Sale, W. S. (1994) Regulation of Chlamydomonas flagellar dynein by an axonemal protein kinase. *J. Cell Biol.* **127,** 1683–1692
99. Francis, S. H., and Corbin, J. D. (1999) Cyclic nucleotide-dependent protein kinases: intracellular receptors for cAMP and cGMP action. *Crit. Rev. Clin. Lab. Sci.* **36,** 275–328
100. Maerker, T., van, Wijk, E., Overlack, N., Kersten, F. F., McGee, J., Goldmann, T., Sehn, E., Roepman, R., Walsh, E. J., Kremer, H., and Wolfrum, U. (2008) A novel Usher protein network at the periciliary reloading point between molecular transport machineries in vertebrate photoreceptor cells. *Hum. Mol. Genet.* **17,** 71–86
101. Williams, D. S. (2008) Usher syndrome: animal models, retinal function of Usher proteins, and prospects for gene therapy. *Vision Res.* **48,** 433–441
102. Abernethy, D. R., and Schwartz, J. B. (1999) Calcium-antagonist drugs. N. *Engl. J. Med.* **341,** 1447–1457
103. Reimao, J. Q., Scotti, M. T., and Tempone, A. G. (2010) Anti-leishmanial and anti-trypanosomal activities of 1,4-dihydropyridines: In vitro evaluation and structure-activity relationship study. *Bioorg. Med. Chem.* **18,** 8044–8053
104. Cole, D. G. (2003) The intraflagellar transport machinery of Chlamydomonas reinhardtii. *Traffic* **4,** 435–442
105. Rosenbaum, J. L., and Witman, G. B. (2002) Intraflagellar transport. *Nat. Rev. Mol. Cell Biol.* **3,** 813–825
106. Okiyoneda, T., Barriere, H., Bagdany, M., Rabeh, W. M., Du, K., Hohfeld, J., Young, J. C., and Lukacs, G. L. (2010) Peripheral protein quality control removes unfolded CFTR from the plasma membrane. *Science* **329,** 805–810
107. Hershko, A. (2005) The ubiquitin system for protein degradation and some of its roles in the control of the cell division cycle. *Cell Death Differ.* **12,** 1191–1197
108. Wilkinson, K. D. (1999) Ubiquitin-dependent signaling: the role of ubiquitination in the response of cells to their environment. *J. Nutr.* **129,** 1933–1936
109. Huang, K., Diener, D. R., and Rosenbaum, J. L. (2009) The ubiquitin conjugation system is involved in the disassembly of cilia and flagella. *J. Cell Biol.* **186,** 601–613
110. Hill, K. L., Hutchings, N. R., Grandgenett, P. M., and Donelson, J. E. (2000) T lymphocyte-triggering factor of african trypanosomes is associated with the flagellar fraction of the cytoskeleton and represents a new family of proteins that are present in several divergent eukaryotes. *J. Biol. Chem.* **275,** 39369–39378
111. Buchanan, K. T., Ames, J. B., Asfaw, S. H., Wingard, J. N., Olson, C. L., Campana, P. T., Araújo, A. P., and Engman, D. M. (2005) A flagellum-specific calcium sensor. *J. Biol. Chem.* **280,** 40104–40111
112. Deleted in proof
113. Lancaster M. A., Schroth J., Gleeson, J. G. (2011) Subcellular spatial regulation of canonical Wnt signaling at the primary cillum. *Nat. Cell Biol.* **13,** 700–707, e pub, May 22